Year : 2019

Characterization of atypical polyester dépositions at the root of Arabidopsis thaliana

Berhin Alice

Berhin Alice, 2019, Characterization of atypical polyester dépositions at the root of Arabidopsis thaliana

Originally published at : Thesis, University of Lausanne

Posted at the University of Lausanne Open Archive http://serval.unil.ch
Document URN : urn:nbn:ch:serval-BIB_2E712200405C9

UNIL | Université de Lausanne
Faculté de biologie
et de médecine

Département de Biologie Moléculaire Végétale

Characterization of atypical polyester depositions at the root of *Arabidopsis thaliana*

Thèse de doctorat ès sciences de la vie (PhD)

présentée à la

Faculté de biologie et de médecine
de l'Université de Lausanne

par

Alice Berhin

Bioingénieur diplômée de l'Université de Louvain-la-Neuve (Belgique)

Jury

Prof. Philippe Christe, Président
Dr. Christiane Nawrath, Directrice de thèse
Dr. Rochus Benni Franke, expert
Dr. Gwyneth Ingram, expert
Dr. Robertas Ursache, expert

Lausanne 2019

UNIL | Université de Lausanne
Faculté de biologie
et de médecine

Ecole Doctorale
Doctorat ès sciences de la vie

Imprimatur

Vu le rapport présenté par le jury d'examen, composé de

Président·e	Monsieur	Prof.	Philippe	**Christe**
Directeur·trice de thèse	Madame	Dre	Christiane	**Nawrath**
Expert·e·s	Monsieur	Dr	Robertas	**Ursache**
	Madame	Dre	Gwyneth	**Ingram**
	Monsieur	Dr	Rochus	**Franke**

le Conseil de Faculté autorise l'impression de la thèse de

Madame Alice Berhin

Master de bioingénieur, Université catholique de Louvain, Belgique

intitulée

Characterization of atypical polyester depositions at the root of *Arabidopsis thaliana*

Lausanne, le 15 août 2019

pour le Doyen
de la Faculté de biologie et de médecine

Prof. Philippe Christe

Acknowledgement

Because a good research is never the work of a single person but of a team for scientific advices and moral support, I cannot thank enough my colleagues, friends and family.

I would like to express my gratitude to my research supervisor Dr. Christiane Nawrath for her guidance, her encouragements and her support.

For their helpful discussions and insistence to put priority on projects, I would like to thank my mid-thesis and thesis committee Dr Rochus Benni Franke, Dr Gwyneth Ingram, Dr Robertas Ursache and Prof. Ted Farmer.

I would also like to acknowledge Prof. Niko Geldner and his lab for welcoming me in their lab meeting and giving their feedback on the projects. I would like to thank also Marie Barberon for her guidance.

I wish to thank our collaborators Damien de Bellis, Prof. Moritz K. Nowack and Dr Rafael A. Buono for their contributions and Prof Mario Serrano and Martha Torres for their kindness and their guidance during our collaboration in Mexico.

I really enjoyed working in a department full of excellent scientists. A special thanks goes to Tonni Andersen, Peter Marhavy, Amélia Amiguet, Ines Barbosa, Rodrigo Siqueira Reis and Steven Moussu for their technical advices and scientific support.

I want to acknowledge for moral support and useful discussions Carolina Elejalde Palmett as my only lab member during the three first years of my PhD. But also Nasim Farahani Zayas and Aurore Guerault for the fresh atmosphere they brought to the lab since their arrival.

I wish to acknowledge in general all the DBMV colleagues for creating a nice ambiance for the successful completion of my thesis work.

Last but not least, I would like to thank Dario Guarino, my partner, for his vital support during good and bad times even with the distance, Michèle and Thierry, my parents, for pushing me to go always further in my carrier, Nuala and Alvaro, my aunt and my uncle, for their support and assistance during my stay in Switzerland and my friends for their constant encouragement.

Table of content

Résumé vulgarisé

A l'heure où le changement climatique se fait sentir, où la population mondiale ne cesse d'augmenter et où la majorité des terres arables sont exploitées, l'agriculture va devoir se tourner de plus en plus vers des terres plus arides et moins propices à la culture. Pour cette raison, la recherche scientifique s'oriente actuellement vers une compréhension plus approfondie de la façon dont la plante s'isole de son environnement pour se protéger de la sécheresse, des substances toxiques et des pathogènes.

Depuis le début du 19ème siècle, de nombreuses recherches ont été effectuées sur la cuticule, une structure lipidique qui recouvre l'épiderme des parties aériennes de la plante. Par ses propriétés hydrophobes, elle limite la diffusion d'eau évitant ainsi à la plante des pertes d'eau par la transpiration, et elle la protège des attaques microbiennes. Parce que le rôle des racines est de puiser l'eau dans le sol, l'absence d'une cuticule couvrant la racine n'a jamais été remise en question.

Nos recherches ont conduit à la découverte d'une cuticule présente sur la coiffe, le bout de la racine. Sous forme d'une cuticule embryonnaire dès le plus jeune stade de développement de l'embryon, elle protège la racine qui sort de son environnement protecteur qu'est la graine, un moment critique pour sa survie dans de nouvelles conditions environnementales jusqu'à ce que d'autres structures soient établies. Elle est aussi présente sur les racines latérales depuis leur formation dans la racine principale et durant leur émergence. Des malformations de racines latérales émergentes lors de l'absence de cuticule mettent également en évidence les propriétés lubrifiantes essentielles de la cuticule.

La découverte d'une cuticule sur la coiffe de la racine contredit les théories fondamentales de la biologie végétale qui affirment que la cuticule est exclusivement spécifique aux parties aériennes de la plante. De plus, elle ajoute un nouvel élément dans la compréhension de l'anatomie, du développement, de la physiologie racinaire et plus particulièrement de la manière dont la plante réagit de façon contrôlée avec son environnement.

Thesis abstract

During land colonization, plants have developed extracellular semi-permeable diffusion barriers to isolate themselves from the environment. Mainly made of polyesters, they prevent the loss of water and nutrients, and protect the plant against biotic and abiotic stresses. In the shoot, the cuticle is a cell wall structure covering the surface of epidermal cells of various organs. In the root, the so far identified diffusion barriers are cell wall modifications of the endodermis forming the Casparian strip and the suberin lamellæ, and cell wall modifications of the phellem forming suberin lamellae at the periderm. In addition, the presence of diffuse suberin in epidermal cells has also been hypothesised. The main constituents of the cuticle and suberin lamellae are respectively cutin and suberin, both aliphatic polyesters.

In this thesis, we discovered that the outer root cap cell layer of young primary roots and lateral roots of *Arabidopsis thaliana* forms also a cuticle-like structure. This root cap cuticle (RCC) is lost together with the first root cap cell layer when the replacement cycles of the outer root cap cells begin at 5 days after germination. Evidence for the presence of a RCC was strengthened by its removal by cutinases, staining with lipid dyes, as well modifications in structure and properties in mutants of several root cap expressed cutin biosynthesis genes. The cutin of the root tip of 2-day-old seedlings is rich in C18:2 dicarboxylic acid, which is the main monomer of the *Arabidopsis* leaf cuticle, but contains also numerous atypical components, including polyunsaturated fatty acids. The RCC of young primary and emerging lateral roots delays the diffusion of molecules into the root tip and protects the root meristem. In consequence, the RCC helps seedlings to establish under different stress conditions. Moreover, the RCC could facilitate the lateral root emergence process by reducing organ adhesion since RCC mutants show organ deformations and delay in lateral root emergence.

In parallel, we have investigated suberin formation in the endodermis in order to find new genes involved in its formation. Up to now, polyester biosynthetic genes have been classified into cutin- and suberin-specific genes. However, we have identified *GPAT4* and *GPAT8,* two cutin biosynthetic genes, as being involved in suberin formation in the roots. By showing that a same gene can be involved in suberin and in cutin formation, we are breaking down

the theory of two independent pathways and going further in the proposal of Fich and its collaboraters suggesting that suberin and cutin are only one polymer which can be deposited in the inner or the outer side of the cell wall.

We have also shown that *GPAT2* and *GPAT3*, two non-characterized genes, are present at the surface of the roots and may contribute together to the formation of an uncharacterized type of polyester impregnating the cell wall. Preliminary results suggest that they also have a role in the interaction with microbes.

To summarize, we discovered a new cuticle deposition at root cap cell, we showed that cutin and suberin pathway are sharing common genes and we identified two genes that could be involved in the formation of an uncharacterized polyester at the surface of the roots. Those discoveries increase the global understanding of root anatomy, development and physiology.

Résumé de la thèse

Au cours de l'évolution d'un milieu aquatique à un milieu terrestre, les plantes ont développé des barrières de diffusion extracellulaires semi-perméables pour s'isoler de leur environnement. Composées principalement de polyesters, celles-ci empêchent les pertes d'eau et de nutriments, et protègent la plante contre des stress biotiques et abiotiques. Dans les parties aériennes de la plante, la cuticule, structure de la paroi cellulaire, couvre la surface des cellules épidermiques de différents organes. Dans les racines, les barrières de diffusion, identifiées jusqu'à présent, sont des modifications de la paroi cellulaire de l'endoderme pour former le cadre de Caspary et des lamelles de subérine, et de la paroi du périderme formant des lamelles de subérine du phellem. De plus, une hypothèse de la présence de subérine diffuse dans les cellules de l'épiderme a aussi été avancée. Les principaux constituants de la cuticule et des lamelles de subérine sont respectivement la cutine et la subérine, tous deux des polyesters aliphatiques.

Durant ma thèse, j'ai découvert que la couche cellulaire externe de la coiffe des jeunes racines primaires et des racines latérales de *Arabidopsis thaliana* forme aussi une structure de type cuticule. Cette cuticule de la coiffe de la racine (RCC) est perdue en même temps que la première couche cellulaire de la coiffe, quand les cycles de remplacement des cellules commencent à 6 jours après germination. La preuve de la présence de cette RCC est renforcée par son ablation par l'application de cutinases et par sa coloration avec des colorants spécifiques aux lipides. De plus, des modifications de sa structure et de ses propriétés ont été observées dans des mutants de plusieurs gènes impliqués dans la voie métabolique de la formation de la cuticule et montrant une expression génique à la coiffe. La cutine de la pointe racinaire de plantules âgées de 2 jours est riche en acide dicarboxylique C18:2, qui est le principal monomère de la cuticule de la feuille d'*Arabidopsis,* mais contient aussi plusieurs composants inhabituels, incluant des acides gras polyinsaturés. La RCC des jeunes racines primaires et latérales retarde la diffusion de molécules toxiques dans la pointe de la racine et protège le méristème racinaire. En conséquence, la RCC aide les plantules à s'établir sous différentes conditions de stress. De plus, la RCC facilite le processus d'émergence des racines latérales par la réduction de l'adhésion des organes entre eux, vu que les mutants de la cuticule présentent des déformations des organes et un retard dans l'émergence des racines.

En parallèle, nous avons investigué la formation de la subérine dans l'endoderme racinaire afin de trouver de nouveaux gènes impliqués dans sa formation. Jusqu'à présent, les gènes impliqués dans la voie métabolique de formation des polyesters ont été classifiés en deux catégories : les gènes spécifiques pour la cutine et ceux spécifiques pour la subérine. Cependant, nous avons identifié *GPAT4* et *GPAT8,* deux gènes impliqués dans la formation de la cutine dans les parties aériennes de la plante, comme étant aussi impliqués dans la formation de la subérine dans la racine. En montrant qu'un même gène peut être impliqué dans la formation de la cutine et de la subérine, nous remettons en question la théorie suggérant la présence de deux voies métaboliques indépendantes et nous approfondissons la théorie de Fich et ses collaborateurs suggérant que la subérine et la cutine sont un seul et unique polymère qui peut être déposé à l'intérieur ou à la surface de la paroi cellulaire.

Nous avons aussi montré que *GPAT2* et *GPAT3*, deux gènes encore non caractérisés, sont présents à la surface de la racine et peuvent contribuer ensemble à la formation d'un type de polyester encore inconnu imprégnant la paroi cellulaire. Les résultats préliminaires suggèrent qu'ils pourraient jouer un rôle dans l'interaction avec les microbes.

En résumé, nous avons découvert une nouvelle cuticule couvrant les cellules de la coiffe, nous avons montré que la cutine et la subérine pourrait être avoir besoin de gènes identiques pour leur formation et nous avons identifié deux gènes qui pourraient être impliqués dans la formation d'un polyester encore non caractérisé à la surface de la racine. Ces découvertes élargissent la connaissance générale de l'anatomie, du développement et de la physiologie racinaires.

Frequently used abbreviations

ABCG	ATP-binding cassette transporters sub-family G
AFST	Aliphatic suberin feruloyl-transferase
BDG	Bodyguard
CUS	Cutin synthase
CYP	Cytochrome P450 oxidase
DCA	α,ω-dicarboxylic acid
DCF	Deficient in cutin ferulate
DCR	Defective in cuticular ridges
EH	Epoxy hydrolase
ER	Endoplasmic reticulum
F5H	Ferulic acid 5-hydrolase
FA	Fatty acid
FAE	Fatty acid elongase complex
FAR	Fatty acyl-CoA reductase
FDA	Fluorescein diacetate
FY	Fluorol Yellow
GC-MS	Gas chromatography-mass spectrometry
GDSL	Glycine-aspartic acid-serine-leucine motif
GPAT	Glycerol-3-phosphate acyltransferase
KCS	3-ketoacyl CoA synthase
LACS	Long chain acyl-CoA synthase
LPA	Lysophosphatidic acid
LTP	Lipid transfer protein
MAG	Monoacylglycerol
PI	Propidium Iodide
RCC	Root cap cuticle
SEM	Scanning electron microscopy
TEM	Transmission electron microscopy
VLCFA	Very long chain fatty acid
WT	Wild type
ω-OH FA	ω-hydroxy fatty acids
9,10,18-trihydroxy C18:1 FA	9,10,18-trihydroxy octadecenoic acid
C18:2 DCA	α,ω-octadecadiendioc acid

List of figures and tables

1. Introduction

1.1. Plant diffusion barriers

480 million years ago, land plants evolved from simple Charophycean freshwater green algae to a more morphologically complex organism with elaborate organs and a two-phase life cycle (Kenrick and Crane, 1997; Richard M. Bateman et al., 1998; Bowman, 2013). Facing new growth conditions like rapid oscillations of humidity and temperature, direct exposure to light, biochemical and mechanical stresses due to the absence of water immersion, plants developed hydrophobic extracellular biopolymers: cutin, suberin and lignin. Those polymer depositions isolate the plants from the surrounding terrestrial environment. By forming semi-permeable diffusion barriers, they restrict exchanges of water, gases and nutrients by limiting permeability, but they also protect the plant against biotic and abiotic stresses (Kolattukudy, 2001). Three diffusion barriers have been identified until now: the Casparian strip, the cuticle and the suberin lamellae. They are respectively made of lignin, cutin and suberin. A fourth additional hypothetical diffusion barrier known as diffuse suberin is covering the surface of the roots (Thomas et al., 2007; Nawrath et al., 2013). The existence of a common precursor to lignin, cutin and suberin in *Physcomitrella patens* mosses was hypothesized by Renault et al. (2017).

1.1.1. Casparian strip

In contrast to aerial organs, roots have unprotected surface that serves for absorbance. The first polymer deposition in inner root layers is the Casparian strip which is a ring surrounding the endodermal cell. Thought for a long time of being made of suberin, the Casparian strip is in fact made of lignin (Naseer et al., 2012). It acts like an apoplastic barrier between the absorbent epidermis and the long distant transporter that is the vascular tissue (Barbosa et al., 2019). From the surface of the root to the central cylinder, solutes can travel through the apoplast, which is called the Apoplastic pathway, from cell to cell via plasmodesmata, the Symplastic pathway, or via membrane-located transport molecules taking solutes from the apoplast to the cytoplasm and the opposite, the Coupled Trans-cellular pathway. The Casparian strip forces solutes to leave the Apoplastic pathway to travel via Symplastic

pathway or Coupled Trans-cellular pathway, in order to reach the central cylinder (Figure 1) (Andersen et al., 2015; Barberon, 2017).

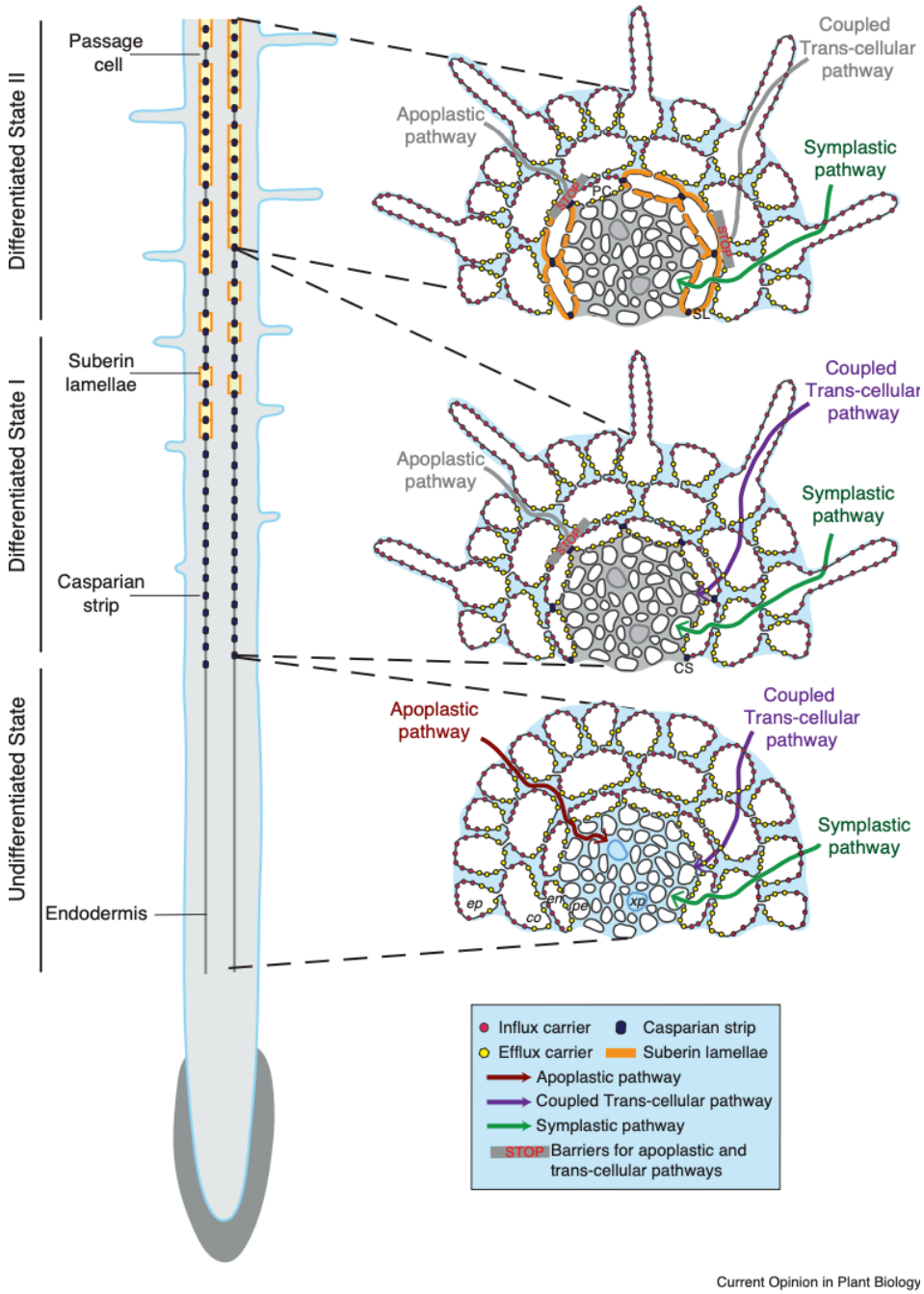

Figure 1: Schematic diagram highlighting the differentiation of the endodermis and the transport of the nutrients and water from the rhizosphere to the vascular tissue from Andersen et al. (2015). The color code is mentioned in the figure.

1.1.2. Cuticle

Cuticle is a hydrophobic layer covering the outer side of the epidermal cell wall of aerial plant organs such as fruits, leaves, primary stems, and flowers (Pollard et al., 2008). Moreover, recently, it has been shown that cuticle can be synthesized *de novo* on newly

exposed residuum cells, after the loss of sepals or petals in abscission zone (Lee et al., 2018). The cuticle is mainly made of a covalently linked cutin matrix. It is subdivided in three layers. Starting from the cell wall side, first, the cuticular layer forms a continuum with the cell wall and is rich in polysaccharides. Then, the hydrophobic cuticle proper, made of cutin embedded with intracuticular waxes, overlays the cuticular layer. In the latter, the epicuticular waxes cover the surface of the cuticle proper as crystals or as amorphous film.

Cuticle composition

Cutin is a structural polyester made up predominantly of aliphatic C16 and C18 oxygenated fatty acids, such as terminal hydroxy (ω-OH FA), mid-chain hydroxy and epoxy acids. Minor compounds are also found such as α,ω-dicarboxylic acids (DCA), glycerol and aromatic compounds like ferulic acid and coumaric acid (Nawrath et al., 2013; Fich et al., 2016; Yang et al., 2016; Bakan and Marion, 2017). Cutin composition differs strongly depending of the species, organs and developmental stages inducing a change in the ultrastructure appearance (Holloway, 1982). In *Arabidopsis thaliana*, flower cutin is rich in 10,16-dihydroxy C16:0 FA, a polyhydroxy acid which is a typical cutin monomer in other species, while stem and leaf cutin is particularly rich in DCAs, mainly C18:2 DCA, and more similar to suberin (Bonaventure et al., 2004; Li et al., 2007a; Li-Beisson et al., 2009; Bakan and Marion, 2017). In DCA-rich cutin, the glycerol content is twice the amount of the DCAs and stays proportional in case of reduction in DCA content (Yang et al., 2016).

Waxes typically consist of very long chain fatty acid (VLCFA) of 24 to 34 carbons, mainly free fatty acids, primary alcohols, aldehydes and alkanes together with secondary metabolites like flavonoids and terpenoids (Pollard et al., 2008; Nawrath et al., 2013).

Cutan is the non-hydrolysable fraction of the cuticle that is left after delipidation and ester bond cleavage by depolymerization. It is made of aliphatic, with C-C or C-O-C bond, and aromatic compounds as well as carbohydrates and is possibly deposed after cutin deposition and cell expansion (Nawrath, 2002; Pollard et al., 2008; Li-Beisson et al., 2016). Little is known about it.

Cuticle localization

In *Arabidopsis*, a patchy cuticle was already observed at the globular stage of the embryo development and an uninterrupted cuticle at the heart stage (Szczuka, 2003; Creff et al.,

2019). Once formed on the embryo, the cuticle continuously grows and is maintained during the entire plant development. Newly formed shoot organs are covered from the beginning by a protocuticle, assumed of a different composition than the mature cuticle (Nawrath et al., 2013). During plant development, the cuticle composition and ultrastructure change due to the environmental and developmental factors, influencing its properties as well (Fabre et al., 2016; Ingram and Nawrath, 2017). However, in case of damage the cuticle is not repaired, instead suberin is sealing the wound (Yang et al. 2012; Nawrath et al., 2013).

Visualization of the cuticle via transmission electron microscopy (TEM) reveals different ultrastructures of the cuticle in leaves, stem and petals (Figure 2). This change in ultrastructure is associated with changes in composition and the polymerization pattern (Holloway, 1982; Nawrath, 2002; Jeffree, 2006; Nawrath et al., 2013). In leaves, the cuticle is an electron dense layer of 20-25 nm. The epicuticular waxes form a thin film at its surface (Nawrath, 2002). In inflorescence stem, the cuticle is also an electron dense layer of 50-80 nm, but with crystals of epicuticular waxes. The surface of the petals and the sepals are covered by nanoridges. The ridge-shaped cuticular layer is electron dense and covered by the electron-lucent cuticular proper of 60-80 nm. The epicuticular waxes are forming a thin film at the surface. Mutant studies show that cutin is needed for nanoridges formation (Li-Beisson et al., 2009; Panikashvili et al., 2009; Mazurek et al., 2017). The formation of the nanoridges on sepals and petals progresses from the tip to the base of the organ following epidermal cell maturation (Hong et al., 2017).

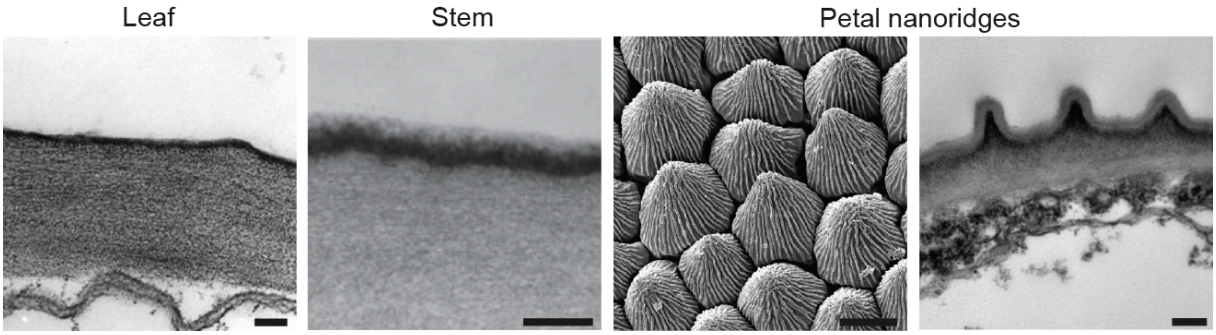

Figure 2: The diversity of the cuticle among the organs adapted from Nawrath et al. (2013). First, it is a leaf cuticle with TEM (Bessire et al., 2007), then a stem cuticle with TEM (Lü et al., 2009) and finally nanoridges of the petal with scanning electron microscopy (SEM) and with TEM (Bessire et al., 2011). Scale bars represent 200 nm for the TEM pictures and 500 nm for the SEM picture.

Cuticle function

The cuticle is a hydrophobic barrier controlling non-stomata gas, solute and water exchanges. Cuticular waxes are thought to be the key factor of the barrier, which increases its permeability by 100 to 1000-fold in case of wax removal while cutin defects have a small effect on the permeability (Isaacson et al., 2009; Schreiber, 2010). Cutin acts as a scaffold in which waxes are hold. Change in cutin amount, composition or structure can affect wax deposition and lead to a defective barrier (Isaacson et al., 2009; Fich et al., 2016). Hence, waxes have a direct function in controlling efflux while cutin has an indirect function as a matrix holding the waxes.

In addition, the cuticle has as well a mechanical barrier function protecting against pathogen attacks and irradiation damages. Several studies have highlighted the role of the cutin in the interaction with microbes (Li et al., 2007a; Isaacson et al., 2009). The most evident prove of the role of cutin during infection is a study on *Carica papaya* fruit where inhibiting the cutinase of a fungus correlated with the loss of its ability to infect (Dickman et al., 1982). However, the alteration of the cuticle can lead to higher sensibility or to the development of a resistance (Raffaele et al., 2009). For instance, a resistance to *Botrytis cinerea* was observed in some cuticle mutants (Bessire et al., 2007; Chassot et al., 2007; Voisin et al., 2009; Bessire et al., 2011). Two hypothesis could explain this resistance: first, the higher cuticle permeability increases the release of antifungal compounds at the surface of the leaf (Bessire et al., 2007); second, the monomers, normally released during the cuticle digestion by fungus cutinase and acting as a signal for appressorium formation, are not formed anymore (Francis et al., 1996; Gilbert et al., 1996). Cutin monomers act as well as a signaling molecule inducing, in fungi, germination of the spores, cutinase gene expression and appressorium formation (Kolattukudy et al., 1995; Francis et al., 1996; Gilbert et al., 1996; Wang et al., 2000).

The cuticle behaves also as lubricant on the surface of organs by keeping them separate from each other during development (Nawrath, 2002; Pollard et al., 2008). Indeed, shoot organ fusion phenotype is observed in several cuticle mutants (Lolle et al., 1998; Wellesen et al., 2001; Kurdyukov et al., 2006a; Bird et al., 2007; Li-Beisson et al., 2009; Panikashvili et al., 2009; Weng et al., 2010). Similarly, the ectopic expression of a cutinase of *Fusarium oxysporum* and of *Arabidopsis thaliana* leads to organ fusion (Sieber et al., 2000; Takahashi

et al., 2010). Organs without cuticle, such as roots, but expressing as well the cutinase do not present any developmental alterations (Sieber et al., 2000). In addition, organ fusion phenotype correlates with cuticle permeability in young organs. Several hypotheses were formulated to explain the formation of organ fusions. It could be explained by the fact that a defective cuticle could allow either inter-organ communication via molecular signals or a possible contact between cell wall homogalacturonans from different organs leading to a crosslink, both impossible in case of a proper functional cuticle (Delude et al., 2016; Ingram and Nawrath, 2017). Moreover, the presence of organ fusions in knockout mutants of genes affecting epidermal developmental suggests a possible direct link between epidermis and cutin formation (Ingram and Nawrath, 2017).

1.1.3. **Suberin lamellae**

Suberin lamellae are made from depositions of suberin, an aliphatic polyester, at the inner side of the cell well, mainly in the roots (Haas and Carothers, 1975).

Suberin lamellae composition

DCAs, glycerols and phenolics are the main components of suberin (Bakan and Marion, 2017). Suberin is mainly characterized by aliphatic compounds namely C18 DCA and ω-OH FA, primary alcohols, VLCFAs of 20 to 24 carbons, and aromatic compounds like ferulic and p-coumaric acids (Pollard et al., 2008; Kreszies et al., 2018). The aromatic and aliphatic domains are esterified to each other and to glycerol to form a polyester (Pollard et al., 2008). In *Arabidopsis thaliana*, the suberin content is very similar to other species.

Suberin-associated waxes, at the opposite of cuticular waxes, have a similar composition to suberin suggesting even a common biosynthetic pathway (Li et al., 2007b). In the periderm, waxes consist of C18-C22 alkyl esters of p-coumaric, caffeic and ferulic acids, C22-C24 monoacylglycerols, C18-C22 primary alcohols, C16-C24 FAs and sterols (Li et al., 2007b).

Suberin lamellae localization

Suberin is deposited either upon wounding and various stress or developmentally in inner tissues, like in the root endodermis (Figure 3), hypodermis, in the bundle sheaths in monocots or in outer tissues such as the phellem of the periderm of secondary roots and stems, in seed coat and in the chalazal plug of the seeds (Pollard et al., 2008; Beisson et al.,

2012). Suberin deposition in the endodermis starts in the differentiated zone by patches before reaching a continuous suberization of the endodermal layer at the exception of the passage cells (Figure 1) (Andersen et al., 2015; Barberon, 2017).

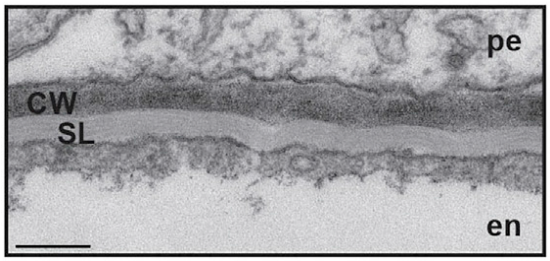

Figure 3: Endodermal suberin lamellae with TEM (Barberon et al., 2016). pe, pericycle; en, endodermal cell; CW, cell wall; SL, Suberin lamellae. The scale bar is 200 nm.

Suberin lamellae function

The impregnation of suberin gives to the endodermis a biotic and abiotic protective role, and a regulatory role for water and nutrient efflux (Barberon et al., 2016). Indeed, similarly to the Casparian strip, suberin deposition is expected to have a role in the uptake regulation of solutes and water and in limiting their lost. While the transport of water and solutes in roots can follow the Apoplastic, Symplastic or Coupled-Trans-cellular pathway, once they reach the endodermis, the suberization of the inner side of the cell wall blocks the coupled-trans-cellular pathway (Figure 1) (Andersen et al., 2015; Barberon, 2017). Nutrient status, through hormonal signals, can modulate suberization of the roots and by consequence nutrient uptake (Barberon et al., 2016). Indeed, enhanced suberization is controlled by salt treatment or potassium and sulfur deficiency through the ABA signaling pathway, while reduction of suberization is associated with iron, manganese and zinc deficiency through ethylene (Barberon et al., 2016).

The suberized endodermis also acts as a cell wall strengthener and as a physical barrier for biotic attack or abiotic damages, in order to protect against opportunist pathogen invasion (Ranathunge et al., 2008). Its induction upon wounding in the shoot illustrates clearly this function.

During the secondary growth of the root, suberin lamellae are present in the phellem layer of the periderm, which mainly has a role in mechanical support, protection against pathogen and limit water and nutrient fluxes.

1.1.4. Diffuse suberin

The presence of diffuse suberin at the epidermal cell walls of *Arabidopsis thaliana* has also been hypothesized based on the identification of suberin deposition at the surface of *Glycine max* (Thomas et al., 2007; Nawrath et al., 2013) and on the observation of epidermal cell auto-fluorescence in *Arabidopsis* roots (Franke et al., 2005). It could have a role in pathogen protection (Thomas et al., 2007; Ranathunge et al., 2008).

1.2. Cutin and suberin pathway

Precusors biosynthesis

Polyesters are constituted of fatty acids that are formed in the plastid and transported to the surface of the endoplasmic reticulum where they undergo different modifications such as acyl-activation, oxidation and esterification (Figure 4).

Initially, fatty acids are activated by a long chain acyl-CoA synthase (LACS family) into an acyl-CoA. The LACS family contains 9 members but only LACS1, LACS2 and LACS4 have been associated with cutin formation (Schnurr et al., 2004; Bessire et al., 2007; Lü et al., 2009; Zhao et al., 2019), LACS2 potential as well with suberin formation (Li-Beisson et al. ,2010).

Before the oxidation, monomers may undergo an elongation step catalyzed by 3-ketoacyl CoA synthase (KCS) in the fatty acid elongase complex (FAE complex). The FAE complex consists of a four step process catalyzes by *β*-ketoacyl-CoA synthase (KCS), *β*-ketoacyl-CoA, reductase, *β*-hydroxyacyl-CoA dehydratase and enoyl-CoA reductase and results in the addition of two carbons to the chain. Proteins such as KCS2/DAISY and KCS20 have been identified to elongate suberin monomers (Franke et al., 2009; Lee et al., 2009b; Kim et al., 2013; Vishwanath et al., 2015).

Sequentially, cutin and suberin monomers are oxidized by cytochrome P450 oxidases (CYP family) such as CYP77s and CYP86s. CYP86A2/ATT1, CYP86A4, CYP86A7 and CYP86A8/LCR hydrolyze the terminal position of cutin precursors (Wellesen et al., 2001; Xiao et al., 2004; Duan and Schuler, 2005; Li-Beisson et al., 2009), while CYP86A1/HORST and CYP86B1/RALPH are their homolog for suberin precursors (Höfer et al., 2008; Compagnon et al., 2009). CYP77A6 is a mid-chain hydrolase for cutin (Li-Beisson et al., 2009). CYP77A4 is able to add an epoxy group to FAs *in vitro*, but *in vivo* studies still have to be conducted (Sauveplane et

al., 2009). CYP86A2 and HTH are adding a second carboxyl group to form DCAs in cutin and CYP86B1/RALPH in suberin (Kurdyukov et al., 2006b; Compagnon et al., 2009; Molina et al., 2009).

Finally, they are esterified to a glycerol by a glycerol-3-phosphate acyltransferase (GPAT family) (Li-Beisson et al., 2016). In cutin, GPAT4, GPAT6 and GPAT8 with their two catalytic sites, acyltransferase and phosphatase, generate monoacylglycerols while in suberin GPAT5 and GPAT7 with a unique acyltransferase site generate lysophosphatidic acids (Yang et al., 2010).

In parallel, characteristic for suberin, the formation of primary fatty alcohols is based on the reduction of activated fatty acids catalyzed by fatty acyl-CoA reductases (FAR) with each for their own carbon length specificity: FAR1, FAR4 and FAR5 (Domergue et al., 2010; Li-Beisson et al., 2016).

In the cytosol, before being exported, precursors can be modified by the members of the BEAT AHCT HCBT1 DAT (BAHD) acyltransferase family. DEFICIENT IN CUTIN FERULATE (DCF) and ALIPHATIC SUBERIN FERULOYL-TRANSFERASE (ASFT/HHT) transfer ferulate-CoA to respectively ω-hydroxy fatty acids in cutin and ω-hydroxy fatty acids and fatty alcohols in suberin (Gou et al., 2009; Molina et al., 2009; Rautengarten et al., 2012). In cutin, epoxy group can be hydrolyzed by EPOXY HYDROLAYSE 1 (EH1) generating two vicinal hydroxyl groups (Pineau et al., 2017). DEFECTIVE IN CUTICULAR RIDGES (DCR) is a diacylglycerol transferase with a function currently under debate. A hypothesis is that DCR catalyzes the transfer of an acyl-CoA to the free OH group of a diacylglycerol in order to form a triacylglycerol (Rani et al., 2010; Molina and Kosma, 2015; Mazurek et al., 2017).

Precursor transport

Afterwards, precursors are hypothesized to be transported across the plasma membrane via ATP-binding cassette (ABC) transporters (Pollard et al., 2008; Fabre et al., 2016). ABCG11, ABCG13 and ABCG32 have been identified as cutin precursor transporter, ABCG2, ABCG6, and ABCG20 as suberin precursor transporter (Panikashvili et al., 2007; Bessire et al., 2011; Panikashvili et al., 2011; Yadav et al., 2014). It is not clear yet if precursors are only exported as such or if they can also form larger oligomers before being exported. Monoacylglycerols are polymerized in the apoplastic compartment suggesting extracellular polymerization and

transport of monoacylglycerols as such (Yeats et al., 2012; Yeats et al., 2014, Bakan and Marion, 2017). However, this does not exclude the export of larger oligomers through a different transport such as cytoplasmic carrier protein, Golgi-mediated vesicles or oleophilic droplets (Pollard et al., 2008).

After the transport to the apoplast, cutin precursors still need to be carried out through the cell wall to the cuticle layer where they are then polymerized; the involvement of lipid transfer proteins (LTP) in this transport has been hypothesized (Kader, 1996). First, LTPg anchored in the plasma membrane could take in charge the cutin precursors from the ABC transporters. Then another LTP could facilitate the transport or the diffusion through the cell wall (Salminen et al., 2018). LTPg1 and LTPg2 are potential candidates for cutin monomer transport (Salminen et al., 2018). LTPg4 and LTPg6 were suggested for suberin transport through the apoplast (Edstam and Edqvist, 2014; Vishwanath et al., 2015).

Polymerization of the precursors

Cutin precursors are polymerized at the outer cell wall by the Glycine-aspartic acid-serine-leucine motif (GDSL) lipase/hydrolases called cutin synthases (CUS). CUS1 and CUS2 cutin polymerization activity was confirmed (Yeats et al., 2012; Yeats et al., 2014; Hong et al., 2017). Member of the α/β-hydrolase BODYGUARD (BDG) family with BDG3, BDG1 could also have a role in cutin polymerization, although its function is unknown (Kurdyukov et al., 2006a; Shi et al., 2011; Fich et al., 2016). Suberin precursors are polymerized at the inner side of the cell wall. However, no synthases have been identified so far, but the members of the CUS family are possible candidates (Li-Beisson et al., 2016).

Another hypothesis for polymerization is the existence of an autocatalytic-polymerization via the so-called cutinsome. A cutinsome is a “building unit of plant cutin produced by self-assembly of cutin monomers in a polar environment where they spontaneously polymerized” said Domínguez et al. (2015). While researches usually consider that precursor transport through plasma membrane and cell wall happens via transporters or lipid transfer proteins, a recent hypothesis suggests that cutinsomes could also transport cutin precursors and even enzymes from the cytoplasm to the outer site of the cell wall (Stępiński et al., 2016).

Regulation of the biosynthesis of cutin and suberin

SHN1/WIN1, SHN2 and SHN3 transcription factors are positive regulators of cutin and possibly suberin biosynthetic genes (Aharoni et al., 2004; Kannangara et al., 2007; Shi et al., 2011). MYB106 transcription factor, regulating SHN1, together with MYB16 control cutin formation and epidermis identity, with a positive feedback as well as ANL2 (ANTHOCYANINLESS 2) and HDG1 (HOMEODOMAINGLABROUS 1) transcription factors (Oshima et al., 2013; Fich et al., 2016). HDG1 depends on the CFL1 (CURLY FLAG LEAF 1) negative regulator of cuticle development (Fich et al., 2016). NFXL2 (NFX1-LIKE2), a repressor of abiotic stress response, increases the expression of *SHN1* to *3* and *BDG* (Fich et al., 2016). MYB9, MYB41 and MYB107 are transcription factors controlling suberin deposition (Kosma et al., 2014; Lashbrooke et al., 2016).

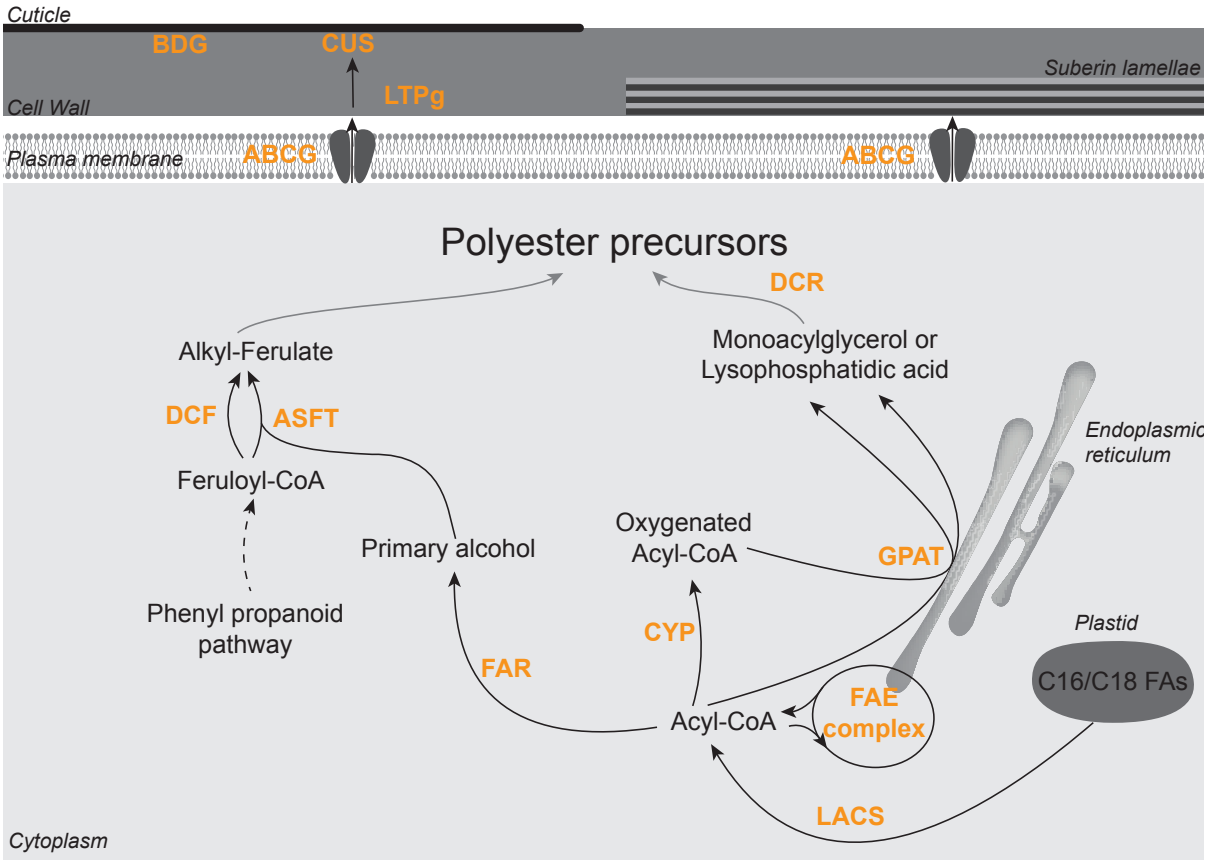

Figure 4: Schematic representation of cutin and suberin biosynthetic pathway. DCF, Deficient in Cutin Ferulate; ASFT, Aliphatic Suberin Feruloyl-Transferase; FAR, Fatty Acyl-CoA Reductase; DCR, Defective in Cuticular Ridges; FAE complex, Fatty Acid Elongase complex; CYP, Cytochrome P450 Oxidase; GPAT, Glycerol-3-Phospate Acyltransferase; LACS, Long Chain Acyl-CoA Synthase; ABCG, ATP-binding Cassette Transporter; LTPg, Lipid Transfer Protein; CUS, Cutin Synthase; BDG, Bodyguard; curvy black arrow, chemical reaction; straight black arrow, transport; grey arrow, affiliation to the polyester precursor pool; orange, name of enzyme; orange ?, enzyme with a unknown function; grey ?, questioning the affiliation of that component to the precursor pool. For details about the cutin and suberin biosynthetic pathway see Section 1.2. Created with biorender.com.

1.3. Plant architecture

Derived from their ancestors growing in water, the first land plants had rhizoids, a structure similar to root hairs, allowing nutrient uptake and attachment the ground (Motte and Beeckman, 2018). With time, the root system evolved and acquired a branched architecture that allowed stronger anchoring in the soil, leading to the possibility of developing bigger size and better acquisition of nutrients and water, while providing a barrier against biotic and abiotic stresses (Motte and Beeckman, 2018).

1.3.1. Plant primary growth

Starting from the seed, the plant develops based on the shoot and root apical meristems, which are formed during embryogenesis.

In dicots, the shoot apical meristem is localized between the two cotyledons and is activated upon germination inducing the production of leaves. Following environmental stimulus, the shoot apical meristem transitions from a vegetative stage to a reproductive stage starting to produce inflorescence meristem (Barton, 2010).

Primary root growth happens at the apical root meristem: in the middle of this meristem, the quiescent center keeps the initials around undifferentiated (Figure 5) (Benfey and Scheres, 2000). At first, the epidermis/lateral root cell initials, by anticlinal division, generate each an epidermal daughter cell and secondly, by periclinal division, they produce a lateral root cap daughter cell. The four columella initials generate the columella cells towards the tip of the root. The endodermis/cortex initials divide first anticlinally generating each a daughter cell that directly goes through a periclinal division to produce a cortical and an epidermal cell (Augstein and Carlsbecker, 2018).

The root is made of several tissues, radially from the outside: first the epidermis, then the cortex, endodermis and the vascular tissue, in the middle. The epidermis is the outer cell layer divided in two types of cells: root hair and non-root hair cells. Due to its direct contact with the environment, the epidermis has an important role in solute and water uptake; the root hairs increase the absorption surface. The cortex is made of only one cell layer in *Arabidopsis,* but it can go up to 10 in certain rice varieties (Di Ruocco et al., 2018). It has a polysaccharide and oil storage function (Augstein and Carlsbecker, 2018). The endodermis

acts as a filter controlling the flux of water and solutes. The vascular tissue includes the pericycle cells, the xylem and the phloem. The pericycle has a function in periderm and lateral root formation. The xylem transports minerals and water from the root to the shoot, while the phloem carries products of the photosynthesis in the opposite direction.

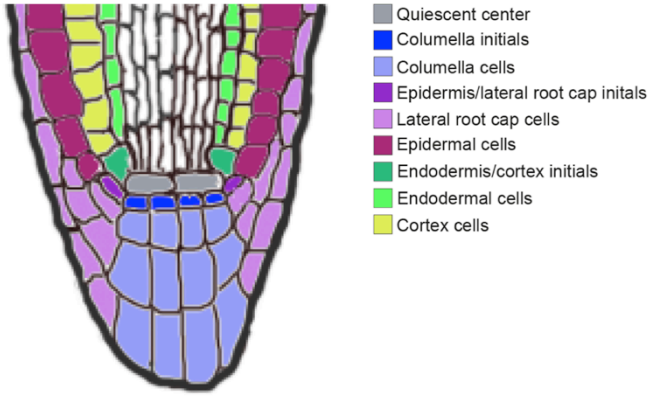

Figure 5: A schematic representation of the root meristem of *Arabidopsis thaliana.* Grey, quiescent center; dark blue, the columella initials; light blue, columella cells; purple, epidermis/lateral root cap initials; pink, lateral root cap cells; dark red, epidermal cells; dark green, endodermis/cortex initials; light green, endodermal cells; yellow, cortex cells.

While the primary root is formed during embryogenesis, lateral roots are established post-embryogenesis and they determine the global root architecture (MacGregor et al., 2008). In *Arabidopsis thaliana*, the auxin released by the dying lateral root cap towards the surrounding cells induces an auxin oscillation that will establish the lateral root position pattern (Xuan et al., 2016). The first step of the lateral root formation is the asymmetric anticlinal division of a pericycle cell facing the xylem pole (Figure 6). To cross the endodermis, triggered by an accumulation of auxin, the endodermal cell above the lateral root primordium gets thinner and the Casparian strip is locally degraded to allow the primordium to pass. The cortical and epidermal cells are pushed apart by the primordium and the middle lamella is enzymatically digested to allow the passage of the primordium. Coordination and intercellular communication of this full process is tightly controlled by auxin efflux (Vilches-Barro and Maizel, 2015; Stoeckle et al., 2018).

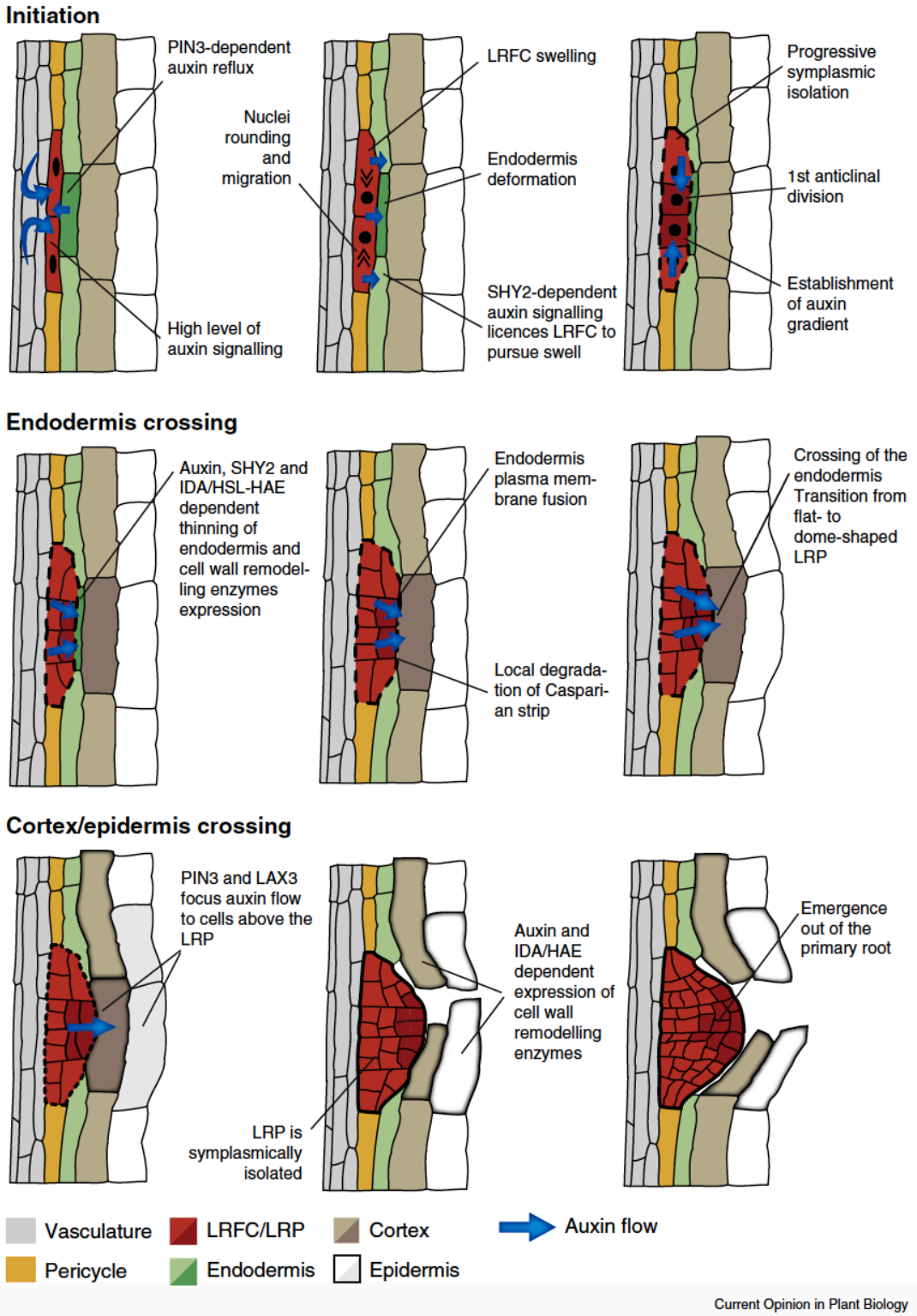

Figure 6: Steps of lateral root formation in *Arabidopsis thaliana* with a detailed explanation of the main events from Vilches-Barro and Maizel (2015). Grey, vascular tissue; yellow, pericycle; red, lateral root founder cells/lateral root primordium; green, endodermis; brown, cortex; white, epidermis; blue arrow, auxin flow. Darker shade illustrates the accumulation of auxin signaling.

1.3.2. Plant secondary growth

The plant secondary growth is needed for long distance transport of water and nutrients, protection against pathogen and for mechanical support (Groh et al., 2002; Lendzian, 2006; Blackmore, 2018). This stage is characterized by the development of the periderm which is made of three cells types: the phellogen producing towards the inside the phelloderm and towards the outside the phellem (Wunderling et al., 2018). The phellem cells are impregnated with suberin and lignin. In *Arabidopsis thaliana*, the periderm is present on the roots and on the hypocotyl. In roots, the periderm develops from the pericycle cells in the central cylinder. To have the periderm as outer layer, the epidermal and the cortex cells break while the endodermal cells undergo programmed cell death (Wunderling et al., 2018). Since phellem cells are continually produced from the inside, the outer layer constantly peels off (Wunderling et al., 2018).

1.4. Thesis layout

The main goal of this thesis is to characterize atypical polyesters with a focus on the *Arabidopsis* roots. At first, the expression pattern of the members of the *GPAT* family is used as a marker to monitor polyester depositions (Chapter 2). Afterwards, our projects focus on the characterization of the role and the nature of the polyester deposition in atypical locations of the root as suggested by the expression pattern of the *GPAT* family. We identified an unexpected cutin deposition at the root cap of primary and lateral roots (Chapter 3). We started to investigate the role of cutin-biosynthetic genes in suberin formation at the endodermis (Chapter 4) and to characterize the function of *GPAT2* and *GPAT3* and their possible role in the formation of an elusive polyester at the surface of the roots (Chapter 5). Lastly, we began to explore the possible function of those three polyesters in the interaction with microbes (Chapter 6).

2. *GPAT* family as a tool to study polyester deposition in *Arabidopsis thaliana*

2.1. Introduction

Plant glycerol-3-phosphate acyltransferase (GPAT) catalyzes the transfer of a fatty acid from an acyl donor to a glycerol-3-phosphate to form lysophosphatidic acid (LPA). LPAs are precursors of multiple glycerolipids such as extracellular polyester, storage or membrane lipids, depending of their subcellular localization.

In *Arabidopsis thaliana*, the GPAT family consists of ten members, ATS1, GPAT1, GPAT2, GPAT3, GPAT4, GPAT5, GPAT6, GPAT7, GPAT8 and GPAT9, and are located in three different sites: in the stoma of chloroplast, bound to the endoplasmic reticulum membrane (ER) or bound to the mitochondrial membrane. ATS1 is the only member of the family located in the chloroplast (Murata and Tasaka, 1997). GPAT1 mitochondria localization was confirmed through a pea mitochondria import assay, excluding at the same time a possible mitochondrial localization of GPAT2 (Zheng et al., 2003). *In vivo* assays in tobacco cells revealed that GPAT8 and GPAT9 are located at the ER with the active acyltransferase domain at C-terminus in the cytosol (Gidda et al., 2009). Their ER-specific retrieval motif was identified at the end of the C-terminus. Based on sequence homology, GPAT2 to GPAT7 have been hypothesised to have an ER retrieval motif, while GPAT1 presents a N-terminal mitochondrial signal peptide (Gidda et al., 2009). However, there are papers that still claim that GPAT2 and GPAT3 are mitochondial localized due to their similarity to GPAT1 (Beisson et al., 2007; Chen et al., 2011a; Chen et al., 2014; Sui et al., 2017; Jayawardhane et al., 2018; Waschburger et al., 2018).

Plant fatty acids, such as C16 and C18, are synthesized in the chloroplast stroma as acyl-carrier-protein-bound form. They can be hydrolyzed to free fatty acids, esterified to coenzyme A, transported to the cytoplasm and later be esterified to glycerol-3-phosphate. Or they can directly esterify to glycerol-3-phosphate to generate LPA, staying in the chloroplast. ATS1 is the only GPAT using acyl-carrier-protein as acyl donor. LPA produced in the chloroplast can directly be used for phosphatidylglycerol synthesis (Murata and Tasaka, 1997; Li-Beisson et al., 2010). The other GPATs use Acyl-CoA as acyl donor in the cytoplasm.

ATS1 and GPAT9 are sn-1 acyltransferase involved in plant storage and membrane lipids (Chen et al., 2011a; Shockey et al., 2015; Waschburger et al., 2018). GPAT1 to GPAT8 are all sn-2 enzymes with a function in extracellular lipids for GPAT4 to GPAT8 and an unclear function for GPAT1 to GPAT3 (Yang et al., 2012). GPAT1 to GPAT8 protein sequences present two trans-membrane domains and four acyltransferase domains with several conserved catalytic sites, which are located after the second trans-membrane domains in the highly conserved C-terminus (Zheng et al., 2003; Beisson et al., 2007; Gidda et al., 2009). The N-terminus is the main source of sequence divergence between the members of the family. GPAT9, the shortest of all GPATs, has three predicted trans-membrane domains in addition to the conserved acyltransferase domains.

Glycerol-3-phosphate acyltransferase activity was confirmed *in vitro* for GPAT1 to GPAT8, at the exception of GPAT2 and GPAT3 for which no activity in yeast and germ wheat with unmodified or ω-oxidized acyl-CoA could be detected (Zheng et al., 2003; Yang et al., 2012).

Phylogenic analyses of *GPAT* family reveal that *GPAT9* is closer to mammalian *GPAT3* and *GPAT4* than to the other *GPATs* suggesting that *GPAT9* branch split from the *GPAT* family before plant and mammals did (Gidda et al., 2009, Waschburger et al., 2018). *GPAT* algae homologs are similar only to *GPAT9* and *ATS1* suggesting that they are more ancient. The sn-2 *GPATs* have appeared in mosses, where homologs could be identified, and have evolved with terrestrial colonization synchronized with adaptation to the new environment, leading to the nickname "Land-plant-specific *GPATs*" (Yang et al., 2010; Yang et al., 2012; Waschburger et al., 2018). In most of the land plants, only one homolog exists for *GPAT4* and *GPAT8* together as well as for *GPAT5* and *GPAT7* implying a lineage specific divergence by duplication event in only a few species like *Arabidopsis thaliana*. *GPAT6* from all plant species is close enough to *GPAT4* and *GPAT8* clade to suggest they may have a common ancestor and have diverged. *GPAT4*, *GPAT6* and *GPAT8* are the most ancient form of land plant *GPATs* because they are similar to *GPATs* from *Physcomytrella patens* and *Sphagnum fallax*. *GPAT1, GPAT2* and *GPAT3* originate from a duplication event in the vascular plants. *GPAT3* homologs have split in two groups separating the monocots from dicots (Waschburger et al., 2018).

In *Arabidopsis thaliana*, land-plant-specific *GPAT*s are coupled in three main groups based on their sequence homology: *GPAT1*, *GPAT2* and *GPAT3* together, *GPAT4*, *GPAT6* and *GPAT8*, *GPAT5* and *GPAT7* (Figure 7).

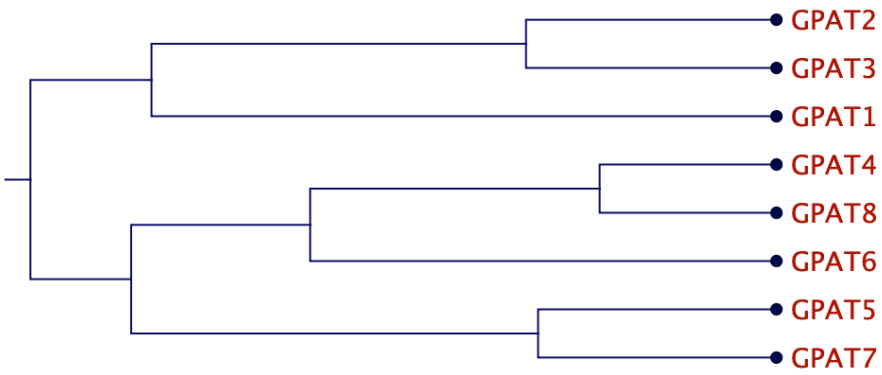

Figure 7: Overview of the phylogenetic relationships between the land plant *GPATs* at the gene level. The tree was constructed with the Unweight Pair Group Method with Arithmetic mean on CLC software (Qiagen) with a bootstrap value of 1000 replicates.

The existence of an 11th *GPAT* has been reported recently with more than 75% similarity to *GPAT5* and *GPAT7*. It is At3G11325 currently annotated as a phospholipid/glycerol acyltransferase (Waschburger et al., 2018)

For our researches, we have decided to focus on ER-localized sn-2 glycerol-3-phosphate acyltransferase family excluding *ATS1, GPAT1* and *GPAT9* because they are involved in the formation of storage or membrane lipids. An overview of the current knowledge on *GPAT2* to *GPAT8* is presented here.

2.1.1. *GPAT2* and *GPAT3* have unknown function

Little is known about the functions of *GPAT2* and *GPAT3*. Even if their structural modeling and similarity of sequence to other *GPAT*s suggests an sn-2 acyltransferase activity; no activity could be revealed when ω-oxidized or unmodified substrates were used (Yang et al., 2012). Biochemical analyses of single knockout mutants were not conclusive: *gpat2* showed no polyester precursor changes in flowers, seeds and leaves; neither *gpat3* in roots, leaves and flowers (Yang et al., 2012). Following RNA based studies from Beisson et al. (2007), *GPAT2* and *GPAT3* show overlapping expression in several tissues: flowers, seeds, roots, leaves and stems.

GPAT2 and *GPAT3* have a higher sequence similarity to the sn-2 *GPATs* rather than to *GPAT9* making them potential candidates for being involved in polyester formation.

2.1.2. *GPAT4, GPAT6* and *GPAT8* are implicated in cutin formation

For this subgroup, *in vitro* studies have revealed bifunctionality of the GPAT4, GPAT6 and GPAT8 enzymes having both a sn-2 acyltransferase and a phosphatase activity (Yang et al., 2012).

The redundant function of *GPAT4* and *GPAT8* was established based on the observation that a *gpat4 gpat8* double mutant contains a strongly reduced cuticle, a phenotype which could not be observed in single mutants. Together with overexpression studies, this provides direct evidence that GPATs catalyze a limiting step of accumulation of cutin (Li et al., 2007a; Li-Beisson et al., 2009). *GPAT4* and *GPAT8* are needed for the specific formation of C16 and C18 DCAs and ω-OH FA (mainly C16:0 DCA and C18:2 DCA) in stem and leaves fitting with *GPAT4* expression in their epidermis (Li et al., 2007a; Yang et al., 2012). Indeed, in *gpat4 gpat8* leaves, the absence of cuticle and the missing cuticular ledge forming the stomatal pore led to a higher permeability and sensitivity to *Alternaria brassiciola* (Li et al., 2007a). *GPAT4* and *GPAT8* are also reported to have a role in nanoridges formation in flowers and in embryonic cuticle (Chen et al., 2014; Fabre et al., 2016, Creff et al., 2019). In contrast to the obvious changes in polyester depositions, *gpat4 gpat8* presents neither changes in membrane and storage lipids nor in wax deposition (Li et al., 2007a).

The loss of function of *GPAT6* leads to formation of a defective cuticle in flowers having as consequence an organ fusion phenotype, a permeability of the petal cuticle and an absence of petal and sepal nanoridges. *In vivo*, GPAT6 is selective for C16 cutin monomers. Indeed, in flowers, *gpat6* has a reduction in 10,16-dihydroxy C16:0 FA, 16-OH C16:0 FA and C16:0 FA (Li-Beisson et al., 2009; Yang et al., 2010). In leaves, *gpat6* presents a slight reduction in the same C16 compounds (Li-Beisson et al., 2009) which may be in link with the trichome expression reported by Li et al. (2012). Similarly, in tomato fruit, *GPAT6* homolog is involved in the formation of cutin with the incorporation of C16 monomers: 9/10, 16 dihydroxy C16:0 FA, C16:0 DCA, 9/10 hydroxy C16:0 DCA, ω-OH C16:0 FA, 10-oxo-ω-OH FA C16:0 FA and C16:0 FA (Petit et al., 2016). *In vitro,* the GPAT6 enzyme can also interact with C18 ω-OH FA

and DCA, but it has a clear selectivity for 16-OH C16:0 FA (Yang et al., 2012). *GPAT6* is not involved with wax or intracellular lipid formation (Li-Beisson et al., 2009).

2.1.3. *GPAT5* and *GPAT7* are involved in suberin formation

With 81% of identity of sequence, *GPAT5* and *GPAT7* form a sub-group in the *GPAT* family (Beisson et al., 2007). *GPAT5* is involved in the formation of the suberin lamellae in the endodermis (Naseer et al., 2012), in the seed coat and hilum sealing (Beisson et al., 2007). In seeds and roots, the *gpat5* mutant displays a strong reduction of C22:0 and C24:0 unsubstituted, ω-oxidated FA and DCA, monomers typical of suberin. A role in the formation of those precursors is supported by the accumulation of the same monomers in the ectopic overexpression of *GPAT5* (Beisson et al., 2007). Due to its seed coat and endodermal suberin defect, *gpat5* is presenting higher sensitivity to salt upon germination and in their seedling establishment rate (Beisson et al., 2007). In flowers, *gpat5* presents a reduction in C22:0, C24:0 and ω-OH C18:2 FA which fits with *GPAT5* expression in the anthers (Beisson et al., 2007). *In vitro*, GPAT5 exhibits the high affinity with C22:0, ω-OH C22:0 and C22:0 DCA acyl-CoAs (C24 ω-OH and DCA acyl-CoA were not tested) and lower activity with C16:0 to C24:0 acyl-CoA (Yang et al., 2012).

GPAT7 is induced upon wounding in leaves which hypothetically could lead to suberin formation, even if no chemotype was visible in leaves or wounded leaves of *gpat7* (Yang et al., 2012).

Thus, *GPAT5* and *GPAT7* are involved in suberin formation, respectively in a constitutive and inducible way and not in membrane and storage lipids (Beisson et al., 2007). However, their single overexpression leads to an increase in sn-2 MAGs and C22-C24 free FAs in stem, which is surprising since GPAT5 and GPAT7 have no phosphatase activity (Li et al., 2007b; Yang et al., 2012).

2.2. Strategy

In this section, we aim to describe polyester deposition, know or unknown, in *Arabidopsis* roots. To this end, the expression pattern of the some of the polyester-related genes was studied and correlated with polyester deposition.

To locate polyester deposition in the roots, we focused on genes already known to be involved in plant polyester synthesis. The *GPAT* family is ideal for that since (1) intensified phylogenetic analysis revealed the existence of 10 members in the family; (2) its members are involved in the biosynthetic pathway of polyesters: cutin (*GPAT4, GPAT6* and *GPAT8*) and suberin (*GPAT5* and *GPAT7*); (3) *GPAT4, GPAT5* and *GPAT8* activity is a limiting step in the production of cutin and suberin (Li et al., 2007a); (4) *in vitro*, the enzymatic activity of GPAT1, GPAT4, GPAT5, GPAT6, GPAT7 and GPAT8 are confirmed (Yang et al., 2012); (5) *GPAT5* is well characterized in the root. At the opposite *GPAT4, GPAT6* and *GPAT8* are only described in the shoot. *GPAT2, GPAT3* and *GPAT7* are very little studied. With still a lot to explore, this acquired knowledge gives us confidence that the GPAT family is an interesting tool to study polyester deposition in the root.

As already mentioned before, *GPAT1, ATS1* and *GPAT9* involved in membrane and storage lipids were not the focus of those researches. From now on, *GPATs* will refer to *GPAT2* to *GPAT8.*

To study the expression of the entire *GPAT* family, we developed transgenic reporter lines consisting of the *GPAT* promoter followed by a nuclear localization signal (NLS) fused to GFP and GUS markers. The nuclear localization was used because it is easier to detect a nuclear signal than ER one. GFP was a tool to identify the expression localized at the cellular level, GUS at the organ level. Through qPCR in various *GPAT* mutants, we investigated if the members of this family have a co-expressional relationship.

2.3. Results

2.3.1. *GPAT*s are expressed in different root cell types

Characterization of the GFP signal of transgenic plants harboring the pGPAT::NLS-GFP-GUS constructs at embryonic stage and in 2-, 5-, 7- and 10-day-old roots revealed gene expression in different cell types and at a wide variety of developmental stages.

Expression studies of the embryo and seed showed that *GPAT2* and *GPAT3* were expressed respectively from the heart stage and the bend cotyledon stage (Figure 8). *GPAT4* was expressed at the seed coat and the outer layer of the endosperm (Figure 8).

At the root tips, *GPAT2* and *GPAT3* were expressed in all the cells of the columella and the lateral root cap cells of the root cap during the entire seedling development (Figure 9). *GPAT4* was expressed only at the outer cell layer of the root cap cells and until the first root cap cell layers get lost, at 6 days (Figure 9). *GPAT5*, *GPAT6*, *GPAT7* and *GPAT8* did not exhibit any visible expression at the root cap (Figure 9).

In the differentiated primary root, *GPAT2* was expressed along the whole root in the epidermis and in the cortex, with an intensity gradient increasing from the elongation zone towards the older part of the root (Figure 10, Figure S1). Expression of *GPAT3* was similar to *GPAT2* at the primary root, but with the gradient towards the tip and a weak additional expression in the stele (Figure 10). *GPAT4*, *GPAT5*, *GPAT6, GPAT7* and *GPAT8* showed expression in the endodermis (Figure 10). All along the differentiation zone, expressions varied. Starting from the younger part of the differentiated zone, the expression of *GPAT5* and *GPAT6* was at first patchy, then it became continuous before getting patchy again in the older part of the root. *GPAT4* has a gradient in the younger part of the undifferentiated zone and a patchy expression in the older differentiated zone. With a similar expression pattern to *GPAT4*, *GPAT8* presented no patchiness but an intensity gradient. In addition to its endodermal expression, *GPAT7* was also expressed in the differentiated epidermis and cortex following a patchy-continuous-patchy pattern (Figure 10).

After lateral root emergence, *GPAT2* and *GPAT3* expression started to be expressed on a similar manner than in the primary root (Figure 11). *GPAT5* and *GPAT6* did not present any expression in emerging lateral roots (Figure 11). In fully developed and differentiated lateral roots, their expression profile was the same as in the primary root. *GPAT4*, *GPAT7* and *GPAT8* were expressed at the early stages of lateral root primordium formation in the primary root (Figure 11). During the differentiation of the lateral root cells, they were first expressed in the root cap cells and in the epidermis. In longer lateral roots, the expression pattern fitted the one of primary roots.

To conclude, considering *GPAT* expression pattern in roots we can subdivide them into two distinct groups. On one side, *GPAT2* and *GPAT3* are both expressed in epidermal and cortex cells all along the root and at root cap. Logically due to their similarity of expression pattern and their close sequence homology, they may be involved together in the formation of one specific polyester deposited in the outer cells of the root. On the other side, expressed in the

endodermis, *GPAT4*, *GPAT5*, *GPAT6*, *GPAT7* and *GPAT8* may be implicated in the formation of one common polyester in endodermis. We hypothesize that they are all implicated in suberin formation, as shown for *GPAT5* (Beisson et al., 2007). In addition, an interesting root cap specific expression is present at the primary and/or at the lateral roots of *GPAT2, GPAT3, GPAT4, GPAT7* and *GPAT8*.

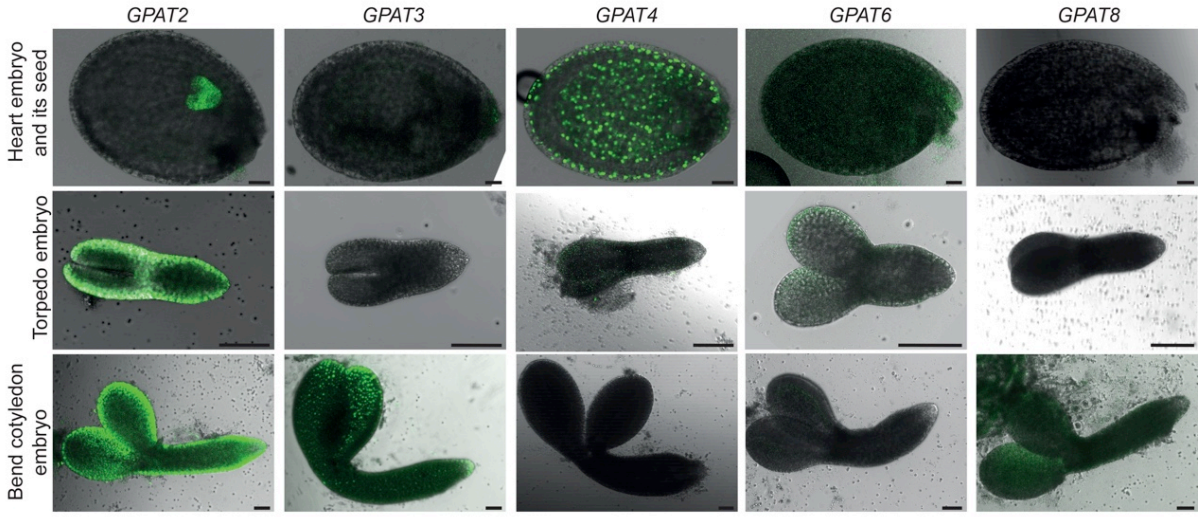

Figure 8: GFP fluorescence of transgenic plants expressing pGPAT::NLS-GFP-GUS for *GPAT2, GPAT3, GPAT4, GPAT6* and *GPAT8* at the heart, torpedo and bend cotyledon embryonic stage and in the seed coat. Scale bars represent 50 µm.

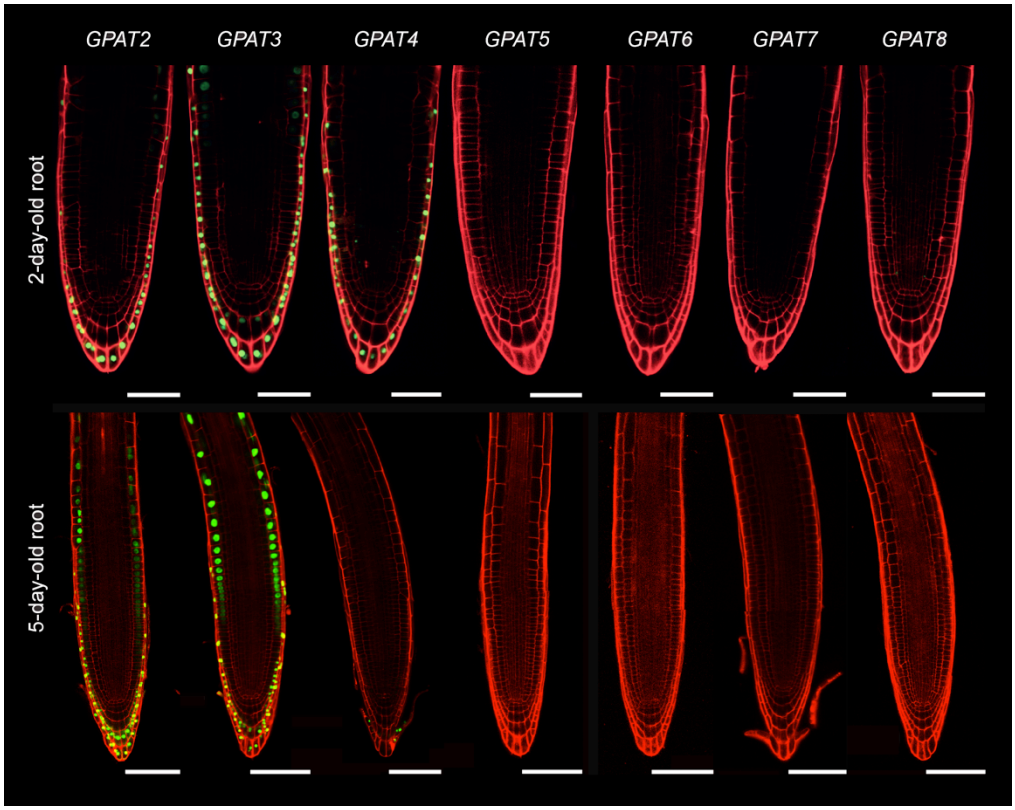

Figure 9: GFP fluorescence of transgenic plants expressing pGPAT::NLS-GFP-GUS at the root cap of a 2-day-old and 5-day-old seedling. Expression profile of *GPAT4* and *GPAT8* at 2-day-old root from Berhin et al. (2019), Figure1D. Propidium Iodide (PI) in red is staining the cell wall. Scale bars represent respectively 50 and 100 µm for the 2- and 5-day-old seedling.

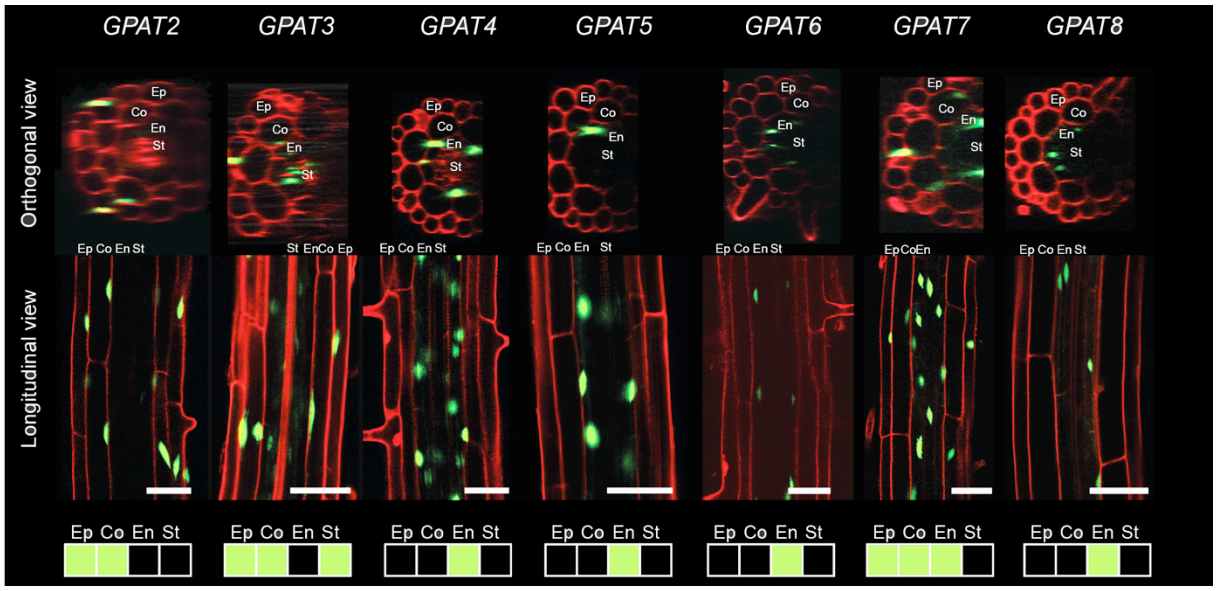

Figure 10: GFP fluorescence of transgenic plants expressing pGPAT::NLS-GFP-GUS at primary root of 5-day-old seedling: orthogonal, longitudinal view and schematic abstract of the expression. PI in red is staining the cell wall. Scale bars represent 50 µm. Ep, Epidermis; Co, Cortex; En, Endodermis; St, Stele.

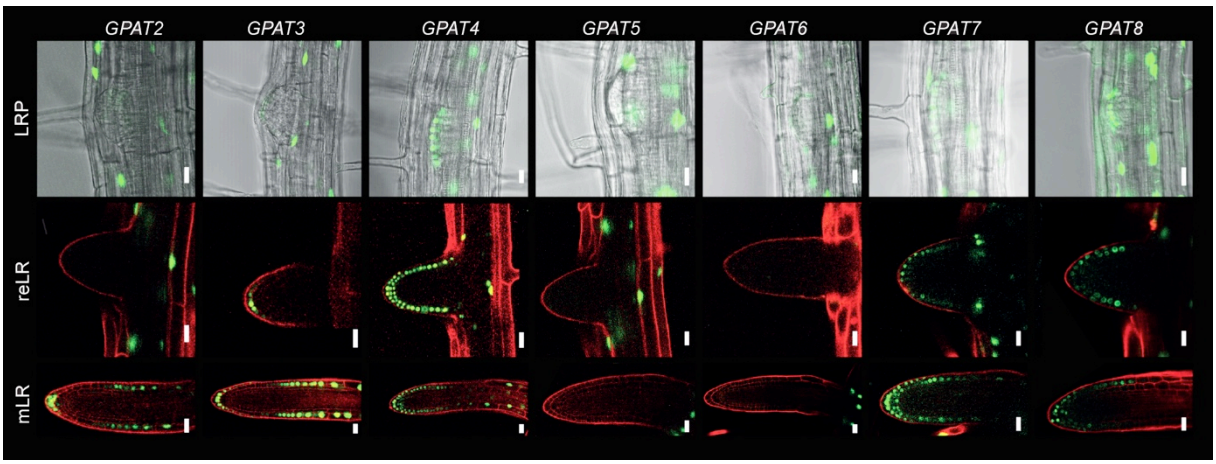

Figure 11: GFP fluorescence of transgenic plants expressing pGPAT::NLS-GFP-GUS at the lateral roots. Expression of *GPAT4* and *GPAT8* from Berhin et al. (2019), Figure 3C. PI is staining the cell wall. LRP, lateral root primordium; reLR, recently emerged lateral root; mLR, mature lateral root. Scale bars represent 20 µm.

2.3.2. *GPAT*s are co-regulated at the transcriptional level

Previous studies suggested that some *GPAT*s have redundant activities (Li et al., 2007a) and are co-regulated (Petit et al., 2016). To have a better overview of the co-expressional relationship between the members of this family, we evaluated the expression level of the *GPATs* via qPCR in various *GPAT* mutants: *gpat4, gpat8* (Li et al., 2007a)*, gpat6-1, gpat6-2* (Li-Beisson et al., 2009)*, gpat5* (Naseer et al., 2012), *gpat7 (gpat7-3* from Yang et al. (2012)), *gpat2 (gpat2-1* from Yang et al. (2012)) and *gpat3 (gpat3-2,* SALK_139115). Beforehand, the two available mutants for *GPAT6* knockouts were compared in term of *GPAT6* level of expression. *gpat6-2* seemed to be a real knockout of *GPAT6* gene while *gpat6-1* was strongly

reduced (Figure 12) confirming the results of Fabre et al. (2016). Therefore *gpat6-2* was tested in this experiment.

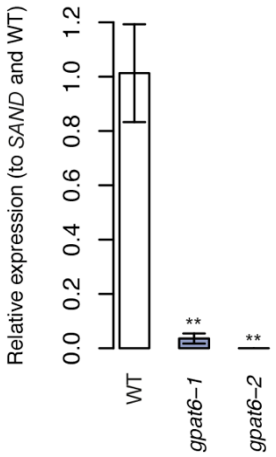

Figure 12: Quantification of the expression level of *GPAT6* in *gpat6-1* and *gpat6-2* mutants. Normalization was performed to the *SAND* reference gene and WT. Displayed values are means with standard errors of three independent biological experiments. Significant differences to WT were determined by Student's t test: **p < 0.01.

First, we confirmed that the expression of each gene is strongly down-regulated in their corresponding mutant, with the exception of *gpat8,* which showed an overexpression (Figure 13). In our design, the primers used were binding to gene after the T-DNA insert. The transcription enhancement of a sequence following a T-DNA insertion is a phenomenon that has been already observed (Ülker et al., 2008; Zubko et al., 2011). In this case, we can be sure that the transcript is not effective since *gpat4 gpat8* has a permeable cuticle as opposed to *gpat4*.

In *gpat4*, the *GPAT5* and *GPAT7* expression was down regulated to at least 80% of the WT, *GPAT6* and *GPAT8* to 50%. The same pattern was visible in *gpat8* where the expression of *GPAT4*, *GPAT5*, *GPAT6* and *GPAT7* was at least 50% lower than in WT. The knockout of *GPAT6* appeared to solely influence the expression of *GPAT5* that was up-regulated by 1.5 fold. In *gpat5* and *gpat7*, the *GPAT4*, *GPAT6* and *GPAT8* behave similarly respectively with a reduction of 40%, 25% and 40%. *GPAT5* and *GPAT7* presented respectively a decrease of 40% and 60% in each another knockout.

GPAT2, *GPAT3* and *GPAT7* knockouts were not influenced by each other, except in *gpat2* where *GPAT3* and *GPAT7* expression level was 50% lower if compared to WT (Figure 14).

In conclusion, the expression of *GPAT*s is co-down-regulated. The general tendency is the decrease of the expression of other genes when one of them is knocked-out, at the exception of *gpat6* in which the expression of *GPAT5* increases, probably due to a compensation mechanism.

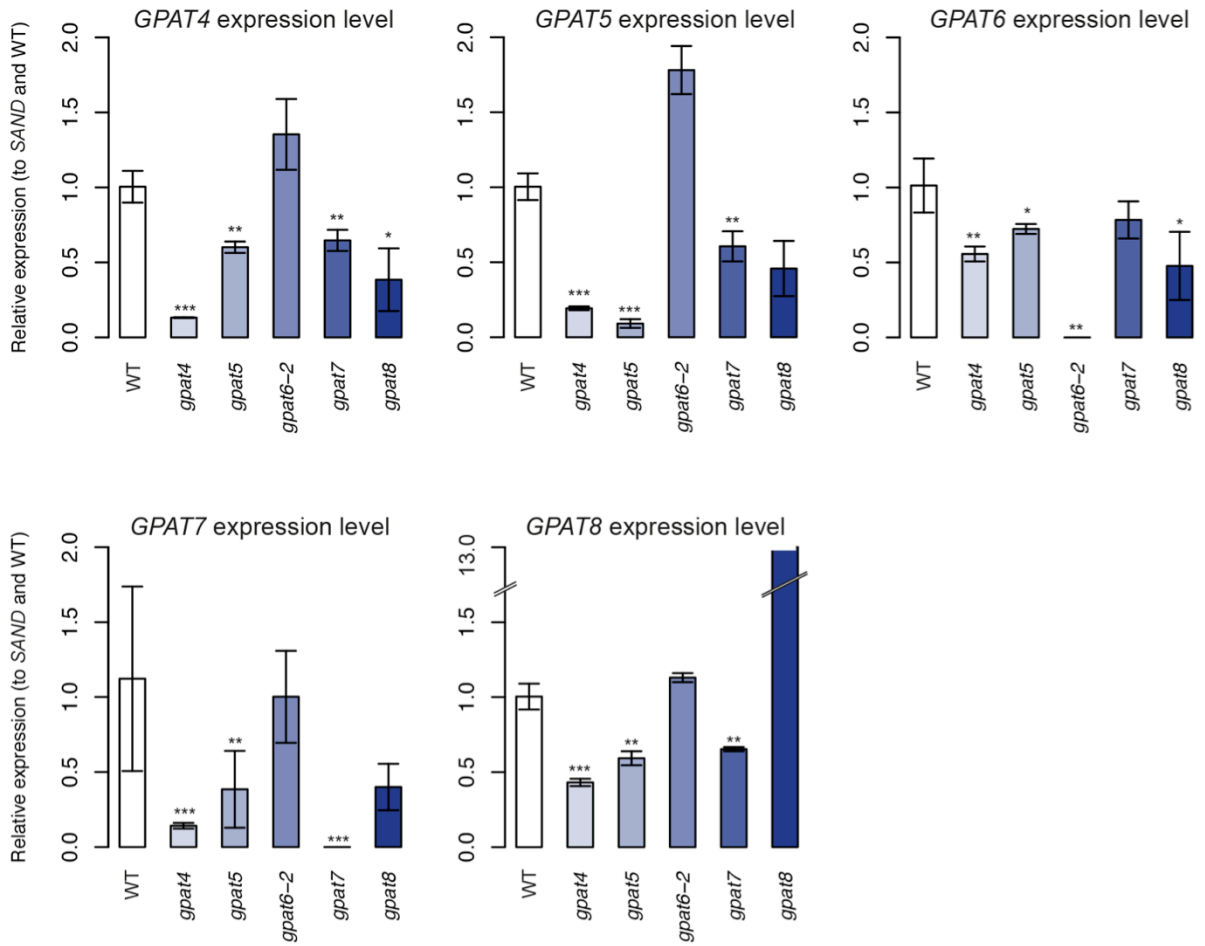

Figure 13: Quantification of the expression level of *GPAT*s expressed in the endodermis when one of them is knocked out. Relative expression of *GPAT4, GPAT5, GPAT6, GPAT7* and *GPAT8* in WT and in different *gpat* mutants normalized to the *SAND* reference gene and WT. Displayed values are means with standard errors of three independent biological experiments. Significant differences to WT were determined by Student's t test: ***p < 0.001; **p < 0.01; *p < 0.05.

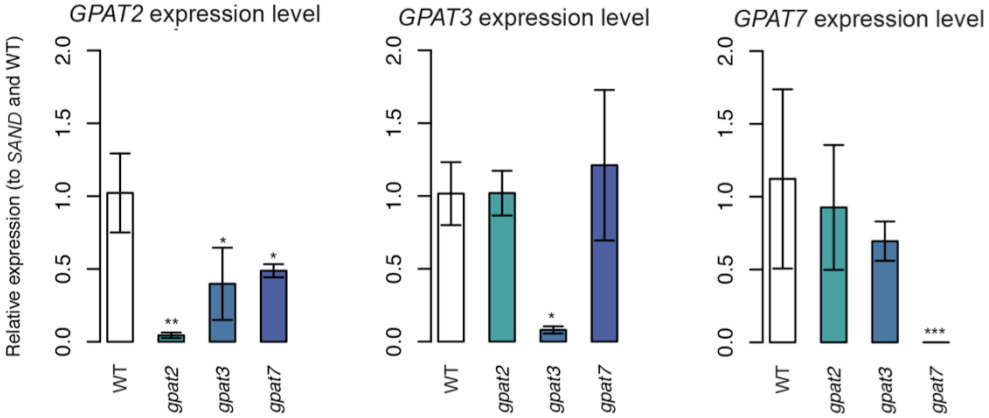

Figure 14: Quantification of the expression level of *GPATs* expressed in the epidermis and cortex when one of them is knocked out. Relative expression of *GPAT2, GPAT3*, and *GPAT7* in WT and in different gpat mutants normalized to the *SAND* reference gene and WT. Displayed values are means with standard errors of three independent biological experiments. Significant differences to WT were determined by Student's t test: ***p < 0.001; **p < 0.01; *p < 0.05.

2.4. Discussion and perspectives

2.4.1. *GPAT2*, *GPAT3* and partially *GPAT7* are co-expressed in the epidermis and the cortex

GPAT2 and *GPAT3* were both expressed in epidermal and cortex cells all along the root and at root cap. Absence of *GPAT2* induced a decrease in the expression of the *GPAT3* but not the opposite. Together with their sequence similarity and co-expression data (GeneMania (Mostafavi et al., 2008) and ATTED II (Aoki et al., 2016)), their common expression suggested that they may act together in the formation of a, so far uncharacterized, specific polyester precursors in the outer layers of the root.

GPAT7 also presents an epidermal and cortical expression, but only in the differentiated part of the root. This partial common expression could indicate that *GPAT7* is forming a different precursor than *GPAT2* and *GPAT3* but for a same polyester at the surface of the roots.

2.4.2. *GPAT4* to *GPAT8* are co-expressed in the endodermis.

In addition to the known *GPAT5* (Beisson et al., 2007, Naseer et al., 2012), *GPAT4*, *GPAT6,* *GPAT7* and *GPAT8* showed endodermal expression. Single gene knockout of *GPAT4*, *GPAT5*, *GPAT7* and *GPAT8* led to a general tendency of expression decrease of the other *GPAT*s. *GPAT6* inactivation influenced only the expression of *GPAT5*, which increased. A decrease of the expression of polyester-related genes when another one was knocked-out, has already been reported by Petit et al. (2016). Indeed, *GPAT4*, *LACS2*, *CYP77s, CYP86s, LTPg1* and *CUS1* are down regulated in *gpat6* tomato fruit (Petit et al, 2016). This shows that the entire polyester pathway is down-regulated and not just the *GPAT*s. The unexpected co-expression between the cutin-related genes, *GPAT4* and *GPAT6,* and a suberin-related gene, *GPAT5,* was confirmed through microarray databases like Genevestigator and Genemania (Hruz et al., 2008; Mostafavi et al., 2008). We can conclude that *GPAT4, GPAT5, GPAT6, GPAT7* and *GPAT8* may be involved in a common pathway in the endodermis; even if *GPAT4*, *GPAT6* and *GPAT8* have been characterized as cutin-related genes in the shoot. It can be hypothesized that they are involved in suberin deposition in the endodermis like *GPAT5* since it is the only known polyester deposition at this location.

While *GPAT5*, *GPAT6* and *GPAT7* expression follows the suberin pattern, the expression of *GPAT4* and *GPAT8* begins earlier (Figure S2), more in synchronization with Casparian strip formation like shown with the similar expression profile of *CASP1* and *SGN1* (Roppolo et al., 2011; Alassimone et al., 2016). Another suberin gene has the similar expression profile, *ASFT* (Naseer et al., 2012). Based on the expression pattern, it was hypothesized that *ASFT* may also allow the integration of ferulic acid esters in the Casparian strip (Naseer et al., 2012) but it is hard to argue on the role of *GPAT*s in the formation of lignin. However, this could suggest a lipid impregnation of the lignin as mentioned by Zeier and Schreiber (1998), although more evidence has to be collected to confirm it. Another hypothesis is that some polyester precursors could be formed before others and only polymerized when the suberin lamellae starts forming.

2.4.3. *GPAT2*, *GPAT3*, *GPAT4*, *GPAT7* and *GPAT8* are co-expressed at the root caps

Expression studies on early primary root development showed that *GPAT2*, *GPAT3* and *GPAT4* were expressed at the root cap. *GPAT4* was only expressed at the outer layer of the root cap and until the first root cap cells are lost, while *GPAT2* and *GPAT3* were expressed in all cells of the root cap and for the whole life of the seedlings. The expression of *GPAT2* and *GPAT3* was already observed at the embryo, surprisingly, *GPAT4* was not (Figure 8), despite of the embryo cuticle absence in the *gpat4 gpat8* double mutant (Creff et al., 2019).

At the lateral roots, *GPAT2* and *GPAT3* were expressed at the root cap after emergence of the primordia, while *GPAT4*, *GPAT8* and *GPAT7* were expressed already at the early formation of the primordia inside the primary root.

Other cuticle-related-genes like *LACS2*, *DCR, ABCG11, LTPG1, LTPG2* and *BDG* have already been reported as being expressed at the root cap, suggesting that a polyester barrier could be formed there (Kurdyukov et al., 2006a; Kurdyukov et al., 2006b; Bird et al., 2007; Lee et al., 2009a; Lü et al., 2009; Panikashvili et al., 2009; Kim et al., 2012; Jakobson et al., 2016).

2.4.4. *GPAT1* could potentially be involved in polyester formation

GPAT1 has a known function but is necessary for tapetum differentiation and pollen development linked to a role to the membrane lipid biosynthetic pathway, similar as *GPAT4* and *GPAT6* (Jayawardhane et al., 2018; Zheng et al., 2003). Indeed, *GPAT1* and *GPAT6* both

act in ER assembly for the tapetum and together in microspore release (Li et al., 2012). Furthermore, *GPAT4* knockout in *Brassica napus* exhibits issues in pollen development (Chen et al., 2014). Since *GPAT4* and *GPAT6* knockouts have the similar defect in pollen development than *GPAT1*, this could indicate that *GPAT1* might be involved in polyester formation as well.

Expression pattern of *GPAT2* to *GPAT8* based on microarray fits quite well to the GFP expression pattern we obtained in pGPAT::NLS-GFP-GUS plants (Beisson et al., 2007). This dataset presents *GPAT1* as well being expressed in the roots and in the leaves. Thus, like *GPAT6, GPAT1* could be also involved in polyester formation.

In vivo studies have shown that GPAT1 can use DCA-CoA as substrates (Yang et al., 2012; Singer et al., 2016). DCAs are specific for extracellular lipids. This ability to use DCAs suggests a possible role in cutin or suberin formation, even if no changes in polymeric FAs were observed in *gpat1* leaves, flowers and seeds (Yang et al., 2012).

The main difference between GPAT1 and the other sn-2 GPATs is its mitochondrial membrane localization. This has been confirmed by the import of GPAT1 in pea mitochondria and the identification of a potential mitochondrial signal peptide (Gidda et al., 2009; Zheng et al., 2003). A further investigation *in vivo* of GPAT1 subcellular localization should be performed using a translational fusion construct to confirm the previous *in vitro* studies. In a similar way, localization of the acyltransferase domain of the protein, inside or outside the organelle, has to be studied. It raises the question whether *GPAT1* could be involved in polyester formation, even if located at the mitochondria instead of the ER as long as its acyltransferase domain is present as well in the cytosol.

In conclusion, *GPAT1* is worth to be investigated for a potential role in polyester formation in the future.

2.5. Conclusion

In summary, the use of the expression profile of the *GPAT* family as a tool led us to the identification of potential novel polyester depositions yet to be identified and to the observation of unexpected overlapping expression of cutin-related genes with suberin-related genes in the endodermis. Those results open many topics of investigation listed here.

GPAT2, GPAT3, GPAT4, GPAT7 and *GPAT8* are expressed at the root cap of the primary and/or the lateral roots. Since they are not the only polyester-related genes that are expressed in those locations and that no polyester deposition is known at the root cap, it would be interesting to investigate the reason of their presence and if applicable, the polyester that they are forming. This served as basis for the research topic presented in the Chapter 3: The root cap cuticle.

Endodermal co-expression and co-regulation at the transcriptional level between the *GPAT4, GPAT5, GPAT6, GPAT7* and *GPAT8* are destabilizing the theory of suberin- and cutin-specific genes in the roots. The possibility of their implication in the formation of suberin in the roots is investigated further in Chapter 4: The role of *GPAT4*, *GPAT6*, *GPAT7* and *GPAT8* in endodermal suberin.

GPAT2 and *GPAT3* are two uncharacterized genes that are intriguing due to their epidermal and cortex cell layer localization that does not match any known polyester deposition. They are both studied in Chapter 5: Characterization of *GPAT2* and *GPAT3* and their role in polyester formation .

Chapter 6: Role of polyester depositions in the interaction with microbes, investigates how polyester deposition at the roots may have a role in microbial interaction through the study of the *GPAT* mutants.

3. The root cap cuticle

3.1. Introduction

The cuticle is “a hydrophobic boundary layer that coats the outer face of the epidermis of aerial plant organs”, defines Fich et al. (2016). Until now, the cuticle has always been considered as shoot specific. The possibility of cuticle deposition at the root surface was never envisioned, because the root is an organ having principally a water absorption function. Hence, cuticle deposition at its surface sounds incompatible.

Based on our preliminary results showing an intriguing expression of polyester-related genes at the root cap of the primary and the lateral roots (Figure 9 and Figure 11), we decided to investigate the possibility of a polyester deposition at the root cap. In this introduction, I introduce the root cap, present the current knowledge on polyester depositions in the root tip and draw the attention to numerous polyester-related genes that are expressed in this organ.

3.1.1. The root cap of the primary and the lateral roots

Found at the tip of the roots, constantly protecting the meristem, the root cap is constituted of the columella and the lateral root cap cells, which are constantly renewed (Figure 5 and Figure 15). At the so-called transition zone, where the epidermal cells start to elongate, the neighboring lateral root cap cells enter a programmed cell death process (Fendrych et al., 2014). They are sloughed off with the outer layer of columella cells that are detached alive. This ensures the constant turnover of the outer root cap layer (Kumpf and Nowack, 2015). NAC transcription factors control tidily this process: FEZ stimulates periclinal division of columella and epidermis/lateral root cap stem cells; SOMBERO (SMB), a negative regulator, promotes differentiation of the cells (Willemsen et al., 2016); BEARSKIN1 (BRN1) and BEARSKIN2 (BRN2) control the maturation of the cells and their detachment (Kamiya et al., 2016).

The root cap is the first tissue of the plant that is in contact with the newly invaded environment. Gravitropism, allowed by the statoliths in the columella cells, and hydrotropism determine the directional growth of the roots (Kumpf and Nowack, 2015). In

addition, root cap cells produce mucilage, a polysaccharide-based matrix having lubricant properties to facilitate the soil invasion. Mucilage, but also other released components (cells, proteins…), may influence the rhizosphere and the interactions with microbes (Kumpf and Nowack, 2015).

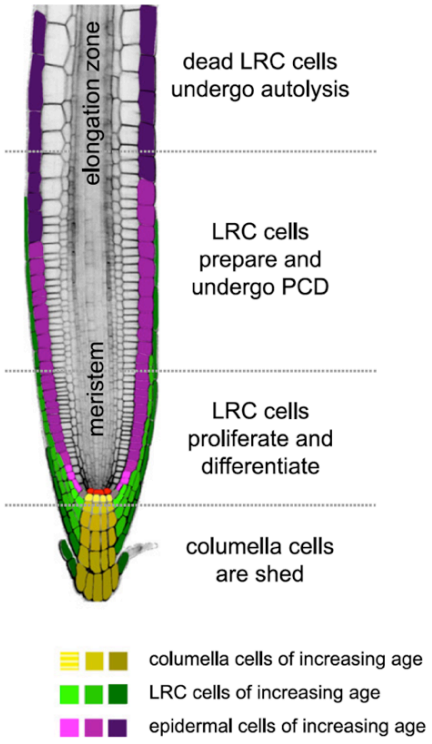

Figure 15: Schematic diagram of *Arabidopsis thaliana* root tip highlighting root cap sloughing off process from Huysmans et al. (2018). Yellow gradient, columella cells; green gradient, lateral root cap cells; pink gradient, epidermal cells; LRC, lateral root cap; PCD, program cell death.

3.1.2. Polyester deposition at the root cap

Polyester depositions have already been reported to be present at the root tips. First, it was observed during metacutinization, which is a process of suberization and lignification of the root cap cells in order to protect from winter conditions. Secondly, a cuticle has been reported at the tip of aerial roots during the aerial growth. However, it disappears when the roots continue their growth in the underground. To close this section we report some hints suggesting that it is worth investigating a possible cuticle formation at the root cap.

Metacutinization of the root tips

Beginning of the 20th century, Scott (1928) already reported the root as being an absorbing organ. The length of the absorbing zone at the tip of the root before the suberization of the endodermis and the exodermis fluctuates in function of the environmental factors (Scott, 1928). A phenomenon called metacutinization has been reported several times in the

literature. (1) In Gymnosperms, as the winter approaches, the roots lose their absorbing function by protecting the root tip with a ligno-suberized layer connecting up to the exodermal suberin. When the warmer season comes, this layer cracks, allowing the growth of the roots (Scott, 1928). (2) In monocots, a similar process has been described at the beginning of autumn, where the outer layer of the root cap cells becomes lignified and suberized in continuity with the exodermis. In this case, the roots are never going to grow again and they are replaced by new developing ones (Scott, 1928). (3) Root caps of dormant roots of several Angiosperm species are also sheltered in a metacutinized layer. When the plant is starting to grow again this ligno-suberized layer is sloughed off (Bowes, 1972).

Metacutinization is characterized by a suberization and lignification of the cell wall (Wilcox, 1954). This suberization is not lamellae like in the endodermis or exodermis (Wilcox, 1954). It is a protection from water loss due to freezing conditions (Wilcox, 1954).

Cuticle on the root tip of aerial roots

Selaginella kraussiana has roots developing from the stem, having aerial organ characteristics first and then subterranean ones. Therefore, in the aerial environment, the root cap is covered by a cuticle. Once in the underground conditions, the root undergoes several structural changes. At that stage, the cuticle is not visible anymore (Grenville and Peterson, 1981).

A potential cuticle at the root tip

In the literature, several independent clues suggested a possible polyester deposition at the tip of the primary and the lateral roots.

(1) Auramine O staining on *Arabidopsis* embryo executed by Szczuka (2003) revealed cuticle presence from the globular stage all the way around the embryo, even on the radicle.

(2) Fluorol yellow staining on lateral roots revealed a staining all along the primordia and the emerging lateral roots. At that time, Li et al. (2017) hypothesized that it was suberin deposition.

(3) Based in the expression profile of *DCR* and *ABCG11*, it has already been suggested, but not investigated, that a cutin-like polymer could be present at the lateral root tips (Panikashvili et al., 2009; Panikashvili et al., 2010).

3.1.3. Root tip expression of polyester-related genes

It has been reported that a few genes involved in polyester formation are expressed at the tip of the primary and lateral roots. However, the role of those genes at that location was unclear. None of the genes classified as suberin-related are expressed at the root tips. At the opposite, cutin-related genes are commonly expressed there (Table 1): *LACS2* (Lü et al., 2009), *HTH* (Kurdyukov et al., 2006b), *DCR* (Panikashvili et al., 2009), *ABCG11* (Bird et al., 2007), *LTPg1* (Lee et al., 2009a), *LTPg2* (Kim et al., 2012), and *BDG* (Jakobson et al., 2016).

3.2. Strategy

The aim of this project is to investigate the presence of an unexpected polyester deposition at the tip of the roots and to characterize it in details, to understand its composition, its formation and its functions.

	Gene name	Primary root	Lateral root	Type of labeling	References
Cutin-related genes (Fich et al., 2016)	*ABCG11*	Yes	Yes	GUS	Bird et al., 2007, Panikashvili et al. 2007
	ABCG12	n.a	n.a		
	ABCG32	n.a	n.a		
	ANL2	n.a	n.a		
	BDG	No[(1)]/ Yes[(2)]	Yes[(1) (2)]	GFP and GUS	[(1)]Jakobson et al. 2016, [(2)]Present work with lines from L. Jackobson
	CFL1	n.a	n.a		
	CUS1	n.a	n.a		
	CUS2	No	No	GFP and GUS	Present work with lines from A. Roeder
	CYP77A4	n.a	n.a		
	CYP77A6	n.a	n.a		
	CYP86A2	n.a	n.a		
	CYP86A4	n.a	n.a		
	CYP86A7	n.a	n.a		
	CYP86A8	n.a	n.a		
	DCF	No	No	YFP	Present work with lines from Mi Yeon Lee
	DCR	Yes	Yes	GFP[(3)] and GUS[(4)]	[(3)]Present work, [(4)]Panikashvili et al. 2009
	GPAT4	Yes	Yes	GFP	Present work
	GPAT6	No	No	GFP	Present work
	GPAT8	No	Yes	GFP	Present work
	HDG1	n.a	n.a		
	HTH	n.a	Yes	GUS	Kurdyukov et al. 2006
	LACS1	No	No	GUS	Lu et al. 2009
	LACS2	Yes	Yes	GUS	Lu et al. 2009
	LACS3	n.a	n.a		
	LACS4	Yes	n.a	GUS	Zhao et al. 2019
	LTPg1	Yes	Yes	GUS	Lee et al. 2009
	LTPg2	Yes	Yes	GUS	Kim et al. 2009
	MYP106	n.a	n.a		
	MYP16	n.a	n.a		
	NFXL2	n.a	n.a		
	SHN1	n.a	n.a		
	SHN2	n.a	n.a		
	SHN3	n.a	Yes	GUS	Aharoni et al. 2004
Suberin-related genes (Vishwanath et al., 2015)	*ABCG2*	n.a	n.a		
	ABCG6	n.a	n.a		
	ANCG20	n.a	n.a		
	ASFT	No	n.a	YFP[(5)] and GUS[(6)]	[(5)]Molina et al. 2009, [(6)]Naseer et al.2012
	CYP86A1/ HORST	Yes[(7)] / No[(8)]	n.a	GFP[(7)] and GUS[(8)]	[(7)]Naseer et al.2012, [(8)]present work with lines from Yuree Lee
	CYP86B1	No	n.a	GUS	Naseer et al.2012
	DAISY/KCS2	n.a	No[(9)]/Yes[(10)]	GUS	[(9)]Lee et al. 2009, [(10)]Franke et al. 2009
	FACT	n.a	n.a		
	FAR1	No	n.a		Naseer et al.2012
	FAR4	No	n.a		Present work with lines from Yuree Lee
	FAR5	n.a	n.a		
	GPAT5	No	No	GFP and GUS	Present work
	GPAT7	No	No	GFP and GUS	Present work
	KCS1	No	n.a	GUS	Naseer et al.2012
	KCS20	No	No	GUS	Lee et al. 2009
	MYP41	n.a	n.a		

Table 1: Table presenting the expression of cutin- and suberin-related genes at the root tip of primary and lateral roots. Columns refer to the type of labeling used and the reference of the published data. n.a, no available data.

3.3. Publication entitled: The root cap cuticle - a cell wall structure for seedling establishment and lateral root formation

Article

Cell

The Root Cap Cuticle: A Cell Wall Structure for Seedling Establishment and Lateral Root Formation

Graphical Abstract

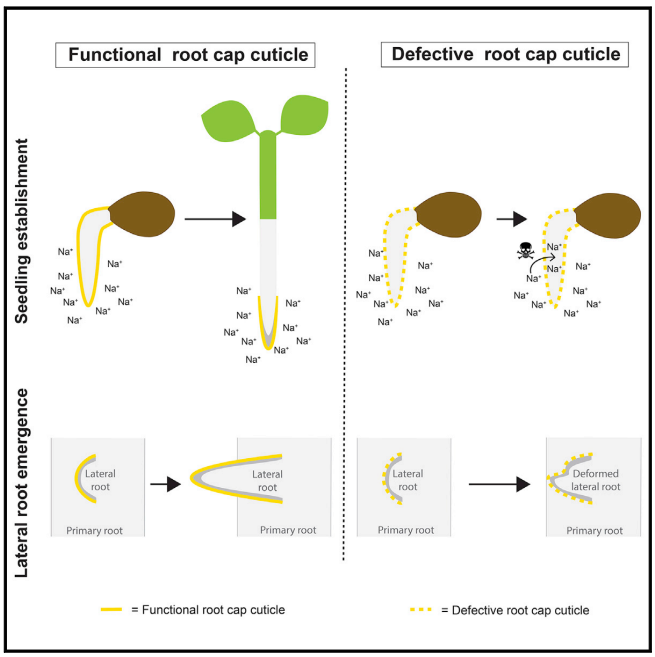

Authors

Alice Berhin, Damien de Bellis, Rochus B. Franke, Rafael A. Buono, Moritz K. Nowack, Christiane Nawrath

Correspondence

christiane.nawrath@unil.ch

In Brief

A cuticle-like cell wall structure on plant root caps protects seedlings from abiotic stress and contributes to proper lateral root outgrowth.

Highlights

- At early developmental stages, root caps of primary and lateral roots form a cuticle
- This polyester-rich cuticle is lost with the removal of the first root cap cell layer
- During germination, the root cap cuticle protects the sensitive root meristem
- The cuticle of young lateral roots facilitates invasive growth and root emergence

Berhin et al., 2019, Cell *176*, 1–12
March 7, 2019
https://doi.org/10.1016/j.cell.2019.01.005

CellPress

Please cite this article in press as: Berhin et al., The Root Cap Cuticle: A Cell Wall Structure for Seedling Establishment and Lateral Root Formation, Cell (2019), https://doi.org/10.1016/j.cell.2019.01.005

Article

Cell

The Root Cap Cuticle: A Cell Wall Structure for Seedling Establishment and Lateral Root Formation

Alice Berhin,[1] Damien de Bellis,[1,2] Rochus B. Franke,[3] Rafael A. Buono,[4,5] Moritz K. Nowack,[4,5] and Christiane Nawrath[1,6,*]

[1]Department of Plant Molecular Biology, University of Lausanne, Biophore Building, 1015 Lausanne, Switzerland
[2]Electron Microscopy Facility, University of Lausanne, Biophore Building, 1015 Lausanne, Switzerland
[3]Institute of Cellular and Molecular Botany, University of Bonn, Kirschallee 1, 53115 Bonn, Germany
[4]Department of Plant Biotechnology and Bioinformatics, Ghent University, Technologiepark 71, 9052 Ghent, Belgium
[5]VIB Center for Plant Systems Biology, Technologiepark 71, 9052 Ghent, Belgium
[6]Lead Contact
*Correspondence: christiane.nawrath@unil.ch
https://doi.org/10.1016/j.cell.2019.01.005

SUMMARY

The root cap surrounding the tip of plant roots is thought to protect the delicate stem cells in the root meristem. We discovered that the first layer of root cap cells is covered by an electron-opaque cell wall modification resembling a plant cuticle. Cuticles are polyester-based protective structures considered exclusive to aerial plant organs. Mutations in cutin biosynthesis genes affect the composition and ultrastructure of this cuticular structure, confirming its cutin-like characteristics. Strikingly, targeted degradation of the root cap cuticle causes a hypersensitivity to abiotic stresses during seedling establishment. Furthermore, lateral root primordia also display a cuticle that, when defective, causes delayed outgrowth and organ deformations, suggesting that it facilitates lateral root emergence. Our results show that the previously unrecognized root cap cuticle protects the root meristem during the critical phase of seedling establishment and promotes the efficient formation of lateral roots.

INTRODUCTION

Higher organisms adapted to the life on land by developing surface modifications protecting themselves against desiccation and other environmental stresses, including pathogen attack. In contrast to animals that incorporate specialized proteins in the extracellular matrix of the skin (Alberts et al., 2015), plants developed lipid-derived modifications on the surface of different organs (Kolattukudy, 2001a; Pollard et al., 2008). Aerial organs of the shoot that are in primary growth stage, such as leaves, flowers, and fruits have acquired a cuticle (Riederer, 2006). The cuticle forms a multi-layered structure of lipid components at the outermost surface of the organ in continuation with the cell wall (Jeffree, 2006). In most species, the main components of the cuticle are an insoluble structural polyester, named cutin, and a mixture of solvent-extractable compounds, commonly called waxes (Holloway, 1982a; Kolattukudy, 1980). Inner border tissues, organs in secondary growth stage, and wounded tissues are protected by lamellae containing suberin, a polymer similar to cutin but with higher amounts of phenolic compounds (Andersen et al., 2015; Franke et al., 2012; Pollard et al., 2008). Importantly, in contrast to cutin, which is primarily deposited on the outermost surface of the cell wall, suberin is formed as part of the secondary cell wall, deposited between the primary wall and the plasma membrane (Kolattukudy, 2001b; Pollard et al., 2008, Nawrath et al., 2013). Other plant organs are protected by specialized lipid-derived cell wall modifications, such as pollen containing sporopollenin and seeds forming seed coats containing suberin (Dominguez et al., 1999; Molina et al., 2006).

The cuticle that is synthesized by the epidermis of the shoot varies strongly in composition, architecture, and properties depending on the species, organ, and developmental stage as well as environmental conditions (Jeffree, 2006). Despite of being a surface structure with diffusion barrier properties, the cuticle has multiple functions beyond plant protection against water loss and abiotic stresses, such as in plant development preventing organ adhesions and fusions (Ingram and Nawrath, 2017; Nawrath et al., 2013). A cuticle can already be identified during early embryogenesis at globular stage when the embryo consists of a few dozen cells (Szczuka and Szczuka, 2003). From this stage on, it continuously expands with the growth of the plant. The cuticle of the embryo has also multiple functions in plant development, for example it plays a role in the establishment of identity of the epidermis of the shoot, in addition to preventing adhesions between embryo and maternal tissues (Ingram and Nawrath, 2017).

The polyester cutin consists predominantly of C16 and C18 oxygenated fatty acids, such as hydroxylated fatty acids and dicarboxylic acids, as well as glycerol. The interconnectivity between the monomers determines the polymer structure and its properties (Bakan and Marion, 2017; Yang et al., 2016). The biosynthesis of cutin comprises the formation of precursors within the cell, their export and the assembly of the polyester

Please cite this article in press as: Berhin et al., The Root Cap Cuticle: A Cell Wall Structure for Seedling Establishment and Lateral Root Formation, Cell (2019), https://doi.org/10.1016/j.cell.2019.01.005

within the cuticle (Fich et al., 2016; Nawrath et al., 2013). A key step of precursor formation is the synthesis of *sn-2*-monoacylglycerols from CoA-activated oxygenated fatty acids by GLYCEROL-3-PHOSPHATE ACYLTRANSFERASES (GPATs) (Beisson et al., 2012). Additional cutin precursors are formed by enzymes of the BAHD family of acyltransferases, such as DEFECTIVE IN CUTICULAR RIDGES (DCR), which is essential for the incorporation of in-chain hydroxylated C16 fatty acids into cutin (Lashbrooke et al., 2016; Panikashvili et al., 2009). After export of cutin precursors to the apoplast, the formation of the cuticular polyester involves enzymes from the α/β hydrolase family, such as BODYGUARD (BDG), as well as cutin synthases from the GDSL-lipase family (Jakobson et al., 2016; Kurdyukov et al., 2006; Yeats et al., 2014).

Roots are very different from aerial organs as they generally grow in the soil and are specialized for the acquisition of water and nutrients, incompatible with the presence of a strong diffusion barrier at their entire surface. Indeed, in the primary growth stage, no visible lipid depositions are located at the surface of the root epidermis. Only deeper inside the root, the endodermis forms cell wall modifications with barrier functions, such as lignified Casparian strips as well as suberin lamellae (Doblas et al., 2017; Geldner, 2013). In addition to the primary root that originates from the embryo, lateral roots are initiated in the vascular cylinder of the primary root through divisions of the pericycle, leading to a branched root system (Van Norman et al., 2013). The emerging lateral root has to grow through the outer cell layers of the primary root, i.e., endodermis, cortex, and epidermis before breaking out, which is described as an invasive growth process (Marsollier and Ingram, 2018; Stoeckle et al., 2018). This lateral root outgrowth is accompanied by various cell and cell wall modifications that lead not only to changes in the anatomy of the overlaying endodermal cell and the breakdown of the Casparian strip, but also to separation of the outer cell layers at the respective positions. These processes are tightly regulated by the plant hormone auxin (Vermeer et al., 2014; Vilches-Barro and Maizel, 2015). After emergence, the lateral root matures establishing all typical cell types of the primary root.

The root cap at the tip of the root is an organ that protects the root meristem, promotes the growth of the root through the soil, and perceives and transmits environmental stimuli, including gravity and nutrient availability (Barlow, 2002; Kumpf and Nowack, 2015). Consisting of central columella cells and adjacent lateral root cap cells, the root cap has a determined size tightly balancing the continuous formation of new cells with elimination of old outer cells (Barlow, 2002). In *Arabidopsis*, the columella cells are sloughed off alive of the tip of the root. Lateral root cap cells are eliminated by programmed cell death, which starts at older cells next to the transition zone and progresses toward the columella cells. Dead and dying lateral root cap cells are detached together with the columella cells, such that the entire outermost root cap cell layer is eliminated in a coordinated manner (Fendrych et al., 2014; Kumpf and Nowack, 2015). Mature root cap cells form mucilage, rich in cell wall polysaccharides, such as pectins, thought to have a lubricant effect for the growth of the root in the soil (Durand et al., 2009).

A root cap is already formed early during the embryo development (Barlow, 2002). Although it is assumed that the root cap protects the root meristem in mature plants, little is known about the molecular mechanisms of root cap biology before the onset of the cell maturation and replacement cycles. Here, we show by histological, chemical, and genetic approaches that the first cell layer of the root cap of the primary root is covered by a hitherto unrecognized root cap cuticle (RCC). Structural modifications of the RCC at the primary root affect the diffusion barrier properties and lead to reduced rates of seedling establishment under osmotic stress and high salt conditions. Increased death of meristematic cells under high salt conditions indicates that the RCC protects the root meristem under stress conditions supporting thus seedling survival. RCC modifications at emerging lateral roots interfere with the process of lateral emergence as evidenced by a slower development of lateral roots and deformations of lateral root primordia reminiscent of organ adhesions. Our findings reveal a role for root caps in their early developmental stage and demonstrate that the RCC has equivalent physiological roles as the cuticle of the shoot.

RESULTS

A Cuticle Covers the Root Cap of the Primary Root

During the analysis of roots of 2-day-old *Arabidopsis thaliana* wild-type (WT) seedlings by transmission electron microscopy (TEM), we noticed that the surface of the cell wall of root cap cells was covered by an electron-opaque layer of 20 nm (18.5 ± 4.5 nm), resembling in thickness and ultrastructure the *Arabidopsis* leaf cuticle (Nawrath et al., 2013) (Figures 1A and 1B). This structure was not present at the root epidermis (Figures 1A and S1A).

The cuticle-like structure of the root cap was well defined from day 1 to 3 of seedling development, but less distinct at day 5, shortly before this first root cap layer is shed and replaced by the underlying, younger root cap layer (Figures 1A and S1B). The RCC was, however, already present at the radicle of the embryo (Figure S1C). Thus, the presence of this cell wall structure is tightly associated with the first root cap cell layer, which is formed during embryogenesis and shed from the seedling root ~5 days after germination (Dubreuil et al., 2018). The cuticle-like surface structure was also noticed in root caps of 2-day-old seedlings of *Brassica napus* and *Solanum lycopersicum* (Figure S1D), suggesting conservation of this root cap structure in higher plants.

In order to strengthen the hypothesis that this newly identified cell wall structure may be a layer containing aliphatic polyesters, fluorol yellow (FY), a dye staining aliphatic polyesters was used (Brundrett et al., 1991; Lux et al., 2005). FY stained the outer cell walls of root cap cells of 1- to 3-day-old WT seedlings (Figures 1B and S1B) but only rarely root caps of 5-day-old roots, confirming that only the first root cap layer generates a RCC (Figure S1B).

To discover the function of this transient RCC, the *CUTICLE DESTRUCTING FACTOR 1* (*CDEF1*) gene encoding an esterase of *Arabidopsis* able to degrade cutin and suberin (Barberon et al., 2016; Naseer et al., 2012; Takahashi et al., 2010) was expressed under the control of the promoter *pLOVE1* (*LOVE GLOVE1*), which is specifically active in the outermost layer of the root

Cell

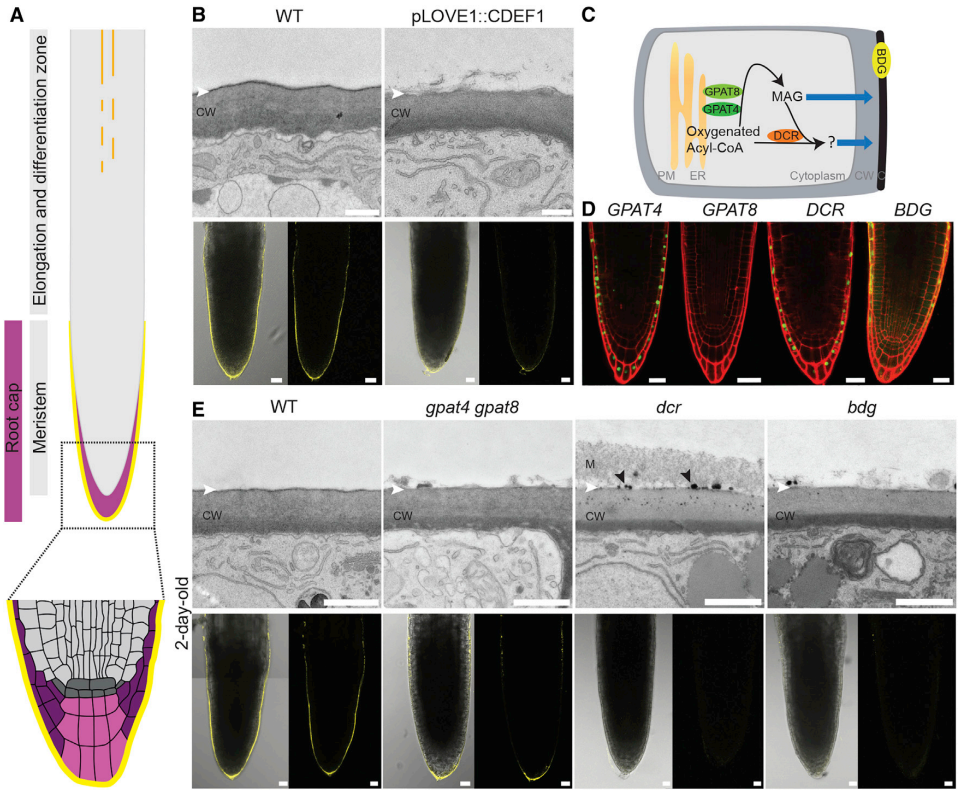

Figure 1. Evidence for a RCC at the Primary Root

(A) Schematic diagram highlighting polyester depositions in the roots of a 3-day-old *Arabidopsis* seedling. Orange, endodermal suberin; yellow, cuticle; pink, root cap cells. Enlargement: light gray, meristematic cells; dark gray, stem cells; light purple, columella cells; dark purple, lateral root cap cells; yellow, cuticle.

(B and E) TEM showing cell wall and cuticle of the outermost lateral root cap cells (top) and median views of the FY staining at the root cap of 2-day-old (B) WT and pLOVE1::CDEF1 plants and (E) WT and mutant plants affected in RCC biosynthesis (bottom; on the left, overlay bright field and fluorescence; on the right, fluorescence only). Scale bars in TEM pictures, 500 nm; in fluorescence micrographs, 20 μm. CW, cell wall; M, mucilage; white arrowhead, expected position of the cuticle; black arrowhead, methanol-soluble material. See also Figures S1 and S2.

(C) Simplified schematic diagram of the cutin biosynthetic pathway. Oxygenated acyl-CoA esters are generated at the endoplasmatic reticulum. They are metabolized by GPATs to monoacylglycerol and may be modified by DCR to precursors of unknown structure before being exported across the plasma membrane and the cell wall where cutin is formed in the cuticle, e.g., by the action of BDG. C, cuticle; CW, cell wall; ER, endoplasmatic reticulum; MAG, monoacylglycerol; PM, plasma membrane; blue arrow, export of precursors.

(D) Gene expression in transgenic plants expressing pGPAT::NLS-GFP-GUS, pDCR::NLS-GFP-GUS and pBDG::GFP at the root cap of a 2-day-old seedling. Scale bars, 20 μm.

cap. The root caps of 2-day-old plants expressing *pLOVE1::CDEF1* did not stain with FY and did not exhibit the electron-opaque cuticle-like layer in TEM (Figure 1B). Similarly, exogenously applied recombinant cutinase also removed the cuticle from the root cap (Figure S1E). Based on these findings, we classified the structural polyester of this newly discovered cell wall structure as a cutin.

Cutin Biosynthesis Genes Are Required for RCC Formation

We hypothesized if the RCC is made of cutin, then known cutin biosynthesis genes may be involved in its formation (Figure 1C). In fact, several genes that are required for the biosynthesis of cutin in organs of the shoot (i.e., *GPAT4*, *DCR*, and *BDG*) are also expressed in the root cap (Figure 1D). The *Arabidopsis* T-DNA knockout mutants *gpat4*, *dcr*, and *bdg* were selected for studying a putative role in RCC formation (Kurdyukov et al., 2006; Li et al., 2007; Panikashvili et al., 2009). Despite the absence of detectable *GPAT8* expression at the root cap (Figure 1C), *gpat8* and the *gpat4 gpat8* double mutants were also included in the study because *GPAT4* and *GPAT8* act redundantly in leaf cutin formation (Li et al., 2007). Impressively, no FY staining was visible at the RCC of *dcr* and *bdg* showing that *DCR* and *BDG* are required for RCC formation (Figure 1E). Similarly, the RCC of the *gpat4 gpat8* double mutant did not stain with FY (Figure 1E), while the RCC of the *gpat4* and *gpat8* single

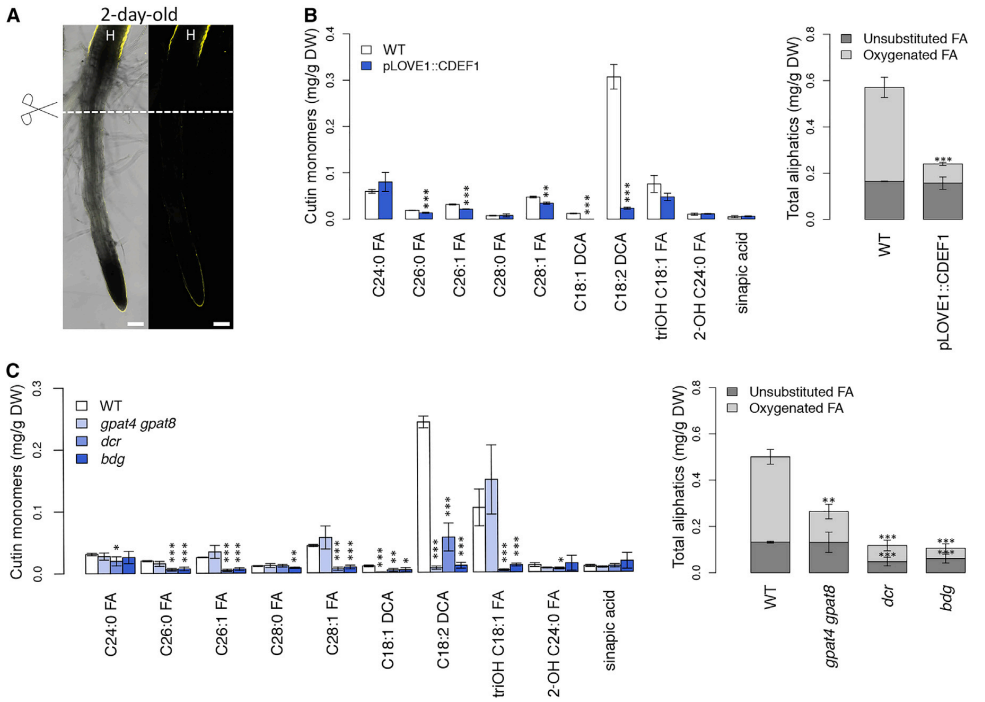

Figure 2. Composition of Cutin of the RCC at the Primary Root

(A) FY staining of the root of a 2-day-old seedling. H, hypocotyl; dashed line, point of sample excision for analysis. Scale bars, 100 μm.

(B and C) Quantification of aliphatic and aromatic ester-bond cutin monomers isolated from 2-day-old roots of (B) pLOVE1::CDEF1 plants and (C) RCC mutants, with their respective WT control. Left graph shows the principal cutin monomers and right graph shows the total of evaluated aliphatic compounds on the left grouped by substance classes. Values represent the means ± SD, n = 3–4. Asterisks denote significant differences to wild-type (WT) as determined by Student's t test: ***p < 0.001; **p < 0.01; *p < 0.05. FA, fatty acid; DCA, dicarboxylic acid; triOH C18:1 FA, 9,10,18-triOH C18:1 FA; DW, dry weight.

mutants stained as in WT (Figure S2A) demonstrating the redundant function of *GPAT4* and *GPAT8* in RCC formation.

TEM revealed that the RCC of *gpat4 gpat8* and *bdg* was less defined and had an eroded appearance (Figure 1E). In *dcr*, however, the continuous layer of cuticle was entirely absent and a broad layer of loose fibrous material, interpretated as mucilage, was present instead (Figure 1E). In addition, electron-dense globular structures were present within the outer half of the cell wall and at the cell wall-mucilage interface in the *dcr* mutant (Figure 1E). This material most likely consisted of unstructured and not completely polymerized cuticular lipids, because it was not visible when the sample was treated with methanol (Figure S2B). That the loosely attached fibrous material visible in TEM of the *dcr* mutant was indeed mucilage could be shown by immunolabeling with the xylogalacturonan-specific LM8 antibody that had been used previously to detect mucilage at *Arabidopsis* root cap cells (Durand et al., 2009) (Figure S2C). Our finding that genes necessary for cutin formation in leaves of *Arabidopsis* were also required for RCC formation further supports its structural analogy with the leaf cuticle.

Moreover, the receptor kinases GASSHO1/SCHENGEN3 (GSO1) and GASSHO2 (GSO2), acting redundantly in cuticle formation of the shoot (Tsuwamoto et al., 2008), act also together in RCC formation, as identified by FY staining (Figures S2D and S2E). TEM revealed, however, that the *gso1 gso2* double mutant has in addition to the disrupted cuticle strong modifications of the cell wall of the outer root cap cell layer (Figure S2E). Modifications of the RCC were also visible in the *smb* mutant defective in the root cap maturation process in TEM as well as by FY staining (Figure S2E).

In summary, RCC formation displays many parallels to shoot cuticle formation, in particular in cotyledons and leaves, but it is also integrated in the regulatory circuits of root cap maturation.

The Polyester of the RCC Represents an Atypical Cutin

In order to characterize the polyesters present in the RCC in more detail, the composition of the esterified lipids and aromatic acids bound to the cell wall were analyzed from root tips of 2-day-old *Arabidopsis* seedlings of different genotypes. We confirmed that at this age the endodermis was not yet suberized (Figure 2A), thus the entire lower root section could be used for the analysis. The most abundant oxygenated monomers of the cutin in the RCC were α,ω-octadecadiendioic acid (C18:2 DCA) and 9,10,18-trihydroxy octadecenoic acid (9,10,18-triOH

C18:1 FA) (Figures 2B and 2C), which are not present in endodermal suberin (Barberon et al., 2016). Despite these monomers indicating a C18 class cutin, very-long chain fatty acids of 26 and 28 carbons in length and their monounsaturated homologs were also present in considerable amounts, which is unusual for cutin (Figures 2B and 2C). Similarly unusual was that *p*-coumaric and ferulic acid, often present in cutin, could not be detected. Instead, sinapic acid was present as the only aromatic ester-bound compound. In summary, despite a high amount of oxygenated C18 fatty acids classically found in cutin, several atypical components were identified in the cell wall-bound ester fraction of the RCC.

In transgenic pLOVE1::CDEF1 plants expressing a cutinase specifically in root cap cells, predominant oxygenated fatty acids were reduced by 80%, while unsubstituted fatty acids as well as sinapic acid were not substantially altered (Figure 2B). In the *gpat4 gpat8* double mutant, the C18:2 DCA was reduced by more than 95% (Figure 2C). The *dcr* and *bdg* mutants showed both a strong reduction in oxygenated fatty acids and a less pronounced reduction of unsubstituted FAs (Figure 2C).

Taken together, the cutin in the RCC of the primary root has an atypical fatty acid composition requiring *GPAT4* and *GPAT8* as well as *DCR* and *BDG* for its synthesis, all of them also required for cutin formation in organs of the shoot.

The Emerging Lateral Root Is Also Covered by a Cuticle

Whether a cuticle is also present at the lateral root was investigated by TEM in 8-day-old WT *Arabidopsis* plants. An electron-opaque cuticle covered the cell wall of the outer most cell layer of the root cap of the lateral root before emergence and after emergence from the primary root (Figures 3A and 3B) that was thicker (36 ± 2.5 nm) than in primary roots. The RCC of the lateral roots stained in WT with FY, similar as in primary roots (Figure 3D). When the lateral root was fully differentiated, the FY staining was specific to the area of the root cap (Figure S3A).

The cutin biosynthesis genes *GPAT4* and *GPAT8* were also expressed at the outermost root cap cell layer in the developing lateral root (Figure 3C). Furthermore, gene expression of *BDG* and *DCR* had equally been reported at the lateral root tip (Jakobson et al., 2016; Panikashvili et al., 2009). Recently emerged lateral roots of *dcr*, *bdg*, and the *gpat4 gpat8* double mutant were characterized by TEM and subjected to the FY staining procedure. In contrast to a strong electron-opaque RCC in WT, the RCC of recently emerged lateral roots in *bdg* and the *gpat4 gpat8* was eroded and did not stain with FY (Figure 3D). *gpat4* and *gpat8* single mutants stained normally (Figure S3B). By contrast, the RCC of *dcr* mutants displayed alternating areas of electron-opaque cuticle and occasional disruptions, but still stained with FY (Figure 3D).

In summary, a cuticle covers root caps of both lateral and primary roots but differences in dimension, ultrastructure, and FY affinity in mutant genotypes indicate a different molecular structure and composition between the two RCCs.

Diffusion Barrier Properties Are Impaired in RCC Mutants

A hallmark of the role of the cuticle of aerial organs is to build a diffusion barrier (Schreiber, 2010). Barrier properties of the RCCs were assessed by dye diffusion assays across the cuticle using toluidine blue and fluorescein diacetate (Barberon et al., 2016; Li et al., 2007; Tanaka et al., 2004). Toluidine blue binds directly to anionic compounds that are present in the cell and in the apoplast (including pectic polysaccharides), while fluorescein diacetate is a cellular tracer that fluoresces only after uptake and cleavage in a living cell. Fluorescein diacetate allows live staining of single roots to highlight dynamic differences in staining between genotypes, while toluidine blue allows the simultaneous assessment of many roots (stained versus not stained).

Staining of the meristem of the primary root with fluorescein diacetate was too fast to allow the characterization of the RCC of the primary root by confocal microscopy (faster than 10 s). The permeability of the RCC of the primary root was thus assessed with toluidine blue in 2-day-old seedlings. In *Arabidopsis* WT plants, the number of roots having a stained meristem increased steadily between 20 s and 135 s, the time when the meristems of all the investigated roots were stained (Figure 4A). In contrast, a comparable staining of all root meristems was observed in pLOVE1::CDEF1 plants and the RCC mutants *bdg* and *dcr* already after 10 s and in the *gpat4 gpat8* double mutant after 20 s demonstrating diminished barrier properties of the RCC of the primary root in these genotypes (Figure 4A).

The barrier properties of the RCC of recently emerged lateral roots could be assessed by fluorescein diacetate. The tip of these lateral roots of WT did not show any fluorescence after a 4-min long incubation in fluorescein diacetate. In contrast, all the mutants that had modifications in the ultrastructure of the RCC at recently emerged lateral roots (i.e., *gpat4 gpat8*, *bdg*, and *dcr*) showed a clear fluorescence signal after a 4-min long incubation period demonstrating their diminished diffusion barrier properties. The strength of fluorescence depended on the genotype being the weakest in *gpat4 gpat8* and the strongest in *bdg* (Figure 4D).

In summary, both the RCC of the primary root as well as of the recently emerged lateral root provide barrier functions limiting the diffusion of molecules.

The RCC of the Primary Root Protects the Seedling against Harmful Compounds

Whether the diffusion barrier properties of the RCC of the primary root may be able to contribute to seedling establishment under abiotic stress conditions was tested in transgenic pLOVE1::CDEF1 lines. CDEF1 expression was restricted to the outermost cell layer of the radicle and young root, thus generating specifically a defective RCC. Mutants in cutin biosynthesis are affected in the deposition of several polyesters present in the seeds and are thus less suitable for these analyses (De Giorgi et al., 2015; Molina et al., 2008; Panikashvili et al., 2009). The development of transgenic pLOVE1::CDEF1 plants barely differed to WT under standard growth conditions. They were, however, much more strongly affected than WT by high salt concentrations (i.e., 100 mM NaCl, 75 mM K_2SO_4, and 100 mM KCl) or the osmotically active compound mannitol (250 mM) (Figure 4B) indicating that the RCC may protect establishing seedlings of harmful compounds.

Whether the RCC protects the meristematic cells of harmful components was investigated in the presence of NaCl because

Please cite this article in press as: Berhin et al., The Root Cap Cuticle: A Cell Wall Structure for Seedling Establishment and Lateral Root Formation, Cell (2019), https://doi.org/10.1016/j.cell.2019.01.005

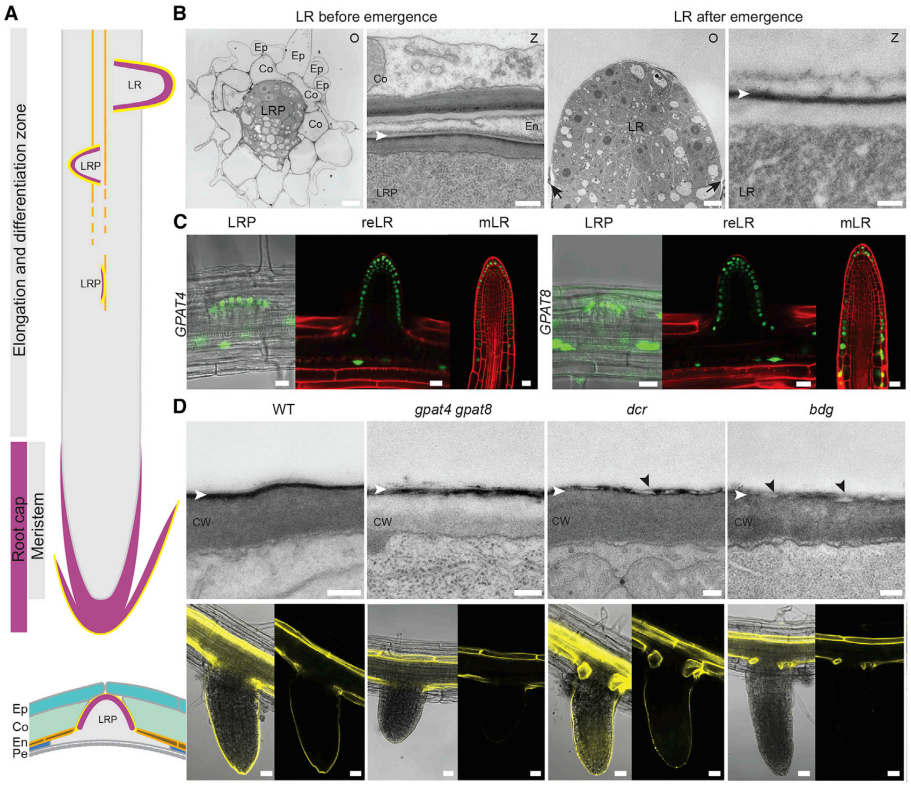

Figure 3. Evidence for a RCC at the Young Lateral Root

(A) Schematic diagram highlighting polyester depositions in a 5-day-old *Arabidopsis* seedling losing the first root cap cell layer. Orange, patchy and continuous suberin deposition; yellow, cuticle; pink, root cap cells. LRP, lateral root primordium; LR, lateral root; Co, cortical cell; En, endodermal cells; Ep, epidermal cell; Pe, pericycle.

(B) TEM showing the lateral root of WT before and after emergence. An overview (O) and an enlarged view (Z) of cell wall and cuticle at the root cap is given. The overview showing the lateral root before emergence was stitched together from multiple TEM pictures. Scale bars, 7 μm in O and 250 nm in Z. For details, see legend of (A); black arrow, cell wall of epidermal cells of the primary root; white arrowhead, expected position of the cuticle.

(C) Gene expression in transgenic plants expressing pGPAT::NLS-GFP-GUS at the lateral root of a 8-day-old seedling. LRP, lateral root promordium; reLR, recently emerged lateral root; mLR, maturelateral root. Scale bars, 20 μm.

(D) TEM pictures showing cell wall and cuticle (top) and median views of the FY staining of the developing lateral root of WT and mutant plants affected in RCC formation after emergence (bottom; on the left, overlay bright field and fluorescence; on the right, fluorescence only). FY stained the suberin of the endodermis and the RCC, when present. Scale bars, 200 nm in TEM pictures; 20 μm in pictures showing FY staining. CW, cell wall; white arrowhead, expected position of the cuticle; black arrowhead, eroded cuticle.

See also Figures S3A and S3B.

the excess of Na^+ ions is known to be toxic for cells and lead to cell death in *Arabidopsis* root tips (Olvera-Carrillo et al., 2015; Zhu, 2016). Propidium iodide, which only enters cells having a compromised plasma membrane integrity was used to identify the presence of dead cells (Truernit and Haseloff, 2008). In the presence of 140 mM NaCl, we found significantly more cell death in the root meristem of 2-day-old pLOVE1::CDEF1 seedlings than in WT (Figure 4C).

In summary, the RCC of the primary root having diffusion barrier functions protect the meristematic cells from toxic compounds during the vulnerable growth stage of seedling establishment.

RCC Defects at Lateral Root Primordia Lead to Delayed Outgrowth of Lateral Roots

Because genes involved in RCC formation of lateral roots are already expressed before lateral root emergence, and the cuticle is well-defined while the lateral root invades the tissues of the primary root (Figure 3B), we investigated whether the RCC of the lateral root primordium may play a role in the process of lateral root emergence. When lateral root initiation was synchronized in vertically growing roots by turning the agar plates by 90° (Voß et al., 2015), the majority of the lateral roots of WT had emerged after 42 h, while the lateral primordia of *gpat4 gpat8*, *dcr*, and *bdg* were still in the outer tissue layers of the primary root (Figure 4E).

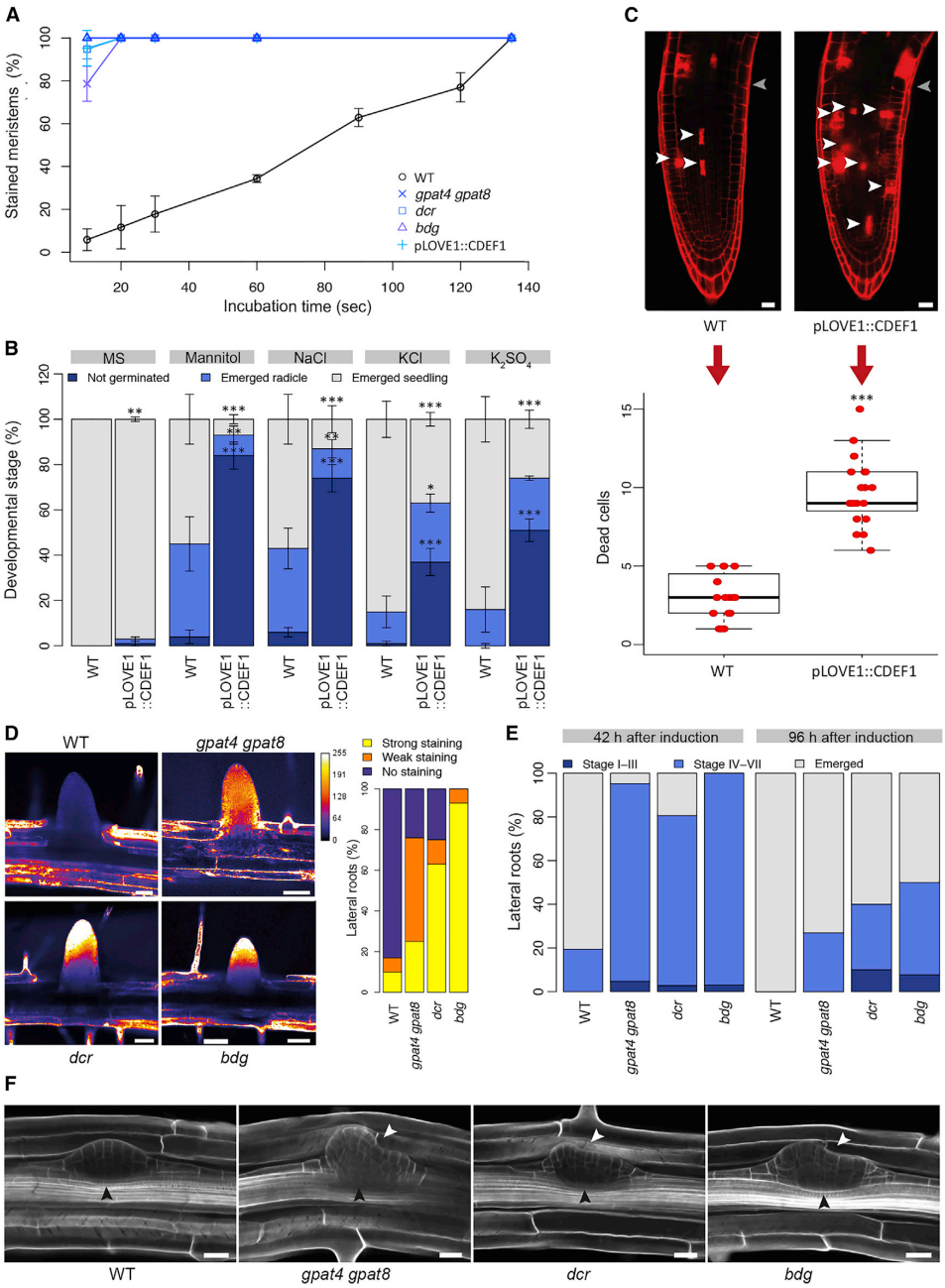

Figure 4. Diffusion Barrier Properties and Biological Roles of RCCs

(A) Penetration of toluidine blue into the meristem of 2-day-old seedlings of different genotypes. Values represent the mean ± SD of the number of stained meristems in a seedling population at indicated time points.

(B) Role of the RCC of primary roots in seed germination and seedling establishment illustrated by studying the impact of mannitol (250 mM), NaCl (100 mM), KCl (100 mM), and K_2SO_4 (75 mM) in the medium during early root development stages on WT and pLOVE1::CDEF1 plants. Values represent the mean ± SD of the

(legend continued on next page)

Even after 96 h, a certain number of lateral root primordia of the RCC mutants had not yet broken through the epidermis, even when the outgrowth process had further advanced, demonstrating a severe retardation of the lateral root emergence process in mutants having RCC defects at lateral root primordia (Figure 4E).

Cuticles of the shoot play an important role during the development of organs by preventing surface interactions when plant organs are in tight contact because cuticle impairments may lead to organ adhesions and fusions (Ingram and Nawrath, 2017). Therefore, we investigated the shape of lateral root primordia during the lateral root emergence process. Deformations of lateral root primordia occurred during the passage through the cortex layer in all three genotypes having RCC modifications at the lateral root primordia (Figures 4F and S3). Such deformations could never be observed at lateral root primordia of WT (Figures 4F and S3). Deformed lateral root primordia could be observed in 5%–11% of the total investigated roots at early (42 h and 48 h) observation times and were not more, but rather less frequent at later observation times (96 h) (2%–7%) indicating that they were a transient phenomenon during the emergence process. The deformations of the lateral root primordia in RCC mutants suggest that the RCC facilitates invasive growth of the lateral root primordia by reducing cell surface interactions causing organ adhesions.

DISCUSSION

The RCC Defines an Early Developmental Stage of Root Caps

Up to now, the root cap has been understood as a structure secreting mucilage and releasing their older cells as single border cells or cell clusters (Barlow, 2002). While this is true for root caps with rapid cell turn-over, our ultrastructure analysis of the cell wall of root caps before the onset of the root cap turnover cycle has revealed an as yet undocumented structure, the root cap cuticle (RCC). Because the RCC is only present on the very first root cap cell layer of primary and lateral roots, it defines a specific developmental and physiological state of root caps.

The Formation of the RCC Is Integrated in Root Cap Cell Differentiation

The receptor kinases GSO1 and GSO2 are required for establishing epidermis-specific functions of cotyledons during embryo development and during seedling establishment in *Arabidopsis* (Tsuwamoto et al., 2008; Xing et al., 2013). Both GSO1 and GSO2 are also essential for the proliferation and differentiation of root cell types in young seedlings, including columella and lateral root cap cells (Racolta et al., 2014). The *gso1 gso2* double mutant, but not both single mutants, has an interrupted RCC at the primary root indicating that *GSO1* and *GSO2* act redundantly in RCC formation. An adherence of the endosperm to the embryo was documented in embryos of the *gso1 gso2* double mutant (Moussu et al., 2017), indicating that these genes are important for generating the appropriate surface structure of organs before and after seedling germination. Interestingly, *GSO2* exhibits an intriguing change in expression from strong root cap expression at 3 days after germination (i.e., when the root cap has a cuticle) to none at 6 days after germination (i.e., when root cap cells have no RCC anymore) (Racolta et al., 2014). This expression pattern underscores that the root cap of young establishing seedlings has different characteristics than the one of older plants.

An additional argument that the formation of the RCC is tightly regulated during the development and differentiation of root cap cells is that the *smb* mutant having a delayed maturation of root cap cells has also a defective RCC (Bennett et al., 2010).

The *Arabidopsis* RCC Consists of a Particular Cutin

The ultrastructure of the RCC was visualized as an electron-opaque layer that resembled the leaf cuticle of *Arabidopsis* WT plants (Nawrath et al., 2013). Indeed, the cutin of the RCC was rich in two components: (1) C18:2 DCA that is the predominate cutin monomer in *Arabidopsis* leaves, but is rather atypical for cutin within the plant kingdom (Bonaventure et al., 2004; Franke et al., 2005), and (2) 9,10,18-triOH C18:1 FA that is a prominent cutin monomer in many species (Beisson et al., 2012; Kolattukudy, 2001a), but is typically absent from any *Arabidopsis* shoot cuticle. As in other organs of *Arabidopsis*, *GPAT4* and *GPAT8* were required for the incorporation of C18:2 DCA in the polyester of the RCC (Li et al., 2007). The incorporation of 9,10,18-triOH C18:1 FA depended strongly on DCR emphasizing the important role of this acyltransferase for the incorporation of mid-chain hydroxylated fatty acids into cutin (Lashbrooke et al., 2016; Panikashvili et al., 2009). BDG plays an important role for the incorporation of C18:2 DCA into cutin of *Arabidopsis* leaves and flowers but leading only to moderate (40%–50%) reductions in the polyester amount of these organs in *bdg* (Jakobson et al., 2016). Here, we

number of seedlings of each genotype having the indicated stage when grown in the presence of the respective compound. Significant differences to WT were determined by Student's t test: ***$p < 0.001$; **$p < 0.01$; *$p < 0.05$.

(C) Salt-induced cell death in the meristem of 2-day-old root of WT and pLOVE1::CDEF1 plants. Dead cells present after a 10-min-long incubation in 140 mM NaCl are visualized by propidium iodide staining. Top: Pictures show the median section of the root tip. White arrowhead, dead cell; gray arrowhead, superior limit of the meristematic zone. Scale bars, 20 μm. Bottom: The number of dead cells present in the entire meristematic zone of each root (as assessed via a z stack) are presented as boxplot. Individual data points are shown as dots. Asterisks denote significant differences to WT as determined by Student's t test: ***$p < 0.001$.

(D) Penetration of the fluorescent cellular tracer fluorescein diacetate into root cap cells and meristematic cells of shortly emerged lateral roots of different genotypes after 4 min of incubation. Relative intensity of the fluorescence is depicted by the color code. Scale bars, 50 μm. Quantitative evaluation is given in the graph to the right showing the number of shortly emerged lateral roots having the indicated staining intensity.

(E and F) Role of the RCC at the lateral root primordium during lateral root emergence. (E) Stages of lateral root primordia 42 h and 96 h after induction were evaluated in WT and in different mutant genotypes having a modified RCC at the lateral root primordium. Stages were determined as described in Casimiro et al. (2003): stage I–III, before breakage into the cortex; stage IV–VII, within the outer layers of the primary root; emerged. (F) Shape of lateral root primordia in WT and different genotypes having a modified RCC at the emerging lateral root. Regular shape of a lateral root primordium of WT. Deformed lateral root primordia of genotypes having RCC modifications at the lateral root. Black arrowhead, lateral root primordium; white arrowhead, primordium deformation. Scale bars, 20 μm. See also Figure S3C.

showed that BDG is also required for the incorporation for 9,10,18-triOH C18:1 FA into cutin resulting in a particular strong reduction (80%) in the total polyester content of the RCC of primary roots in *bdg*. Overall, the incorporation of oxygenated monomers into cutin of the RCC occurs very well in accordance with our current understanding of cutin synthesis in *Arabidopsis* (Fich et al., 2016; Nawrath et al., 2013). In the future, the RCC might be a useful tool for studying the incorporation and the functional relevance of its atypical polyester monomers (i.e., C26 and C28 acids as well as sinapic acid).

The RCC had a different ultrastructure during the course of development of root cap cells analogous to maturing cuticles in aerial tissues. In aerial tissues, changes in the cuticle ultrastructure are associated with changes in cutin composition, structure, and properties (Fabre et al., 2016; Jeffree, 2006; Nawrath et al., 2013), which still would need to be investigated in more detail for the RCC.

The RCCs of Primary and Emerging Lateral Roots Form a Diffusion Barrier

One of the principal and best-studied features of cuticles of the shoot is that they form a diffusion barrier separating the respective plant organ from the surrounding environment (Riederer, 2006). The barrier properties of the cuticle of different species and organs of the same species vary widely (Schreiber and Schönherr, 2009). Nevertheless, the cuticles have protective functions in their respective cellular context. The incubation time necessary to stain the meristem below the RCC of the primary root was shorter than for tissues below shoot cuticles grown under similar conditions (Moussu et al., 2017; Tanaka et al., 2004). The cellular processes in root cap cells as well as the environmental conditions below-ground differ from shoots where cuticles are in an aerial environment. This might explain why the RCCs evolved different properties. It may also be an argument for aliphatic wax molecules, typically associated with leaf cuticles, being the important determinant for the transport barrier properties of cuticles, more than the amount and composition of the cutin polyester itself (Kosma et al., 2009; Schreiber, 2010; Zeisler-Diehl et al., 2018). Whether the cutin in the RCC is associated with some type of waxes remains to be elucidated.

The RCC of the Primary Root Protects the Root Meristem

The cuticle of the shoot with its function as diffusion barrier influences the uptake and loss of a wide variety of molecules, including water, nutrients, volatiles, and toxic compounds (Riederer, 2006; Schreiber and Schönherr, 2009; Valeska Zeisler-Diehl et al., 2017). The hypersensitivity of plants having a permeable RCC to hyperosmotic conditions and salt stress indicate that the RCC has similar broad functions as diffusion barrier at the root cap during seedling establishment. Because diffusion barriers function in both directions (i.e., in uptake and loss of solutes), the RCC may prevent an even faster water loss under osmotic stress conditions that would cause an irreversible cell damage. During salt stress, not only water is lost by the osmotic differential, but also ions will diffuse into the plant reaching toxic concentrations faster than when a RCC is present. Higher death rates of meristematic cells in the presence of toxic concentrations of NaCl could be observed in pLOVE1::CDEF1 plants supporting this hypothesis. Even though a transient structure, the results point to crucial role of the RCC of primary roots in protecting the meristem in the stage when it is very small and highly susceptible to stress conditions and thus gives the seedling some time to adapt and to put other protective mechanisms in place (Zhu, 2016).

Cuticles of the shoot are also implicated in the interaction of plants with its microbial environment. Susceptibility or resistance of the plant are the outcome of complex processes that are not predictable solely based on structure, amount, and composition of the cuticle (Ziv et al., 2018). Sensitivity of seedling establishment toward biotic stresses has recently been shown by inhibition of germination in the presence of bacterial pathogens (Chahtane et al., 2018). Whether the protective functions of the RCC will also extend to the interaction with the biotic environment will be a topic of future studies.

The RCC of the Lateral Root Promotes Lateral Root Emergence

Lateral root formation, one of the key steps for the adaptive remodeling of root system architecture, determines the efficiency of the root in nutrient acquisition. The mechanisms of lateral root emergence are therefore a focus of current plant research (Stoeckle et al., 2018; Van Norman et al., 2013; Vilches-Barro and Maizel, 2015). Lateral root emergence is an invasive growth process (Marsollier and Ingram, 2018) because the lateral root primordia, initiated at the pericycle deeply within the primary root, have to penetrate through the different overlying tissue layers to emerge (Figure 3A). During the entire emergence process the lateral root primordium is in very tight contact with the surrounding tissue layers. Therefore, the presence of a substance functioning as "lubricant" during lateral root emergence has been hypothesized (Marsollier and Ingram, 2018). Here, we showed that lateral roots having impairments in the RCC of the primordium are strongly slowed down during the emergence process and have deformations giving experimental evidence for a role of the RCC of the lateral root primordia in the prevention of surface interactions of different organs.

The cuticle of aerial organs has important functions in the prevention of organ adhesions during plant development that manifest themselves in organ deformations (e.g., during the rapid outgrowth of petals from the floral bud) (Ingram and Nawrath, 2017). Under certain circumstances, fusions between organs of the shoot may be seen in plants having a permeable shoot cuticle that are characterized by the formation of a single cell wall between the organs and tissue breakage when the fusion is disrupted (Nawrath et al., 2013). In the investigated RCC mutants, no signs have been observed that deformations at the lateral root primordium were solved by tissue breakage or remained permanent, but instead a decrease in the number of organ deformations over time, indicating that organ adhesions, not organ fusions, occurred.

Interestingly, the radicle of the *gso1 gso2* double mutant did not separate from the endosperm (Moussu et al., 2017) suggesting that a cuticular structure on the radicle might have similar functions in preventing organ adhesions during embryo development.

Conclusions

Plant cuticles of different aerial organs have been studied since the middle of the 19th century and have so far been exclusively associated with epidermal tissues of the shoot. Suberin lamellae, by contrast, have been seen in many other tissues of shoots and roots (Holloway, 1982b; Kolattukudy, 1980; Pollard et al., 2008). Therefore, it has been deduced that only shoot epidermal cells and protodermal cells of the embryo, as their precursor, can synthetize a cuticle, and not root tissues (Barlow, 2002). Our discovery of a cuticle at the root cap now challenges this dogma.

The RCC of young primary roots and emerging lateral roots play important roles in root physiology and development. During the critical first days after germination, the RCC serves as a diffusion barrier, protecting the vulnerable seedling meristem and giving thus the seedling some time to adapt to environmental challenges. In lateral root formation, the RCC serves as a specialized surface structure that prevents adhesions of newly forming organs, similar as the cuticle of aerial organs does. The discovery of the RCC adds a new element to our understanding of root anatomy, development, and physiology.

STAR★METHODS

Detailed methods are provided in the online version of this paper and include the following:

- KEY RESOURCES TABLE
- CONTACT FOR REAGENT AND RESOURCE SHARING
- EXPERIMENTAL MODEL AND SUBJECT DETAILS
  - Plant material
  - Growth conditions
- METHOD DETAILS
  - Generation of constructs
  - Cutin digestion, cuticle staining and permeability assays
  - Germination and root growth assays
  - Immunofluorescence labeling
  - Fluorescence Microscopy
  - Transmission electron microscopy
  - Chemical analyses
- QUANTIFICATION AND STATISTICAL ANALYSIS

SUPPLEMENTAL INFORMATION

Supplemental Information includes four figures and one table and can be found with this article online at https://doi.org/10.1016/j.cell.2019.01.005.

ACKNOWLEDGMENTS

We greatly appreciated helpful discussions and technical advice of Robertas Ursache, Tonni Anderson, Peter Marhavy, Evangelia Vogiatzaki, Steven Moussu, and Gwyneth Ingram. Particular thanks go to Niko Geldner and Marie Barberon for their discussions, sharing of unpublished information, and critical comments on the manuscript. Furthermore, we thank Willy Blanchard for his contribution to the artwork. The NASC stock center, Fred Beisson, Gwyneth Ingram, Liina Jakobson, and Niko Geldner are thanked for providing us with seed stocks and Mario Serrano for supplying us with cutinase. Furthermore, we thank Bruno Humbel and Arnaud Paradis for leading the Electron Microscopy Facility and the Imaging Facility of UNIL, respectively. This work was supported by the Swiss National Science Foundation (31003A_170127 to C.N.) and the ERC (starting grant PROCELLDEATH; Project Number 639234 to M.K.N.).

AUTHOR CONTRIBUTIONS

Conceptualization, A.B., C.N., and M.K.N.; Methodology, A.B. and D.d.B.; Investigation, A.B. and D.d.B., Validation, A.B., R.B.F., and C.N.; Resources, R.A.B. and M.K.N.; Writing–Initial Draft, C.N.; Writing–Review & Editing, A.B., M.K.N., and R.B.F., Visualization, A.B., Supervision and Funding Acquisition, C.N.

DECLARATION OF INTERESTS

The authors declare no competing interests.

Received: June 30, 2018
Revised: November 23, 2018
Accepted: January 2, 2019
Published: February 14, 2019

REFERENCES

Alberts, B., Johnson, A., Lewis, J., Morgan, D., Raff, M., Roberts, K., and Walter, P. (2015). Molecular Biology of the Cell, Sixth Edition (Garland Science, Taylor and Francis Group).

Ali, M.A., Shah, K.H., and Bohlmann, H. (2012). pMAA-Red: a new pPZP-derived vector for fast visual screening of transgenic Arabidopsis plants at the seed stage. BMC Biotechnol. *12*, 37.

Andersen, T.G., Barberon, M., and Geldner, N. (2015). Suberization - the second life of an endodermal cell. Curr. Opin. Plant Biol. *28*, 9–15.

Bakan, B., and Marion, D. (2017). Assembly of the cutin polyester: from cells to extracellular cell walls. Plants (Basel) *6*, E57.

Barberon, M., Vermeer, J.E.M., De Bellis, D., Wang, P., Naseer, S., Andersen, T.G., Humbel, B.M., Nawrath, C., Takano, J., Salt, D.E., and Geldner, N. (2016). Adaptation of root function by nutrient-induced plasticity of endodermal differentiation. Cell *164*, 447–459.

Barlow, P.W. (2002). The root cap: cell dynamics, cell differentiation and cap function. J. Plant Growth Regul. *21*, 261–286.

Beisson, F., Li-Beisson, Y., and Pollard, M. (2012). Solving the puzzles of cutin and suberin polymer biosynthesis. Curr. Opin. Plant Biol. *15*, 329–337.

Bennett, T., van den Toorn, A., Sanchez-Perez, G.F., Campilho, A., Willemsen, V., Snel, B., and Scheres, B. (2010). SOMBRERO, BEARSKIN1, and BEARSKIN2 regulate root cap maturation in Arabidopsis. Plant Cell *22*, 640–654.

Bonaventure, G., Beisson, F., Ohlrogge, J., and Pollard, M. (2004). Analysis of the aliphatic monomer composition of polyesters associated with Arabidopsis epidermis: occurrence of octadeca-cis-6, cis-9-diene-1,18-dioate as the major component. Plant J. *40*, 920–930.

Brundrett, M.C., Kendrick, B., and Peterson, C.A. (1991). Efficient lipid staining in plant material with sudan red 7B or fluorol [correction of fluoral] yellow 088 in polyethylene glycol-glycerol. Biotech. Histochem. *66*, 111–116.

Casimiro, I., Beeckman, T., Graham, N., Bhalerao, R., Zhang, H., Casero, P., Sandberg, G., and Bennett, M.J. (2003). Dissecting Arabidopsis lateral root development. Trends Plant Sci. *8*, 165–171.

Chahtane, H., Nogueira Füller, T., Allard, P.M., Marcourt, L., Ferreira Queiroz, E., Shanmugabalaji, V., Falquet, J., Wolfender, J.L., and Lopez-Molina, L. (2018). The plant pathogen *Pseudomonas aeruginosa* triggers a DELLA-dependent seed germination arrest in *Arabidopsis*. eLife *7*, e37082.

Clough, S.J., and Bent, A.F. (1998). Floral dip: a simplified method for Agrobacterium-mediated transformation of *Arabidopsis thaliana*. Plant J. *16*, 735–743.

De Giorgi, J., Piskurewicz, U., Loubery, S., Utz-Pugin, A., Bailly, C., Mène-Saffrané, L., and Lopez-Molina, L. (2015). An endosperm-associated cuticle is

required for Arabidopsis seed viability, dormancy and early control of germination. PLoS Genet. *11*, e1005708.

Doblas, V.G., Geldner, N., and Barberon, M. (2017). The endodermis, a tightly controlled barrier for nutrients. Curr. Opin. Plant Biol. *39*, 136–143.

Dominguez, E., Mercado, J.A., Quesada, M.A., and Heredia, A. (1999). Pollen sporopollenin: degradation and structural elucidation. Sex. Plant Reprod. *12*, 171–178.

Dubreuil, C., Jin, X., Grönlund, A., and Fischer, U. (2018). A local auxin gradient regulates root cap self-renewal and size homeostasis. Curr. Biol. *28*, 2581–2587.e3.

Durand, C., Vicré-Gibouin, M., Follet-Gueye, M.L., Duponchel, L., Moreau, M., Lerouge, P., and Driouich, A. (2009). The organization pattern of root border-like cells of Arabidopsis is dependent on cell wall homogalacturonan. Plant Physiol. *150*, 1411–1421.

Fabre, G., Garroum, I., Mazurek, S., Daraspe, J., Mucciolo, A., Sankar, M., Humbel, B.M., and Nawrath, C. (2016). The ABCG transporter PEC1/ABCG32 is required for the formation of the developing leaf cuticle in Arabidopsis. New Phytologist *209*, 192–201.

Fendrych, M., Van Hautegem, T., Van Durme, M., Olvera-Carrillo, Y., Huysmans, M., Karimi, M., Lippens, S., Guérin, C.J., Krebs, M., Schumacher, K., and Nowack, M.K. (2014). Programmed cell death controlled by ANAC033/SOMBRERO determines root cap organ size in Arabidopsis. Curr. Biol. *24*, 931–940.

Fich, E.A., Segerson, N.A., and Rose, J.K.C. (2016). The plant polyester cutin: biosynthesis, structure, and biological roles. Annu. Rev. Plant Biol. *67*, 207–233.

Franke, R., Briesen, I., Wojciechowski, T., Faust, A., Yephremov, A., Nawrath, C., and Schreiber, L. (2005). Apoplastic polyesters in Arabidopsis surface tissues–a typical suberin and a particular cutin. Phytochemistry *66*, 2643–2658.

Franke, R.B., Dombrink, I., and Schreiber, L. (2012). Suberin goes genomics: use of a short living plant to investigate a long lasting polymer. Front. Plant Sci. *3*, 4.

Geldner, N. (2013). The endodermis. Annu. Rev. Plant Biol. *64*, 531–558.

Holloway, P.J. (1982a). The chemical constitution of plant cutins. In The Plant Cuticle, D.F. Cutler, K.L. Alvin, and C.E. Price, eds. (Academic Press), pp. 45–86.

Holloway, P.J. (1982b). Structure and histochemistry of plant cuticular membranes: An overview. In The Plant Cuticle, D.F. Cutler, K.L. Alvin, and C.E. Price, eds. (Academic Press), pp. 1–32.

Ingram, G., and Nawrath, C. (2017). The roles of the cuticle in plant development: organ adhesions and beyond. J. Exp. Bot. *68*, 5307–5321.

Jakobson, L., Lindgren, L.O., Verdier, G., Laanemets, K., Brosché, M., Beisson, F., and Kollist, H. (2016). BODYGUARD is required for the biosynthesis of cutin in Arabidopsis. New Phytol. *211*, 614–626.

Jeffree, C.E. (2006). The fine structure of the plant cuticle. In Biology of the Plant Cuticle, M. Riederer and C. Müller, eds. (Blackwell Publishing), pp. 11–125.

Kolattukudy, P.E. (1980). Cutin, suberin and waxes. In The Biochemistry of Plants,, *vol. IV*, P.K. Stumpf, ed. (Academic Press), pp. 571–645.

Kolattukudy, P.E. (2001a). Cutin from plants. In Biopolymers, Y. Doi and A. Steinbüchel, eds. (Wiley-VCH), pp. 1–35.

Kolattukudy, P.E. (2001b). Suberin from plants. In Biopolymers, Y. Doi and A. Steinbüchel, eds. (Wiley-VCH), pp. 41–68.

Kosma, D.K., Bourdenx, B., Bernard, A., Parsons, E.P., Lü, S., Joubès, J., and Jenks, M.A. (2009). The impact of water deficiency on leaf cuticle lipids of Arabidopsis. Plant Physiol. *151*, 1918–1929.

Kumpf, R.P., and Nowack, M.K. (2015). The root cap: a short story of life and death. J. Exp. Bot. *66*, 5651–5662.

Kurdyukov, S., Faust, A., Nawrath, C., Bär, S., Voisin, D., Efremova, N., Franke, R., Schreiber, L., Saedler, H., Métraux, J.P., and Yephremov, A. (2006). The epidermis-specific extracellular BODYGUARD controls cuticle development and morphogenesis in Arabidopsis. Plant Cell *18*, 321–339.

Lashbrooke, J., Cohen, H., Levy-Samocha, D., Tzfadia, O., Panizel, I., Zeisler, V., Massalha, H., Stern, A., Trainotti, L., Schreiber, L., et al. (2016). MYB107 and MYB109 homologues regulate suberin deposition in angiosperms. Plant Cell *28*, 2097–2116.

Li, Y., Beisson, F., Koo, A.J.K., Molina, I., Pollard, M., and Ohlrogge, J. (2007). Identification of acyltransferases required for cutin biosynthesis and production of cutin with suberin-like monomers. Proc. Natl. Acad. Sci. USA *104*, 18339–18344.

Li-Beisson, Y., Shorrosh, B., Beisson, F., Andersson, M.X., Arondel, V., Bates, P.D., Baud, S., Bird, D., Debono, A., Durrett, T.P., et al. (2013). Acyl-lipid metabolism. Arabidopsis Book *11*, e0161.

Lux, A., Morita, S., Abe, J., and Ito, K. (2005). An improved method for clearing and staining free-hand sections and whole-mount samples. Ann. Bot. *96*, 989–996.

Malamy, J.E., and Benfey, P.N. (1997). Organization and cell differentiation in lateral roots of Arabidopsis thaliana. Development *124*, 33–44.

Marsollier, A.-C., and Ingram, G. (2018). Getting physical: invasive growth events during plant development. Curr. Opin. Plant Biol. *46*, 8–17.

Molina, I., Bonaventure, G., Ohlrogge, J., and Pollard, M. (2006). The lipid polyester composition of *Arabidopsis thaliana* and *Brassica napus* seeds. Phytochemistry *67*, 2597–2610.

Molina, I., Ohlrogge, J.B., and Pollard, M. (2008). Deposition and localization of lipid polyester in developing seeds of *Brassica napus* and *Arabidopsis thaliana*. Plant J. *53*, 437–449.

Moussu, S., Doll, N.M., Chamot, S., Brocard, L., Creff, A., Fourquin, C., Widiez, T., Nimchuk, Z.L., and Ingram, G. (2017). ZHOUPI and KERBEROS mediate embryo/endosperm separation by promoting the formation of an extracuticular sheath at the embryo surface. Plant Cell *29*, 1642–1656.

Naseer, S., Lee, Y., Lapierre, C., Franke, R., Nawrath, C., and Geldner, N. (2012). Casparian strip diffusion barrier in Arabidopsis is made of a lignin polymer without suberin. Proc. Natl. Acad. Sci. USA *109*, 10101–10106.

Nawrath, C., Schreiber, L., Franke, R.B., Geldner, N., Reina-Pinto, J.J., and Kunst, L. (2013). Apoplastic diffusion barriers in Arabidopsis. Arabidopsis Book *11*, e0167.

Olvera-Carrillo, Y., Van Bel, M., Van Hautegem, T., Fendrych, M., Huysmans, M., Simaskova, M., van Durme, M., Buscaill, P., Rivas, S., Coll, N.S., et al. (2015). A conserved core of programmed cell death indicator genes discriminates developmentally and environmentally induced programmed cell death in plants. Plant Physiol. *169*, 2684–2699.

Panikashvili, D., Shi, J.X., Schreiber, L., and Aharoni, A. (2009). The Arabidopsis *DCR* encoding a soluble BAHD acyltransferase is required for cutin polyester formation and seed hydration properties. Plant Physiol. *151*, 1773–1789.

Pfister, A., Barberon, M., Alassimone, J., Kalmbach, L., Lee, Y., Vermeer, J.E.M., Yamazaki, M., Li, G., Maurel, C., Takano, J., et al. (2014). A receptor-like kinase mutant with absent endodermal diffusion barrier displays selective nutrient homeostasis defects. eLife *3*, e03115.

Pollard, M., Beisson, F., Li, Y., and Ohlrogge, J.B. (2008). Building lipid barriers: biosynthesis of cutin and suberin. Trends Plant Sci. *13*, 236–246.

Racolta, A., Bryan, A.C., and Tax, F.E. (2014). The receptor-like kinases GSO1 and GSO2 together regulate root growth in Arabidopsis through control of cell division and cell fate specification. Dev. Dyn. *243*, 257–278.

Riederer, M. (2006). Introduction: biology of the plant cuticle. In Biology of the Plant Cuticle, M. Riederer and C. Müller, eds. (Blackwell Publishing), pp. 1–10.

RStudio Team (2015). RStudio: Integrated Development for R. RStudio, Inc., Boston, MA. https://www.rstudio.com.

Schindelin, J., Arganda-Carreras, I., Frise, E., Kaynig, V., Longair, M., Pietzsch, T., Preibisch, S., Rueden, C., Saalfeld, S., Schmid, B., et al. (2012). Fiji: an open-source platform for biological-image analysis. Nat. Methods *9*, 676–682.

Schreiber, L. (2010). Transport barriers made of cutin, suberin and associated waxes. Trends Plant Sci. *15*, 546–553.

Schreiber, L., and Schönherr, J. (2009). Water and Solute Permeability of Plant Cuticles (Springer Berlin Heidelberg).

Stoeckle, D., Thellmann, M., and Vermeer, J.E.M. (2018). Breakout-lateral root emergence in *Arabidopsis thaliana*. Curr. Opin. Plant Biol. *41*, 67–72.

Szczuka, E., and Szczuka, A. (2003). Cuticle fluorescence during embryogenesis of *Arabidopsis thaliana* (L.) Heynh. Acta Biol. Cracov. Ser. Bot. *45*, 63–67.

Takahashi, K., Shimada, T., Kondo, M., Tamai, A., Mori, M., Nishimura, M., and Hara-Nishimura, I. (2010). Ectopic expression of an esterase, which is a candidate for the unidentified plant cutinase, causes cuticular defects in *Arabidopsis thaliana*. Plant Cell Physiol. *51*, 123–131.

Tanaka, T., Tanaka, H., Machida, C., Watanabe, M., and Machida, Y. (2004). A new method for rapid visualization of defects in leaf cuticle reveals five intrinsic patterns of surface defects in Arabidopsis. Plant J. *37*, 139–146.

Truernit, E., and Haseloff, J. (2008). A simple way to identify non-viable cells within living plant tissue using confocal microscopy. Plant Methods *4*, 15.

Tsuwamoto, R., Fukuoka, H., and Takahata, Y. (2008). *GASSHO1* and *GASSHO2* encoding a putative leucine-rich repeat transmembrane-type receptor kinase are essential for the normal development of the epidermal surface in Arabidopsis embryos. Plant J. *54*, 30–42.

Ursache, R., Andersen, T.G., Marhavý, P., and Geldner, N. (2018). A protocol for combining fluorescent proteins with histological stains for diverse cell wall components. Plant J. *93*, 399–412.

Valeska Zeisler-Diehl, V., Migdal, B., and Schreiber, L. (2017). Quantitative characterization of cuticular barrier properties: methods, requirements, and problems. J. Exp. Bot. *68*, 5281–5291.

Van Norman, J.M., Xuan, W., Beeckman, T., and Benfey, P.N. (2013). To branch or not to branch: the role of pre-patterning in lateral root formation. Development *140*, 4301–4310.

Vermeer, J.E.M., von Wangenheim, D., Barberon, M., Lee, Y., Stelzer, E.H.K., Maizel, A., and Geldner, N. (2014). A spatial accommodation by neighboring cells is required for organ initiation in Arabidopsis. Science *343*, 178–183.

Vilches-Barro, A., and Maizel, A. (2015). Talking through walls: mechanisms of lateral root emergence in *Arabidopsis thaliana*. Curr. Opin. Plant Biol. *23*, 31–38.

Voß, U., Wilson, M.H., Kenobi, K., Gould, P.D., Robertson, F.C., Peer, W.A., Lucas, M., Swarup, K., Casimiro, I., Holman, T.J., et al. (2015). The circadian clock rephases during lateral root organ initiation in *Arabidopsis thaliana*. Nat. Commun. *6*, 7641.

Willemsen, V., Bauch, M., Bennett, T., Campilho, A., Wolkenfelt, H., Xu, J., Haseloff, J., and Scheres, B. (2008). The NAC domain transcription factors FEZ and SOMBRERO control the orientation of cell division plane in Arabidopsis root stem cells. Dev. Cell *15*, 913–922.

Xing, Q., Creff, A., Waters, A., Tanaka, H., Goodrich, J., and Ingram, G.C. (2013). ZHOUPI controls embryonic cuticle formation via a signalling pathway involving the subtilisin protease ABNORMAL LEAF-SHAPE1 and the receptor kinases GASSHO1 and GASSHO2. Development *140*, 770–779.

Yang, W., Pollard, M., Li-Beisson, Y., and Ohlrogge, J. (2016). Quantitative analysis of glycerol in dicarboxylic acid-rich cutins provides insights into Arabidopsis cutin structure. Phytochemistry *130*, 159–169.

Yeats, T.H., Huang, W., Chatterjee, S., Viart, H.M.F., Clausen, M.H., Stark, R.E., and Rose, J.K.C. (2014). Tomato Cutin Deficient 1 (CD1) and putative orthologs comprise an ancient family of cutin synthase-like (CUS) proteins that are conserved among land plants. Plant J. *77*, 667–675.

Zeisler-Diehl, V., Müller, Y., and Schreiber, L. (2018). Epicuticular wax on leaf cuticles does not establish the transpiration barrier, which is essentially formed by intracuticular wax. J. Plant Physiol. *227*, 66–74.

Zhu, J.-K. (2016). Abiotic stress signaling and responses in plants. Cell *167*, 313–324.

Ziv, C., Zhao, Z., Gao, Y.G., and Xia, Y. (2018). Multifunctional roles of plant cuticle during plant-pathogen interactions. Front. Plant Sci. *9*, 1088.

Please cite this article in press as: Berhin et al., The Root Cap Cuticle: A Cell Wall Structure for Seedling Establishment and Lateral Root Formation, Cell (2019), https://doi.org/10.1016/j.cell.2019.01.005

STAR★METHODS

KEY RESOURCES TABLE

REAGENT or RESOURCE	SOURCE	IDENTIFIER
Antibodies		
Monoclonal antibody to xylogalacturonan	Plantprobes	LM8
Anti-Rat IgG–FITC antibody produced in goat	Sigma-Aldrich	Cat#F6258; RRID: AB_259695
Chemicals, Peptides, and Recombinant Proteins		
Fluorol Yellow 088	Sigma-Aldrich	Cat#F5520
Aniline Blue diammonium salt	Sigma-Aldrich	Cat#415049
Toluidine Blue	Sigma-Aldrich	Cat#89640
Fluorescein diacetate	Sigma-Aldrich	Cat#F7378
ω-pentadecalacton	Sigma-Aldrich	Cat#W2840009
Methylheptadecanoate	Sigma-Aldrich	Cat#H4515
N, O- bis(trimethysilyl)-trifluoroacetamide with trimethylchlorosilane (BSTFA)	Sigma-Aldrich	Cat#15238
Pyridine	Sigma-Aldrich	Cat#270970
Methyl acetate	Sigma-Aldrich	Cat#296996
Sodium methoxide	Sigma-Aldrich	Cat#156256
Dichloromethane	Sigma-Aldrich	Cat#650463
Calcolfluor white (Fluorescent brightener 28)	Polysciences	Cat#4359
Xylitol	Sigma-Aldrich	Cat#X3375
Sodium deoxycholate	Sigma-Aldrich	Cat#30970
Urea	Sigma-Aldrich	Cat#51456
Potassium hexacyanoferrate(II) trihyadrate	Sigma-Aldrich	Cat#60280
Low viscosity Embedding media Spurr	EMS	Cat#14300
Osmium tetroxide 4%	EMS	Cat#19150
Experimental Models: Organisms/Strains		
Arabidopsis: gpat4	Li et al., 2007	SALK_106893
Arabidopsis: gpat8	Li et al., 2007	SALK_095122
Arabidopsis: gpat4 gpat8	Li et al., 2007	Cross between *gpat4* and *gpat8*
Arabidopsis: dcr-2	Panikashvili et al., 2009	SALK_128228
Arabidopsis: bdg-1	Kurdyukov et al., 2006	W32 mutant
Arabidopsis: gso1-1/sng3-1	Pfister et al., 2014	SALK_064029
Arabidopsis: gso2-1	Tsuwamoto et al., 2008	SALK_130637
Arabidopsis: gso1-1 gso2-1	Moussu et al., 2017	Cross between *gso1-1* and *gso2-1*
Arabidopsis: smb-3	Willemsen et al., 2008	SALK_143526
Arabidopsis: pLOVE1::CDEF1	This study	Transgenic Col-0
Arabidopsis: pGPAT4::NLS-GFP-GUS	This study	Transgenic Col-0
Arabidopsis: pGPAT8::NLS-GFP-GUS	This study	Transgenic Col-0
Arabidopsis: pDCR::NLS-GFP-GUS	This study	Transgenic Col-0
Arabidopsis: pBDG::GFP	Jakobson et al., 2016	Transgenic Col-0
Oligonucleotides		
For all oligonucleotides used for genotyping and cloning	See Table S1B	N/A
Recombinant DNA		
All recombinant DNA needed for the generation of transgenic lines are described in the subsection of the Method Details- Generation of constructs	This paper	N/A

(*Continued on next page*)

Continued

REAGENT or RESOURCE	SOURCE	IDENTIFIER
Software and Algorithms		
Fiji	Schindelin et al., 2012	https://fiji.sc/#; RRID: SCR_002285
Rstudio	RStudio Team, 2015	https://www.rstudio.com/; RRID: SCR_000432

CONTACT FOR REAGENT AND RESOURCE SHARING

Further information and requests for resources and reagents should be directed to and will be fulfilled by the Lead contact Christiane Nawrath (christiane.nawrath@unil.ch).

EXPERIMENTAL MODEL AND SUBJECT DETAILS

Plant material

Arabidopsis thaliana accession Col-0 was used in this work along with *Brassica nigra* and *Solanum lycopersicum* L. ''Moneymaker.'' All *Arabidopsis* seeds were maximally 3-month-old for the characterization of the RCC.

Arabidopsis thaliana mutants were already described: *gpat4, gpat8, gpat4 gpat8* (Li et al., 2007), *dcr-2* (Panikashvili et al., 2009), *bdg-1* (Kurdyukov et al., 2006), *smb-3* (Willemsen et al., 2008), *gso1/sng3-3* (Pfister et al., 2014), *gso2-1* (Tsuwamoto et al., 2008) and *gso1/sng3-3 gso2-1* (Moussu et al., 2017). Gene numbers and genotyping primers are described in Tables S1A and S1B.

Growth conditions

For the characterization of the RCC plants were grown under sterile conditions. Seeds were surface sterilized with chlorine gas. After 2-3 days of vernalization at 4°C, plants were grown on ½ MS (Murashige and Skoog, 500mg/l MES, pH 5.7), 0.7% agar at 22°C, under continuous light (100 μmol m^{-2} s^{-1}). With the exception of the seedlings for polyester extraction and salt stress assays, plants were grown vertically. For transformation and seed amplification plants were grown on soil under continuous light (100 μmol m^{-2} s^{-1}) at 20°C and 65% humidity.

METHOD DETAILS

Generation of constructs

To generate pENTRY L4-pGPAT4-R1 and pENTRY L4-pGPAT8-R1, 1.7 kb and 2.2 kb fragments upstream of each *GPAT* were amplified, respectively, and cloned into pDONR P4-P1 using KpnI and XbaI restriction site. pENTRY L4-pLOVE1-R1 was generated by amplifying a 2.1 kb fragment upstream of *LOVE1* and recombining it into pDONR P4-P1. To generate pENTRY-L1-NLS-GFP-GUS-L2, *NLS-GFP-GUS* was amplified from a pDEST containing B1-NLS-GFP-B2-GUS-B3 and recombined into pDONR221. All primers used are shown in Table S1B. pENTRY L1-CDEF1-L2 was previously described (Naseer et al., 2012). pGPAT4::NLS-GFP-GUS, pGPAT8::NLS-GFP-GUS and pLOVE1::CDEF1 were generated by recombining the corresponding entry clones into the pMMA-Red vector (Ali et al., 2012) using the Gateway Technology (Lifesciences). pLOVE1::H2A-GFP was generated by recombining pENTRY-L4-pLOVE1-R1 and pENL1-GAL4-VP16-L2 into the destination vector pB9-H2A-UAS-7m24GW. This vector contains a HISTONE 2A-6 (H2A) coding sequence (At5g59870) fused to eGFP and driven by the repetitive UAS promoter (Olvera-Carrillo et al., 2015). pBDG::GFP was previously described (Jakobson et al., 2016). All constructs were transformed in *Agrobacterium tumefaciens* and then in *Arabidopsis thaliana* accession Col-0 using the floral dip method (Clough and Bent, 1998): inflorescences were dipped into a 5% sucrose/0.05% Silwet L-77 solution containing *Agrobacterium* for 2-3 s and kept at high humidity for 24 h. Transformed seeds were selected based on their red fluorescence (Ali et al., 2012).

Cutin digestion, cuticle staining and permeability assays

The polyester of the RCC was digested *in vitro* by a recombinant cutinase (Unilever). Samples were fixed in acetone 90% for 30 min at −20°C, washed several time in 0.2M K_2HPO_4 pH8 and placed in a tube with 100 μg/ml cutinase in 0.2M K_2HPO_4 pH8 for three days, the negative control plants were incubated in 0.2M K_2HPO_4 without cutinase.

The polyester of the RCC of primary roots was specifically digested *in vivo* in transgenic pLOVE1::CDEF1 lines. In order to evaluate whether the pLOVE1 promoter was suitable to express a cutinase specifically in the outer root cap cell layer its activity was evaluated in several independent pLOVE1::H2A-GFP lines (Figure S4A). Furthermore, several independent transgenic pLOVE1::CDEF1 lines were investigated for giving consistent results in respect to the RCC degradation (Figure S4B).

For visualization of cell wall polyesters, the Fluorol Yellow 088 protocol from Naseer et al. (2012) was modified to remove background staining in lipid-rich organs and validated (Figure S4C). Shortly, seedlings were incubated in Fluorol Yellow 088

(0.01% in methanol) during 3 days for investigations of roots and for three weeks for aerial parts of the plants. Specimen were then counterstained with aniline blue (0.5% in water) for minimum 1 h at RT and rinsed in water. 10 roots each were studied in three independent experiments.

For studying the permeability of the RCC with toluidine blue, 10-12 roots were harvested in 0.5 x liquid MS medium and then simultaneously incubated in an aqueous solution of 0.05% toluidine blue/0.1% Tween 20 during the indicated time (10-135 s) followed by a quick washing step in water. Samples were instantaneously evaluated under the Axio Zoom V16 microscope (Zeiss) coupled to an Axiocam 512 Color camera for the presence or absence of dark-blue staining of the meristematic cells (Figure S4D). A staining of the mucilage at the columella (Figure S2) was present at all times in WT and mutants (Figure S4C). The experiment was repeated three times.

For studying the permeability of the cuticle with fluorescein diacetate (FDA) (5 μg/ml in ½ MS) (Barberon et al., 2016), 25 lateral roots of the same developmental stage originating from 3 independent experiments were individually investigated by direct application of FDA to the root on the microscope slide, immediately mounted and observed as described below. The same microscope and same settings were used for the analysis and a 4-min incubation period was selected for comparison of the different genotypes. The Fire scale of relative intensity was used for the comparison (Schindelin et al., 2012).

Germination and root growth assays

Salt stress assays were conducted by placing seeds on medium containing 75 mM of K_2SO_4, 250 mM of mannitol, 100 mM of KCl or 100 mM of NaCl, respectively. Four replicates were evaluated for each treatment (50-100 seeds each) and 3 for controls. Experiments were repeated independently three times and a representative dataset is presented. Salt concentrations had been optimized to minimize the effects on plant development of WT by using 50-200 mM of K_2SO_4, 200-400 mM of mannitol, 100-200 mM of KCl or 100-200 mM of NaCl.

NaCl-induced cell death assay was conducted by incubating of 2-day-old seedlings in ½ MS medium containing 140 mM NaCl for 10 min. Seedlings were subsequently treated for 10 s with propidium iodide (PI) (10 μg/mL) and immediately observed under the microscope (Olvera-Carrillo et al., 2015). The number of dead cells was determined by counting the cells fully stained by PI in the entire meristem using a z-stack of pictures. 16-20 meristems were observed per genotype. Experiments were repeated independently two times and a representative dataset is presented.

Lateral root emergence was induced on 5-day-old seedlings by turning the plate of 90°C (Voß et al., 2015). Stages of lateral root emergence were evaluated after 42 h or 96 h, using mutant roots having a comparable length to WT. Roots were fixed and cleared by the following incubation steps: 4% HCl/20% methanol solution for 15 min at 57°C, 7% NaCl/60% ethanol solution for 15 min at RT, rehydrated by 10 min incubation in 60%, 40%, 20%, 10% ethanol. Specimens were mounted in 50% glycerol/5% ethanol and stages of lateral root emergence were determined using a Leica DM5000B microscope (Malamy and Benfey, 1997). Experiments were repeated independently three times (n = 20-30) and a representative dataset is presented.

To study the shape of lateral root primordia seedlings were fixed, cleared and stained with Calcofluor as described in Ursache et al. (2018). Briefly, the seedling was fixed in 4% paraformaldehyde for 1 h, then washed twice in 1x PBS and cleared overnight in Clearsee (10% Xylitol/15% Sodium deoxycholate/25% Urea). Afterward the specimens were staining in 0.1% Calcofluor white in Clearsee for 1 h and washed in Clearsee for max 30 min before being imaged, as described below. Adhesion frequency was assessed by studying 90 - 160 seedlings of each genotype at the early observation time (42 h and 48 h) and approximately 100 seedlings at the late observation time (96 h).

Immunofluorescence labeling

To label mucilage, the protocol of Durand et al. (2009) was used to detect xylogalacturonan-associated epitopes with the LM8 antibody, which was revealed with a fluorescein isothiocyanate (FITC)-conjugated goat anti-rat antibody. Briefly, 2-day-old seedlings were fixed for 30 min in 4% paraformaldehyde/1% glutaraldehyde/50 mM PIPES pH 7.0/1 mM $CaCl_2$ and washed in 50 mM PIPES pH 7.0 with 1 mM $CaCl_2$. After a 30 min incubation in 3% low-fat milk/PBS (phosphate-buffered saline) pH 7.2 as blocking solution, seedlings were washed in 0.05% Tween 20 (PBST) and incubated overnight with the LM8 antibody (1:5 in 0.1%PBST) at 4°C. Samples were then washed 5 times in 0.01% PBST and incubated for 2 h at 28°C in FITC-conjugated goat anti-rat as secondary antibody (1:50 in 0.1% PBST). A minimum of 30 roots of each genotype was studied.

Fluorescence Microscopy

Most fluorescent microscopy studies were performed on the confocal laser-scanning microscope ZEISS 700 with an excitation at 488 nm and detection with BP 490-555 nm for GFP, FY, FDA and LM8, and respectively at 555 nm and LP 640 nm for PI. PI (10 μg/mL) was used for staining the cell wall of the roots during the study of gene expression by direct application on the slide. Calcofluor staining was studied on the confocal ZEISS LSM 880 Airyscan with an excitation at 405 nm and detection at 425-475 nm. Red seeds selection was performed under the stereomicroscope Leica 6000 equipped with a DSR filter.

Transmission electron microscopy

The protocol for transmission electron microscopy of Barberon et al. (2016) was slightly modified. Roots were fixed in a 2.5% glutaraldehyde solution in 0.1 M phosphate buffer pH 7.4 (PB) for 1 h at RT followed by a postfixation (1 h at RT) in a freshly made solution of

1% osmium tetroxide and 1.5% potassium ferrocyanide in PB and then washed in distilled water. Dehydration steps were then gradually performed in ethanol solution (30%, 50%, 70% for each 40 min, 100% twice for 1 h). The infiltration with Spurr resin at 33% in ethanol for 4 h, 66% for 4 h and 100% for 8 h twice was achieved before polymerization at 60°C for 48 h. Root tips were cut longitudinally in ultrathin sections of 50 nm of thickness and studied with a FEI CM100 transmission electron microscope (FEI, Eindhoven, the Netherlands) coupled with a TVIPS TemCamF416 digital camera (TVIPS GmbH, Gauting, Germany) (acceleration voltage of 80 kV). The ultrastructure of the root cap cell wall and cuticle was investigated over the entire length of the root cap in 2-3 independent root tip preparations per genotype and representative pictures were taken. Cuticle thickness was determined by taking 4 pictures per root and 5 measurements per picture for 5 primary roots and 3 lateral roots at a magnification of 20.000 (0.5101 nm/pixel). The ultrastructure of the RCC at the emerging LR was investigated at the stage when the lateral root had just emerged from the primary root and thus its exact position could be identified by light microscopy.

Chemical analyses

The protocol for the determination of ester-bond lipids previously described in Barberon et al. (2016) was adapted. 200 mg of seeds were grown on nylon mesh (200 μm pore size). After two days, the roots were shaved off after flash freezing and extracted in isopropanol/0.01% butylated hydroxytoluene (BHT). They were then delipidized three times (1 h, 16 h, 8 h) in each of the following solvents, i.e., chloroform-methanol (2:1), chloroform-methanol (1:1), methanol with 0.01% BHT, under agitation before being dried for 3 days under vacuum. Depolymerization was performed by base catalysis (Li-Beisson et al., 2013). Briefly, dried plant samples were transesterified in 2 mL of reaction medium. 20 mL reaction medium was composed of 3 mL methyl acetate, 5 mL of 25% sodium methoxide in dry methanol and 12 mL dry methanol. The equivalents of 5 μg of methyl heptadecanoate and 10 μg of ω-pentadecalactone/sample were added as internal standards. After incubation of the samples at 60°C for 2 h 3.5 mL dichloromethane, 0.7 mL glacial acetic acid and 1 mL 0.9% NaCl (w/v) Tris 100 mM pH 8.0 were added to each sample and subsequently vortexed for 20 s. After centrifugation (1500 g for 2 min), the organic phase was collected, washed with 2 mL of 0.9% NaCl, and dried over sodium sulfate. The organic phase was then recovered and concentrated under a stream of nitrogen. The resulting cutin monomer fraction was derivatized with BFTSA/pyridine (1:1) at 70°C for 1 h and injected out of hexane on a HP-5MS column (J&W Scientific) in a gas chromatograph coupled to a mass spectrometer and a flame ionization detector (Agilent 6890N GC Network systems). The temperature cycle of the oven was the following: 2 min at 50°C, increment of 20°C/min to 160°C, of 2°C/min to 250°C and 10°C/min to 310°C, held for 15 min. 3 independent experiments were performed with 3-4 replicates for each genotype, respectively, and a representative dataset is presented. The amounts of unsubstituted C16 and C18 fatty acids were not evaluated because of their omnipresence in the plant and in the environment.

QUANTIFICATION AND STATISTICAL ANALYSIS

For the germination assay, the cell death assay and the chemical analyses of the cutin composition, presented values are the mean ± standard deviation. Student's t-test analyses were performed to highlight differences between WT and other genotypes. Asterisks illustrate the p value: $p < 0.001$ is ***, $p < 0.01$ is ** and $p < 0.05$ is *.

Number of repetitions and replicates are mentioned for each experiment in the METHOD DETAILS.

Cell

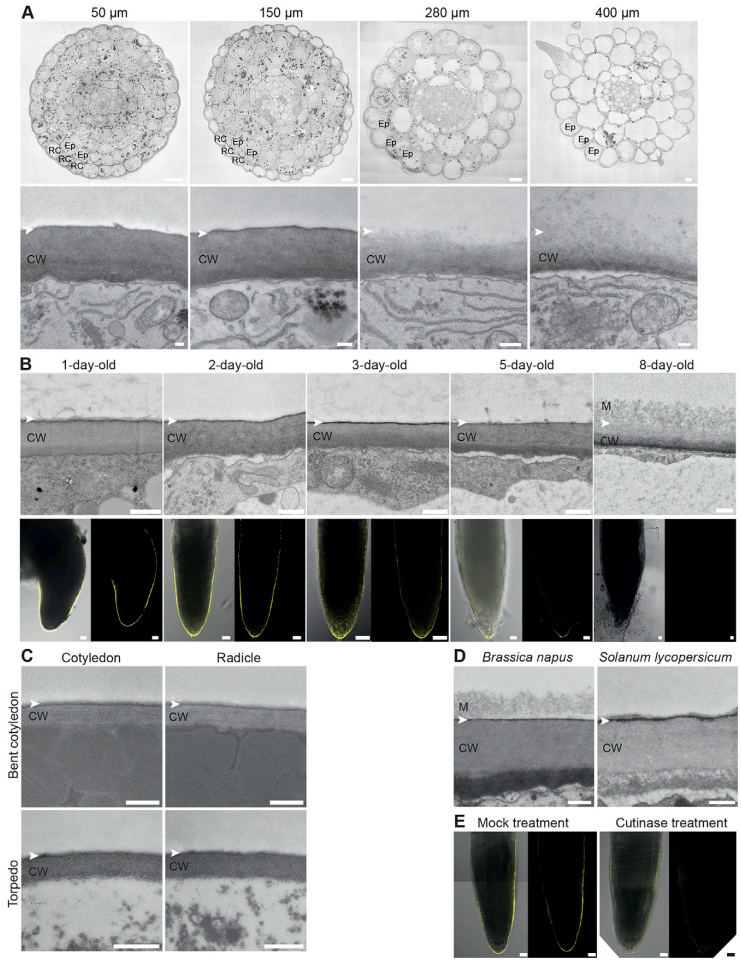

Figure S1. RCC of the Primary Root of *Arabidopsis* and Other Plant Species and Its Degradation by Cutinase *In Vitro*, Related to Figure 1B

(A) Transversal root sections at the indicated distance from the extremity of the root tip of a 2-day-old WT seedling, as visualized by TEM (top) and zoom to the outer cell wall of the outermost cell layer (bottom). At 50 and 150 µm, lateral root cap cells form the outermost cell layer of the root tip having an electron-opaque layer at the surface of the outer cell wall. At 280 and 400 µm, epidermal cells form the outermost cell layer having no electron-opaque layer. The scale bars in the overview represent 10 µm and in the zoom 200 nm. Overview pictures are stitched together from multiple TEM pictures.

(B) TEM pictures of root tips of WT showing cell wall and cuticle of the outermost lateral root cap cells (top) and median views of the FY staining at the root cap at indicated ages (bottom; on the left, overlay bright field and fluorescence; on the right, fluorescence only). With the loss of the first root cap cells, the RCC is not present anymore. Scale bars in TEM pictures represent 500 nm and in fluorescence micrographs 20 µm.

(C) Cell wall and cuticle ultrastructure of embryonic organs at torpedo and bent cotyledon stage, as visualized by TEM. Scale bars represent 500 nm.

(D) Lateral root cap cells of 2-day-old seedlings of *Brassica napus* and *Solanum lycopersicum*, both having an electron-opaque layer at the outside of the primary cell wall in TEM. Scale bars represent 500 nm.

(E) Median views of FY staining of the tips of 2-day-old roots treated with recombinant cutinase and respective controls showing the absence of the RCC after cutinase treatment. Scale bars represent 20 µm.

CW, cell wall; Ep, epidermal cell; M, mucilage; RC, root cap cell; white arrow head, expected position of the RCC.

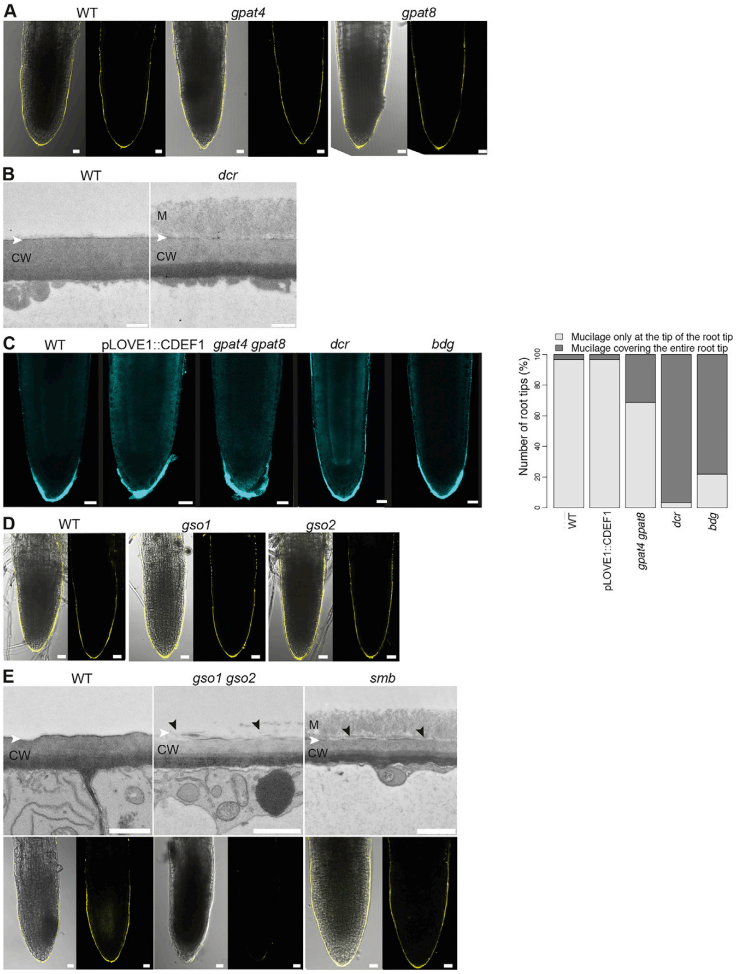

Figure S2. Characterization of the RCC and Other Cell Wall Structures in Different Genotypes, Related to Figure 1E

(A) Median views of FY staining at the RCC of the primary root of 2-day-old *gpat4* and *gpat8* mutants in comparison to WT (on the left, overlay bright field and fluorescence; on the right, fluorescence only). Scale bars represent 20 μm.

(B) Ultrastructure of cell wall and cuticle of lateral root cap cells of 2-day-old root after a 3-day-long methanol-treatment. Although the ultrastructure of the cell wall is not largely altered in WT, in *dcr* mutant, globular electron-opaque depositions in the cell wall and at the cell wall-mucilage interface visible without methanol treatment (Figure 1E) were not present anymore. Scale bar represents 500 nm.

(C) Mucilage deposition at the root cap of 2-day-old seedlings as assessed by immunolabelling with the LM8 antibody detecting xylogalacturonan-associated epitopes of *Arabidopsis* root caps (Durand et al., 2009). Quantitative evaluation of mucilage localization in the observed root tips is shown on the right of representative picture. Scale bars represent 20 μm.

(D) Median view of FY staining of the RCC of the primary root of *gso1* and *gso2* in comparison to WT (on the left, overlay bright field and fluorescence; on the right, fluorescence only). Scale bars represent 20 μm.

(E) Alterations in the cell wall and cuticle ultrastructure of the outermost lateral root cap cells (top) and median views of the FY staining at the root cap (bottom; on the left, overlay bright field and fluorescence; on the right, fluorescence only) of WT, *gso1 gso2* mutant having no RCC and *smb* mutant having an interrupted RCC. Scale bars in TEM pictures represent 500 nm and in pictures showing FY staining 20 μm.

CW, cell wall; M, mucilage; black arrowhead, interruption of the cuticle; white arrowhead, expected position of the RCC.

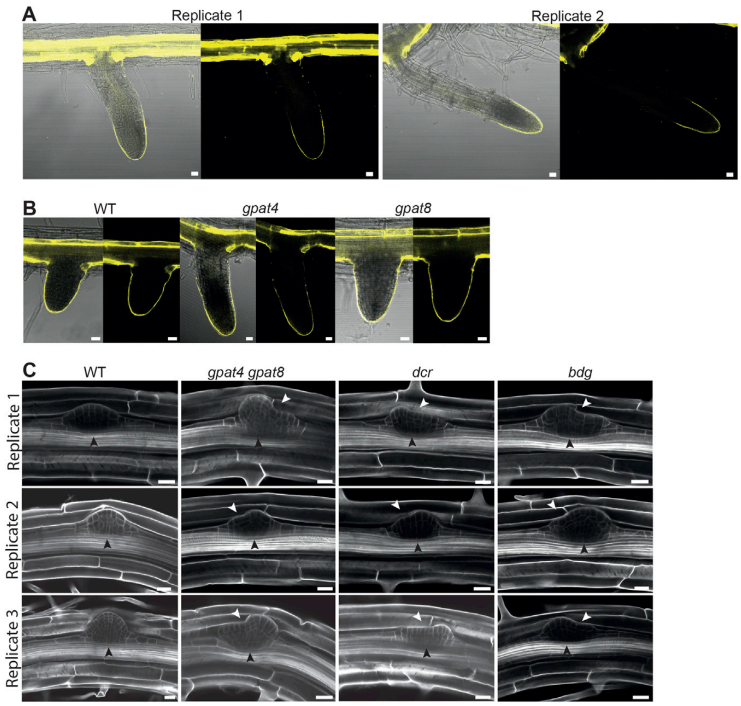

Figure S3. The RCC of the Lateral Root and Its Role in Lateral Root Emergence, Related to Figures 3D, 4D, and 4E

Median views of FY staining in 8-day-old WT seedlings (A) at the RCC of lateral roots having different lengths and (B) at the RCC of shortly-emerged lateral roots of *gpat4* and *gpat8* in comparison to WT (left, overlay bright field and fluorescence; right, fluorescence only). As expected, the suberin of the endodermis is also stained. Scale bars represent 20 μm.

(C) Shape of lateral root primordia in WT and different genotypes having a modified RCC at the emerging lateral root. Regular shape of lateral root primordia of WT. Deformed lateral root primordia of genotypes having RCC modifications at the lateral root primordium. Black arrowhead, lateral root primordium; white arrowhead, primordium deformation. Scale bars represent 20 μm.

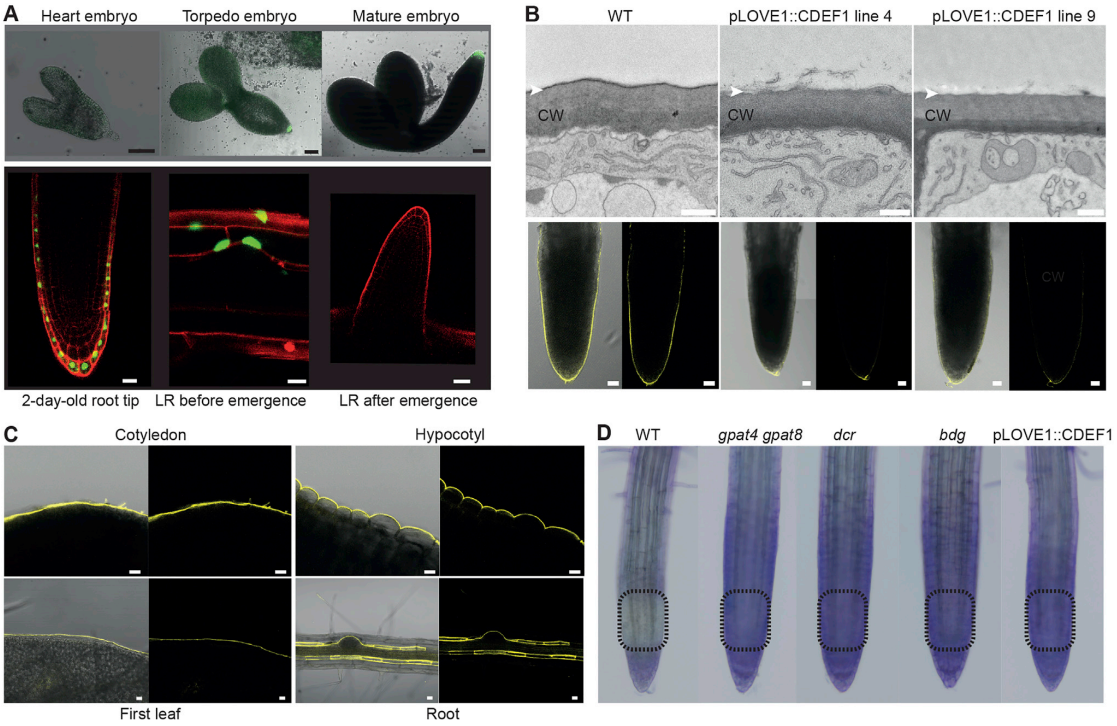

Figure S4. Generation of pLOVE1::CDEF1 Plants, Fluorol Yellow and Toluidine Blue Staining, Related to STAR Methods

(A) Activity of pLOVE1 was assessed in different organs and at different developmental stages in transgenic *Arabidopsis* lines expressing pLOVE1::H2A-GFP. Scale bars represent 50 μm (top row) and 20 μm (bottom row).

(B) Ultrastructure of cell wall and cuticle of the outermost lateral root cap cells as visualized by TEM (top) and median views of the FY staining at the root cap of WT and different transgenic lines expressing pLOVE1::CDEF1 having no RCC (bottom: on the left, overlay bright field and fluorescence; on the right, fluorescence only). Scale bars represent 500 nm (top) and 20 μM (bottom). CW, cell wall; white arrowhead, expected position of RCC. pLOVE1::CDEF1 line 4 has been selected to be shown as representative pLOVE1::CDEF1 line in Figure 1B together with its WT control.

(C) Various organs of 8-day-old WT seedlings were stained with FY using the modified staining protocol showing that cutin and suberin can be stained. Scale bars represent 20 μm.

(D) Toluidine blue staining of the primary root of 2-day-old seedlings of WT and different genotypes having RCC modifications after 30 s of incubation. The staining at the extremity of the root tip is due to the mucilage at the columella cells (See Figure S2C) that also stains with toluidine blue. Dashed box; zone of evaluation.

3.4. Additional results and discussions

The key results and main discussions of this project are in the publication of Berhin et al. (2019). However, some additional experiments and observations were not included in the publication. They are presented and discussed here.

3.4.1. Several cutin biosynthetic genes are expressed at the root tips

As previously stated, several known genes are mentioned in the literature as being expressed at the tip of the primary and the lateral roots: *LACS2*, *HTH, DCR*, *ABCG11, LTPg1, LTPg2* and *BDG* (Table 1), suggesting that they could be involved in the root cap cuticle (RCC) biosynthesis pathway. In order to identify more genes, we examined the expression pattern of some well-characterized polyester-related genes. In addition to *GPAT4*, *GPAT8*, *DCR* and *BDG* (Berhin et al. 2019, Figure 1C), we have also investigated the non-published expression of *FAR4*, *GPAT2*, *GPAT3*, *GPAT5*, *GPAT6*, *GPAT7*, *DCF* and *CUS2* at the root tips. Additionally, we also reinvestigated the already published expression patterns of *CYP86A1, CYP86B1, ASFT* and *ABCG11* (Bird et al., 2007; Panikashvili et al., 2007; Molina et al., 2009; Naseer et al., 2012).

GPAT2, GPAT3 and GPAT7 are also expressed at the tip of the primary and/or the lateral roots like GPAT4 and GPAT8

As described in our publication (Berhin et al. 2019, Figure 1D and 3C), *GPAT4* exhibited root cap expression at the primary and the lateral roots. *GPAT8* expression was detected only in the lateral roots, although its presence at the primary root tip was expected due to its known redundancy with *GPAT4* (Li et al., 2007a). In addition, as already described in the section 2.4.3, *GPAT2* and *GPAT3* were also expressed at the primary root tip from the embryonic stage and in the lateral roots after the emergence of the primordia (Figure 8, Figure 9 and Figure 11). In contrast to other *GPAT* genes, *GPAT2* and *GPAT3* were expressed in every cell layers of the root cap. *GPAT7,* which was not present at the primary root, showed expression at the lateral roots at early stages after initiation of the lateral root primordia (Figure 9 and Figure 11). *GPAT5* and *GPAT6* were not expressed at all in root tips (Figure 9 and Figure 11).

DCR is expressed at the root cap of primary and lateral roots

The *DCR* expression pattern had already been studied with pDCR::GUS transgenic line revealing an expression at the primary and lateral root tips (Panikashvili et al., 2009). Expression pattern analysis using via pDCR::NLS-GFP fusion showed a specific expression in the outer layer of the root cap cells, and a lateral root expression starting already during the early stages of the primordium (Figure 16 and Berhin et al.,2019, figure 1D).

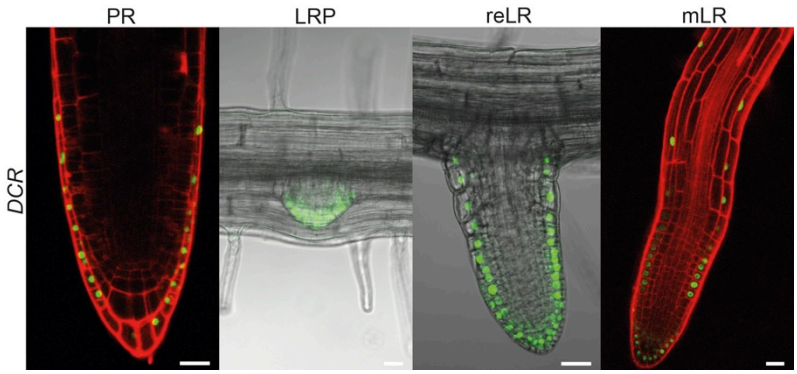

Figure 16: GFP fluorescence of transgenic plants expressing pDCR::NLS-GFP-GUS at the root cap of a 2-day-old primary root and lateral roots. Pictures overlay the gene expression in green and PI staining in red as background for PR and mLR and the bright field for LRP and reLR. Scale bar is 20 µm. PR, primary root; LRP, lateral root primordium; reLR, recently emerged lateral root; mLR mature lateral root. Expression of *DCR* at primary root from Berhin et al. (2019), Figure 1D.

DCF is not expressed at the root tips

The *DCF* expression pattern was studied through the reporter line pDCF::YFP. No expression was observed in root tips, neither in the entire root system with the exception of one endodermal cell next to the side of lateral root formation (Figure 17).

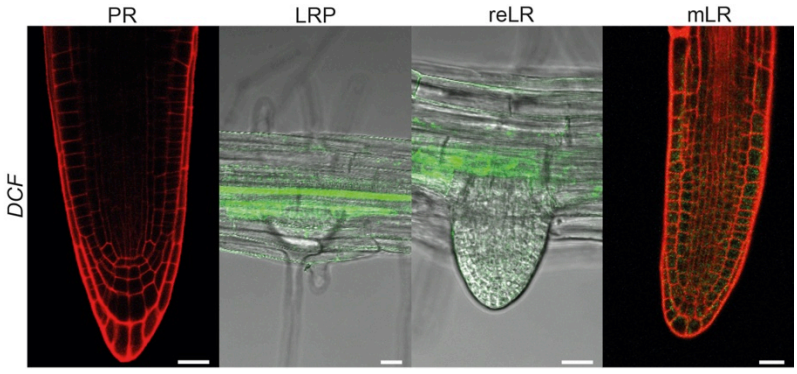

Figure 17: GFP fluorescence of transgenic plants expressing pDCF::NLS-GFP-GUS at the root cap of a 2-day-old primary root and lateral roots. Pictures overlay the gene expression in green and PI staining in red as background for PR and mLR and the bright field for LRP and reLR. Scale bar is 20 µm PR. primary root; LRP, lateral root primordium; reLR, recently emerged lateral root; mLR mature lateral root.

ABCG11 is polarly expressed at the root cap of primary and lateral roots

ABCG11 was reported to be expressed at the tip of the primary and the lateral roots (Bird et al., 2007; Panikashvili et al., 2007). A detailed study of *ABCG11* expression pattern, via the reporter line pABCG11::NLS-GFP-GUS, showed that it was expressed in the outer cell layer of root cap of the primary and lateral roots from the earliest development stage and nowhere else in the roots (Figure 18). ABCG11 subcellular localization, studied using pABCG11::CITRINE-ABCG11, was polar at the plasma membrane of the root cap.

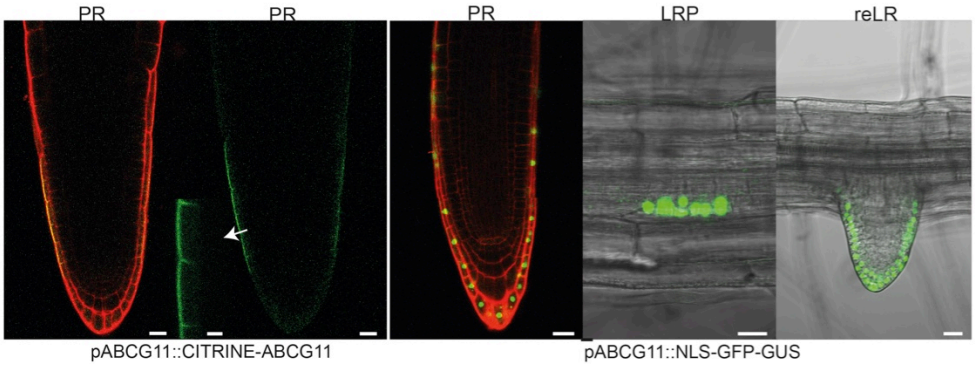

Figure 18: GFP fluorescence of transgenic plants expressing pABCG11::CITRINE-ABCG11 and pABCG11::NLS-GFP-GUS at the root cap of a 2-day-old primary root and lateral roots. For pABCG11::CITRINE-ABCG11, the first picture presents the overlay of the gene expression in green with PI in red. The second picture is the gene expression alone. For pABCG11::NLS-GFP-GUS, pictures overlay the gene expression in green and PI staining in red as background for PR and the bright field for LRP and reLR. The white arrow highlights a zoom. Scale bar is 20 µm in the main pictures and 5 µm in the zoom. PR, primary root; LRP, lateral root primordium; reLR, recently emerged lateral root.

CUS2 is not expressed at the root tips

The *CUS2* expression pattern was studied through the reporter line pCUS2::NLS-GFP. No expression at all could be observed in the root (Figure 19).

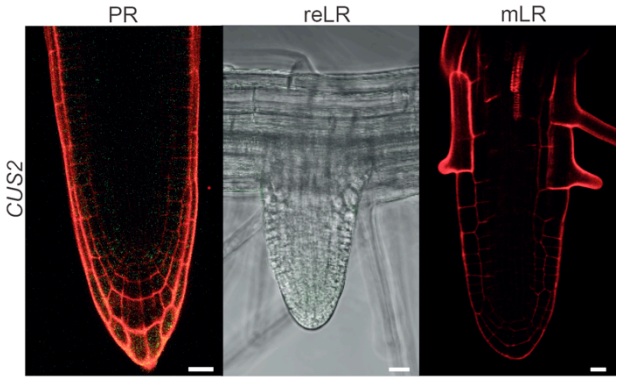

Figure 19: GFP fluorescence of transgenic plants expressing pCUS2::NLS-GFP at the root cap of a 2-day-old primary root and lateral roots. Pictures overlay the gene expression (which is absent here) and PI staining in red as background for PR and mLR and the bright field for reLR. Scale bar is 20 µm PR. primary root; reLR, recently emerged lateral root; mLR mature lateral root.

BDG is expressed at the root cap of primary and lateral roots

The *BDG* expression pattern has already been described in the central cylinder of the root, at the tip of lateral roots from the earliest point in lateral root development and slightly at the superior border of the primary root cap (Jakobson et al., 2016). By looking ourselves at the same lines p*BDG*::GFP, an additional expression in the primary root cap cell was visible (Figure 20 and Berhin et al.,2019, figure 1D).

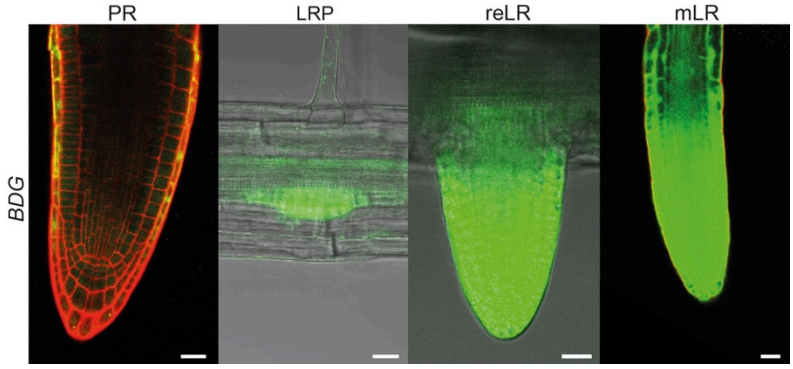

Figure 20: GFP fluorescence of transgenic plants expressing pBDG::GFP at the root cap of a 2-day-old primary root and lateral roots. Pictures overlay the gene expression in green and PI staining in red as background for PR and mLR and the bright field for LRP and reLR. Scale bar is 20 µm PR. primary root; LRP, lateral root primordium; reLR, recently emerged lateral root; mLR mature lateral root. Expression of *BDG* at primary root from Berhin et al. (2019), Figure 1D.

GSO1 and GSO2 are expressed at the root cap of the primary root

Two receptors like kinase, *GSO1* also called *SGN3* and *GSO2*, are required for normal development of the epidermis and cuticle formation in the embryo and the shoot (Tsuwamoto et al., 2008). Both genes studied via pGSO1::NLS-GFP-GUS and pGSO2::NLS-m3xVENUS are expressed at the root cap of the primary root (Figure 21).

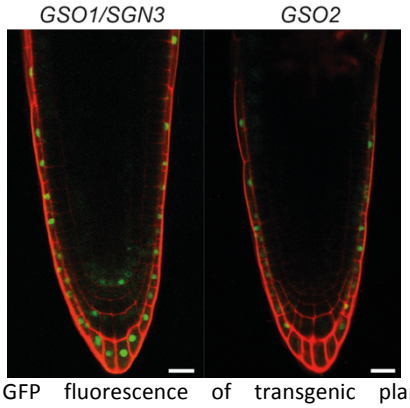

Figure 21: GFP fluorescence of transgenic plants expressing pGSO1::NLS-GFP-GUS and pGSO2::NLS-3xVENUS at the root cap of the primary root of a 2-day-old seedling. Pictures overlay the gene expression in green and PI staining in red as background. Scale bar is 20 µm.

FAR4, CYP86A1, CYP86B1 and ASFT are not expressed in the root tips

The expression patterns of some genes known to be required for suberin formation were studied through reporter lines: pFAR4::NLS-GFP-GUS, pCYP86A1::NLS-GFP-GUS, pCYP86B1::NLS-GFP-GUS and pASFT::NLS-GFP-GUS. Expression data from Naseer et al. (2012) suggested an expression of *CYP86A1* at the primary root (via GUS reporter from pCYP86A1::NLS-GFP-GUS). By studying those lines using GFP, no signal was detected (Figure 22). No expression was observed in the root tips for *FAR4, ASFT* and *CYP86B1* (Figure 22). The endodermal expression previously reported was confirmed (Domergue et al., 2010; Naseer et al., 2012).

Figure 22: GFP fluorescence of transgenic plants expressing pFAR4::NLS-GFP-GUS, pCYP86A1::NLS-GFP-GUS, pCYP86B1::NLS-GFP-GUS and pASFT::NLS-GFP-GUS at the root cap of the primary root of a 2-day-old seedling. Pictures overlay the gene expression in green (which is absent here) and PI staining in red as background. Scale bar is 20 µm.

3.4.2. RCC can be stained with lipid dyes

In order to visualize the RCC in an easier and faster way than TEM, we tested different dyes for their ability to stain cuticle.

Nile Red

Nile Red is a dye known to stain suberin (Ursache et al., 2018). However, it stains the suberin of the endodermis higher in the root than fluorol yellow, suggesting a staining of late formed suberin. Theoretically, knowing the composition similarity between cutin and suberin, Nile Red could potentially stain the RCC. During our attempt of staining with Nile Red coupled with ClearSee, endodermal suberin was clearly visible (Figure 23). Nevertheless, neither the leaf cuticle nor the RCC from primary and lateral roots were stained. Nile red is not an adequate staining for cuticle studies.

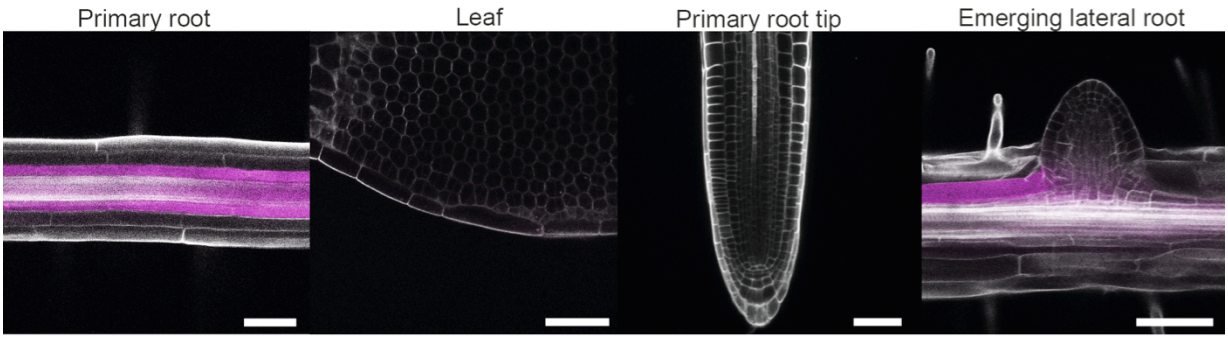

Figure 23: Nile Red staining of the WT plant primary root, leaf, primary root tip and emerging lateral root. Nile red is in purple. Calcofluor White in white is staining the cell wall. Scale bar is 50 µm.

Auramine O

Auramine O has been reported to stain lignin, cutin and suberin (Ursache et al., 2018). It has already been used to stain *Arabidopsis* embryo and endosperm cuticle, and tomato fruit cuticle (Szczuka, 2003; Buda et al., 2009; Fawke et al., 2018; Loubéry et al., 2018; Creff et al., 2019). In addition, Auramine O stains cuticular edge of the stomata and the cuticle on the trichome, according to Ursache et al. (2018). In our hands, Auramine O stained clearly lignin in the Casparian strip and the xylem (Figure 24). The cuticle of the leaf and the hypocotyl was visible as well (Figure 24). However, the RCC of the primary and the lateral roots was detectable at the same level than the background rejecting the hypothesis of a specific RCC binding by Auramine O (Figure 24).

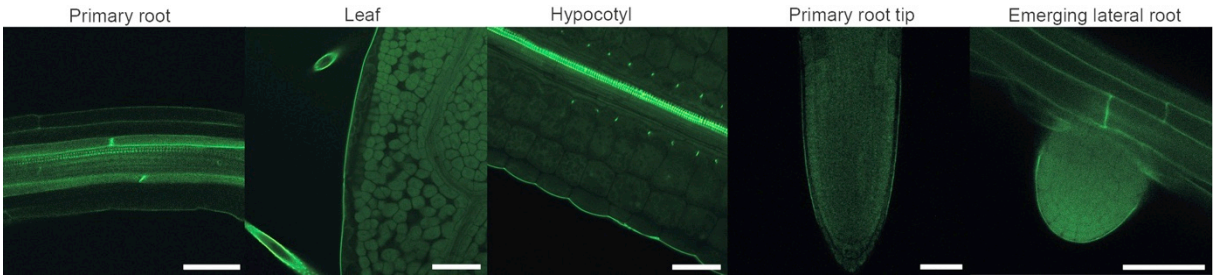

Figure 24: Auramine O staining of the WT plant primary root, leaf, hypocotyl, primary root tip and emerging lateral root. Scale bar is 50 µm.

Sudan Red

Sudan Red 7B colors waxes and lipids, including suberin and cutin. Inspired by the staining of the leaf cuticle from De Giorgi et al., (2015), we stained the RCC from the primary root. The RCC was visible, however the workload to prepare the sample and the difficulty to observe it did not make this technique the most suitable for screening mutants.

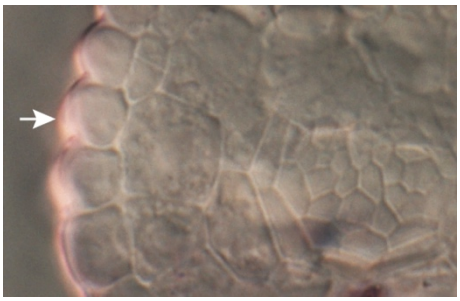

Figure 25: Sudan Red 7B of the WT plant primary root tip. Red staining, Sudan red; white arrow, stained cuticle.

Fluorol yellow

In Berhin et al. 2019, we presented a new protocol combining fluorol yellow (FY) and methanol. It was widely inspired by the fluorol yellow in lactic acid protocol (Lux et al., 2005; Barberon et al., 2016). FY combined with aniline blue, its counter staining, highlighted specifically lipids. Methanol has here two functions: solvent and delipidizer. It is used as a solvent for FY, which avoids the warming steps due to the use of lactic acid, leading to root tip explosion in the previous protocol. In addition, the methanol removes all non-polymerized fatty acids. The meristem of 2-day-old roots is full of fatty acids coming from the seeds resulting in a high signal background. Methanol removes them leaving only polymerized polyester deposition such as cutin and suberin. Used until now only to stain suberin, this technique successfully stains the cuticle of leaves too (Berhin et al. 2019, figure S4C). A mutant study on leaves shows the efficiency of the staining for screening for defective cuticle mutants (Figure 26): *gpat4 gpat8* and *lacs2* mutants showed a defective cuticle on the first leaves and the cotyledons, *bdg* only in leaves, while *dcr* presented no change in staining.

External application of a recombinant cutinase on cotyledons and leaves followed by a FY staining revealed a digestion and a removal of the cuticle (Figure 27). An identical procedure performed on the 2-day-old roots led to the same results suggesting that both the leaf cuticle and the RCC can be digested by an external cutinase (Berhin et al. 2019, Figure S1E). A similar absence of staining was observed in pLOVE1::CDEF1 plants, having a cutinase specifically expressed in the root cap (Berhin et al. 2019, Figure 1A and S4B). In conclusion, FY has been shown to be a useful tool to stain the RCC and to highlight defective cuticles in mutants.

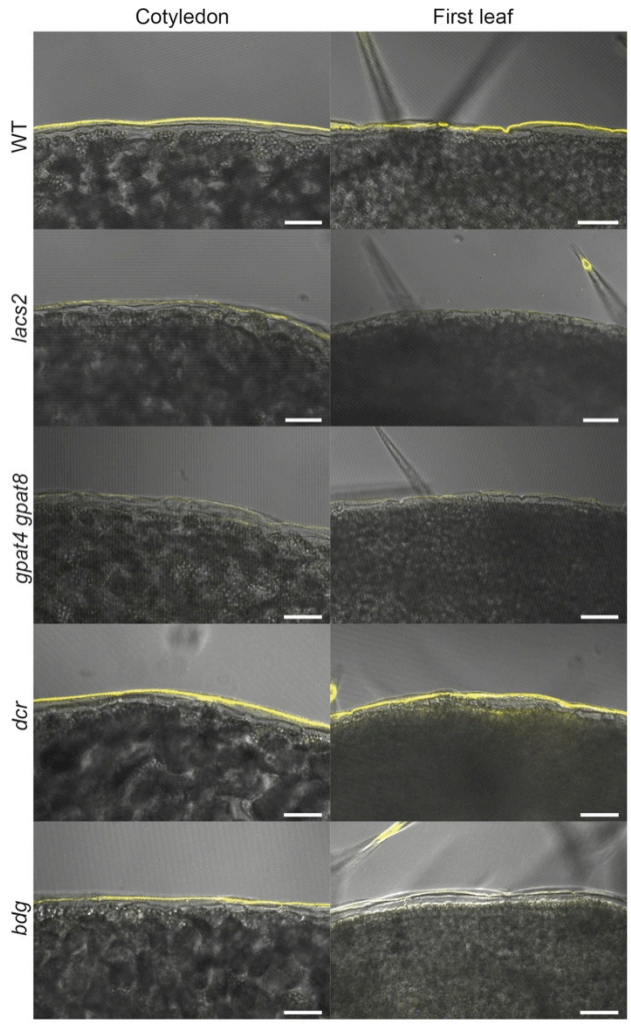

Figure 26: FY on the cotyledon and the first leaf of WT, *lacs2, gpat4 gapt8, dcr* and *bdg.* The FY staining is in yellow overlaying the bright field picture. Scale bar is 50 µm.

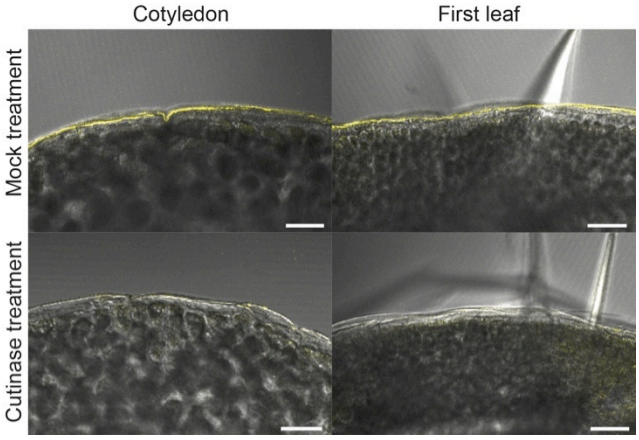

Figure 27: FY on the cotyledon and the first leaf of WT, *lacs2, gpat4 gapt8, dcr* and *bdg.* The FY staining is in yellow overlaying the bright field picture. Scale bar is 50 µm.

3.4.3. A cuticle covers the root cap of the primary and the lateral roots and needs cutin biosynthetic genes for its formation

RCC at the primary root

The RCC was first visualized via TEM. It is a black electron dense layer of 18.5 +/-4.5 nm similar to the leaf cuticle (Figure 2 and Berhin et al. 2019, Figure 1B). It is specific to the root cap cells from the embryonic stage until the loss of the first root cap cell layer at approximately 6 days after germination (Berhin et al. 2019, Figure 1B, S1C and S1B). *Solanum lycopersicum* and *Bassica napus* also have an RCC (Berhin et al. 2019, Figure S1D). The RCC is not an artifact linked to growth conditions since plants grown on soil and in liquid had a similar cuticle (Figure 28); however, its appearance change could be due to the environment. By cutting the root orthogonally at several position along the root tip, it was observed that as long as there are root cap cells, the cuticle is visible. From the point where the outer layer is made of epidermal cells the cuticle is not present anymore (Berhin et al. 2019, Figure S1A). Hence, the RCC is specific to the root cap cells.

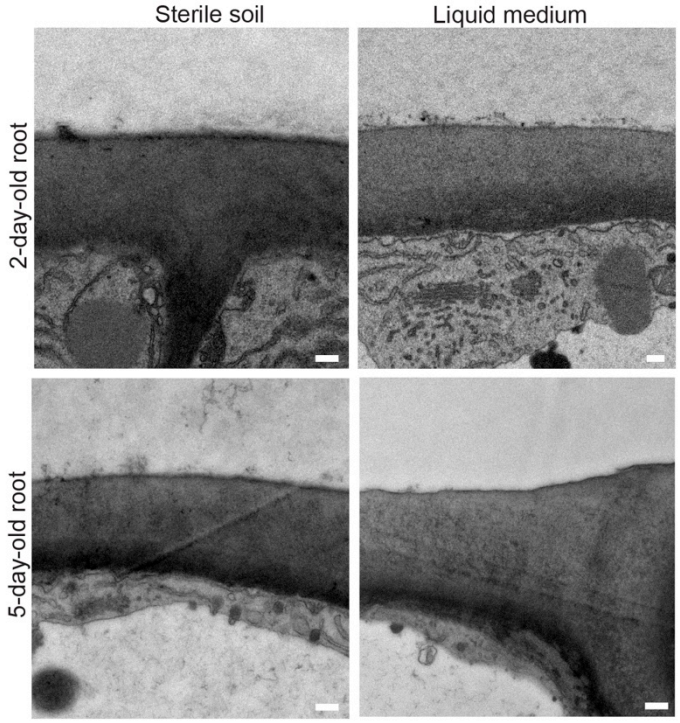

Figure 28: Ultrastructure of cell wall and cuticle of the outermost lateral root cap cells as visualized by TEM at the root cap of 2-day-old and 5-day-old WT seedling grown in sterile soil and in liquid medium. The scale is 200 µm.

Since the electron dense layer was deposited at the outer side of the cell wall like a cuticle and that the cutin biosynthetic genes were predominantly expressed at the root cap, we started to investigate mutants. In Berhin et al. 2019, *gpat4 gpat8*, *dcr* and *bdg* have already been shown to have a defective cuticle at the primary root (Berhin et al. 2019, Figure 1E). Those results proved that *GPAT4, GPAT8*, *DCR* and *BDG* are involved in RCC biosynthesis. *gso1 gso2,* mutant for two receptor kinases acting in shoot cuticle formation, did not present any FY staining fitting with the absence of RCC at the TEM (Berhin et al., 2019, Figure S2D and S2E). FY staining on *smb*, mutant of a transcription factor involved in root cap maturation, suggested the presence of the RCC. Nevertheless, TEM revealed that the RCC has holes, details that could not be noticed with the resolution of the staining pictures (Berhin et al., 2019, Figure S2E). In addition to the mutants, pLOVE1::CDEF1 lines, having a cutinase specifically expressed at the root cap, were presenting a defective cuticle as well (Berhin et al. 2019, Figure 1B and S4B). The defective RCC observed in cutin gene mutants and its digestion by a cutinase confirms that the RCC is made of a polyester similar to cutin.

Those results show that FY can be a useful tool to screen easily in order to identify new mutants, keeping in mind that sometimes even a defective RCC can be stained, like in the case of *smb*.

Based on the interesting expression profile of their gene at the root tip (Kim et al., 2012; Kurdyukov et al., 2006b; Lee et al., 2009a; Lü et al., 2009), *lacs2*, *gpat2*, *gpat3*, *hth* and *ltpg1 ltpg2* mutants have been investigated, along with *fah1* and *eh1*. The primary root of *lacs2* could not be stained with FY. TEM confirmed that the RCC was defective (Figure 29 and Figure 30). Similarly to *lacs2*, *gpat2* RCC presented no staining with FY and an altered cuticle with TEM at the primary root tip (Figure 29 and Figure 30), suggesting the implication of both genes in the RCC biosynthetic pathway. The staining of *gpat3* was not affected at the primary root and TEM confirmed the presence of a RCC with a normal ultrastructure (Figure 29 and Figure 30). *hth* presented also no phenotype at the primary root with FY (Figure 30). *ltpg1 ltpg2-1* was not lacking staining at the primary root (Figure 30) neither were *ltpg1 ltpg2-2* and *ltpg1 ltpg2-3* (data not shown). If a TEM analysis would show no defect in the cuticle, this could suggest a redundancy of *LTPg1* and *LTPg2* with another member of the *LTPg* family; to be investigated further.

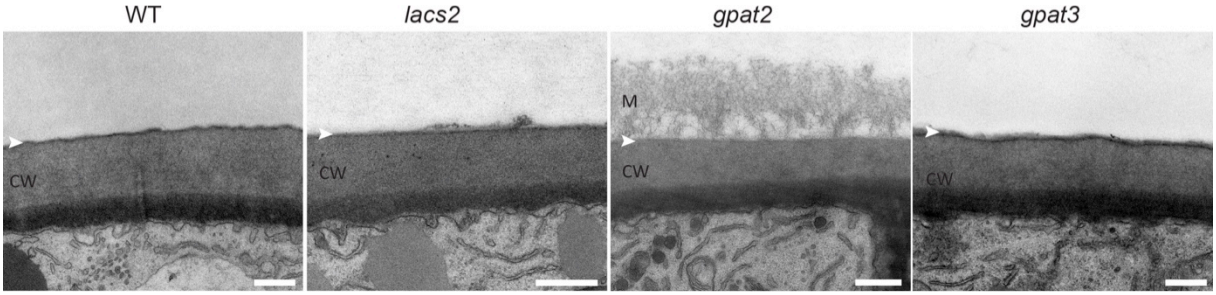

Figure 29: TEM showing cell wall and cuticle of the outermost lateral root cap of 2-day-old WT, *lacs2, gpat2* and *gpat3*. Scale bar is 500 nm; CW, cell wall; M, mucilage; white arrowhead, expected position of the cuticle.

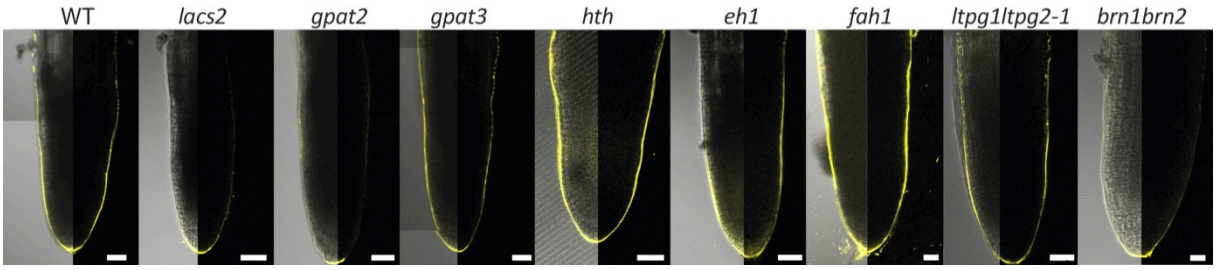

Figure 30: Median views of the FY staining at the root cap of 2-day-old WT, *lacs2, gpat2, gpat3, hth, eh1, fah1, ltpg1 ltpg2-1* and *brn1 brn2* (on the left, overlay bright field and fluorescence; on the right, fluorescence only). Scale bar is 20 µm.

Participating in the formation of compounds that are part of the RCC composition (see section 3.4.4), *eh1* and *fah1* have been tested even though their expression profile is unknown. *EH1* is involved in the conversion of 18-hydroxy 9,10-epoxy C18:1 FA into 9,10,18 hydroxy C18:1 FA which is present in the RCC (Pineau et al., 2017). The absence of FY phenotype in *eh1*, if confirmed by TEM, suggests that another of the seven members of the *EH* family may be implicated in the RCC biosynthetic pathway alone or with redundancy (Figure 30). *fah1* is the mutant of a ferulic acid 5-hydrolase (F5H) which is involved in the phenylpropanoid pathway leading to the formation of synapic acid, present in RCC composition (Anderson et al., 2015). The absence of change in the ultrastructure of *fah1* RCC observed with FY (Figure 30), if confirmed by TEM, could imply that: (1) seeing the small amount of synapic acid present in the RCC, its absence may not be enough to make the RCC defective; (2) *F5H* is not involved in the formation of synapic acid at the RCC.

brn1 brn2, double mutant defective in root cap maturation and cell detachment (Kamiya et al., 2016), was tested as well with FY and showed an absence of staining. Similar to *smb*, the effect on the RCC of the knockout of those two transcription factors suggests that the formation of the RCC is integrated in the regulatory pathway of root cap maturation (Figure 30).

In order to show that the modifications in the RCC of the *dcr* mutant were really due to the lack of *DCR* function at the outer root cap cell layer, *DCR* was expressed specifically in the

root cap cells using *LOVE1* promoter. RCC deficiencies were complemented by this construct as well as by an analogous construct harboring the *DCR* promoter. Similarly, to show that the RCC modifications in the *gpat2* mutant are due to the knockout of the gene, *gpat2* was complemented with pGPAT2::GPAT2. The complementation was confirmed by FY staining. pDCR::DCR perfectly complemented *dcr* as well as pGPAT2::GPAT2 did for *gpat2* (Figure 31). The complementation of *dcr* with pLOVE1::DCR proved that for RCC formation, the protein is needed in the outer layer of the root cap cells (Figure 31).

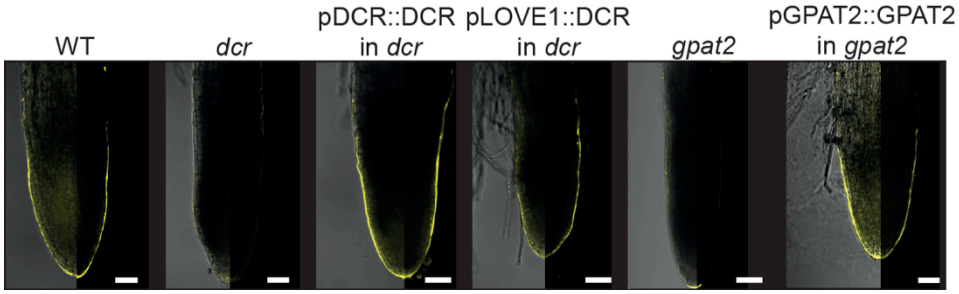

Figure 31: Median views of the FY staining at the root cap of 2-day-old seedlings: WT, *dcr, dcr* complemented with pDCR::DCR, *dcr* complemented with pLOVE1::DCR, gpat2 and *gpat2* complemented with pGPAT2::GPAT2 (on the left, overlay bright field and fluorescence; on the right, fluorescence only). Scale bar is 20 µm.

A filamentous structure covering the defective cuticle of *dcr*, *gpat2* and *smb* (Figure 29 and Berhin et al. (2019), Figure 1E) was confirmed to be mucilage by immunolabeling using xylogalacturonan-specific LM8 antibody (Figure 32, Berhin et al. (2019), Figure S2E), previously shown to detect mucilage at *Arabidopsis* roots (Durand et al., 2009). This suggests that a defective RCC affects in certain cases the mucilage production or the mucilage release from the root tip. Weirdly *gso1 gso2* did not have any particular mucilage accumulation when investigated in TEM but revealed a huge amount of mucilage all around the root tip with LM8 immunolabeling (Figure 32). The *gso1 gso2* defective cell wall could make the retention of the mucilage by the roots more difficult, leading to loss of the mucilage during the TEM preparation procedure.

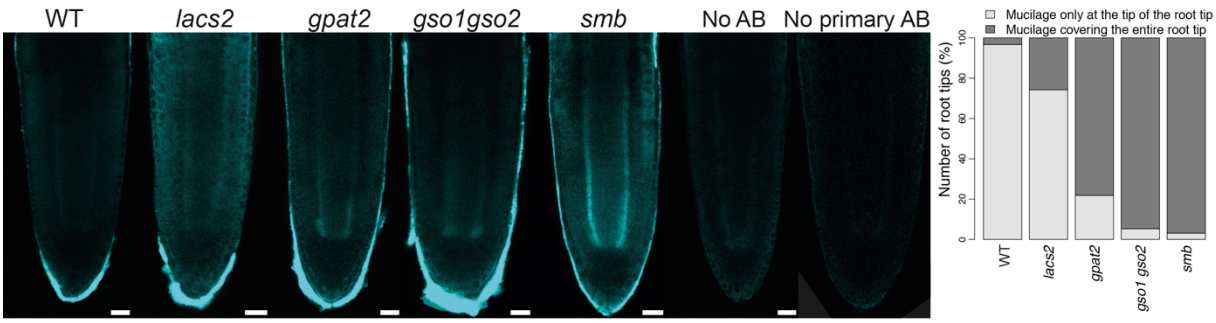

Figure 32: Mucilage deposition at the root cap of 2-day-old seedlings as assessed by immunolabeling with the LM8 antibody detecting xylogalacturonan-associated epitopes of *Arabidopsis* root caps (Durand et al., 2009). Quantitative evaluation of mucilage localization in the observed root tips is shown on the right of representative pictures. Scale bars represent 20 µm.

RCC at the lateral roots

Despite the ultrastructural similarity to the RCC of the primary root, the RCC of the lateral roots is twice thicker with 36 nm +- 2.5 nm. The cuticle is present before the emergence from the primary root: it could be already seen in developmental stage 3 (Berhin et al. 2019, Figure 3B and Damien de Bellis, unpublished). *gpat4 gpat8*, *dcr* and *bdg* showed to have a defective cuticle at shortly-emerged lateral roots despite differences in RCC ultrastructure (Berhin et al. 2019, Figure 3D). At the magnification used for the FY study, *dcr* presented a clear FY staining of the lateral root RCC. However, similarly to *smb* at the primary root, TEM revealed a change of RCC structure (Berhin et al. 2019, Figure 1E and 3C).

Based on the reported expression of *LACS2, GPAT2, GPAT3, GPAT7, HTH, LTPG1* and *LTPG2* at the lateral roots, the RCC was investigated in the respective mutants in order to identify whether there are involved in the formation of the RCC (Figure 11) (Kurdyukov et al., 2006b; Lee et al., 2009a; Lü et al., 2009; Kim et al., 2012). *lacs2* showed a defective cuticle at the emerging lateral roots suggesting its implication in RCC biosynthetic pathway (Figure 33 and Figure 34). *gpat2* and *gpat3* had a RCC similar to WT at the emerging lateral roots (Figure 33 and Figure 34). The staining, visible at first in emerging lateral roots, disappeared of the root cap in mature lateral roots at a stage where it is still present in the WT. This suggests that *GPAT2* and *GPAT3* are involved in RCC formation after the emergence of the lateral roots fitting with their expression in the mature lateral root (Figure 11 and Figure 35). Before jumping to conclusion, it has to be confirmed that the mutants are not losing prematurely their first root cap layer. A similar phenomenon was observed in *hth*; this should be more documented in the future based on a detailed study of *HTH* expression. *gpat7* had a staining similar to the WT suggesting a functional RCC at the lateral root primordia (Figure 34). Similarly to the primary root, *ltpg1 ltpg2* did not present any lack of staining at the lateral roots (Figure 34).

Unfortunately, pLOVE1::CDEF1 line could not be used to study the RCC of the lateral roots because the *LOVE1* promoter is active in the lateral root only after lateral root emergence (Berhin et al. 2019, Figure S4A).

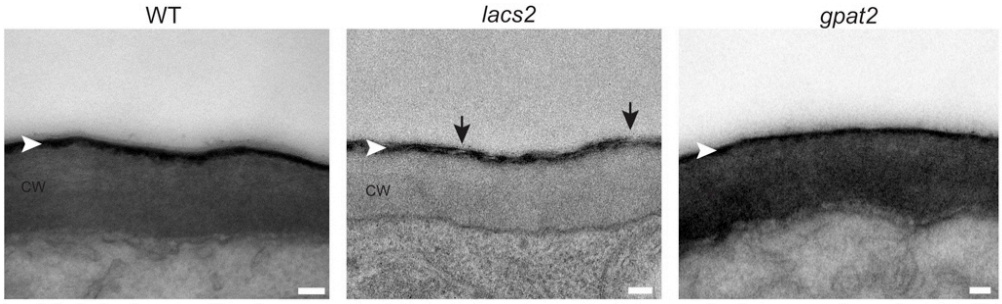

Figure 33: TEM showing cell wall and cuticle of the developing lateral root of WT, *lacs2, gpat2* and *gpat3*. Scale bar is 100 nm; CW, cell wall; M, mucilage; white arrowhead, expected position of the cuticle; black arrow, modified RCC.

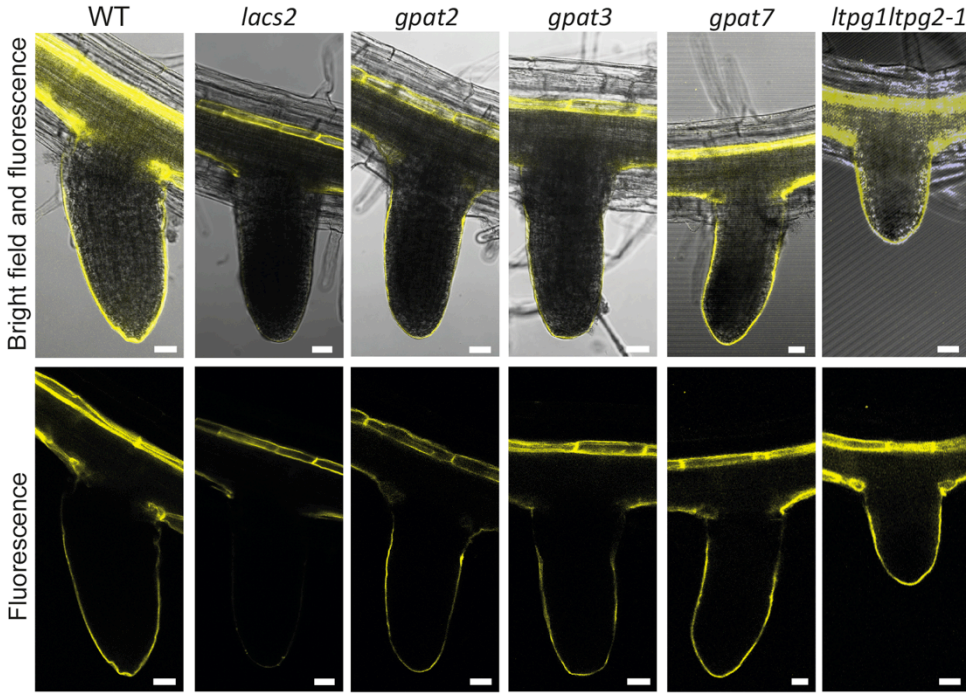

Figure 34: Median views of the FY staining of the developing lateral root of WT, *lacs2, gpat2, gpat3, gpat7* and *ltpg1 ltpg2* (on the top, overlay bright field and fluorescence; on the bottom, fluorescence only). FY stained the suberin of the endodermis and the RCC, when present. Scale bars represent 20 µm.

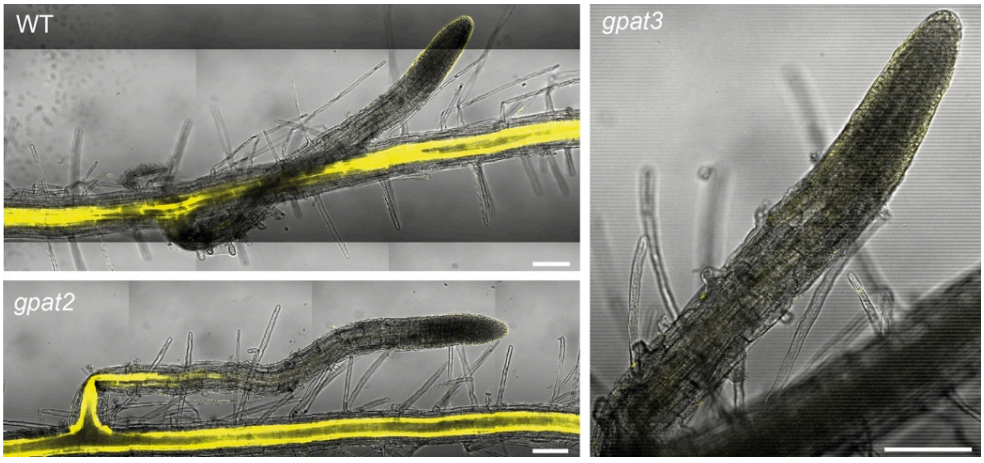

Figure 35: FY staining of the mature lateral root of WT, *gpat2* and *gpat3 (*overlay bright field and fluorescence). FY stained the suberin of the endodermis and the RCC, when present. Scale bars represent 100 µm.

3.4.4. The polyester of the RCC is an atypical cutin

In Berhin et al (2019), the root cap cuticle composition was established. The RCC extraction was executed in 2-day-old roots; no suberization was observed at that stage (Berhin et al (2019), Figure 2A). The main components of the RCC were C18:2 DCA and 9,10,18-trihydroxy C18:1 FA implying a C18 class cutin (Berhin et al (2019), Figure 2B). Unusual monomers like C26:0, C26:1, C28:0 and C28:1 were also present. Surprisingly, the unique detectable aromatic compound was sinapic acid. Coumaric and ferulic acids usually present in cutin were not present in the RCC.

The study, via biochemical analyses with gas chromatography-mass spectrometry (GC-MS) of the RCC composition of mutant plant presenting a defective cuticle, highlighted the role of certain genes in the RCC biosynthetic pathway. *GPAT4* and *GPAT8,* which have shown in stem to be involved in the formation of oxygenated FAs including C18:1 and C18:2 DCA, confirmed the same in the RCC (Li et al., 2007a). Indeed, a 95% reduction of C18:1 and C18:2 DCA was perceived in *gpat4 gpat8* mutant (Berhin et al (2019), Figure 2C). *DCR* has a role in incorporation of 9/10,16-OH C16:0 FA in leaves, seeds and flowers (Panikashvili et al., 2009). At the RCC, the strongest reduction (95%) was observed in 9,10,18-trihydroxy C18:1 FA (Berhin et al (2019), Figure 2C). *BDG* plays a role in the synthesis or the incorporation of unsaturated C18 monomers. Fitting with that theory, *bdg* at the RCC presented strong decrease of C18:2 DCA and 9,10,18-trihydroxy C18:1 FA (Berhin et al (2019), Figure 2C). By expressing a cutinase specifically at the root cap (pLOVE1::CDEF1), we induced the degradation of the RCC. The composition of the RCC in those lines was affected the strongest in C18:2 DCA and C18:1 DCA (Berhin et al (2019), Figure 2B). This indicates that CDEF1 may cleave specific bonds releasing DCAs. A reduction of the unsaturated compounds C26:0, C26:1 and C28:1 was also observed in pLOVE1::CDEF1, *bdg* and *dcr*.

Since *lacs2* and *gpat2* have a defective RCC at the primary root, the same biochemical analysis was performed. *LACS2* is known to be necessary for the incorporation of all types of oxygenated FAs (Bessire et al., 2007). Its knockout had a significant reduction only in C18:2 DCA (95%) at the RCC (Figure 36). Little is known about *GPAT2* and its relation with cutin formation. In the RCC, the *gpat2* mutant had the strongest reduction in the very long chain fatty acids of C26 and C28 and their monounsatured homologs (Figure 37). A mild reduction

of 40% and 50% was respectively detected for C18:2 DCA and 9,10,18-trihydroxy C18:1 FA monomers.

Taken together those results highlight the atypical composition of the RCC, which requires *LACS2*, *GPAT2*, *GPAT4*, *GPAT8*, *DCR* and *BDG* to be synthesized. At the exception of *GPAT2,* which is uncharacterized up to now, those genes are all also required for cutin formation in the shoot. Further investigations could unveil the whole biosynthetic pathway.

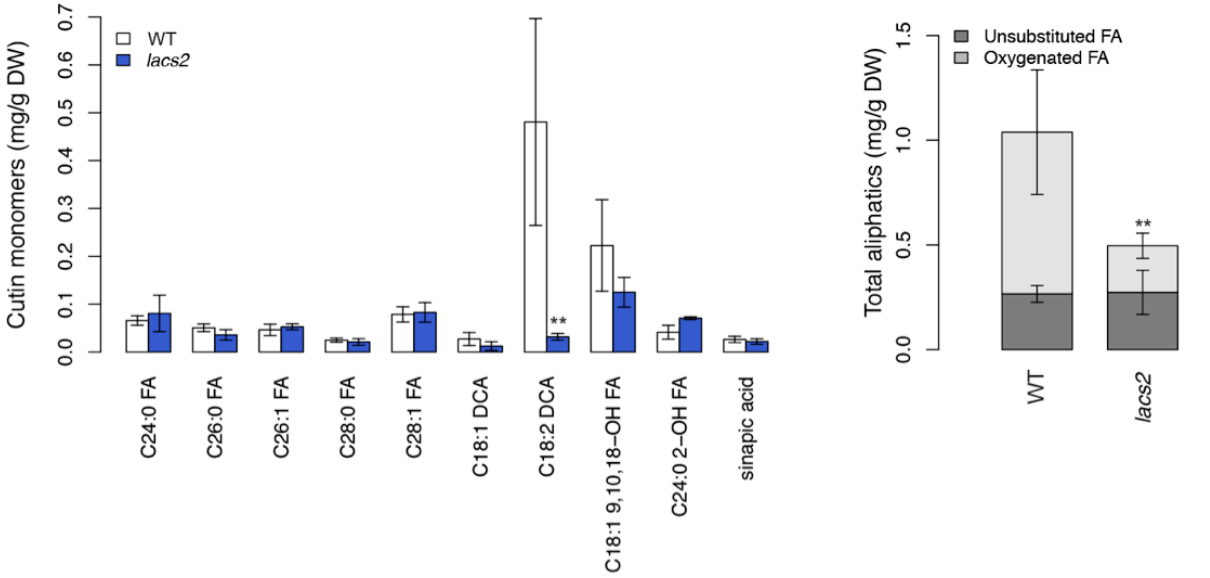

Figure 36: Quantification of aliphatic and aromatic ester-bond cutin monomers isolated from 2-day-old roots of *lacs2* in comparison to WT. Left graph shows the principal cutin monomers and right graph shows the total of evaluated aliphatic compounds on the left grouped by substance classes. Values represent the means ± SD, n = 3–4. Asterisks denote significant differences to as determined by Student's t-test: ***p < 0.001; **p < 0.01. FA, fatty acid; DCA, dicarboxylic acid; trihydroxy C18:1 FA, 9,10,18-trihydroxy C18:1 FA; DW, dry weight.

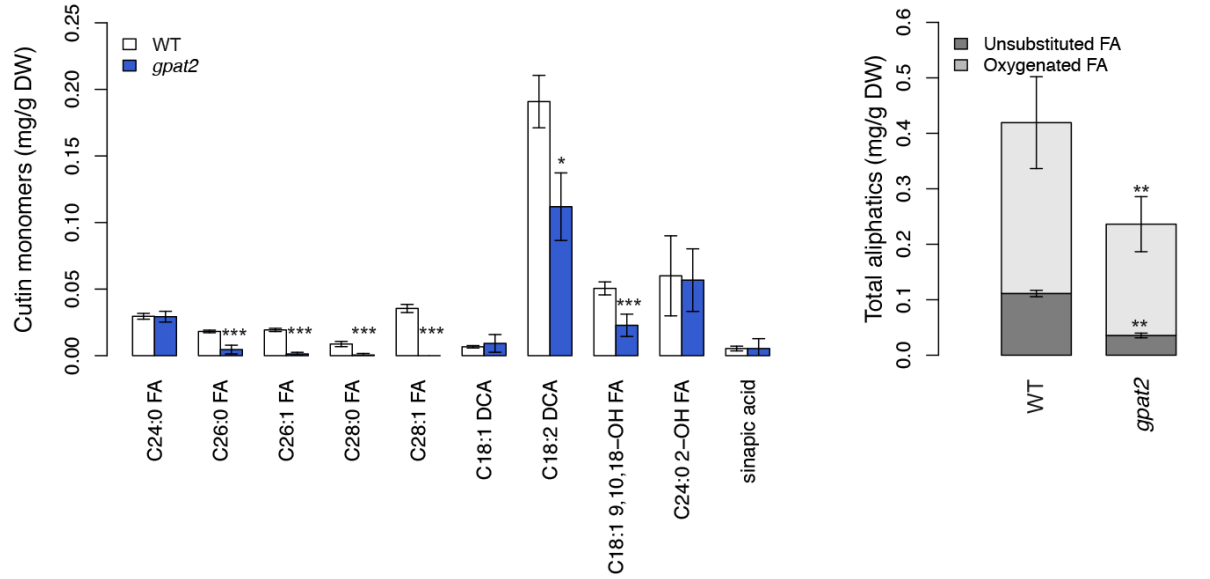

Figure 37: Quantification of aliphatic and aromatic ester-bond cutin monomers isolated from 2-day-old roots of *gpat2* in comparison to WT. Left graph shows the principal cutin monomers and right graph shows the total of evaluated aliphatic compounds on the left grouped by substance classes. Values represent the means ± SD, n = 3–4. Asterisks denote significant differences to as determined by Student's t-test: ***p < 0.001; **p < 0.01; *p < 0.05. FA, fatty acid; DCA, dicarboxylic acid; trihydroxy C18:1 FA, 9,10,18-trihydroxy C18:1 FA; DW, dry weight.

3.4.5. **Diffusion barrier properties are impaired in RCC mutants**

Permeability to toluidine blue

A kinetic analysis of the diffusion of toluidine blue into the meristem of the primary root comparing WT and mutants showed a penetration 6 to 10 times faster depending on the mutant genotype (Berhin et al., 2019, Figure 4A). Staining at one specific chosen time point illustrates this dynamic (Berhin et al., 2019, Figure S4D).

Staining with toluidine blue on lateral roots was showing promising preliminary results with WT primordia not stained after 4 min, while *bdg* primordia were colored at 1 min already (data not shown). However, an approach using fluorescein diacetate (FDA) was more informative, since it gives also information on the staining intensity.

Permeability to fluorescein diacetate

FDA is a cellular tracer that becomes fluorescent when entering living cell. At the primary root, FDA application resulted in saturating fluorescence less than 30 seconds later, making it impossible to study the penetration dynamics (lower concentrations of FDA have been used without success) (Figure 38). At the lateral roots, on the other hand, FDA was taking more time to diffuse through the RCC. This difference of permeability is probably due to the thickness of the cuticle, which is twice thicker in the lateral roots than in the primary root, but also possibly different molecular structure or composition. In addition, waxes also have an important function in permeability, therefore. Their presence at the RCC of primary and the lateral root has to be investigated.

4 minutes after application of FDA, differences between mutants to WT were highlighted (Berhin et al., 2019, Figure 4D). With its fully functional cuticle, WT did not show any FDA penetration after 4 minutes of staining. *bdg* showed a strong permeability which was expected due to unstructured cuticle observed at the lateral root cap with TEM (Berhin et al., 2019, Figure 1E). *dcr* displayed a strong permeability which was expected due to the holes observed at the RCC with TEM. *gpat4 gpat8* had an intermediate phenotype with a weaker permeability than *bdg* or *dcr* but still more permeable than WT. A similar phenotype was observed in *gpat4 gpat8* etiolated cotyledons having a confirmed cutin monomer deficiency (Creff et al., 2019). In addition to those results, *lacs2* was also studied. *lacs2* did showed only a weak any increased permeability which may be explained by a modified but

still clearly present RCC (Figure 33 and Figure 38). *gpat2* used as a control behaved similarly to WT since *GPAT2* was not expressed at the lateral roots at this stage (Figure 38).

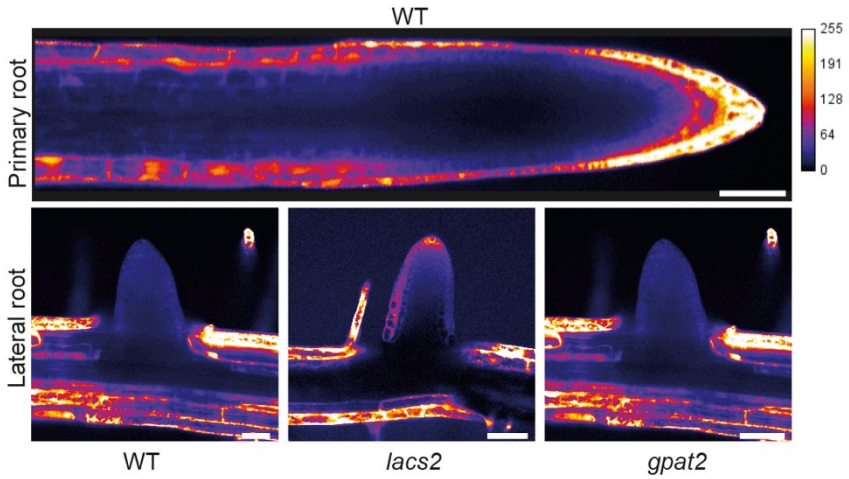

Figure 38: Penetration of the fluorescent cellular tracer fluorescein diacetate into root cap cells and meristematic cells of 2-day-old WT primary root and of shortly emerged lateral roots of WT, lacs2 and gpat2 after respectively 30 sec and 4 min of incubation. Relative intensity of the fluorescence is depicted by the color code. Scale bars, 50 µm.

Permeability to propidium Iodide

Frequently used in root studies to image the cell walls, it is common knowledge that PI does not enter easily into lateral root primordia. Preliminary tests confirmed that the RCC was the reason of this absence of penetration. In WT, *gpat2* and *lacs2*, after 30 seconds, none of primordia were stained, while 100% of them were in *bdg* and *dcr*. *gpat4 gpat8,* which always had an intermediate phenotype, presented 10% of non-stained primordia, 45% weakly stained and 45% strongly stained (Figure 39). Results are similar than with FDA for the lateral roots. At the primary root as well since WT was already stained after 30 seconds.

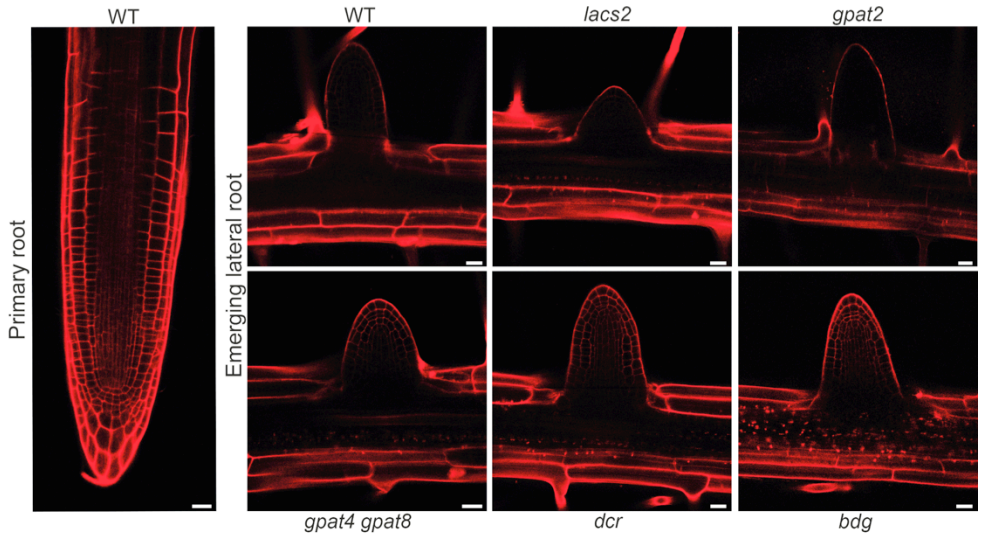

Figure 39: Penetration of the Propidium Iodide into root cap cells and meristematic cells of 2-day-old WT primary root and of shortly emerged lateral roots of WT, *lacs2, gpat2, gpat4 gpat8, dcr* and *bdg* after respectively 30 sec and 4 min of incubation. Scale bars represent 20 µm.

3.4.6. The RCC of the primary root protects the seedlings against harmful compounds

Permeability to radiolabeled ions

Inspired by the study on the radioactive phosphate uptake into the meristem via phosphate transporter (Kanno et al., 2016), we wanted to study whether the RCC plays a role as diffusion barrier to biological relevant ions and not only to dyes. We imagined an assay where the uptake of radiolabeled SO_4 and PO_4 could be followed in WT and mutants in order to show that more ions could enter the meristem in case of a defective cuticle. SO_4 and PO_4 were chosen for their natural presence in the environment and for their availability as radiolabelled (with ^{33}P and ^{35}S). The key points of the experiment were to limit the uptake of the radiolabel ions to only the root cap and to keep the integrity of the seedlings. 2-day-old seedlings were used to avoid the presence of endodermal suberin, which is present at older stages, and to be sure that the RCC was not yet gone. The small size of the 2-day-old seedlings was a real challenge. First, the root was drying in less than 10 seconds obliging us to keep a humid environment via humid filter application or agar blocks. Secondly, the radiolabel solution had to be precisely applied on the root tip only. Using drops, filter papers and vaseline as barrier, the radiolabelled solution was always spreading along the root due capillary forces. Thus, unfortunately, we had to abandon this experiment, as it was not doable on such small seedlings.

In vivo permeability to salt

The role of the RCC to protect the seedlings from salt and osmotic stresses was investigated. For that, seeds were grown on plates under different stress conditions and their state of development was evaluated after two days: not germinated, only the radicle emerged, or radicle and cotyledons emerged. Concentrations of salts were selected to impact as less as possible the WT seedlings. At 150 mM NaCl, 150 mM KCl, 100 mM K_2SO_4 and 400 mM mannitol had a strong impact on the germination of the WT seeds; similar results were obtained by Beisson et al. (2007). In order to have a second osmotic stress compound, we tried to establish a germination assay on PEG8000. However, plates are made by applying overnight a solution of PEG on a MS plate and dried, inducing a lot of variation in the plate humidity. This variability had a negative impact on the reproducibility of the data. Further

analyses were not carried on with PEG. Thus, germination assays were performed only under the following conditions: 100 mM NaCl, 100 mM KCl, 75 mM K_2SO_4 and 250 mM mannitol.

The comparison between WT and pLOVE1::CDEF1 plants highlighted a delay in seed germination and emergence of the radicle out of the seeds under all tested conditions. This underlined the importance of the RCC during seedling establishment and the impact on the development of the seedling in case of a defective RCC (Berhin et al., 2019, Figure 4B).

The study of the RCC mutants in the same conditions gave similar results (Figure 40). After 2 days under NaCl stress conditions, *lacs2, bdg* and *gpat4 gpat8* had a reduction of fully developed seedlings due to non-germination of the seeds and *lacs2* also an increase of seedlings at the stage of radicle emergence. Similarly, under KCL stress conditions, the reduction of fully developed seedling was due to a delay in germination for *gpat4 gpat8*, an increase of seedlings at the stage of radicle emergence for *lacs2* and both for *bdg*. Under NaCl and KCl growth conditions, *gpat2* was behaving like WT. K_2SO_4 in the medium induced a delay in development of the seedlings with an increase of non-germinated seeds and radicle emergence stage seedlings for *lacs2, gpat4 gpat8, bdg*, and only an increase of the radicle stage for *gpat2.* Osmotic stress mimicked by mannitol generated a development delay with more non-germinated seeds for *gpat4 gpat8* and more seedlings with only the radicle emerged for *lacs2* and both for *bdg* and *gpat2*. Surprisingly, under none of those conditions, *dcr* has presented difference with WT.

Studying the growth of *lacs2*, *gpat4 gpat8* and *bdg* under salt and osmotic stresses, gave results globally similar to the pLOVE1::CDEF1. However, with only the data from the RCC mutants, it would have been hard to claim that the effect was specific to the RCC since they may also have a defective seed coat, endosperm cuticle and embryo cuticle at the cotyledons potentially affecting the germination.

The seed coat is a suberin deposition at the surface of the seed. *gpat5* is a mutant presenting a defective suberization of the seed hilum and a change in its seed suberin composition (Beisson et al., 2007). It has a higher sensitivity to salt upon germination. However, at the concentration of NaCl, KCl and K_2SO_4 we used, only a slight difference (max 10 %) was observed with the WT (Beisson et al., 2007). Moreover, an increase of seed coat permeability, like *gpat5* has, does not lead to an increase of sensitivity to osmotic stress (Wang et al., 2011). To test the permeability of the seed coat, we used tetrazolium, a dye

that is reduced to red substrates when it enters the embryo where it is reduced by NADPH-dependent reductases (Beisson et al., 2007). Results showed that none of the mutants were as permeable as *gpat5* (Figure 41). Together, the low impact on germination under our salt conditions of a mutant having tetrazolium permeability and the fact that neither of our mutants showed a strong permeability to tetrazolium, we can suppose that, for none of those mutants, the seed coat has an implication in the observed higher sensitivity to salt during germination.

If seed coat is not defective, endosperm cuticle and cotyledon embryo cuticle most likely are. *bdg* has a defective endosperm cuticle (De Giorgi et al., 2015). *lacs2* has a similar phenotype that *bdg* in term of viability and dormancy suggesting a defective endosperm cuticle as well (De Giorgi et al., 2015). *gpat4 gpat8* has a defective embryo cuticle (Creff et al., 2019). In addition, the expression pattern of *GPAT4* in the seeds suggests that it could be involved in endosperm cuticle formation as well while *GPAT2* is not (Figure 8). The expression pattern of *GPAT2* (Figure 8), *LACS2*, *DCR* and *BDG* expression suggests an implication of those genes in the embryo cuticle formation with potentially a defective embryo cuticle in case of knockout of those genes (Panikashvili et al., 2009; Jakobson et al., 2016; Creff et al., 2019).

It is hard based on the RCC mutant results to establish which phenotype can be attributed to a defect of the endosperm cuticle or a cuticle defects at the cotyledon or the RCC or an accumulation of the three of them. From our knowledge no further control test could have been done to answer those questions. The *LOVE1* promoter is active only in the radicle of the embryo, making *CDEF1* expression specific to the basal part of the embryo only (Berhin et al., 2019, Figure S4A), and pLOVE1::CDEF1 plants the most suitable for the study.

In this assay, we evaluated the rate of germination and establishment of the seedlings after 2 days under salt or osmotic stresses. The detailed evaluation of the testa rupture would have been an additional criterion to fully understand if the non-germinating seeds stopped developing after or before seed opening, facilitating the entrance of the compounds.

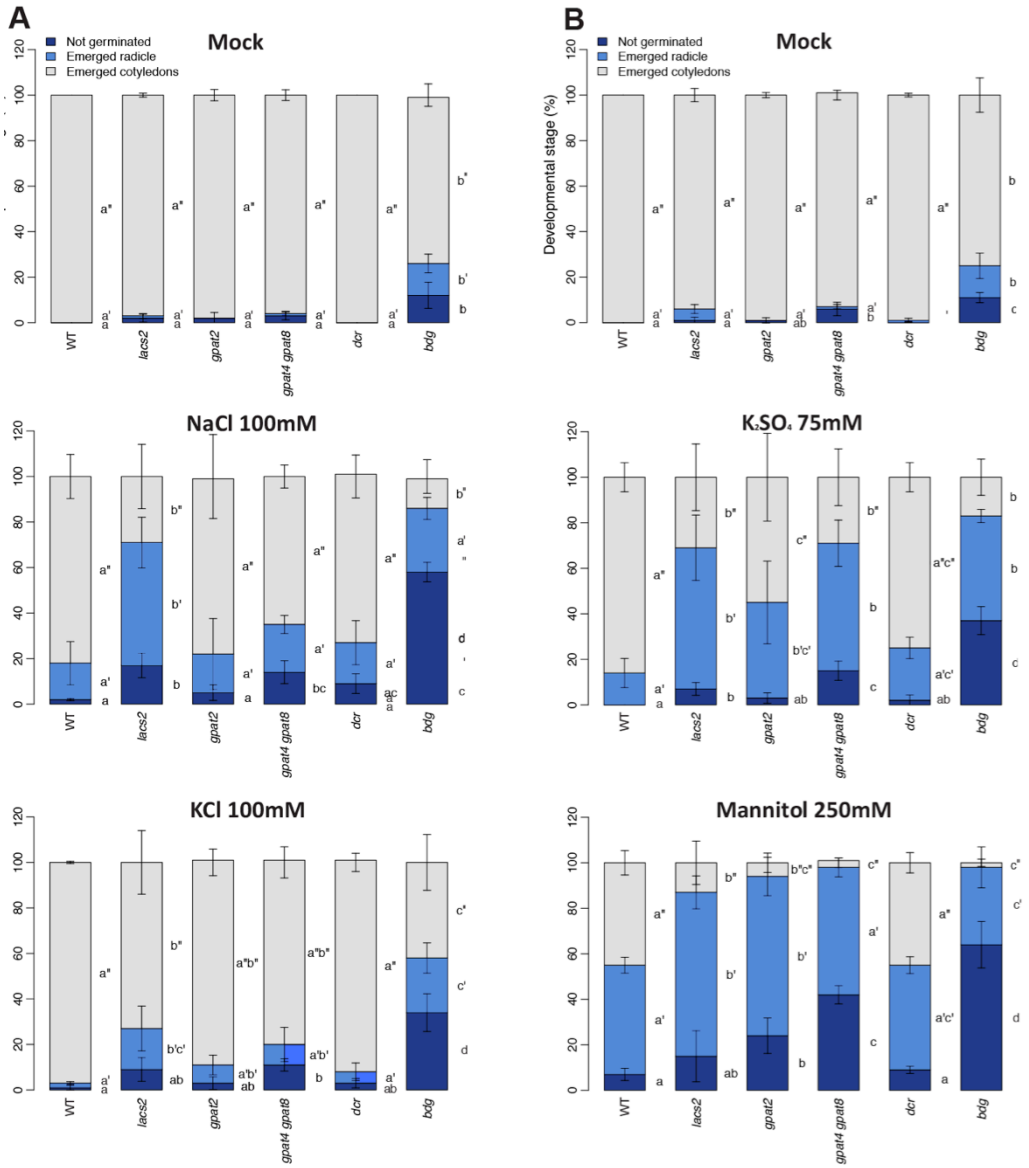

Figure 40: Evaluation of the impact on WT, *lacs2, gpat2, gpat4 gpat8, dcr* and *bdg* of medium with mannitol (250 mM), NaCl (100 mM), KCl (100 mM), and K_2SO_4 (75 mM) during early root development stages. Values represent the mean ± SD of the number of seedlings of each genotype having the indicated stage when grown in the presence of the respective compound (n=50-100). Significant differences to WT were determined by ANOVA. Each letter represents a significant variation between a genotype in a specific growth condition ($p < 0.05$.).

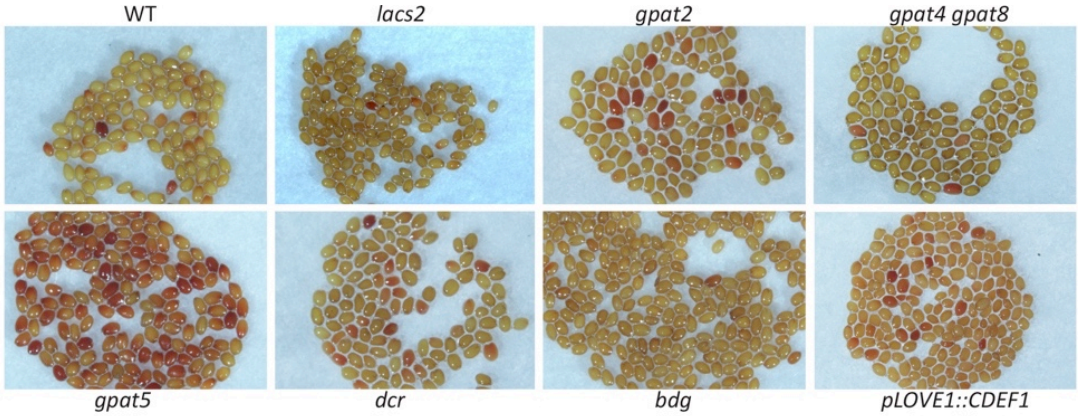

Figure 41: Tetrazolium staining on WT, *lacs2, gpat2, gpat4 gpat8, gpat5, dcr, bdg* and pLOVE1::CDEF1 highlithing the permeability of the seed coat. *gpat5* is the positive control.

Sensitivity of meristematic cells to high sodium concentrations

Until now, higher permeability to staining and higher sensitivity to salt and osmotic stresses have been shown when in presence of a defective cuticle, but it is not clear what impact it can have on seedling establishment. Previous data have shown that the incubation of a 5-day-old roots in 140 mM of NaCl for 6h kills cells in the meristem (Olvera-Carrillo et al., 2015). By adapting this to our 2-day-old roots, using 140mM of NaCl for 10 minutes, we could show that meristematic cells are dying faster in roots with a defective cuticle highlighting the role of the RCC in the protection of the meristem against harmful compounds (Berhin et al 2019, Figure 4C). Interestingly, meristematic cells were always dying first, suggesting that cells types detect and react to abiotic stress in different manner.

The same experiment was conducted overnight with 400 mM of mannitol (double amount than in the seedling growth experiments). But no cell death was observed, neither in WT or pLOVE1::CDEF1 seedlings indicating that osmotic and salt stresses act differently on the root meristem.

Even though the RCC is a transient structure, the results point to a crucial role of the RCC in protecting the meristem in the stage when it is very small and highly susceptible to stress conditions. Thus, the RCC gives the seedling some time to adapt, and perhaps helps to put other protective mechanisms in place (Zhu, 2016).

RCC of the primary root acts as a lubricant

Based on the theory of Marsollier and Ingram (2018), we hypothesized that the RCC is a lubricant covering the root tip helping it to emerge from the seeds but also to penetrate in the soil. However, we could not bring any evidence to support this theory. Indeed it has been attempted to develop an experiment where seeds were germinated on plate with agar from 0.7% to 1.4%. However, the high sensitivity of small seedlings and the variability in humidity of the plate had a bigger impact on the root penetration in the agar than the genotype itself, generating irreproducible data. Further analyses were not carried on.

3.4.7. RCC defects at primordia lead to delayed outgrowth of lateral roots

Lateral root emergence through the primary root

The speed of emergence of lateral roots in the RCC mutants is slower than in the WT (Berhin et al. 2019, Figure 4E) and some of their primordia have a deformed shape likely due to adherence of the lateral root primordium to the adjacent cells during the emergence through the primary root (Berhin et al. 2019, Figure 4F). Organ fusion and adhesion is a process that has been already observed in shoot cuticle mutants (Ingram and Nawrath, 2017). Hence, cuticle is a layer that is needed in the entire plant during development to avoid organ fusion or adhesion. Quantification in time revealed that 5-11% of the primordia are missed shaped 42h after bending while it drops to 2-7% at 48h and 96h. Moreover, fully emerged primordia grew normally. Both those observations suggest a transient phenomenon link to organ adhesion more than an organ fusion where cell walls are fused. The strong adhesion during lateral root emergence through the primary root could be the origin of the delay in lateral root outgrowth supporting the theory of Marsollier and Ingram (2018), proposing the presence of a lubricant at the surface of the lateral roots which could be our RCC.

Similarly to *gpat4 gpat8, dcr* and *bdg* (Berhin et al., 2019, Figure 4E), lacs2 have shown a delay in lateral root emergence after 42h of induction (Figure 42). While 80% of lateral roots were emerged in WT, lacs2 had none. Surprisingly, gpat2 is also presenting a delay in lateral root emergence while its RCC is not defective (Figure 33 and Figure 42). This could be explained by the fact that *GPAT2* is also expressed in cortex and epidermis, where it has an unknown function. Ideally, the expression of *CDEF1*, specifically at the lateral roots, would have been the perfect control, but we could not find any adequate promoter for such construct.

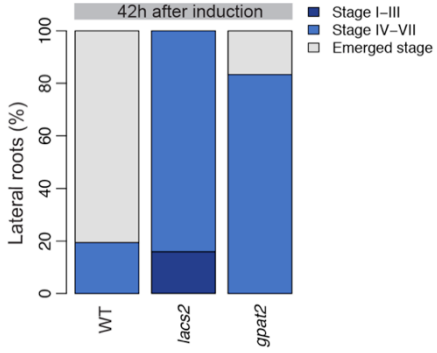

Figure 42: Stages of lateral root primordia 42 h after induction were evaluated in WT and in *lacs2* and *gpat2* at the lateral root primordium. Stages were determined as described in Casimiro et al.(2003): stage I–III, before breakage into the cortex; stage IV–VII, within the outer layers of the primary root; emerged, outside of the primary root.

Instead of inducing the lateral root formation like we previously did, another way to show that lateral root primordia have a delay in emergence was to count the number of lateral roots per seedling. From the hypocotyl towards the tip, lateral roots are emerged and getting smaller until the non-emerged primordium stage is reached closer to the tip. We noticed that among the emerged lateral roots, we could sometimes observe a single non-emerged lateral root, that we called delayed primordium. No difference was observed between WT and the RCC mutants in the number of non-emerged primordium suggesting a normal initiation of the lateral root formation. However, the number of delayed primordia increased in the mutants and the number of emerged lateral root deceased, indicating a delay in the emergence of some lateral roots (Figure 43). These data meet the conclusion obtained in the previous assay where the lateral roots were induced upon bending: a defective RCC delays the emergence of lateral roots.

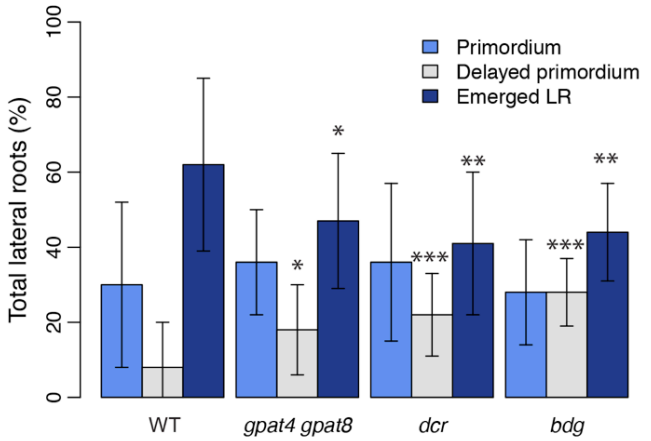

Figure 43: Observation of the emergence of the lateral root on 8-day-old seedlings of WT, *gpat4 gpat8, dcr* and *bdg.* Three categories were established: Primordium, lateral root primordium close to the tip of the root; Emerged LR, lateral root that has emerged out of the primary root; Delayed primordium, primordium localized in the zone where all lateral roots are already emerged. Values represent the means ± SD, n = 8–10. Asterisks denote significant differences to as determined by Student's t test: ***p < 0.001; **p < 0.01; *p < 0.05.

Impact of sucrose on the lateral root development

Contradictory reports claim that mutants having impairments in the cuticle of the shoot, such as *bdg* and *dcr*, have more lateral roots than WT at the opposite of what we observed (Kurdyukov et al., 2006a; Panikashvili et al., 2009; Wu et al., 2015). The origin of this discrepancy lays in the use of sucrose in the culture medium, as revealed by MacGregor et al. (2008). In our studies, no sucrose is present in the medium.

As a control, we have grown RCC mutant having an obvious phenotype at the lateral roots with 0% and 1% sucrose in the medium. The addition of the sucrose clearly increased the number of lateral root formation, but it did not influence in any way the RCC phenotype at the lateral roots. This confirms that the increase of lateral roots in cuticle mutants is not related to the loss of the RCC phenotype but due to the uptake of the sucrose by the permeable leaves.

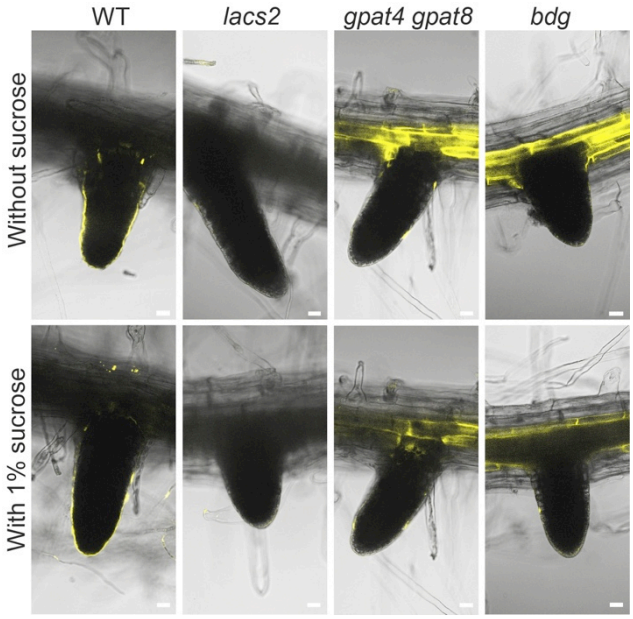

Figure 44: Median views of the FY staining of the developing lateral root of WT, *lacs2, gpat4 gpat8* and *bdg* with 1% of sucrose ad without any sucrose (overlay bright field and fluorescence). FY stained the suberin of the endodermis and the RCC, when present. Scale bars represent 20 µm.

3.4.8. No evidence links the role of hormones to the RCC formation

It has been reported that hormones can induce or inhibit polyester formation (Barberon et al., 2016). As a preliminary study, we screened several hormone mutants. This experiment was done quickly during the reviewing process of the paper, hence the mutants used were the ones we could obtain in a short time frame.

To study the possible involvement of ABA in RCC formation, *aba2, abi3-8* and *abi5-8* were tested. *aba2* is an ABA deficient mutant biosynthesis while *abi3* and *abi5* are ABA insensitive mutants (Barberon et al., 2016; L'Haridon et al., 2011). *aba2* and *aba3* have a permeable shoot cuticle and a decrease of suberin deposition in the roots (Barberon et al., 2016; L'Haridon et al., 2011). *ABI5* is targeting cutin biosynthetic genes (De Giorgi et al., 2015). No change in FY could be observed at the root cap of those mutants (Figure 45 and Figure 46).

Mutants like *abi1, snrk2.2 snrk2.2 snrk2.6* and *pyr1 pyl1 pyl2 pyl4 pyl5* that have shown to have a shoot permeable cuticle or *abi4* with a reduced suberization in the roots could still be studied (Barberon et al., 2016; Cui et al., 2016). To understand if ethylene can have an impact on the regulation of RCC pathway, *etr1* and *ein2* mutants were studied. *etr1* is an ethylene resistant mutant insensitive to cytokinin and which has an inhibition of lateral root development (Laplaze et al., 2007; Barberon et al., 2016). *ein2* is an ethylene insensitive mutant. No FY changes could be observed in those mutants (Figure 45 and Figure 46). *ein3* presenting a reduced suberization of the root could still be studied (Barberon et al., 2016). The relation between cuticle formation and cytokinin is poorly understood, but shoot cuticle mutants have alterations in cytokinin perception (De Giorgi et al., 2015; Ingram and Nawrath, 2017). *LOG3, LOG4* and *AHP6,* which regulate cytokinin activity, are expressed in the lateral root primordia (Kuroha et al., 2009; Moreira et al., 2013). Their mutants, *log3 log4* and *ahp6,* presented no FY phenotype (Figure 45 and Figure 46). Knowing the importance of auxin during the process of lateral root formation, *aux1-7, aux1-21, yuc2 yuc5 yuc6 yuc8* and *d6pk*, auxin mutants, were tested. None showed a defective cuticle (Figure 45 and Figure 46). Since exogenous application of gibberellic acid is known in agriculture to enhance cuticle thickness, it would be worth to investigate some mutants like *ga1,* a mutant known for its cutin reduction (Shi et al., 2011; Doaigey et al., 2013).

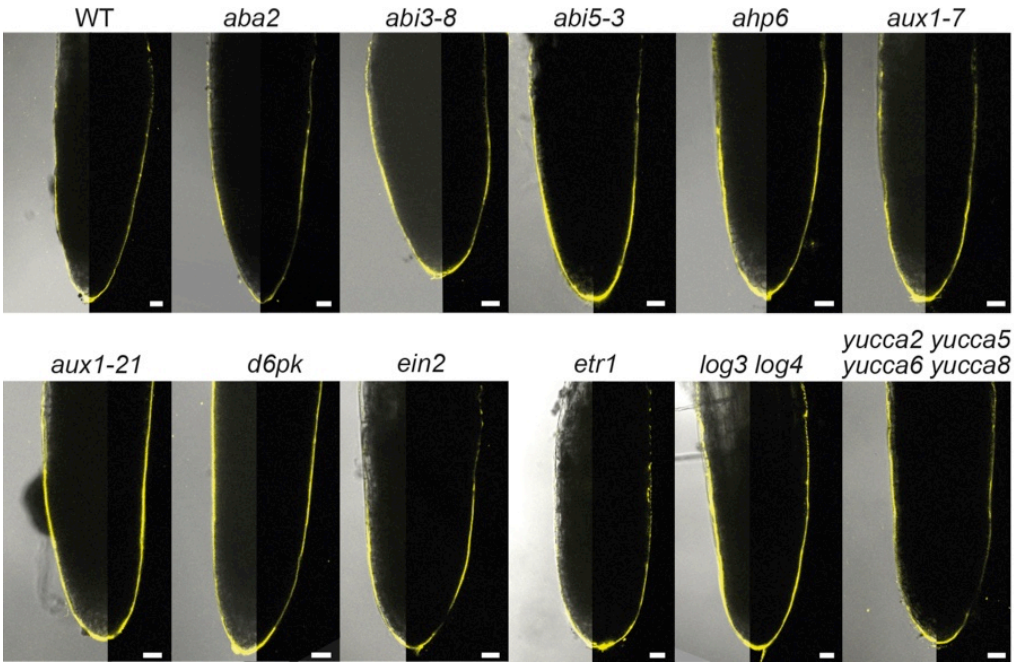

Figure 45: Median views of the FY staining at the root cap of 2-day-old WT, *aba2, abi3-8, abi5-3, ahp6, aux1-7, aux1-21, d6pk,ein2, etr1, log3 log4* and *yuc2 yuc5 yuc 6 yuc8* (on the left, overlay bright field and fluorescence; on the right, fluorescence only). Scale bar is 20 µm.

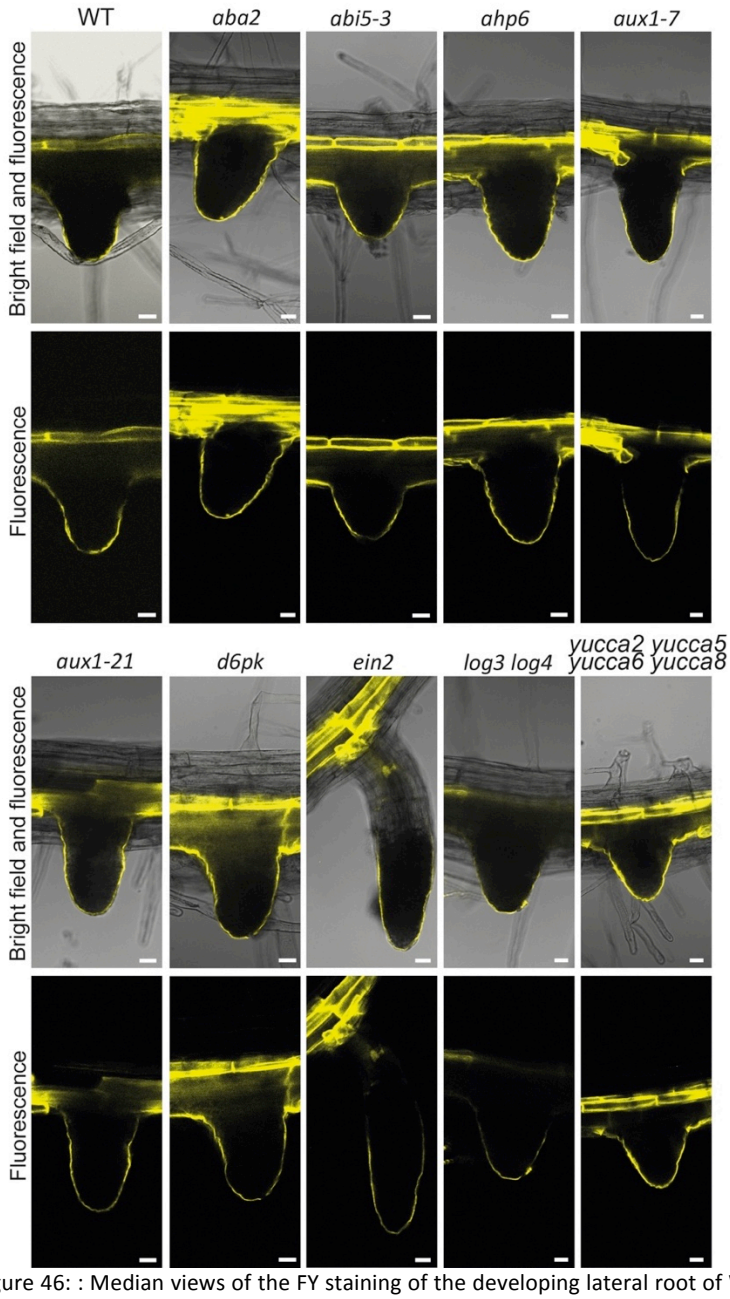

Figure 46: : Median views of the FY staining of the developing lateral root of WT, *aba2, abi5-3, ahp6, aux1-7, aux1-21, d6pk, ein2, log3 log4* and *yuc2 yuc5 yuc6 yuc8* (on the trop, overlay bright field and fluorescence; on the bottom, fluorescence only). FY stained the suberin of the endodermis and the RCC, when present. Scale bars represent 20 µm.

None of those results could confirm the link between RCC formation and hormones. Cuticle is more complex to study than suberin. An increase of cutin may not be visible by FY. Ideally, performing biochemical analysis would be the best way to see if there is an accumulation of cutin monomers. However, since a defective cuticle should be visible with FY, we can conclude that none of the studied mutants can inhibit RCC formation: more mutants should be investigated. The exogenous application of abscisic acid, gibberellic acid, ethylene or

cytokinin is another approach worth a try, in order to identify a cuticle defect link to one of them similarly to what Barberon et al. (2016) have done with suberin.

3.5. Perspectives

Opening a new field of research, the characterization of the RCC is far from being over. Several perspectives and ideas of future studies are here exposed.

Identification of the entire RCC biosynthetic pathway

During the course of our research, we have identified 6 genes that are involved in the biosynthetic pathway of RCC: *LACS2*, *GPAT2*, *GPAT4*, *GPAT8*, *DCR* and *BDG*. More genes like *GPAT3*, *GPAT7*, *F5H, HTH, LTPG1* and *LTPG2* have been investigated by FY, but a deeper analysis with TEM and biochemistry would really allow to conclude on their implication in the RCC formation. Negative results would lead to the investigation of other family members to study them alone or as multiple knockouts in case of possible redundancy. *ABCG11,* expressed at the root cap, still needs to be studied as well. Other genes, with an unknown expression pattern but an activity potentially at the origin of the formation of monomers present in the RCC composition, should still be investigated. For example, enzymes catalyzing the oxidation and polymerization step could be for sure uncovered.

Examination of the possible presence of wax at the RCC

Shoot cuticle is made of cutin and waxes. Intracuticular waxes are deposited within the cutin matrix while extracuticular waxes are deposited at the surface of the cuticle as crystals or film (Yeats and Rose, 2013). We have identified that the RCC is made of cutin, but whether there is wax deposition still has to be investigated. Several genes are known to be involved in wax formation (Samuels et al., 2008). The expression at the lateral roots of *CER3* and *CER17* has been reported (Kurata et al., 2003; Yang et al., 2017). It is a first hint in the direction of the possible presence of waxes at the RCC.

Role of the RCC during the emergence from the seeds

Cuticle prevents adhesion of plant aerial organs (Ingram and Nawrath, 2017). Organ fusion is a common phenomenon observed within or between shoot organs in cuticle mutants. During embryo development, the cuticle has an important function in the separation of embryo and the endosperm. Embryo with a defective cuticle presents a failed separation

embryo/endosperm (Tsuwamoto et al., 2008; Yang et al., 2008; Xing et al., 2013). The identification of the embryo sheath, defective in the mutants having a defective cuticle as well, calls into question the involvement of each structure. In addition to a role in properly separating organs, the primary root RCC could have a lubricant and protective function allowing a smooth emergence of the radicle out of the seed, similarly to the lateral roots (Marsollier and Ingram, 2018; Berhin et al., 2019). This has to be studied more in details.

Role as a barrier protecting primordia of enzyme digesting the middle lamellae of the endodermal cells

A key step of the lateral root formation is the crossing of the endodermal cells made possible by the digestion of their middle lamellae. This digestion is delicate since it has to digest the endodermal lamellae and not alter the lateral root primordium cell wall. A hypothesis is that the demethylesterification of the endodermal cell wall could restrict the digestion only to those tissues by the pectate lyses that degrade specifically demythylesterified pectin (Laskowski et al., 2006). With the discovery of the RCC, another hypothesis could be that the cuticle protects primordia from the digestion enzymes. This has to be investigated further.

Role in the interaction with microbes

The cuticle is a physical barrier against pathogen (Nawrath, 2002). Nevertheless, it has been shown that several cuticle mutants in the leaves have a higher resistance to some pathogen due to the constant production and diffusion of anti-fungal components through the permeable cuticle (Chassot et al., 2007; Serrano et al., 2014). The interaction between RCC and microbes has to be explored to see if the RCC can be considered as well as a barrier to protect from microbe invasion. If it is the case, it can be expected to see in some cases, a resistance to pathogen in RCC mutants, like in the leaves.

Identification of signals controlling RCC formation

Little is known about changes in cutin composition in response to stresses. At the opposite, suberin deposition has shown to be regulated by the salt present in the environment through hormone induction (Barberon et al., 2016).

In Berhin et al. (2019), the RCC permeability and composition was assessed only under standard conditions but we would like to investigate if the plant could protect itself from

dangerous environment by modulating the RCC. The study of the permeability of the RCC in function of the surrounding environment would feature the potential plasticity of the RCC. The evaluation of the RCC composition under stress conditions and the identification of stresses and of hormones influencing RCC formation would be big steps in the cuticle field.

The root cap cuticle has been characterized as present on the root tip until the sloughing off of the first root cap cell layer. It would be interesting to investigate if this RCC could be reformed at a later stage under certain stress condition. An approach through the study of induction of cuticle-related transcription factor under stress condition could be an option.

Characterization of a similar structure in monocots

No root organ fusion has been reported (Ingram and Nawrath, 2017). However inter-tissue fusion was already observed. In rice, the knockout of *ONION3 (ONI3)*, a putative, ω-alcohol dehydrogenase, homolog of *HTH*, presents a fusion of the root epidermis and root cap in addition to the classic organ fusion in the shoot (Akiba et al., 2014). In the shoot, organ fusion is usually attributed to cuticle defects. In rice, the zone between the root cap and the meristem is called the root cap junction and is characterized by a thick cell wall boundary making the root cap cells easily detachable (Wang et al., 2014). The observation of tissue fusion in *oni3* suggests the possible presence of a polyester deposition at its surface.

In addition, RCC have not yet been studied in monocots. Thus, both of those points have to be characterized deeper.

3.6. Conclusion

Plant cuticles have been studied closely and from every angle for centuries. In contrast to suberin lamellae found in different tissues of the roots and shoots, the cuticle has only been characterized in the epidermal cells of the shoot (Pollard et al., 2008). Moreover, a cuticle at the root was imagined not to be compatible with the function of water and nutrient uptake. Without being able to prove the opposite, the specific localization of the cuticle at the epidermis of the aerial organ was a define feature of the cuticle (Fich et al., 2016). Our innovative research led to the discovery of a cuticle where least expected, at the root cap of the primary and lateral roots.

In this chapter and the quoted paper, we showed that the RCC is of a crucial importance for root physiology and development. It is present from early stages of root development: in the embryo for the primary root and at the early stage of the lateral root primordium formation. The RCC protects the meristem until the first loss of the outer root cap cell layer. During the delicate developmental stage of germination and seedling establishment, the RCC acts as a diffusion barrier protecting the meristem from saline and osmotic stresses. In addition, at the lateral roots, the RCC has also a lubricant function preventing adhesion during the emergence of the lateral roots through the tissues of the primary root, similarly to the cuticle in the shoot. Its composition consists of an atypical cutin and we already identified six genes involved in its biosynthetic pathway: *LACS2, GPAT2, GPAT4, GPAT8, DCR* and *BDG*.

This discovery opens a new chapter in the characterization of cuticle in plants. More studies on this new structure can be expected in the future.

3.7. Collaborators and contributions

In this study, I designed, performed and analyzed all the experiments, at the exception of TEM preparation of the samples and imaging, that was executed by Damien de Bellis. Rochus B. Franke contributed at the identification of the monomers for the GC-MS analyses. Rafael A. Buono and Moritz K. Nowack suggested us to work with *LOVE1* promoter and provided the pLOVE1::H2A-GFP line. In addition, the sudan staining and imaging was performed by Sylvain Loubery.

I prepared all the figures and actively participated in the writing and reviewing of the manuscript.

4. The role of *GPAT4*, *GPAT6*, *GPAT7* and *GPAT8* in endodermal suberin formation

4.1. Introduction

Suberin deposition at the endodermis has been already well investigated and several genes are known to be involved in its formation, such as *GPAT5*. Surprisingly *GPAT4*, *GPAT6*, *GPAT7* and *GPAT8* are also expressed in the endodermis of the roots (Figure 10) and we thus aimed to investigate their possible function in suberin formation.

Here, I shortly introduce the suberin deposition in the endodermis and present some evidences on why *GPAT4, GPAT6, GPAT7* and *GPAT8* could also be involved in suberin formation.

4.1.1. Endodermal suberin and its plasticity

Suberin is deposited at the inner side of cell wall of the differentiated endodermal cells and it can be stained with FY (Naseer et al., 2012). A study of the uptake of FDA through the root reveals that this deposition blocks the Apoplastic and Trans-cellular transport pathway (Barberon, 2016; Barberon et al., 2017). Suberin deposition has been considered for a long time as static. Recent researches have highlighted the plasticity of suberin deposition depending of the availability of nutrients (Barberon, 2016; Barberon et al., 2017). This adaptation is mediated by two antagonist hormones: ABA and ethylene. Salt treatment or potassium and sulfur deficiency stimulate ABA signaling pathway, which induces suberin biosynthesis pathway leading to over-suberization. In contrast, iron, manganese and zinc deficiency enhance ethylene production that leads to a reduction of the suberization. Ionomic data shows that over-suberized roots tend to increase their potassium accumulation and to decrease the magnesium and calcium while at the opposite less suberized roots increase their magnesium, calcium and sodium accumulation and decrease potassium. Thus, the nutrient-dependent suberization plasticity affects nutrient transport in both directions, from the stele to avoid leakage and from the cortex to control influxes.

Intriguingly, ABA treatment enhances at the same time suberin deposition in the cortex cells (Barberon, 2016; Barberon et al., 2017).

4.1.2. Role in endodermal suberin formation of *GPAT5* and potentially also *GPAT4, GPAT6, GPAT7* and *GPAT8*

GPAT5 is a well-characterized gene involved in suberin formation in the endodermis. Its corresponding mutant presents a delay in endodermal suberization and changes in suberin composition with mainly reduction in C22 and C24 fatty acids derivatives (Beisson et al., 2007; Naseer et al., 2012).

The investigation of *GPAT4* to *GPAT8* expression in the roots (see Chapter 2) confirmed the expression of *GPAT5* in the endodermis, but also highlighted the presence of *GPAT4*, *GPAT6*, *GPAT7* and *GPAT8* in the same cell layer (Figure 10). Studies of the expression level of those genes in each of their single mutant backgrounds showed a tight relation between one another, i.e. a down regulation of the other *GPAT* genes, when one gene is knocked out or an overexpression of *GPAT5* in *gpat6-2* (Figure 13). A down regulation phenomenon has already been reported by Petit *et al. (2016)* in *gpat6* tomato fruit where many genes from the cutin biosynthetic pathway were down regulated, including *GPAT4*.

Since suberin is the only so far described polyester deposited in the endodermis, we hypothesized that *GPAT4*, *GPAT6*, *GPAT7* and *GPAT8* may be also involved in suberin formation.

GPAT4 and *GPAT8* are required to produce C16:0 DCA, C18:0 DCA, C18:1 DCA, C18:2 DCA and ω-OH C18:2 FA in stem and leaf cutin (Li et al., 2007a; Fabre et al., 2016). Those are compounds that are also present in suberin, even when in different amounts. *GPAT4* homologs in *Brassica napus* that were confirmed to be involved in leaf cutin formation are also expressed in the endodermis of the root and in the seed coat, suggesting a role in suberin formation (Chen et al., 2011b). Moreover, like *GPAT5, GPAT4* was identified in phellem of cork oak (Marum et al., 2011). This information suggests a possible role of *GPAT4* in suberin formation and in consequence *GPAT8* also since they are known to be redundant.

GPAT6 is needed for the formation of 10,16-dihydroxy C16:0 FA, ω-OH C16:0 FA and C16:0 FA in flowers (Li-Beisson et al., 2009; Yang et al., 2010). Similarly in tomato fruit *GPAT6* is

involved in the formation 9/10,16-dihydroxy C16:0 FA, C16:0 DCA, 9/10-hydroxy C16:0 DCA, ω-OH C16:0 FA, 10-oxo-ω-OH C16:0 FA and C16:0 FA (Petit et al., 2016). This suggests that *GPAT6* is mainly using C16 fatty acid derivatives as substrate, which are also present in suberin in the form of C16:0 DCA and ω-OH C16:0 FA monomers. To a lower extent also changes in other components of suberin, C18:0 DCA and ω-OH C18:1, C18:2 and C18:3 FAs, were also observed in *GPAT6* knockout and overexpression lines (Li-Beisson et al., 2009; Fabre et al., 2016; Mazurek et al., 2017). *In vitro* assays have shown the possibly of GPAT6 enzyme to also use ω-OH C18:1 FA and C18:1 DCAs as substrate (Yang et al., 2017). The enzymatic activity of GPAT6 does not exclude a role in suberin monomer formation.

GPAT7 has only been identified as mandatory for suberin formation upon wounding in leaves (Yang et al., 2012). It is unknown which monomer formation depends on *GPAT7* activity. With its high sequence similarity with *GPAT5, GPAT7* is a good candidate for suberin formation in the endodermis.

4.2. Strategy

Based on the expression pattern of *GPAT4, GPAT6, GPAT7* and *GPAT8* in the endodermis of the root, we investigated the role of those genes in endodermal suberin formation.

gpat4 gpat6-1 gpat8 triple mutant was generated to knockout simultaneously all three genes that have an acyltransferase and a phosphatase domain. Furthermore, we generated *gpat5 gpat7* to knockout this clade of *GPAT*s that was commonly associated with suberin formation and having only an acyltransferase domain but no phosphatase domain. Using those mutants, FY was used to monitor suberin deposition in the mutant roots in order to see a possible delay in suberin formation in the endodermis when genes are knocked-out. In addition, biochemical analyses revealed which monomers were affected by the knockout and the possible function of those genes in suberin formation.

4.3. Results

4.3.1. *GPAT4, GPAT5, GPAT7* and *GPAT8* are involved in endodermal suberization

FY staining has been shown to be a useful tool to study a delay in suberization due to the knockdown of suberin genes, i.e GPAT5, HORST, FAR1, FAR5 (Naseer et al., 2012; Andersen

et al., 2018). The percentage of suberization of the roots was evaluated starting from the first suberized cell, not localized around an emerging lateral root. None of the single mutants displayed a delay in suberization at the exception of *gpat5* that had 15% less of the root suberized. In contrast, the knockout of *gpat7* in addition to *gpat5* reduced the suberization zone by 40% compared to WT and by 25% to *gpat5* (Figure 47). A reduction similar to *gpat5* was observed in *gpat4 gpat8* having a suberization of 50% of the root, instead of 65% in WT (Figure 47). Interestingly, *gpat4 gpat6-1 gpat8* did not present a stronger reduction of suberization than *gpat4 gpat8*.

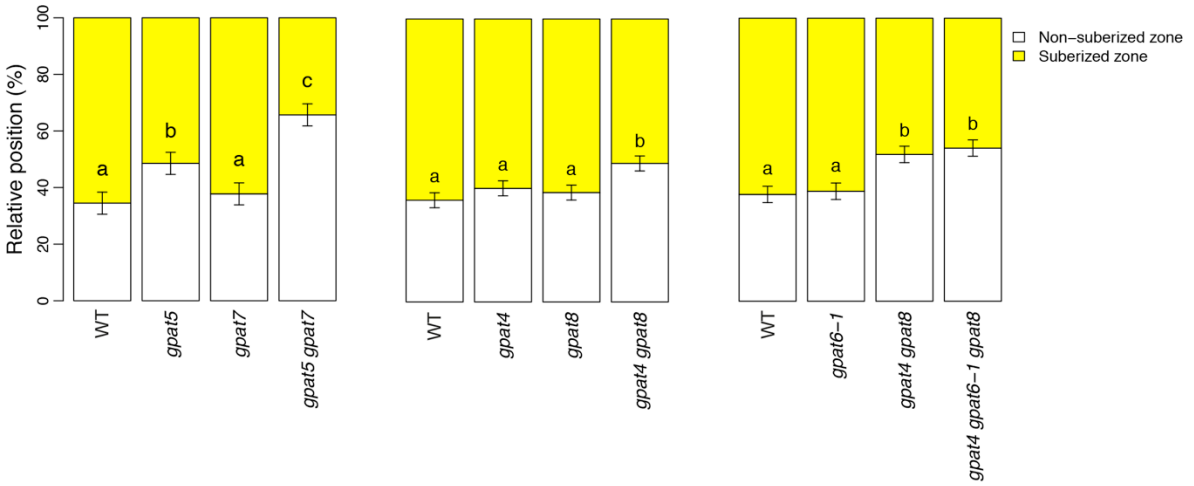

Figure 47: Quantification of the percentage of the suberization in the root using FY as a staining in WT*, gpat5, gpat7, gpat5 gpat7, gpat4, gpat8, gpat6-1, gpat4 gpat8* and *gpat4 gpat6-1 gpat8*. Significant differences to WT were determined by ANOVA. Each letter represents a significant variation between a genotype in a specific growth condition ($p < 0.05$.).

4.3.2. *GPAT7* is redundant to *GPAT5*

Biochemical analyses with gas chromatography-mass spectrometry (GC-MS) were done on 5-day-old roots in order to investigate fatty acid monomer changes in single and double knockouts.

In these analyses, the *gpat7* was found to have no changes in the fatty acid composition and content when compared to WT (Figure 48).

Yet, in *gpat5,* the amount of aliphatic polyesters was reduced: C20:0 FA of 85%, C22:0 FA of 75%, C24:0 FA of 55%, ω-OH C16:0 FA of 40%, ω-OH C18:1 FA of 60%, ω-OH C20:0 FA of 80%, ω-OH C22:0 FA of 60%, ω-OH C24:0 FA of 40%, C16:0 DCA of 30%, C18:2 DCA of 35% and C18:1 DCA of 45% when compared to WT (Figure 48). In the double knockout, these were further reduced: C22:0 FA of 85%, C24:0 FA of 55%, ω-OH C20:0 FA of 90%, ω-OH C22:0 FA of 90%, ω-OH C24:0 FA of 80% and C18:1 DCA of 30% in comparison to *gpat5*, at

the opposition, ω-OH C16:0 FA was slightly increased (Figure 48). *gpat5 gpat7* is similar to *gpat5* for the content of C20:0 FA, ω-OH C18:1 FA and C18:2 DCA, meaning that *GPAT7* knockout has no impact on the formation of those fatty acids. A slight increase but non-significant of the primary alcohols observed could be the results of a compensation mechanism. Light variations in C20:0 DCA and C22:0 DCA were also observed but they are hard to perfectly quantify since really close to the detection limit.

In the analysis, it is necessary to mention that C24:0 alcohol was not detected. Contrarily, C18:0 DCA and C24:0 DCA were detected, however their peak was fused to another compound making the quantification impossible.

Hence, those results showed significant reduction in aliphatic monomers of suberin, such as C20:0 FA, ω-OH C20:0 FA and C18:2 DCA due to *GPAT5* knockout and C22:0 FA , C24:0 FA, ω-OH C18:1 FA, ω-OH C22:0 FA, ω-OH C24:0 FA and C18:1 DCA due to the knockout of *GPAT5* and amplified by the knockout of *GPAT7*.

While analyzing aromatic acids, it is important to note that plants can only make trans acids. cis acids depend of the isomerization during sample procession. Ideally, they should be summed up. For ferulic acid, depending of the purity of the cis peak, researchers tend to present only the trans. In our case, both peaks were clean so both data can be considered (Figure 49). For the coumaric acid, in general, even the trans peak is quite variable due to possible impurities. In this study, cis and trans coumaric acid could be detected, even if in traces, and the peaks were not pure. Quantification was still attempted to evaluate if there was a possible strong reduction. Results presented no detectable change in coumaric acid and ferulic acid in any of the mutants (Figure 49).

In conclusion, *gpat7* has no phenotype on its own but combined with *gpat5*, it amplifies *gpat5* phenotype. This is an evidence of the redundancy of both genes with *GPAT5* being the dominant factor. Their knockdown affects unsubstituted and oxygenated fatty acids but not the aromatics.

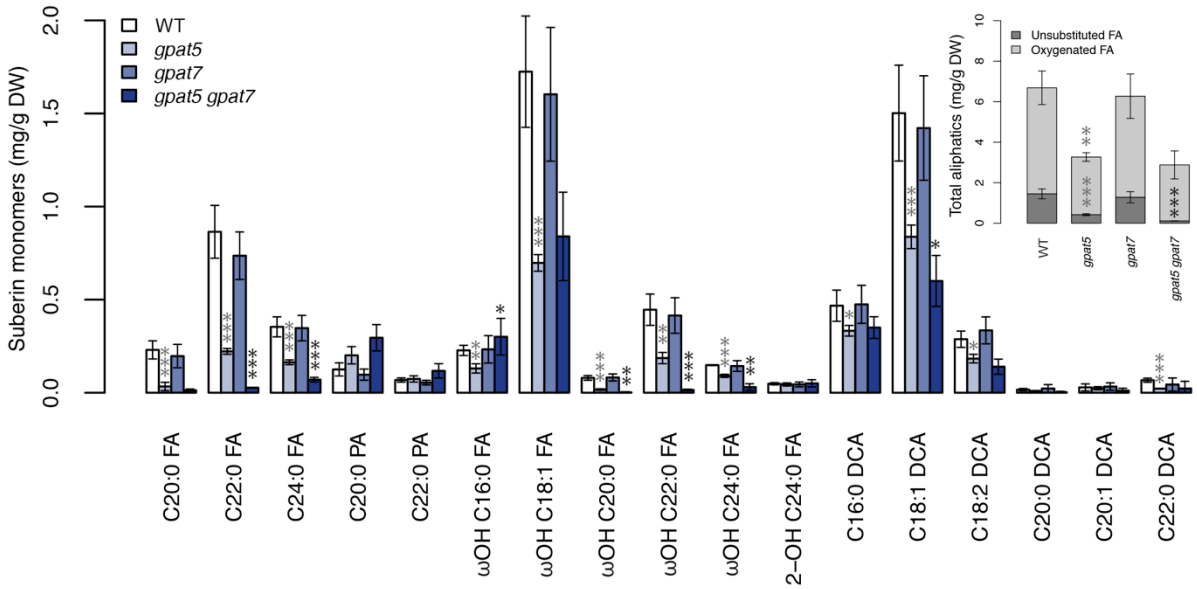

Figure 48: Quantification of aliphatic ester-bond cutin monomers isolated from 5-day-old roots of *gpat5, gpat7* and *gpat5 gpat7* in comparison to WT. Left graph shows the principal cutin monomers and right graph shows the total of evaluated aliphatic compounds on the left grouped by substance classes. Values represent the means ± SD, n = 3–4. Asterisks denote significant differences to as determined by Student's t-test: ***p < 0.001; **p < 0.01; *p < 0.05. Grey asterisks, statistic significance of *gpat5* compared to WT; black asterisks, statistic significance of *gpat5 gpat7* compared to *gpat5* FA, fatty acid; DCA, dicarboxylic acid; PA, primary alcohol; DW, dry weight.

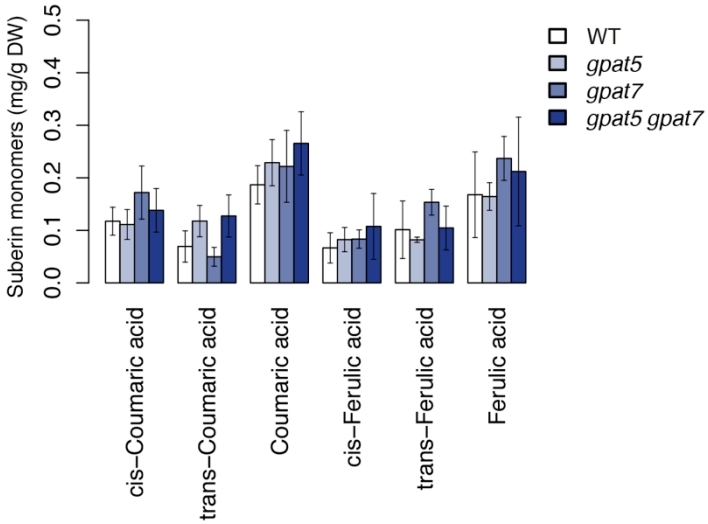

Figure 49: Quantification of aromatic ester-bond cutin monomers isolated from 5-day-old roots of *gpat5, gpat7* and *gpat5 gpat7* in comparison to WT. Values represent the means ± SD, n = 3–4. Significant differences were determined by Student's t-test: no data were significantly different at p < 0.05. DW, dry weight.

4.4. Discussions and perspectives

4.4.1. *GPAT7* acts redundantly with *GPAT5* in the formation of suberin

Redundancy is common in gene families containing a large number of members. In the *GPAT* family, *GPAT4* and *GPAT8* were already reported to act redundantly in cutin formation at the leaves and the root cap. (Li et al., 2007a; Li-Beisson et al., 2009, Berhin et al.,2019). It was previously suggested that there is a redundancy between *GPAT5* and another *GPAT* family member (Li et al., 2007b). *GPAT7* is constitutively expressed in the root endodermis (Figure 10) and implicated in formation of wound-induced suberin in the leaves (Yang, et al.,2012). Moreover, GPAT7 is similar to GPAT5 in term of sequence (Figure 7) and enzymatic activity (Yang, et al.,2012). Those reasons made *GPAT7* the best candidate to be redundant with *GPAT5*.

GPAT7 knockout does not have any impact on the suberin deposition neither on polyester monomer profile (Figure 47 and Figure 48). Nevertheless, its combination with *gpat5* mainly enlarged the delay in suberization and the monomer difference already existing between *gpat5* and WT. Beisson *et al.* (2007) did not report any change in C18:1 ω-OH FA content in one-week-old roots, as we did in 5-day-old roots. However, they obtained similar data in three-week-old roots. This confirms that C18:1 ω-OH FA incorporation in suberin depends of *GPAT5* and *GPAT7* activity. The reduction of 70% unsaturated and 50% oxygenated FAs in *gpat5*, respectively compared to WT, and 90% and 50% in *gpat5 gpat7* might underlie the general decrease in suberization observed with FY staining of these mutants, with 25% less suberization in *gpat5* and 40% in *gpat5 gpat7* compared to WT. The delay in suberization of *gpat5* was already reported by Naseer et al. (2012). The study of C20:0 DCA, C22:0 DCA, C24:0 DCA was not appropriate in roots since their amount are low, at the opposite of the seeds where Beisson *et al.* (2007) could show the role of *GPAT5* in C22:0 and C24:0 DCA. No change in aromatics was observed in any of the mutants confirming the previous results obtained on *gpat5* roots and seeds (Beisson et al., 2007). Our results also get along with the *in vitro* activity of *GPAT5* presenting a higher affinity for oxygenated C22:0 and unsubstituted C20-C24 than for oxygenated C16:0 and C18:0 (Yang et al., 2012).

Those results allow us to conclude that, in roots, *GPAT7* is constitutively involved in suberin formation and is redundant with *GPAT5*. Beisson *et al.* (2007) established that *GPAT5* is

supplying C20:0, C22:0 and C24:0 fatty acid derivatives to the polyester pathway while the variation in C16 and C18 monomers would be linked to a compensation mechanism: this hypothesis can be extended to *GPAT7*. The compensation mechanism is linked to the fact that suberin is a complex structure in which the reduction of the incorporation of one compound can have a direct impact on the incorporation of others compounds and this may vary in function of the organs and the polymer structure (Beisson et al., 2007).

4.4.2. *GPAT4* and *GPAT8* act in both cutin and suberin biosynthesis

In leaves and at the root cap, *GPAT4* and *GPAT8* were already characterized as redundant since only the double knockout has a permeable cuticle (Li et al., 2007a; Li-Beisson et al., 2009, Berhin et al.,2019). In the roots, the same phenomenon is observed with a delay of suberization of the endodermis only visible in *gpat4 gpat8*. However, the delay of suberization in *gpat4 gpat6-1 gpat8* was not enhanced compared to *gpat4 gpat8* suggesting that *GPAT6* is not redundant to *GPAT4* and *GPAT8*. Before claiming it, the study of *gpat6-2* alone should be performed since this allele is knocked out while *gpat6-1* is only reducing *GPAT6* expression (Figure 12). A first quick attempt of isolation of *gpat4 gpat6-2 gpat8* failed (Delphine Le Roux, unpublished). Another effort to isolate this triple mutant should be attempted taking in account the tapetum defect of *GPAT6* knockout during the cross (Li et al., 2012). Perhaps the full knockout of *GPAT6* could highlight an involvement in root suberization and maybe also a redundancy with *GPAT4* and *GPAT8*. However, lethality of the three main genes required for cutin formation may not be ruled out.

It has to be noted that even if *gpat6-1* does not exhibit a delay in suberization, it could influence the amount of suberin deposited. Unfortunately, the quantification of the suberization by the fluorescence of FY is not possible due to sensitivity to light and its rapid bleaching. A possibility would be to do this quantification with another suberin staining like Nile Red, but only for the suberin in the older part of the roots (Ursache et al., 2018).

The logical next step is to do a biochemical analysis using GC-MS in order to identify any change in monomer composition in *gpat6-1* and to confirm which monomers are affected in *gpat4 gpat8*. This will be a challenging experiment in term of workload for *gpat4 gpat8* because only 10% of its roots behave like WT, while for the rest of the seedlings, the root stops growing after 3-4 days.

The hypothesized redundancy of *GPAT6* with *GPAT4* and *GPAT8* is based on their strong sequence similarity, their phosphatase activity in addition to the acyltransferase activity, and that they are all involved in cutin formation in the shoot. However, the expression profile of *GPAT6* in the endodermis is more similar to *GPAT5* (Figure S1) together with the fact that *GPAT5* expression increased when *GPAT6* was knocked down (Figure 13), suggests that *GPAT6* could be redundant to *GPAT5*. The study of *gpat5 gpat6-2* could clear up this hypothesis.

By those results, we were able to show that *GPAT4* and *GPAT8* are not only involved in cutin formation in the shoot, but also in suberin formation in the roots suggesting that both pathways are maybe not so independent from each other and have common genes. The reported expression of *LACS2* and *SHN3* in the endodermal cells supports also this hypothesis (Aharoni et al., 2004; Lü et al., 2009).

4.4.3. **Global perspectives**

Understand the role of the phosphatase activity in vivo

It is interesting to see that at the same location, are expressed four genes from the same family (*GPAT4, GPAT5, GPAT7* and *GPAT8*) and that they are involved in the formation of one and only polyester, the suberin. The common acyltransferase activity attaches the fatty acid to a glycerol-3-phosphate forming LPA. At the opposite of GPAT5, in addition, GPAT4, GPAT6 and GPAT8 also have a phosphatase domain as second catalytic site. *In vitro*, the phosphatase removes the phosphate from the LPA to form a MAG (Yang et al., 2010). Nevertheless, the relevance of the phosphate *in vivo* in term of fatty acid composition or polymerization is not entirely clear.

CUS1, an enzyme involved in cutin polymerization, catalyzes the formation of oligomers from MAGs suggesting that MAGs are transported as such to the apoplast (Yeats et al., 2012; Yeats et al., 2014). LPAs could be transported under a different form of precursors and by different mechanisms, or polymerized by other enzymes.

In order to understand this better, in the future we would like to complement the mutants with a mutated phosphatase version of the protein. Yang et al. (2010) has successfully knocked-down the phosphatase activity, by mutation of two amino acids in the motif III domain of the phosphatase of GPAT6 (K178L, D200K). Those amino acids are conserved in

GPAT4, GPAT6 and GPAT8 but not in GPAT5 and GPAT7 (Figure 50). Based on this work, we could complement mutants with a mutated version of the gene, encoding for a protein not having a phosphatase, and non-mutated version expressed under their native promoter. This study could cover leaves, flowers, seeds and roots. *gpat4 gpat8* could be complemented with the mutated and non-mutated version of *GPAT4* and *GPAT8* individually and use to study the role of the phosphatase in cutin of the leaves and suberin of the roots. Preliminary results to screen the lines will be easily obtained by TB staining on the (partially-) complemented *gpat4 gpat8* mutant leaves. *gpat6-2* could be complemented with the mutated and native non-mutated version of *GPAT6* to study cutin in flowers. Study of organ fusions in flowers will be a useful tool for screening the lines. In the roots, we could expect that *gpat4 gpat6-1 gpat8* seedlings having no *GPAT* with a phosphatase site in the endodermis would present the most interesting phenotype, however until now we could not prove a redundancy of *GPAT6* with *GPAT4* and *GPAT8.*

To understand how similar are the acyltransferase domains of the so-called "cutin-related" genes compared to the "suberin-related" genes, the mutated version of *GPAT4, GPAT6* and *GPAT8* could be transformed under the *GPAT5* promoter in *gpat5* to see whether it complements. Tetrazolium penetration study through the seed hilum will help to quickly assess the full complementation.

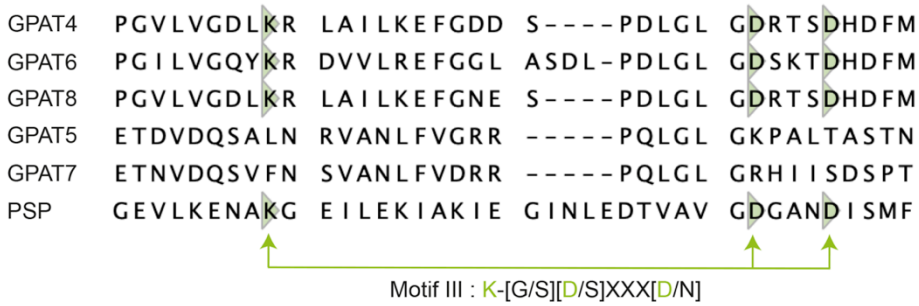

Figure 50: Alignment of the GPAT4 to GPAT8 with phosphoserine phosphatase from *Methanococcus jannaschii* (PSP) in order to highlight the conservation of the key amino acids of the motif III of the phosphatase domain. Figure was adapted from Yang et al. (2010).

Investigation of the lipid impregnation of lignin

With an expression similar to *GPAT5* starting patchy in the differentiated zone where the suberin starts to synthesize, the involvement of *GPAT6* in suberin formation was obvious to

hypothesize. At the opposite, *GPAT4* and *GPAT8* expression starting earlier in the undifferentiated zone did not give a clear hint that those could be involved in suberin formation (Figure S2). The delay in suberization in *gpat4 gpat8*, however supported this role.

The expression of *GPAT4* and *GPAT8* genes in non-differentiated cells could suggest that some polyester precursors are formed before others and only polymerized later when the suberin lamellae starts forming. Another hypothesis is the existence of a lipid impregnation in the Casparian strip lignin. This was already suggested by Zeier and Schreiber (1998) after extraction of the Casparian strip from monotocs. The synchronization of the expression of *GPAT4* and *GPAT8* with Casparian strip specific-gene has to be confirmed.

Lipid impregnation of the lignin could be not only specific to the Casparian strip but to all lignin deposition. The presence of lignin and suberin in the periderm is already confirmed (Wunderling et al., 2018). In a similar way, expression in the stele has also been observed for *GPAT3* (Figure 10), *BDG* and *DAISY* (Franke et al., 2009; Jakobson et al., 2016), although the specific cell type expressing the genes has to be studied. Hence, fatty acids deposition in the stele has to be as well investigated to see if lipid impregnation of lignin from the xylem is observed.

Investigation of the contribution of those genes in periderm suberization

Until now, no suberin biosynthesis gene knockout has been associated to peridermal defect in *Arabidopsis thaliana* at the exception of *GPAT5*, *CYP86A1* and *CYP86B1* (Delude et al., 2016; de Silva, 2018). The association of *GPAT4*, *GPAT7* and *GPAT8* with involvement in the suberin pathway, hypothesized based on FY, and their presence in the roots suggested that they could be involved in the periderm suberin formation, too. First, their pattern of expression should be studied in roots old enough to have entirely developed periderm. Secondly, observing FY staining changes between mutants and WT would be the best method to show their involvement in periderm suberization. Finally, a detailed analysis of the suberin composition in WT and mutants could complete the story.

Investigation of the involvement of those genes in suberin-associated waxes

Suberin-associated waxes have been identified at the periderm of 7-week-old *Arabidopsis* plants and contain, among other components, C22-C24 MAGs (Li et al., 2007b). MAGs are typically produced by GPATs having a phosphatase activity such as GPAT4, GPAT6 and GPAT8. Surprisingly, the plant with a knockout or an overexpression of *GPAT5,* without phosphatase activity, present a change in MAG total amount (Li et al., 2007b). This suggests the co-regulation with another *GPAT* having a phosphatase activity. It would be interesting to characterize the presence and the composition of the suberin-associated wax in the endodermis and in addition to investigate the role of the other *GPAT*s in wax formation at the endodermis.

4.5. Conclusion

In this chapter, we defined *GPAT7* as being involved in endodermal suberization and redundant to *GPAT5*, which is the dominant factor. The here described involvement of *GPAT4*, *GPAT6* and *GPAT8* in endodermal suberization as well showed already a delay in suberization in *gpat4 gpat8* confirming the right direction of the project. Detailed quantification of the suberin composition in this mutant is the next step as well as establishing a link between *GPAT6* and suberization. In addition, an investigation of the role of the phosphatase of *GPAT4*, *GPAT6* and *GPAT8* in cutin and suberin *in vivo* would uncover the function of this phosphate in polyester biosynthetic pathway. In the same line of thought, the role of the genes in periderm suberization could be explored.

Until now, polyester biosynthetic genes have been classified into cutin- and suberin-specific genes in function of which polyester their knockout affects. By showing that a same gene can be involved in suberin and in cutin formation, we are breaking down this theory and going further in the proposal of Fich et al. (2016) suggesting that suberin and cutin are only one polymer which can be deposited in the inner or the outer side of the cell wall. Thinking about cutin and suberin as two polymers with similar composition and common genes in their pathway, make us wonder how the cell knows if the monomers has to be polymerized at the inner or outside of the cell wall. The presence of cutin and suberin deposition in a unique cell can suggest a possible differentiation of suberin and cutin monomers by the plants (Kosma et al., 2014). This mechanism would be interesting to investigate.

4.6. Collaborators and contributions

In this study, I designed, performed and analyzed all the experiments. Rochus B. Franke contributed at the identification of the monomers for the GC-MS analyses.

5. Characterization of *GPAT2* and *GPAT3* and their role in polyester formation in the outer cell layers of the root

5.1. Introduction

GPAT2 and *GPAT3* are both expressed in the epidermis and the cortex cells from the tip to the top of the roots (Figure 10) indicating a different function of those genes compared to the other members of the *GPAT* family. This intriguing expression questions the nature of the fatty acids they are forming but also their function in a location where no polyester deposition has been characterized. In this introduction, I summarize the state of the knowledge on those two genes and *CYP709B2*, a candidate gene for working in the same pathway.

5.1.1. *GPAT2* and *GPAT3*: state of knowledge

Little is known about *GPAT2* and *GPAT3*. They are expressed in flowers, leaves, stem, seeds and roots (Beisson et al., 2007). But biochemical analyses on mutants were not conclusive: *gpat2-1* showed no polyester precursor changes in flowers, seeds and leaves and *gpat3-1* in roots, leaves and flowers (Yang et al., 2012). Their enzymatic activity is still to be elucidated (Yang et al., 2012).

GPAT2 and GPAT3 sub-cellular localization is a subject of debate. Through a pea mitochondria import assay, Zheng et al. (2003) excluded a possible import of GPAT2 in the mitochondia. The ER-specific retrival motif identified at the C-terminus of GPAT8, prooven to be ER-localized, presents sequence homology with motif in GPAT2 and GPAT3 sequence (Gidda et al., 2009). GPAT3 homolog in rice was shown to be ER-localized with GFP-tagging of the protein (Men et al., 2017). However, others papers claims that GPAT2 and GPAT3 are mitochondial localized based on their sequence homology to the mitochondial GPAT1 (Beisson et al., 2007; Chen et al., 2011a; Chen et al., 2014; Sui et al., 2017; Jayawardhane et al., 2018; Waschburger et al., 2018).

GPAT2 and *GPAT3* relative similarity with the sn-2 *GPAT*s rather than *GPAT9* makes them potential candidates as gene involved in polyester formation.

5.1.2. *CYP709B2,* gene coding for a potential ω-1, ω-2 hydroxylase

The *CYP709B2* (AT2G46950) is part of Cytochrome P450 monoxygenase (CYP) family. CYP proteins catalyze the oxidation step of the polyester formation. Based on co-expression data, CYPedia classified *CYP709B2* as involved in "Fatty acid elongation and wax and cutin metabolism" (Ehlting et al., 2008).

In *Arabidopsis*, little is known about *CYP709B2.* It could be related to saline stress and induced by auxin (Goda et al., 2004; Kandel et al., 2005). In wheat, *CYP709* family was pointed out as having a hydrolase function (Morant and Reichhart, 2004). *CYP709C1*, homolog of *CYP709B1, CYP709B2* and *CYP709B3* in *Arabidopsis*, is coding for ω-1, ω-2 hydroxylase (Kandel et al., 2005). However, detection of enzymatic activity of *Arabidopsis* CYP709Bs in yeast was not conclusive (Kandel et al., 2007). Preliminary studies suggested that the three members of the family have different biological function (Mao et al., 2013).

5.2. Strategy

The aim of this project is to characterize *GPAT2* and *GPAT3* in order to understand their role in *Arabidopsis thaliana* and to identify and possibly link their function to polyester formation at the surface of the roots. As a first step, we studied the expression pattern of the genes in the whole plants using GUS and GFP. Then, we isolated *gpat2* and *gpat3* mutants and generated a double mutant. Overexpression lines were also developed. Hoping to amplify mutant and overexpression line phenotype we studied them together with *CYP709B2*. We tested all those plants for cuticle deficiency in the leaves and at the root cap through FY and TB staining as well as GC-MS and chlorophyll leaching studies.

5.3. Results

5.3.1. *GPAT2* and *GPAT3* are expressed in roots, leaves and flowers

Apart from root expression (Section 2.3.1), *GPAT2* and *GPAT3* were also expressed in the aerial part of the plant: in the leaves, petals, sepals and stamen (Figure 51). The leaf

expression was specific to epidermal cells (Figure 52). In addition, *GPAT2* was also present at the stigmata.

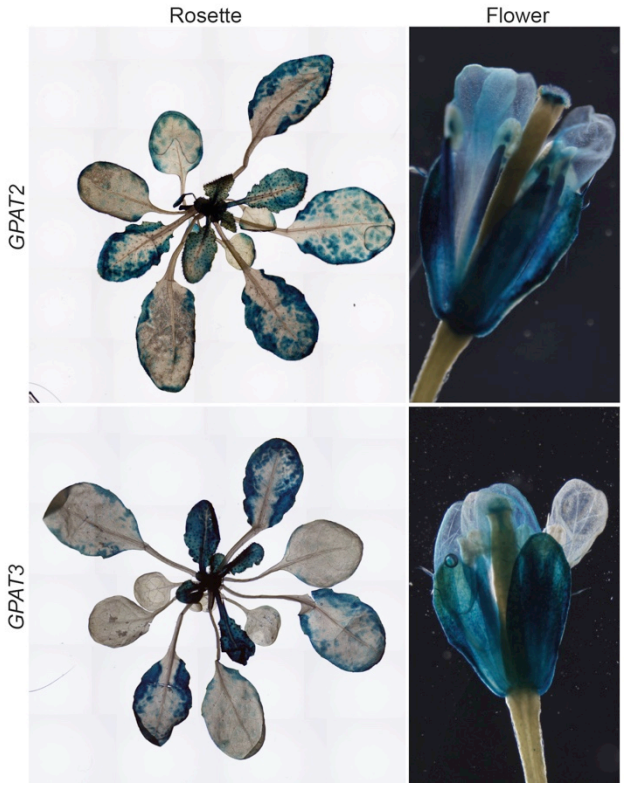

Figure 51: GUS staining of transgenic plants expressing pGPAT2::NLS-GFP-GUS and pGPAT3::NLS-GFP-GUS in leaves and flowers.

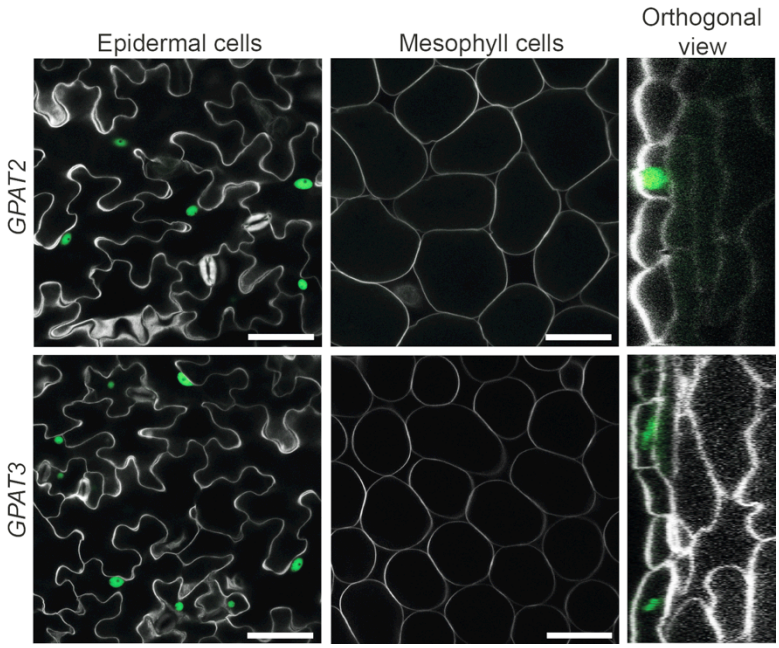

Figure 52: GFP fluorescence in transgenic plants expressing pGPAT2::NLS-GFP-GUS and pGPAT3::NLS-GFP-GUS in epidermis and the mesophyll cells of the leaves. Calcofluor in white is staining the cell wall. Scale bar represents 50 µm.

5.3.2. *CYP709B2*, coding for a potential polyester hydrolase, is present in roots and flowers

We decided to investigate *CYP709B2*, a gene encoding a potential hydroxylase because of it co-expresses with *GPAT2* (ATTED database (Aoki et al., 2016)). In the roots, RNA based expression profiles indicated a strong expression at the root cap and in the endodermal cells. In the shoot, it showed typical cutin-related expression pattern: petals, anthers and in siliques (Winter et al., 2007).

An expression study using pCYP709B2::NLS-GFP-GUS showed expression in petals and sepals and in very young developing leaves. In roots, *CYP709B2* was expressed in the root cap cells of primary and lateral roots, in the cortex and endodermis (Figure 53 and Figure 54).

CYP709B2 had an interesting common expression pattern with *GPAT2* and *GPAT3* in the sepals and petals, at the root cap of the primary and the lateral root and in cortex.

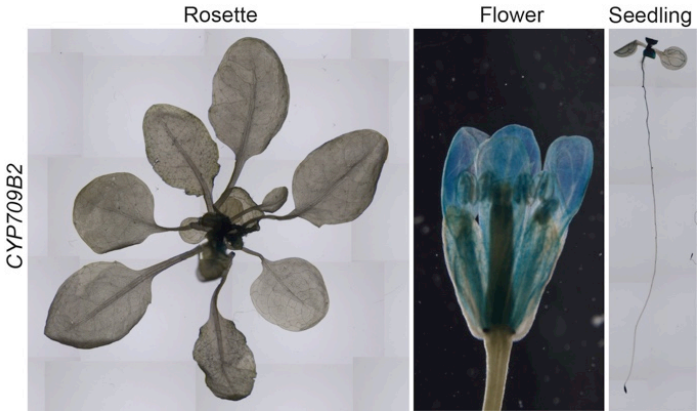

Figure 53: GUS staining of transgenic plants expressing pCYP709B2::NLS-GFP-GUS in leaves, flowers and 8-day-old seedling.

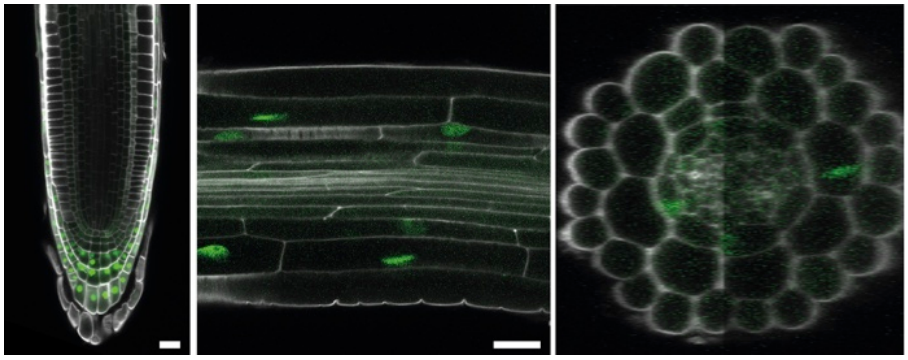

Figure 54: GFP fluorescence in transgenic plants expressing pCYP709B2::NLS-GFP-GUS at the primary root tip, the primary root via a longitudinal and orthogonal view. Calcofluor in white is staining the cell wall. Scale bar represents 20 µm.

5.3.3. **Assessment of *GPAT2* and *GPAT3* functions in polyester formation**

Mutants have no obvious cutin phenotype

The first step to study a gene is to obtain its knockout plant. For *GPAT3*, only two alleles were available from NASC, the European *Arabidopsis* Stock Center (Alonso et al., 2003), gpat3-1 (SALK_028578, Yang et al. (2012)) and gpat3-2 (SALK_139115) with a T-DNA insertion respectively in the unique intron and at the end of the last exon. For *GPAT2*, three alleles were selected among the ones available: *gpat2-1* (SALK_118230, Yang et al. (2012)) and *gpat2-2* (SALK_51152) with a T-DNA insertion in the first exon, and gpat2-3 (SALK_64530) with it in the 5' UTR. *gpat2*-1 and *gpat3*-2 were selected to work for their T-DNA insertion in the exon. For ease of the future discussion, they will be mentioned in the rest of this work as *gpat2* and *gpat3*. Since *GPAT2* and *GPAT3* have a similar expression pattern and as previous biochemical and phenotypic studies on the single mutants revealed no difference to the WT (Yang et al., 2012), further studies were performed on the newly isolated double mutant *gpat2 gpat3* to reveal whether these genes are redundant.

gpat2, *gpat3* and their double mutant *gpat2 gpat3* had no obvious phenotype in the shoot: no changes in the FY staining (Figure 55), no organ fusion, no permeability to TB and no water loss which makes sense since no change in cutin composition in the leaves could be detected neither (data not shown). Only a slight non-explainable accelerated growth in the double mutants was visible (data not shown). To summarize, a simple and classical analysis for cuticle defective mutant did not lead to any conclusion. A biochemical analysis of the flowers could still be performed in the future.

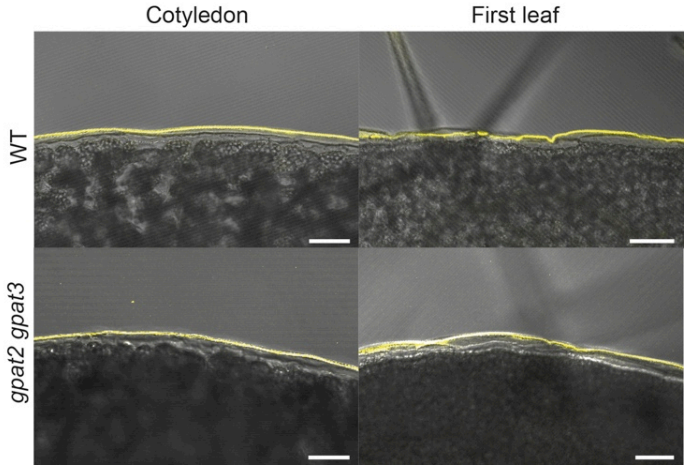

Figure 55: Fluorol yellow on the cotyledon and the first leaf of WT and *gpat2 gpat3* (overlay bright field and fluorescence). Scale bar is 50 µm.

Overexpression of GPAT2, GPAT3 and CYP709B2 resulted in cuticle permeability and organ fusion

Li et al., (2007a) showed that co-overexpression of *GPAT5* combined with *CYP86A1,* when single overexpressing line did not have any phenotype, leads to a strong phenotype in suberin formation because two consecutive steps of the polyester formation is altered. In a similar way, studying *GPAT2* and *GPAT3* with *CYP709B2* in a double loss-of-function mutant or overexpressing lines could highlight the likelihood that both enzymes are working together. *gpat2* and *gpat3* were crossed with the potentially interesting *cyp709b2-1* (SALK_020401, second exon mutation, Mao et al. (2013)). *GPAT2*, *GPAT3* and *CYP709B2* were overexpressed under the *UBQ10* promoter alone or in a combination of two.

No developmental phenotype could be observed in the mutants or the overexpression lines except for the combined overexpression of *GPAT3* and *CYP709B2.* This combined overexpression presented organ fusion, permeability, no cutin composition change but an accumulation of waxes. Overexpression levels were confirmed via qPCR (data not shown). Although exciting, it is worth highlighting that those results are preliminary because they were obtained using T2 segregating plants, hence they need to be repeated including the single overexpression lines and the appropriate controls.

Organ fusions were observed on the double *GPAT3* and *CYP709B2* overexpression line between leaves, stems, flowers but also stem and leaves together, flowers and leaves (Figure 56). TEM on a fused leaf and sepal showed on the edge of the junction an accumulation of cuticle with a non-continuous shape (Figure 57 A, B, C and E). The junction of both organs was identified by the two epidermal layers having no chloroplast. In between the epidermal layers, were present zones where the cuticle is missing, the cell walls were fused and zones where there was locally a cuticle on both side of the cell walls (Figure 57 D).

The rosette of lines overexpressing *GPAT3* and *CYP709B*2 were tested in a chlorophyll leaching assay. A strong permeability of the leaves with the loss of most of the chlorophyll after 5 min was observed while WT was only close to reach that level after 2 h (Figure 58).

Leaf cutin extraction from the lines double overexpressing *GPAT3* and *CYP709B2* showed no change in the cuticle composition (data not shown). Wax analysis from the same organ showed strong accumulation of the C24 and C26 acids (Figure 59).

Figure 56: Organ fusion in transgenic plants expressing pUBQ10::GPAT3 and pUBQ10::CYP709B2. From left to right: fusion flower-leaf, flower-flower, stem-leaf and stem-stem.

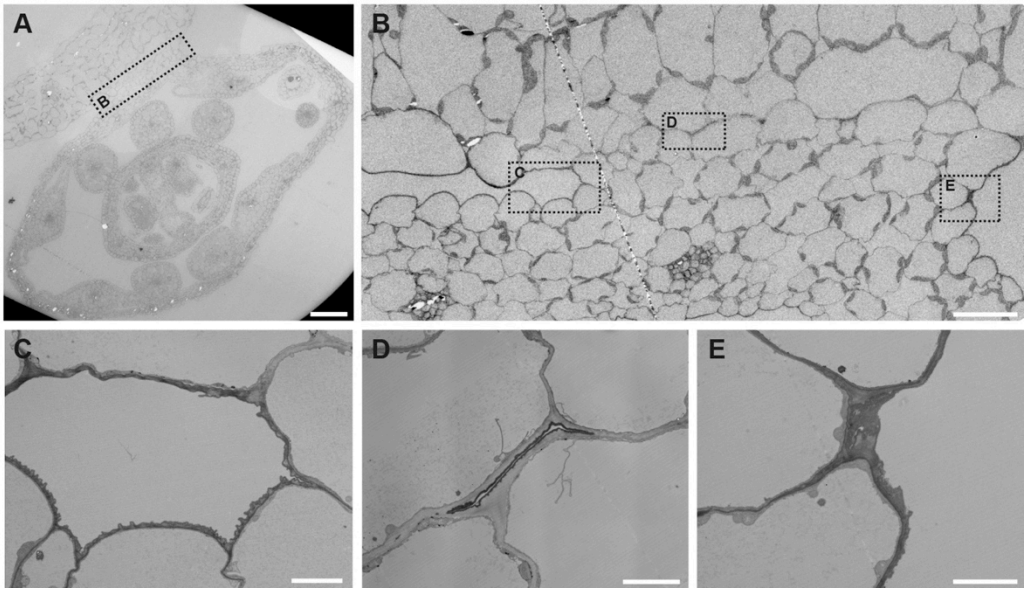

Figure 57: TEM showing organ fusion between a leaf and a sepal in transgenic plants expressing pUBQ10::GPAT3 and pUBQ10::CYP709B2. (A) overview of the leaf and the flower, (B) zoom on the fused area, (C and E) Edge of the fused zone, (D) junction between the two epidermal layer. Scale bars represent (A) 100 µm, (B) 30 µm and (C, D and E.) 5 µm

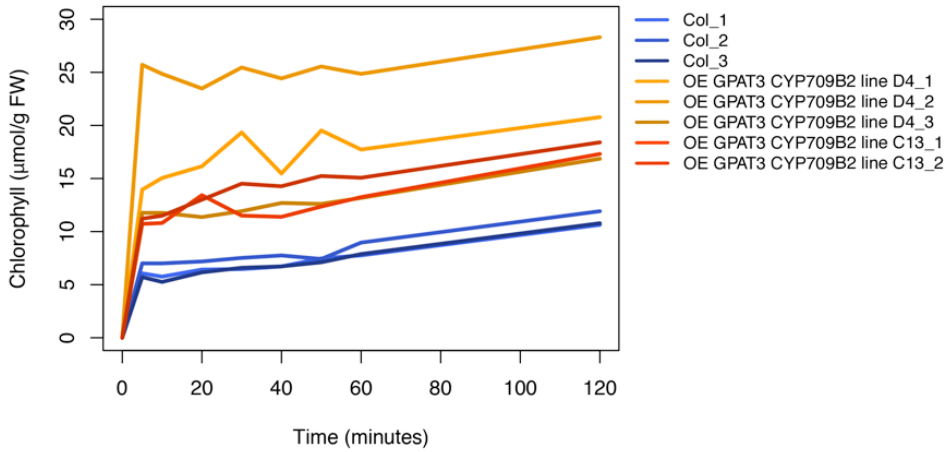

Figure 58: Chlorophyll release from WT (blue shade) and transgenic plants expressing pUBQ10::GPAT3 and pUBQ10::CYP709B2 (line D4, orange shade; line C13, red shade). Data represent independent plants.

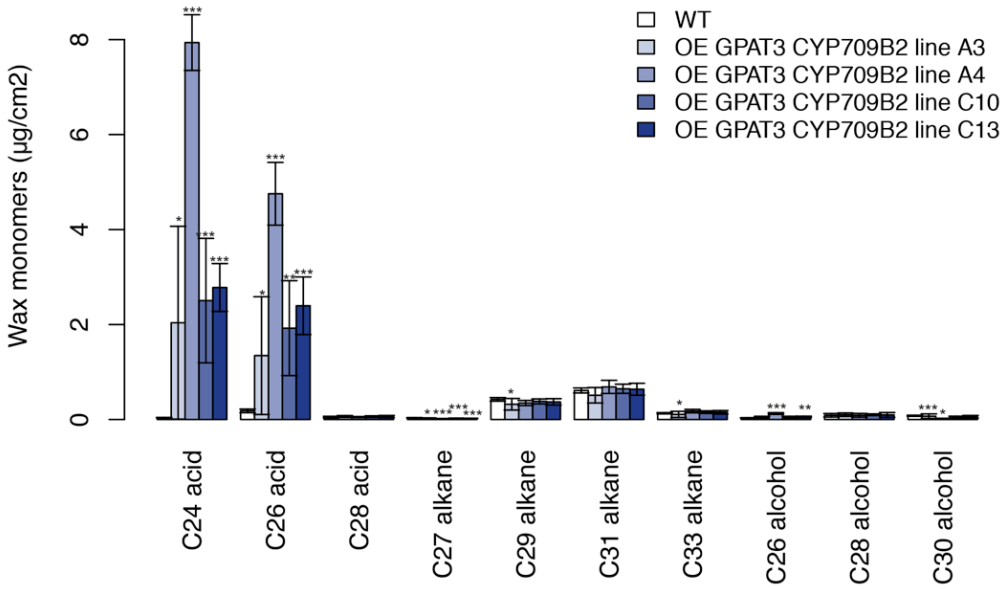

Figure 59: Quantification of wax monomers isolated from 5-week-old rosettes of transgenic plants expressing pUBQ10::GPAT3 and pUBQ10::CYP709B2 in comparison to WT. The overexpression lines were in T2 so still segregating. Values represent the means ± SD, n = 3–4. Asterisks denote significant differences to as determined by Student's t-test: ***p < 0.001; **p < 0.01; *p < 0.05. DW, dry weight.

RCC formation depends on GPAT2 expression

As presented above in section 3.4, *gpat2* is involved in the formation of the root cap cuticle. Indeed, TEM and FY analyses showed a defective cuticle in *gpat2* at the primary root, but not in *gpat3* (Figure 29 and Figure 30). FY was also tested on the other alleles of the mutants (*gpat2-2, gpat2-3* and *gpat3-1*) confirming the same results (data not shown). Furthermore, RCC composition analysis showed reduction in the long chain fatty acid like C26:0 FA, C26:1 FA, C28:0 FA, C28:1 FA and in C18:2 DCA and C18:1 9,10,18-trihydroxy FA (Figure 35).

In addition, germination and establishment assay showed that *gpat2* was not more affected by 100 mM of NaCl and KCl than WT (See section 3.4.6). However, the presence of 75 mM of K_2SO_4 or 250 mM of mannitol delayed the full emergence of the cotyledons (Figure 40) suggesting a role for *GPAT2* in protecting against certain salt and osmotic stresses.

Cutin extraction from the RCC of *gpat3-1*, *gpat3-2* and *gpat2 gpat3-2* gave unexpected results. Focusing on the very long chain fatty acid, the double mutant seemed to have a stronger phenotype than *gpat2* alone, suggesting that the knockout of *gpat3-2* made the phenotype stronger. The study of *gpat3* single mutant alleles was confusing. *gpat3-2*, used for constructing the double mutant, over-accumulated C26:0 FA, C26:1 FA and C28:1 FA compared to WT. The recent sequencing of all SALK lines with next generation sequencing revealed that *gpat3-2* has five other T-DNA insertions, hence, the over-accumulation could

be linked to the other mutations. However, *gpat3-1,* having a single T-DNA insertion, was similar to WT suggesting either an absence of RCC phenotype or that the T-DNA insertion in an intron might not affect the expression of the gene. In a few words, the unclear knockout of *GPAT3* leads to the impossibility to conclude anything about its activity. Future works will need to focus on producing a reliable *gpat3* null mutant.

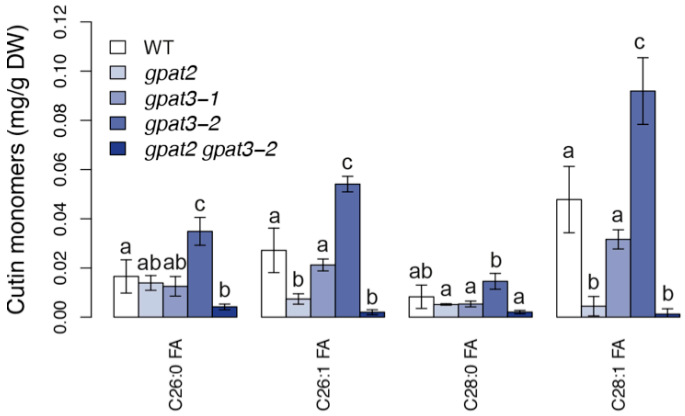

Figure 60: Quantification of C26:0, C26:1, C28:0 and C28:1 cutin monomers isolated from 2-day-old roots of *gpat2, gpat3-1, gpat3-2* and *gpat2 gpat3-2* in comparison to WT. Values represent the means ± SD, n = 3–4. Significant differences to WT were determined by ANOVA. Each letter represents a significant variation between a genotype in a specific growth condition ($p < 0.05$). FA, fatty acid; DW, dry weight.

5.4. Discussion and perspectives

This project is only starting but preliminary results show promising perspectives.

The expression pattern at the root in the epidermis-cortex, at the root cap and in the shoot in leaf epidermis divided this project in three sub-studies.

Firstly, the root cap expression led to the discovery of their potential role in the formation of the RCC. *gpat2* presented a defective RCC and a specific reduction in very long chain fatty acids like C26:0, C26:1, C28:0 and C28:1. Those compounds are specific to the RCC and have not been reported before in cutin composition. The changes in C18:2 DCA and C18:1 9,10,18 trihydroxy FA may be a compensation mechanism. Even if we showed that the *GPAT2* is involved in RCC formation, it is still needed to understand why *GPAT2* is still expressed even after RCC sheding off from the tip and why *GPAT2* is expressed in all root cap cells layers, while the other genes involved in the RCC biosynthesis are only expressed at the outer layer of the root cap cells. This observation suggest *GPAT2* could be involved fatty acid

modification in inner layers, and either independently in polyester formation at the RCC as well or that the defective RCC is only a consequence of another change at the root cap cells.

Secondly, their common expression in the leaf epidermis suggests a function in cuticle formation. In addition, the overexpression of *GPAT3* and *CYP709B2,* leading to an organ fusion plant having a permeable cuticle, is pointing in the direction of a role at the surface of the epidermis. The phenotype close to the one of a cuticle mutant, but without any change in cutin composition, suggests a change in cutin structure. Waxes are often also linked to the permeability of the cuticle. In this case, the increase of C24 and C26 acids could disorganize wax crystals and intracuticular waxes leading to an increase of permeability. A similar phenomenon was seen with the overexpression of *GPAT5* and *CYP86A1* that also changed the structure of the cuticle leading to an increase in permeability (Li et al., 2007a).

Thirdly, root epidermal and cortical expression of *GPAT2* and *GPAT3* is interesting and directly suggests that these genes may be involved in the novel cell wall modifications, for example diffuse suberin like already hypothesized for other species (Thomas et al., 2007; Ranathunge et al., 2008) or another unknown polyester deposited at the surface of the root that is not forming a distinct layer like cutin or suberin. Since the phenolic compounds of the suberin show a specific fluorescent signal when exposed to UV, analyses of the auto-fluorescence spectrum at the root epidermis of *gpat2* and *gpat3* should allow us to investigate if the diffuse suberin is affected (Ranathunge et al., 2008). If *GPAT2* and *GPAT3* are involved in the formation of lipids bound to the call wall, the polyester composition of the single and double mutants could be worth studying. Given the high level of suberin in the endodermis, which may hide smaller polyester composition changes in the root during polyester monomer analyses, a strategy to decrease suberin content in the endodermis could be developed using pELTP::abi1-1 construct: pELTP is an ENDORDERMAL LIPID TRANSFER PROTEIN promoter, specific to the endodermis and *abi1-1* is a dominant negative allele of ABI1 that suppresses ABA signaling and as consequence the formation of the suberization (Barberon et al., 2016). Transgenic plants containing this construct will have greatly reduced suberin in the endodermis. This should help to see any polyester changes in the roots of the *gpat2, gpat3* and *gpat2 gpat3* by means of GC-MS analysis. In parallel, one could also hypothesize that *GPAT2* and *GPAT3* are involved in the formation of solvent-extractable compounds. Periderm suberin-associated waxes have been studied by dipping a

whole roots in chloroform for 1 min (Li et al., 2007b). With a similar protocol, we could extract the non-covalently bound FAs at the surface of the roots. The epidermal expression could imply a role of those genes in the interaction with microbe or stress interaction.

As already mentioned, this project is still on going. A key point to elucidated before going further is whether the *gpat3* mutant is a true knockout, because until now *gpat3* has never shown any clear phenotype. As mentioned in section 5.3.3, *gpat3-1* has a T-DNA insertion in the unique intron and *gpat3-2* has it in the end of the second and last exon, which does not certify that GPAT3 is not active as truncated protein. *gpat3-2* was shown to carry many other mutations in its background making a clear link between genotype and phenotype impossible. In the last few years, the development of CRISPR-CASP9, as a user-friendly technique, is a real asset to be able to knock out a gene with certainty; by using such technique, we could induce a frame shift at the beginning of *GPAT3*. Once the CRISPR-*gpat3* will be generated, we could repeat permeability assay and biochemical analyses on leaf cuticle and RCC but as well flowers to understand the function of *GPAT3*. In addition, for the overexpression study, most of the analyses will have to be repeated on the lines in the T3 generation and with the appropriate controls (WT, single mutants). The presence as well of *GPAT7* at the cortex and the epidermis in the differentiated zone (Figure 10) suggests that it could participate in the formation of the same polyester; a triple mutant *gpat2 gpat3 gpat7* should be generated.

Last but not least, as introduced before, the subcellular localization of GPAT2 and GPAT3 has not been elucidated yet. Enzymes involved in polyester formation are typically localized at the endoplasmic reticulum, thus it might be postulated that GPAT2 and GPAT3 are localized there. To fill this gap in the literature, we would like to express independently both proteins followed by a CITRINE under their native promoter in lines developed by Nelson et al. (2007), which expressed specifically CFP at the ER or the mitochondria. Since a tag at the C- or N-terminus is not affecting the GPATs functionality (Gidda et al., 2009), we will only proceed with one contruct for each.

5.5. Conclusion

Although this project has only started, promising preliminary results are showing (1) an interesting expression pattern of *GPAT2* and *GPAT3* with a root cap expression linked to the

RCC biosynthesis, an epidermal expression linked to a possible formation of polyester at the surface of the root and a leaf expression hypothetically indicating a link with cuticle formation, (2) a role of *GPAT2* in very long chain fatty acid formation at the RCC and (3) a co-expression with *CYP709B2*, potentially coding for a hydrolase, which overexpressed with *GPAT3,* led to no change in cutin composition but an increase in wax coupled a strong permeability of the cuticle. Moreover, useful tools have been already developed (mutants and overexpression lines). This promising project will lead to a better characterization of the last two unknown *GPAT*s and to identify their function in polyester formation.

5.6. Collaborators and contributions

In this study, I designed, performed and analyzed all the experiments on my own.

6. Role of polyester depositions in the interaction with microbes

6.1. Introduction

Polyester depositions are present in the roots as endodermal suberin, peridermal suberin, root cap cuticle, diffuse suberin or other kinds of FAs deposition at the surface of the root. We have already shown how useful could be the *GPAT* family to study polyester formation in the roots. We would like to use their mutants as a tool to identify the possible role of FA deposition in the roots in the interaction with microbes. In this introduction, I briefly introduce the role of FAs in the interaction with microbes and *Piriformospora indica*, a fungus that we will use for this study.

6.1.1. Interaction between fatty acids and microbial colonization

Polyester barriers have a protection role to prevent invasion by microbes. Any alteration of this barrier can lead to higher sensibility or development of a resistance (Raffaele et al., 2009). For instance, in leaves, *gpat4 gpat8* has already shown to be more sensitive to *Alternaria brassicicola* (Li et al., 2007a) whereas a resistance to *Botrytis cinerea* was observed in *lacs2* and *bdg* (Bessire et al., 2007; Chassot et al., 2007). This resistance could be due either to a higher cuticle permeability which increases the release of antifungal compounds at the surface of the leaf (Bessire et al., 2007) or to the absence of monomers, that should be released during the cuticle digestion by fungus cutinase, acting as a signal for appressorium formation, like in *Magnaporthe grisea* and *Erysiphe graminis* (Francis et al., 1996; Gilbert et al., 1996). It is complex to study since infected mutant phenotypes vary with the infecting organism. For example, while *lacs2* inhibits the germination of *B. cinerea* spores, it is sensitive to *Erysiphe cichoracearum (Tang et al., 2007)*.

Even without any epidermal diffusion barrier, symbiosis in the roots shows some similarities with the colonization of the leaves. In *Medicago truncatula*, REQUIRED FOR ARBUSCULAR MYCORRHIZATION (*RAM2*) has been identified as a homolog to a *GPAT* with a phosphatase site, potentially *GPAT6* (Wang et al., 2012). *RAM2* knockout mutant, *ram2* when colonized by *Glomus intraradices,* a mycorrhizal fungus, has a reduced colonization due to a decrease

of hyphopodia formation. This can be rescued with the exogenous application of C16:0 FA. Similarly, *Phytophtora palmivora* presented less appressorium formation on *ram2* roots than on WT. The application of C16:0 FA recovered the infection. Thus, *RAM2* is involved in the production of C16:0 monomers acting necessary for mycorrhizal hyphopodia and appressoria formation (Wang et al., 2012). This suggests that FAs have an important role in the interaction between the plant and the microorganism. In *Benthamiana* leaves, *gpat6* mutant is more susceptible to *Phytophtora infestans* but more resistant to *B. cinerea* (Fawke et al., 2018). The amount of infection of *P. infestans* in NB*GPAT6* overexpression lines were reduced in the leaves but increased in the roots (Fawke et al., 2018). In tomato as well, *gpat6* mutant is more susceptible to *P. infestans* and *palmivora* but more resistant to *B. cinerea* (Fawke et al., 2018). Hence, *GPAT6* seems to have an important function in the interaction with microbes.

In arbuscular mycorrhizal and pathogenic fungi, fatty acids produced by the plant host are transferred to the fungi (Jiang et al., 2017; Luginbuehl et al., 2017). *RAM2* has been identified as key factor in the formation of those FAs.

In conclusion, FAs have key roles in the interaction between plant-microbes and *GPAT*s could be a crucial point in these processes. However, different reactions of the plants (even organs) to different pathogens are observed and can be link to their lifestyle.

6.1.2. *Piriformospora indica*

P. indica is an arbuscular mycorrhiza-like fungi belonging to the *Basidomycota* phylum in the *Sebacinales* order (Varma et al., 1999; Schafer et al., 2007). This fungus has been identified in the Thar dessert for the first time on woody shrubs, but it has a really wide spectrum of infection. *P. indica* promotes the growth of *Arabidopsis* under low nutrient soil and other (a)biotic stresses (Banhara et al., 2015). Such interaction leads to a systemic induced resistance protecting the plant from various root and leaf pathogens (Schafer et al., 2007).

P. indica colonization is specific to the epidermal and cortex cell layers in the whole root at the exception of the elongation zone and the meristem where there is no infection (Jacobs et al., 2011). First, chlamydiospores germinated and colonized the surface of the root (1dpi). Then, starts the intra and inter-cellular colonization at already 2dpi where first host cells stay alive then die after 3dpi. During the biotrophic colonization, the hyphae are extracytosolic

growing into the cells via an invagination of the plasma membrane which proves that at first the fungi development is not depending on the root cell death and does not induced any defense response (Jacobs et al., 2011). At 7 and 14 dpi, sporulation takes place respectively extracellularly and intracellularly.

6.2. Strategy

The aim is to understand how polyester depositions at the root surface may have a role in microbial interaction through the study of specific mutants. In collaboration with Prof. Mario Serrano (Universidad Nacional Autonóma de México), we started to investigate the role of the *GPATs* and in consequence the function of the polyesters that they are forming in the beneficial interaction between *Arabidopsis thaliana* and *Piriformospora indica*. First, the expression level of the *GPATs* from infected plants and non-infected plants was measured via qPCR in order to determine if they are induced after infection. Then, the degree of colonization of the roots of different *GPAT* mutants by *P. indica* was also be studied using qPCR on fungal DNA. *gpat2* and *gpat3* was used to study the interaction of microbes with a still uncharacterized polyester deposition at the surface of the roots and *gpat4*, *gpat5*, *gpat6*, *gpat7* and *gpat8* with suberin in the endodermis and at the periderm. Labeling of the fungi to visualize it in microscopy illustrated the results obtained by qPCR.

6.3. Preliminary results

It is needed to mention that all those data have been generated in less than two months, experimental set up and basic optimization included. Those experiments need to be repeated and optimized; suggestions are given in the discussion. In this study, plants were one-week-old when infected and observed after 14 days.

6.3.1. Colonization by *P. indica* has no impact on the expression of the *GPATs*

GPAT expression level from infected plants and non-infected plants has been measured via qPCR in order to determine if there is a difference. The average of the values tends to point out that there is no difference in the expression of the genes (Figure 61).

The variability between samples is really high, even in the non-infected sample. The experiment needs to be repeated and optimized before being able to draw any conclusion.

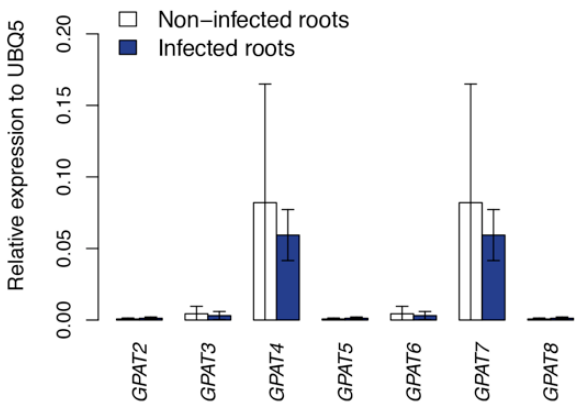

Figure 61: Relative expression of *GPAT* genes in non-infected roots versus infected roots compared to UBQ5. No statistical differences are visible comparing infected and non-infected roots with a $p<0.05$ in a Student's t-test.

Seeing the expression at the outer layer of the root of certain *GPATs*, a role in the interaction with microbes may be hypothesized. For this reason, the degree of colonization of the roots of different *GPAT* mutants by *P. indica* has been studied. A qPCR was performed on extracted DNA of infected WT and mutants with *Arabidopsis* specific primer (*AtUBQ5* - At3g62250 (Daneshkhah et al., 2013)) and *P. indica* specific primers (*PiITS* - P. Indica Internal Transcribed Spacer (Khatabi et al., 2012)) amplifying in both cases a reference gene of the respective organism. The amount of fungi quantified on the mutant roots was compared to the amount on WT. *gpat2 gpat3, gpat4 gpat6-1 gpat8, gpat5 gpat7* and corresponding single mutant were tested (Figure 62).

gpat2 gpat3 was less infected than WT. At the opposite, in *gpat4 gpat6-1 gpat8* and *gpat5 gpat7* more fungi were detected. Single mutants have a less strong phenotype: *gpat3* was significantly more colonized; *gpat2* had slightly less colonization and *gpat4* slightly more but the difference was not statistically significant; *gpat6-1*, *gpat7* and *gpat8* did not show any change. Based on the results obtained so far, it appears that *GPAT*s could have a role in the interaction with *P. indica.*

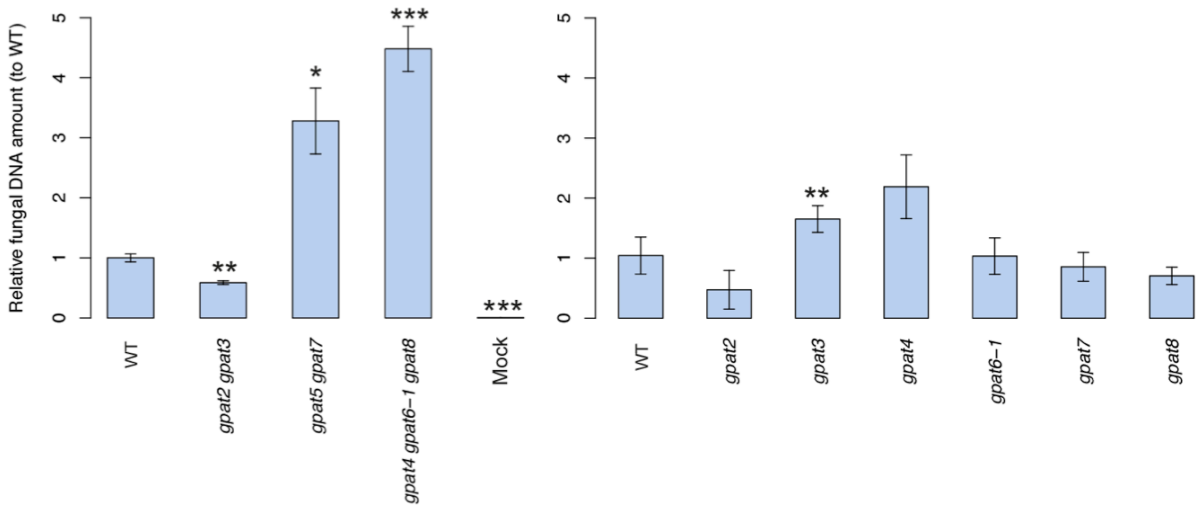

Figure 62: Quantification of fungal DNA relative of *gpat2 gpat3, gpat5 gpat7, gpat4 gpat6-1 gpat8,gpat2, gpat3, gpat4, gpat6-2, gpat7* and *gpat8*. Due to technical issues, *gpat5* was not tested. Mock includes non-infected WT seedlings. Significance is indicated by asterisks calculated using Student t-test: ***p-value < 0.001, p-value < 0.01, *p-value < 0.05.

6.3.2. *gpat2 gpat3* shows less penetration points while *gpat4 gpat6-1 gpat8* shows more

In line with the qPCR, *P. indica* penetration in the root has been studied by labeling of fungus plasma membrane using Wheat Germ Agglutinin Alexia Fluor 488 Conjugate and of plant cell wall with PI (Figure 63). The amount of penetration points in the roots was different for *gpat4 gpat6-1 gpat8* and *gpat2 gpat3* mutants compared to WT. In *gpat2 gpat3*, *P. indica* was never observed inside the roots. In *gpat4 gpat6-1 gpat8*, the penetration happened much more than in WT. No conclusion will be drawn because the experiment has been done only once. Repetitions of the experiments are needed to confirm the results. Single mutants and *gpat5 gpat7* also needs to be studied.

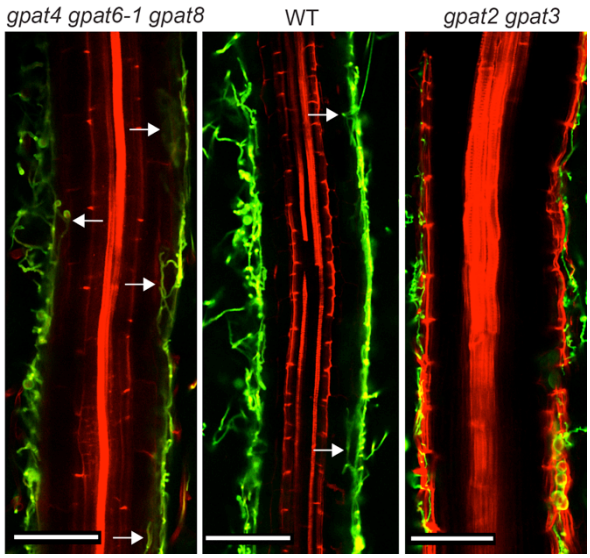

Figure 63: Visualization of the colonization of *P. indica* in WT, *gpat2 gpat3* and *gpat4 gpat6-1 gpat8* by fungus labeling using Wheat Germ Agglutimim Alexia Fluor 488 Conjugate and staining of plant cell with propidium iodide. The arrows are indicating penetration of the fungi in the root. Scale bars represent 100 µm.

6.4. Discussion and perspectives

6.4.1. Focus on the results

GPAT2 and GPAT3 have a role in the colonization of the roots by the P. indica

Colonization study with *P. indica* shows a lower infection rate in *gpat2 gpat3* compared to WT. *gpat2* and *gpat3* alone seem to have an opposite tendency: *gpat2* has a slight reduction of infection compared the WT, but *gpat3* is more infected. In the double mutant, the phenotype linked to *GPAT2* is overtaking the one linked to *GPAT3*. It is important to keep in mind the uncertainty around *gpat3* mutant (section 5.4).

Acting as a biochemical signal, C16 FAs in the roots are needed for appressorium formation and penetration of *Glomus intraradices* in the roots of *Medicago truncatula*. A disruption of C16 production leads to an absence of infection (Wang et al., 2012). In *Arabidopsis thaliana*, lipid signaling could also have a role in the appressorium formation, which could justify the lower infection of *gpat2* if *GPAT2* is involved in the formation of a signaling FA. The epidermal and cortical localization of *GPAT2* fits to such a role. In this case, the FA involved in such interaction needs to be identified. Then exogenous application of the identified FA for rescuing the phenotype is the best way to prove its function (Wang et al., 2012).

If confirmed, the increase of infection observed with *gpat3* could be linked to a mechanical process. By studying soybean cultivars, it has been highlighted that, in soya, the amount of diffuse suberin has an impact on the sensitivity to *Phytophthora sojae (Ranathunge et al., 2008)*. *GPAT3*-dependant monomers could be forming the diffuse suberin at the outside of the root; hence the absence of this polyester could destabilize the cell wall reinforcement and it would make the penetration of a fungus into epidermal cells easier. This could explain the higher colonization of the roots in *gpat3.* Moreover, *GPAT3* expression in the outer layers of the root supports such hypothesis.

The reduction of infection in *gpat2 gpat3* highlights the importance of detection of the plant for the appressorium formation over the weakening of the suberin barrier. The overexpression lines of *GPAT2* and *GPAT3* generated in section 5.3.3 would be a useful tool to use in comparison to the mutants.

If the experiment is continued on 3-week-old plants like it has been done here, an investigation of the expression of *GPAT2* and *GPAT3* expression during periderm formation would be crucial.

GPAT4 to GPAT8 are involved in the suberization of the periderm

Interaction with *P. indica*, a beneficial fungus, has shown that *gpat4 gpat6-1 gpat8* is more colonized than WT. Individually, *gpat4*, *gpat6-1* and *gpat8* were not reflecting alone the phenotype obtained in the triple mutant. The increase of infection in the triple mutant shows that *GPAT4*, *GPAT6* and/or *GPAT8* are also involved in the colonization process but are redundant to each other, or at least two of them are. The redundancy of *GPAT4* and *GPAT8* has already been shown in the leaves (Li et al., 2007a) and in the roots (section 4.4.2). Studying *gpat4 gpat8* in comparison with *gpat4 gpat6-1 gpat8* will reflect the importance of *GPAT6* in the infection. *GPAT6* does not have to be hastily excluded since it has shown to be a key gene in microbe interaction in other species (Wang et al., 2012; Fawke et al., 2018)

gpat5 gpat7 has also an increase of the invasion by *P. indica* but *gpat7* alone is not responsible of this phenotype. *gpat5* has not been tested due to technical issues but we expect a weaker profile than the double mutant since both genes have shown to be redundant (section 4.4.1).

Earlier, in addition to *GPAT5*, we hypothesized that *GPAT4*, *GPAT6*, *GPAT7* and *GPAT8* are involved in endodermal suberin lamellae formation (section 4.4.2). At a later stage, those genes, including *GPAT5*, could also be involved in the suberization of the periderm. A loss of function of those genes would lead to a non/less suberized periderm, easier for fungi to penetrate. This hypothesis is supported by the detection of *GPAT4* and *GPAT5* cork oak homolog expression in suberin-rich phellem (Marum et al., 2011). Moreover, the link between suberization and pathogen infection has already been studied: potato tuber, suberized upon wounding, is not infected anymore by *Erwinia carotovora* and *Fusarium sambucium* (Lulai and Corsini, 1998).

A useful control to confirm that the colonization of a non-suberized periderm leads to an increase of penetration of the fungi in the root is to infect pCASP1::CDEF1 line by *P. indica*. Expressed under pCASP1, an endodermal specific promoter, *CUTICLE DESTRUCTION*

FACTOR1 encoding for a plant cutinase, degrades the suberin of the endodermis and the periderm (Naseer et al., 2012).

6.4.2. **Focus on the techniques**

Different ways to evaluate possible changes in GPAT expression

The first experiment evaluated the total level of *GPAT* expression in the roots and could have highlighted changes in intensity of expression. However, to complete those results, it is necessary to look at the localization of the expression during infection using the GFP-tagged lines and confocal microscopy. Indeed, an induction of expression in a few cells next to the penetration point of the fungi would not be seen by qPCR as well as a shift in the localization of the gene expression. In case of expression next to the point of penetration, a test of wounding the root with a laser would confirm or not if the expression is due to the wounding itself or to the detection of the fungi, a necessary control since *GPAT7* is induced up on wounding.

As mentioned before, the results obtained with qPCR on the whole root system had a significantly high variability between samples. The experiment needs to be repeated under more uniformed growth conditions before being able to draw any conclusion. The use of another or an additional reference gene should be also tested.

The adequate stage of growth in function of which polyester is studied

Apart from the technical improvement, the age of the plants can be adapted to specifically study certain polyester deposition: germination to 5 days to study the role of the RCC in the pathogen interaction at the primary root, 5-10 days for the RCC at the lateral roots, before 3-16 days for the epidermis and the suberized endodermis, 16-21 days for periderm forming inside the primary root, 27 days for periderm as the outer cellular layer (Wunderling et al., 2018).

Specific technical improvements for those experiments

In less than two months experiments were set up and optimized, and a first batch of results was collected. Several suggestions can be made to improve the quality of those data.

First, the *Arabidopsis* seedlings were 3-week-old and having a size which is really unhandy and hard to study at the microscope. Moreover, at that age the periderm covers a big part of the root system which makes hard the study of the epidermis alone.

Secondly, the samples are grown in a way that after two weeks of co-cultivation, the roots are barely infected, penetration points are visible, but the fungi did not develop much in the roots. The key issue is that the disc of fungi is placed at 1 cm from the root tip, so time is lost while waiting for both to enter in contact.

Thirdly, the current growth conditions with the plant growing horizontally on a paper filter is far from being close to natural conditions.

To improve, by taking in account those three observations, it will be necessary to work on younger roots and to make the contact root-fungus faster. For that we suggest following another protocol using chlamydiospores instead of hyphae, where they study the infection after only 3 days of infection (Jacobs et al., 2011; Reitz et al., 2012). With such protocol, the age of the plant easily adapted to study specifically different stage of the root development and seedlings can be grown following the gravitropic forces.

Fourthly, before DNA extraction, it was necessary to remove hyphae at the surface of the roots to quantify only the ones inside. For this, we vortexed the roots several time, some mucilage was seen floating in the buffer (Banhara et al., 2015). However, a more effective way to do it would be to sterilize the surface of the roots with NaOCl (Haegi et al., 2013).

Finally, different qPCR primers for *P.Indica* amplification have been published (Bütehorn et al., 2000; Daneshkhah et al., 2013; Jacobs et al., 2011; Khatabi et al., 2012; Qiang et al., 2012). By testing them for primer efficiency and dissociation curve, we selected a pair of primers, which afterwards showed an amplification of non-infected *Arabidopsis thaliana*. A selection of new primers from the literature or new design of primers based on the genome sequence of *P. indica* is essential (Zuccaro et al., 2011).

Study of the interaction with other pathogens

In a broader way, other microbes could be used to see if the interaction with the mutants is similar to the one with *P. indica*: for instance, *Colletotrichum tofieldiae*, the only other fungus establishing a beneficial interaction with *Arabidopsis* (Hiruma et al., 2016), or a

biotrophic and a necrotrophic fungus or even other type of organisms like nematodes or bacteria.

6.5. Conclusion

This project is still ongoing, but preliminary results are promising and motivate us to continue to the investigation. With the first results, we can already see that the *GPATs* may play important roles in the interaction with fungal organisms. *GPAT2* is needed for the infection to happen, while *GPAT4, GPAT5, GPAT6, GPAT7* and *GPAT8* absence facilitates the invasion. They act redundantly in those processes. The decrease of hyphopodium formation due to an absence of C16:0 monomers at the surface of the roots when colonized by *Glomus intraradices* underlines the importance of the FA deposition at the surface of the roots and a potential role of the *GPATs* (Wang et al., 2012).

With better-established methods, this project may clarify how in *Arabidopsis thaliana* FAs and polyester deposition at the root surface impact on microbial interactions.

6.6. Collaborators and contributions

In this study, I designed, performed and analyzed all the experiments. Mario Serrano and Martha Torres provided *P. indica* and helped in setting up the experiments. Xochitl Alvarado-Affantranger contributed in the imaging.

7. Conclusion and outlines

Since the middle of 19th century, polyester depositions, like cuticle and suberin lamellae, have been studied in different plant organs. Cuticle is specific to outer side cell walls of epidermal cells and is found on fruits, leaves, primary stems, and flowers (Pollard et al., 2008). The suberin lamellae are made of depositions of suberin at the inner side of the cell wall (Haas and Carothers, 1975). Genes encoding key steps of their biosynthetic pathway have been characterized in *Arabidopsis thaliana* independently. Several of those genes are expressed in unexpected tissues like the root cap of primary and lateral roots were reported (Bird et al., 2007; Panikashvili et al., 2009; Jakobson et al., 2016). With this work, we investigated atypical polyester deposition in the roots using the *GPAT* family as a tool to monitor formation of cutin and suberin precursors. This strategy turned out to be efficient.

The *GPAT* expression revealed precursor formation at the root cap of primary and lateral roots. Based on that, we discovered that the outer root cap cell layer of young primary and lateral roots forms a cuticle-like structure. The so-called root cap cuticle is observed in *Arabidospsis thaliana*, *Brassica napus* and *Solanum lycopersicum* and is present from the embryonic stage until the sloughing off of the first root cap cell layer, 6 days after germination. In addition to a staining with lipid dyes, an altered RCC ultrastructure observed in a transgenic line expressing a plant cutinase at the root cap, as well as in several cutin biosynthesis genes mutants, suggested that the electron-dense layer is of lipidic nature. Cuticle composition of a 2-days-old *Arabidopsis* seedlings reveals an RCC made of cutin rich in C18:2 dicarboxylic acid, main monomer of the *Arabidopsis* leaf cuticle, with numerous atypical components. Instead of presenting the typical p-coumaric and ferulic acid, the only aromatic was synapic acid. Unsaturated very long chain fatty acids were also identified. The RCC of the primary root acts as a diffusion barrier protecting the meristem of toxic components during the most vulnerable stage of their development to support their establishment. At the lateral roots, in addition to the role of diffusion barrier, the RCC prevents organ adhesion during lateral root emergence through the primary root, causing a delay in outgrowth and a misshapen of the primordia. Organ adhesion is similar to the organ fusion observed in shoot cuticle mutants. The main features of the shoot cuticle, which has a role as a diffusion barrier to protect the plant from its surrounding environment and

preventing organ adhesion, are characterizing as well the RCC. Globally, cuticles can be considered as having protective functions depending on their localization explaining the different degree of intensity of those features. Until now, the cuticle has always has been associated with epidermal tissues of the shoot. This discovery of the RCC implies an update of this theory. Tena (2019) has kindly underlined the importance of our research on the RCC: “Textbook-changing discoveries are becoming scarce these days. Identifying a new anatomical structure in plants is a significant advance and modifies the way we will consider young roots from now on“.

In addition, we showed that *GPAT7,* like *GPAT5*, a suberin-related gene, but also *GPAT4* and *GPAT8*, cutin-related genes, are involved in suberin formation in the endodermis. By showing that the same gene can be involved in suberin and in cutin formation, we are challenging the theory of two distinct cutin and suberin pathways. Our observation join the theory of Fich et al. (2016) suggesting that suberin and cutin are only one polymer which can be deposited in the inner or the outer side of the cell wall.

Following the expression of polyester-related genes, to identify new polyester deposition, was a successful strategy that can continue further. Indeed, the expression of *GPAT2, GPAT3* and *GPAT7* suggested the presence of a polyester formation at the root surface. Which polyester are they forming and what its role are the main questions that we are currently trying to answer. A possible function in the interaction with the rhizosphere and with microbes is an option. In a similar way, expression in the stele has also been observed in *GPAT3*, but also reported for *BDG* and *DAISY* (Franke et al., 2009; Jakobson et al., 2016), hence polyester deposition in the stele is another path to investigate.

In conclusion, our researches have challenged two main dogmas by demonstrating that the cuticles are not specific to aerial part of the plants and the genes classified cutin-related can also be involved in suberin formation. In addition, preliminary data suggest the presence of a GPAT2- and GPAT3-dependant unknown polyester at the root surface and an interaction between root fatty acids and with pathogens.

8. Materials and methods

8.1. Growth conditions

For most of experiments, plants were grown under sterile conditions. Seeds were surface sterilized with chlorine gas. After 2-3 days of vernalization at 4°C, plants were grown on plates with ½ MS (Murashige and Skoog, 500 mg/l MES, pH 5.7), 0.7% agar at 22°C, under continuous light (100 mmol $m^{-2} s^{-1}$). With the exception of the seedlings for RCC polyester extraction and salt stress assays, plates were grown vertically. For transformation and seed propagation plants were grown on soil under continuous light (100 mmol $m^{-2} s^{-1}$) at 20°C and 65% humidity. For leaf cutin and wax extraction and chlorophyll leaching, plants were also grown on soil but under 10 h light conditions.

8.2. Plant material

Arabidopsis thaliana accession Col-0 was used in this work along with *Brassica napus* and *Solanum lycopersicum* L. ‘‘Moneymaker.’’ All *Arabidopsis* seeds were maximally 3-month-old for the characterization of the RCC. *Arabidopsis thaliana* mutants were already described: *lacs2*-3 (Bessire et al., 2007), *hth-12* (Kurdyukov et al., 2006b), *gpat4*, *gpat8*, *gpat4 gpat8* (Li et al., 2007a), *gpat5* (Naseer et al., 2012), *gpat6-1* and *gpat6-2* (Li-Beisson et al., 2009), *dcr*-2 (Panikashvili et al., 2009), *eh1* (Pineau et al., 2017), *fah1* (Anderson et al., 2015), *ltpg1-1 ltpg2-1, ltpg1-1 ltpg2-2, ltpg1-1 ltpg2-3* (Kim et al., 2012), *bdg*-1 (Kurdyukov et al., 2006a), *gso1/sng3*-3 (Pfister et al., 2014), *gso2-1* (Tsuwamoto et al., 2008), *gso1/sng3-3 gso2-1* (Moussu et al., 2017), *brn1 brn2* (Bennett et al., 2010), *smb-3* (Bennett et al., 2010), *aba2-1, abi3-8, abi5-3* (Barberon et al., 2016), *ahp6* (Andersen et al., 2018), *aux1-7* (Pickett et al., 1990), *aux1-21* (Vandenbussche et al., 2010), *d6pk* (Marhava et al., 2018), *ein2-1* (Feng et al., 2015), *etr1-1* (Barberon et al., 2016) and *log3 log4* (Andersen et al., 2018). *yuc2 yuc5 yuc6 yuc8* was kindely provided by Vinicius Costa Galvao. *gpat2-1* (SALK_118230, Yang et al. (2012)), *gpat2-2* (SALK_051152), *gpat2-3* (SALK_64530), *gpat3*-2 (SALK_139115), *gpat7*-3 (Yang et al., 2012) and *cyp709b2-1* (SALK_020401, Mao et al. (2013)) were ordered at NASC, the European *Arabidopsis* Stock Center (Alonso et al., 2003). *gpat2-1 gpat3-2, gpat4 gpat6-1 gpat8*, *gpat5 gpat7-3, gpat2-1 cyp709b2-1* and *gpat3-2 cyp709b2-1* were obtained by

crosses of the respective single mutants. Gene numbers and genotyping primers are described in Table S1 and S2.

8.3. Generation of constructs

To generate pENTRY L4-pGPAT-R1, between 1.7 kb and 2.2 kb fragments upstream of each *GPAT* were amplified, and cloned into pDONR P4-P1 using KpnI and XbaI restriction site, same for pENTRY L4-pDCR-R1 with 2.9 kb promoter fragment and pENTRY L4-pCYP709B2-R1 with a fragment of 2.1 kb. pENTRY L4-pLOVE1-R1 was generated by amplifying a 2.1 kb fragment upstream of *LOVE1* and recombining it into pDONR P4-P1. pENTRY L4-pABCG11-R1 was provided by Céline Terrattaz (unpublished).

To generate pENTRY-L1-GPAT2-L2, pENTRY-L1-GPAT3-L2 and pENTRY-L1-CYP709B2-L2, their respective gene was amplified and recombined into pDONR221. To generate pENTRY-L1-NLS-GFP-GUS-L2, *NLS-GFP-GUS* was amplified from a pDEST containing B1-NLS-GFP-B2-GUS-B3 and recombined into pDONR221. pENTRY L1-CDEF1-L2 was previously described (Naseer et al., 2012), and pENTRY L1-DCR-L2 provided by Marion Rebeaud (unpublished). Primers used for cloning are available at the table S3.

pGPAT2::NLS-GFP-GUS, pGPAT3::NLS-GFP-GUS, pGPAT4::NLS-GFP-GUS, pGPAT6::NLS-GFP-GUS, pGPAT7::NLS-GFP-GUS, pGPAT8::NLS-GFP-GUS, pABCG11::NLS-GFP-GUS, pDCR::NLS-GFP-GUS, pCYP709B2::NLS-GFP-GUS, pLOVE1::CDEF1, pLOVE1::DCR, pDCR::DCR and pGPAT2::GPAT2 were generated by recombining the corresponding entry clones into the pMMA-Red vector (Ali et al., 2012) using the Gateway Technology (Lifesciences). pUBQ10::GPAT2, pUBQ10::GPAT3 and pUBQ10::CYP709B2 were generated into pH7m24GW and pB7m24GW vectors. pLOVE1::H2A-GFP was generated by recombining pENTRY-L4-pLOVE1-R1 and pENTRY L1-GAL4-VP16-L2 into the destination vector pB9-H2A-UAS-7m24GW. This vector contains a HISTONE 2A-6 (H2A) coding sequence (At5g59870) fused to eGFP and driven by the repetitive UAS promoter (Olvera-Carrillo et al., 2015).

All constructs were transformed in *Agrobacterium tumefaciens* and then in *Arabidopsis thaliana* accession Col-0 using the floral dip method (Clough and Bent, 1998): inflorescences were dipped into a 5% sucrose / 0.05% Silwet L-77 solution containing Agrobacterium for 30 seconds and kept at high humidity for 24 h. Transformed seeds were selected based on their red fluorescence (Ali et al., 2012). All the tagged lines and pLOVE1::CDEF1 were

transformed in Col-0. pLOVE1::DCR and pDCR::DCR were transformed for complementation in *dcr-2* and pGPAT2::GPAT2 in *gpat2-1*.

pGPAT5::NLS-GFP-GUS (Naseer et al., 2012), pBDG::GFP (Jakobson et al., 2016), pCUS2::GFP-GUS (Hong et al., 2017), pCYP86A1::NLS-GFP-GUS, pCYP86B1::NLS-GFP-GUS, pASFT::NLS-GFP-GUS (Naseer et al., 2012), pGSO1/SNG3::NLS-GFP (Pfister et al., 2014) were previously described. pGSO2::NLS-3xmVENUS was kindly provided by Satoshi Fujita (unpublished), pDCF::YFP by Mi Yeon Lee (unpublished), pABCG11::ABCG11-CITRINE by Celine Terrattaz (unpublished) and pFAR4::NLS-GFP-GUS by Yuree Lee (unpublished).

8.4. Evaluation of the expression of *GPAT* genes

Expression pattern

The expression pattern in the whole plant was first studied via GUS staining. Samples of lines expressing GUS were fixed for 20 min in ice cold 90% acetone for fixation and wash 3 x in 50 mM phosphate buffer saline (PBS). They were then incubated overnight at 37°C in a solution of 2% Triton X-100 / 2 mM Ferrocyanide / 0.1% Ferricyanide / 1 mM X-Gluc / 50 mM PBS (phosphate-buffered saline) with a vaccum pre-step for sample other than roots. Samples were then dehydrated with an ethanol serie (70%, 80%, 90%, 100%) for min 20 min each step. Pictures were taken under the Axio Zoom V16 microscope (Zeiss) coupled to an Axiocam 512 Color camera.

For studying the expression pattern at the organ level, a GFP was used combined with confocal microscopy (See section 8.10).

Expression level

For the detailed analysis of the total expression level, qRT-PCR was used. Using Maxwell® System RNA Purification Kit (Promega), RNA was extracted from 5-day-old roots according to the instructions of the manufacturer. cDNA was synthesized based on 1000 ng of RNA with M-MLV Reverse Transcriptase, RNase H Minus, Point Mutant (Promega). Three samples of each *GPAT* mutants and WT plants were independently harvested. One sample was containing 60 seedlings. *GPAT* genes have been amplified using SYBR® Select Master Mix from in the Stratagen MX3005P qPCR machine (Agilent Technology). The level of expression was established by the $2^{-\Delta\Delta Ct}$ method of (Schmittgen and Livak, 2008), ΔΔCt being the

difference between the raw threshold cycle (Ct) obtained by the primers specific to the reference gene to the one of the studied gene. Details about primer sequences are available in the Table S4.

8.5. Polyester digestion

In vitro cuticle digestion

The polyester of the RCC was digested *in vitro* by a recombinant cutinase (Unilever). Samples were fixed in acetone 90% for 30 min at 20°C, washed several time in 0.2 M K_2HPO_4 pH 8 and placed in a tube with 100 mg/ml cutinase in 0.2M K_2HPO_4 pH 8 for three days, the negative control plants were incubated in 0.2 M K_2HPO_4.

In vivo cuticle digestion

The polyester of the RCC of primary roots was specifically digested *in vivo* in transgenic pLOVE1::CDEF1 lines. In order to evaluate whether the *LOVE1* promoter was suitable to express a cutinase specifically in the outer root cap cell layer its activity was evaluated in several independent pLOVE1::H2A-GFP lines (Berhin et al. 2019, Figure S4A). Furthermore, several independent transgenic pLOVE1::CDEF1 lines were investigated for giving consistent results in respect to the RCC degradation (Berhin et al. 2019, Figure S4B).

8.6. Cuticle and suberin staining

Fluorol yellow

For visualization of cell wall polyesters, the Fluorol Yellow 088 protocol from Naseer et al. (2012) was modified to remove background staining in lipid-rich organs and validated (Berhin et al. 2019, Figure S4C). Shortly, seedlings were incubated in Fluorol Yellow 088 (0.01% in methanol) during 3 days for investigations of roots and for three weeks for aerial parts of the plants. Specimen were then counterstained with aniline blue (0.5% in water) for minimum 1 h at RT and rinsed in water. For the study of the RCC mutants, 10 roots were studied in three independent experiments. For the quantification of the suberin along the root, seedlings were entirely taken in picture via tile scan and the suberization was manually measured. 6-8 roots of 5 days were measured each time. The experiment was repeated three times.

Auramine O and Nile red

Other stainings, like Auramine O 0.1% and Nile Red 0.05% were directly prepared in Clearsee solution (10% Xylitol, 15% Sodium deoxycholate, 25% Urea) following protocol from Ursache et al. (2018). Samples were first fixed in fresh 4% paraformaldehyde in PBS 1 x for 30 min for roots, 2 h for leaves then wash 2-3 times in 1 x PBS solution. Samples were incubated in the Clearsee solution for one night for roots and one week for shoots. Then, they were incubated overnight in a Clearsee solution containing 0.1% Auramine O or 0.05% Nile Red. Samples were then washed in Clearsee washed again for 30-60 min. The Auramine O stained samples were then studied. The Nile Red stained samples were washed an additional hour in Clearsee before being stained in Clearsee solution containing 0.1% Calcofluor for 45 min and then washed again 30 min. Samples were mounted in Clearsee.

Sudan red

For Sudan Red staining, the procedure De Giorgi et al. (2015) was followed. Roots were first dehydrated with series of ethanol dilution (10%, 30%, 50%, 70%, 96%, 100%) for minimum 30 min. Following Technovit kit protocol, sample were incubated overnight in 1:1 mix of Ethanol 100% - Solution A (20 ml of Basic Resin, 0.2 g of Harderner powder and 400 µl of PEG400), then 3 h at 4°C in Solution A pure before being embedded in a solution of 40 µl of hardener liquid and 600 µl of Solution A. 10 µm-thick sections were cut with a microtome and stained with Sudan Red 7B 0.1% diluted in 1:1 mix of PEG400 and glycerol 90% for 15 min.

8.7. Assessment of diffusion barrier properties

Toluidine blue

For studying the RCC permeability with toluidine blue, 10-12 roots were harvested in 0.5 x liquid MS medium and then simultaneously incubated in an aqueous solution of 0.05% toluidine blue / 0.1% Tween 20 during the indicated time (10-135 seconds) followed by a quick washing step in water. Samples were instantaneously evaluated under the Axio Zoom V16 microscope (Zeiss) coupled to an Axiocam 512 Color camera for the presence or absence of dark-blue staining of the meristematic cells (Berhin et al. 2019, Figure S4D). A staining of the mucilage at the columella cells (Berhin et al. 2019, Figure S2) was present at

all times in WT and mutants (Berhin et al. 2019, Figure S4C). The experiment was repeated three times.

Fluorescein diacetate and Propidium iodide

For studying the RCC permeability with fluorescein diacetate (FDA) (5 mg/ml in ½ MS) (Barberon et al., 2016), 25 lateral roots of the same developmental stage originating from 3 independent experiments were individually investigated by direct application of FDA to the root on the microscope slide, immediately mounted and observed as described below. The same microscope and same settings were used for the analysis and a 4-min incubation period was selected for comparison of the different genotypes. The Firescale of relative intensity was used for the comparison (Schindelin et al., 2012). Similarly, PI (10 mg/ml) was used also to measure permeability after 4 min.

Tetrazolium red

Tetrazolium Red was used to study the permeability of the seed coat. Seeds were incubated for 24 h at 30°C in 1% Tetrazolium Red (Pineau et al., 2017).

Chlorophyll leaching

Chlorophyll leaching is a technique testing the permeability of a cuticle (Sieber et al., 2000). Full rosettes were incubated in 30 ml of 80% ethanol gently shaking in the dark. After 0, 5, 10, 15, 20, 30, 40, 50, 60 and 120 min, 200 µl was taken off from the tubes and the absorbance was measured. Chlorophyll content was deduced by the absorbance at 664 and 647 nm: Chlorophyll (µM/g of fresh weight)= (7.93 x Absorbance at 664 + 19.53 x Absorbance at 647)/ fresh weight in gram.

8.8. Germination and root growth assays

Salt stress assay

Salt stress assays were conducted by placing seeds on medium containing 75 mM of K_2SO_4, 250 mM of mannitol, 100 mM of KCl or 100 mM of NaCl, respectively. Four replicates were evaluated for each treatment (50-100 seeds each) and 3 for controls. Experiments were repeated independently three times and a representative dataset is presented. Salt concentrations had been optimized to minimize the effects on plant development of WT by

using 50-200 mM of K_2SO_4, 200-400 mM of mannitol, 100-200 mM of KCl or 100-200 mM of NaCl.

NaCl-induced cell death assay

NaCl-induced cell death assay was conducted by incubating of 2-day-old seedlings in ½ MS medium containing 140 mM NaCl for 10 min. Seedlings were subsequently treated for 10 seconds with PI (10 mg/mL) and immediately observed under the microscope (Olvera - Carrillo et al., 2015). The number of dead cells was determined by counting the cells fully stained by PI in the entire meristem using a z-stack of pictures. 16-20 meristems were observed per genotype. Experiments were repeated independently two times and a representative dataset is presented.

Lateral root emergence was induced on 5-day-old seedlings by turning the plate of 90°C (Voss et al., 2015). Stages of lateral root emergence were evaluated after 42 h or 96 h, using mutant roots having a comparable length to WT. Roots were fixed and cleared by the following incubation steps: 4% HCl / 20% methanol solution for 15 min at 57°C, 7% NaCl / 60% ethanol solution for 15 min at RT, rehydrated by 10 min incubation in 60%, 40%, 20%, 10% ethanol. Specimens were mounted in 50% glycerol / 5% ethanol and stages of lateral root emergence were determined using a Leica DM5000B microscope (Malamy and Benfey, 1997). Experiments were repeated independently three times (n = 20-30) and a representative dataset is presented.

Lateral root stage and shape assay

To study the shape and the stage of lateral root primordia seedlings were fixed, cleared and stained with Calcofluor as described in Ursache et al. (2018). Briefly, the seedling was fixed in 4% paraformaldehyde for 1 h, then washed twice in 1 x PBS and cleared overnight in Clearsee (10% Xylitol, 15% Sodium deoxycholate, 25% Urea). Afterward the specimens were staining in 0.1% Calcofluor white in Clearsee for 1 h and washed in Clearsee for max 30 min before being imaged, as described below. Adhesion frequency was assessed by studying 90-160 seedlings of each genotype at the early observation time (42 h and 48 h) and approximately 100 seedlings at the late observation time (96 h).

Total lateral root count

The same Clearsee with Calcofluor technique was used to quantify the total primordia and lateral root number present on 8-day-old roots. The counting started from the tip of the root. Every primordium still clearly inside the primary root was counted as “Primordium”. Then going up in the root, at one point the first emerged lateral root is visible and was counted as “Emerged lateral root”. From that point on, all primordia found still inside the root were counted as “Delayed primordium”.

8.9. Immunofluorescence labeling

To label mucilage, the protocol of Durand et al. (2009) was used to detect xylogalacturonan-associated epitopes with the LM8 antibody, which was revealed with a fluorescein isothiocyanate (FITC)-conjugated goat anti-rat antibody. Briefly, 2-day-old seedlings were fixed for 30 min in 4% paraformaldehyde / 1% glutaraldehyde / 50 mM PIPES pH 7.0 / 1 mM $CaCl_2$ and washed in 50 mM PIPES pH 7.0 with 1 mM $CaCl_2$. After a 30 min incubation in 3% low-fat milk / PBS pH 7.2 as blocking solution, seedlings were washed in 0.05% Tween 20 (PBST) and incubated overnight with the LM8 antibody (1:5 in 0.1% PBST) at 4°C. Samples were then washed 5 times in 0.01% PBST and incubated for 2 h at 28°C in FITC-conjugated goat anti-rat as secondary antibody (1:50 in 0.1% PBST). A minimum of 30 roots of each genotype was studied.

8.10. Fluorescence Microscopy

Most fluorescent microscopy studies were performed on the confocal laser-scanning microscope ZEISS 700 with an excitation at 488 nm and detection with BP 490-555 nm for GFP, CITRINE, VENUS, FY, FDA and LM8, and LP 640 nm for PI. Calcofluor staining was studied on the confocal ZEISS LSM 880 Airyscan with an excitation at 405 nm and detection at 425-475 nm, Auramine as well respectively at 488 nm and at 505-530 nm and Nile Red at 561 nm and 600-650 nm. For staining the cell wall of the roots during the study of gene expression, PI (10 mg/mL) by direct application on the slide or Calcofluor (following the procedure in section 8.8) were used. Red seeds selection was performed under the stereomicroscope Leica 6000 equipped with a DSR filter. Confocal laser scanning microscopy to study *P. indica* were performed either on an Olympus FV1000 (Upright BX61WI). Wheat Germ Agglutinin Alexia Fluor 488 Conjugate (Invitrogen) was used for the labeling of the

fungus plasma membrane at a concentration of 10 µg/mL in PBS after a 15 min treatment at 96°C in KOH 10% to make the root permeable (Banhara et al., 2015).

8.11. Transmission electron microscopy

The TEM protocol developed of Barberon et al. (2016) was slightly modified. Samples were fixed in a 2.5% glutaraldehyde solution in 0.1M phosphate buffer pH 7.4 (PB) for 1 h at RT followed by a postfixation (1 h at RT) in a freshly made solution of 1% osmium tetroxide and 1.5% potassium ferrocyanide in PB and then washed in distilled water. Dehydration steps were then gradually performed in ethanol solution (30%, 50%, 70% for each 40 min, 100% twice for 1 h). The infiltration with Spurr resin at 33% in ethanol for 4 h, 66% for 4 h and 100% for 8 h twice was achieved before polymerization at 60°C for 48 h. Root tips were cut longitudinally in ultrathin sections of 50 nm of thickness. The organ fusion sample of a sepal with a leaf was cut orthogonally in ultrathin sections as well. Samples were studied with a FEI CM100 transmission electron microscope (FEI, Eindhoven, the Netherlands) coupled with a TVIPS TemCamF416 digital camera (TVIPS GmbH, Gauting, Germany) (acceleration voltage of 80 kV).

The ultrastructure of the root cap cell wall and cuticle was investigated over the entire length of the root cap in 2-3 independent root tip preparations per genotype and representative pictures were taken. Cuticle thickness was determined by taking 4 pictures per root and 5 measurements per picture for 5 primary roots and 3 lateral roots at a magnification of 20.000 (0.5101 nm/pixel). The ultrastructure of the RCC at the emerging lateral root was investigated at the stage when the lateral root had just emerged from the primary root and thus its exact position could be identified by light microscopy.

The organ fusion sample of a sepal with a leaf is part of some preliminary results and was only repeated once.

8.12. Chemical analyses

Cutin extraction

The protocol for the determination of ester-bond lipids previously described in Barberon et al. (2016) was adapted. 200 mg of seeds were grown on nylon mesh (200 mm pore size). After two days, the roots were shaved off after flash freezing and extracted in isopropanol / 0.01% butylated hydroxytoluene (BHT). They were then delipidized three times (1 h, 16 h, 8 h) in each of the following solvents, i.e., chloroform-methanol (2:1), chloroform-methanol (1:1), methanol with 0.01% BHT, under agitation before being dried for 3 days under vacuum. Depolymerization was performed by base catalysis (Li-Beisson et al., 2013). Briefly, dried plant samples were transesterified in 2 mL of reaction medium. 20 mL reaction medium was composed of 3 mL methyl acetate, 5 mL of 25% sodium methoxide in dry methanol and 12 mL dry methanol. The equivalents of 5 mg of methyl heptadecanoate and 10 mg of pentadecalactone/ sample were added as internal standards. After incubation of the samples at 60°C for 2 h 3.5 mL dichloromethane, 0.7 mL glacial acetic acid and 1 mL 0.9% NaCl (w/v) Tris 100 mM pH 8.0 were added to each sample and subsequently vortexed for 20 s. After centrifugation (1500 g for 2 min), the organic phase was collected, washed with 2 mL of 0.9% NaCl, and dried over sodium sulfate. The organic phase was then recovered and concentrated under a stream of nitrogen. The resulting cutin monomer fraction was derivatized with BFTSA/pyridine (1:1) at 70°C for 1 h and injected out of hexane on a HP-5MS column (J&W Scientific) in a gas chromatograph coupled to a mass spectrometer and a flame ionization detector (Agilent 6890N GC Network systems). The temperature cycle of the oven was the following: 2 min at 50°C, increment of 20°C /min to 160°C, of 2°C /min to 250°C and 10°C /min to 310°C, held for 15 min. 3 independent experiments were performed with 3-4 replicates for each genotype, respectively, and a representative dataset is presented. The amounts of unsubstituted C16 and C18 fatty acids were not evaluated because of their omnipresence in the plant and in the environment.

Wax extraction

Wax extraction was executed as advised in Kurdyukov et al. (2006a). 12 five-week-old leaves were harvested and dipped for 30 sec in chloroform. 3 mg of teracosane was added to the chloroform as an internal standard. Solvent was evaporated under a delicate flow of nitrogen. The resulting wax monomer fraction was derivatized with BFTSA / pyridine (1:1) at 70°C for 1 h and injected out of hexane on a HP-5MS column (J&W Scientific) in a gas chromatograph coupled to a mass spectrometer and a flame ionization detector (Agilent

6890N GC Network systems). The temperature cycle of the oven was the following: 2 min at 50°C, increment of 40°C /min to 200°C, of 3°C /min to 310°C, held for 30 min. The wax extraction presented in this work was part of preliminary results and so was only done once.

8.13. *Arabidopsis thaliana* with *Piriformospora indica*: co-cultivation and quantification

Co-cultivation

For this procedure a part of the method 1 and 2 of Johnson *et al*. (2011) has been followed: A 5 mm plugs of 4-week-old *P. indica* were placed in the middle of a modified PNM plate covered by a sterile filter. Four 7-day-old plantlets grown on ½ MS medium were placed surrounding the plug. Plates were incubated 14 days at 22°C under continuous light coming from the top (80 µmol.m^{-2}.s^{-1}) (Johnson, 2011).

Evaluation of the infection

Per sample, 20 mg of roots (min 4 roots) were harvested at 14 days after infection by *P. indica* (Banhara et al., 2015) and DNA was extracted using protocol STE buffer. The qPCR amplification was completed on 10 ng of DNA using Maxima SYBR Green/ROX qPCR Master Mix (2x) from Thermo Scientific in the 7300 Real Time PCR System (Applied Biosystems). Primers used for quantification of *P. indica* and *Arabidopsis thaliana* are respectively: PiITS - *P. indica* Internal Transcribed Spacer (Khatabi et al., 2012) and AtUBQ5 (Daneshkhah et al., 2013) (Table S4). Three samples of each mutant were tested, with three technical repetitions. The rate of fungal colonization was established by the $2^{-\Delta\Delta Ct}$ method of Schmittgen and Livak (2008), ΔΔCt being the difference between the raw threshold cycle (Ct) obtained by the primers specific of the fungi to the one of the plant.

Expression level of GPATs in case of infection

For the quantification of GPAT level expression in infect and non-infected roots, using trizol (Invitrogen), RNA was extracted from 200 mg of roots according to the instructions of the manufacturer. cDNA was synthesized based on 1000 ng of RNA with RevertAid H minus First Strand cDNA Synthesis Kit (Thermo Scientific). Three samples of non-infected and infected wild type plants (Col-0) were harvested. GPAT genes were amplified using Maxima SYBR Green/ROX qPCR Master Mix (2x) from Thermo Scientific in the 7300 Real Time PCR System

(Applied Biosystems). Details about primer sequences are available in the Table S4. The $2^{-\Delta\Delta Ct}$ method were used to quantify the difference of expression when the plant is infected or not.

References

Aharoni, A., Dixit, S., Jetter, R., Thoenes, E., van Arkel, G., and Pereira, A. (2004). The SHINE clade of AP2 domain transcription factors activates wax biosynthesis, alters cuticle properties, and confers drought tolerance when overexpressed in Arabidopsis. The Plant cell *16*, 2463-2480.

Akiba, T., Hibara, K., Kimura, F., Tsuda, K., Shibata, K., Ishibashi, M., Moriya, C., Nakagawa, K., Kurata, N., Itoh, J.*, et al.* (2014). Organ fusion and defective shoot development in *oni3* mutants of rice. Plant Cell Physiol *55*, 42-51.

Alassimone, J., Fujita, S., Doblas, V.G., van Dop, M., Barberon, M., Kalmbach, L., Vermeer, J.E.M., Rojas-Murcia, N., Santuari, L., Hardtke, C.S.*, et al.* (2016). Polarly localized kinase SGN1 is required for Casparian strip integrity and positioning. Nature Plants *2*, 16113.

Ali, M.A., Shah, K.H., and Bohlmann, H. (2012). pMAA-Red: a new pPZP-derived vector for fast visual screening of transgenic Arabidopsis plants at the seed stage. BMC Biotechnology.

Alonso, J.M., Stepanova, A.N., Leisse, T.J., Kim, C.J., Chen, H., Shinn, P., Stevenson, D.K., Zimmerman, J., Barajas, P., Cheuk, R.*, et al.* (2003). Genome-Wide Insertional Mutagenesis of Arabidopsis thaliana. Science *301*, 653-657.

Andersen, T.G., Barberon, M., and Geldner, N. (2015). Suberization — the second life of an endodermal cell. Current Opinion in Plant Biology *28*, 9-15.

Andersen, T.G., Naseer, S., Ursache, R., Wybouw, B., Smet, W., De Rybel, B., Vermeer, J.E.M., and Geldner, N. (2018). Diffusible repression of cytokinin signalling produces endodermal symmetry and passage cells. Nature *555*, 529-533.

Anderson, N.A., Bonawitz, N.D., Nyffeler, K., and Chapple, C. (2015). Loss of FERULATE 5-HYDROXYLASE Leads to Mediator-Dependent Inhibition of Soluble Phenylpropanoid Biosynthesis in *Arabidopsis*. Plant physiology *169*, 1557-1567.

Aoki, Y., Okamura, Y., Tadaka, S., Kinoshita, K., and Obayashi, T. (2016). ATTED-II in 2016: A Plant Coexpression Database Towards Lineage-Specific Coexpression. Plant Cell Physiol *57*, e5.

Augstein, F., and Carlsbecker, A. (2018). Getting to the Roots: A Developmental Genetic View of Root Anatomy and Function From Arabidopsis to Lycophytes. Frontiers in Plant Science *9*.

Bakan, B., and Marion, D. (2017). Assembly of the Cutin Polyester: From Cells to Extracellular Cell Walls. Plants (Basel, Switzerland) 6.

Banhara, A., Ding, Y., Kuhner, R., Zuccaro, A., and Parniske, M. (2015). Colonization of root cells and plant growth promotion by Piriformospora indica occurs independently of plant common symbiosis genes. Front Plant Sci *6*, 667.

Barberon, M. (2017). The endodermis as a checkpoint for nutrients. New Phytologist *213*, 1604-1610.

Barberon, M., Vermeer, J.E., De Bellis, D., Wang, P., Naseer, S., Andersen, T.G., Humbel, B.M., Nawrath, C., Takano, J., Salt, D.E.*, et al.* (2016). Adaptation of Root Function by Nutrient-Induced Plasticity of Endodermal Differentiation. Cell *164*, 447-459.

Barbosa, I.C.R., Rojas-Murcia, N., and Geldner, N. (2019). The Casparian strip—one ring to bring cell biology to lignification? Current Opinion in Biotechnology *56*, 121-129.

Barton, M.K. (2010). Twenty years on: The inner workings of the shoot apical meristem, a developmental dynamo. Developmental Biology *341*, 95-113.

Beisson, F., Li, Y., Bonaventure, G., Pollard, M., and Ohlrogge, J.B. (2007). The acyltransferase GPAT5 is required for the synthesis of suberin in seed coat and root of *Arabidopsis*. The Plant cell *19*, 351-368.

Beisson, F., Li-Beisson, Y., and Pollard, M. (2012). Solving the puzzles of cutin and suberin polymer biosynthesis. Curr Opin Plant Biol *15*, 329-337.

Benfey, P.N., and Scheres, B. (2000). Root development. Current biology : CB *10*, R813-815.

Bennett, T., van den Toorn, A., Sanchez-Perez, G.F., Campilho, A., Willemsen, V., Snel, B., and Scheres, B. (2010). SOMBRERO, BEARSKIN1, and BEARSKIN2 Regulate Root Cap Maturation in *Arabidopsis*. The Plant cell *22*, 640-654.

Berhin, A., de Bellis, D., Franke, R.B., Buono, R.A., Nowack, M.K., and Nawrath, C. (2019). The Root Cap Cuticle: A Cell Wall Structure for Seedling Establishment and Lateral Root Formation. Cell *176*, 1367-1378.e1368.

Bessire, M., Borel, S., Fabre, G., Carraca, L., Efremova, N., Yephremov, A., Cao, Y., Jetter, R., Jacquat, A.C., Metraux, J.P*., et al.* (2011). A member of the PLEIOTROPIC DRUG RESISTANCE family of ATP binding cassette transporters is required for the formation of a functional cuticle in Arabidopsis. The Plant cell *23*, 1958-1970.

Bessire, M., Chassot, C., Jacquat, A.C., Humphry, M., Borel, S., Petetot, J.M., Metraux, J.P., and Nawrath, C. (2007). A permeable cuticle in *Arabidopsis* leads to a strong resistance to *Botrytis cinerea*. EMBO J *26*, 2158-2168.

Bird, D., Beisson, F., Brigham, A., Shin, J., Greer, S., Jetter, R., Kunst, L., Wu, X., Yephremov, A., and Samuels, L. (2007). Characterization of *Arabidopsis* ABCG11/WBC11, an ATP binding cassette (ABC) transporter that is required for cuticular lipid secretion. The Plant journal : for cell and molecular biology *52*, 485-498.

Blackmore, S. (2018). How Plants Work: Form, Diversity, Survival. Ivy Press, 114-115.

Bonaventure, G., Beisson, F., Ohlrogge, J., and Pollard, M. (2004). Analysis of the aliphatic monomer composition of polyesters associated with *Arabidopsis* epidermis: occurrence of octadeca-cis-6, cis-9-diene-1,18-dioate as the major component. The Plant journal : for cell and molecular biology *40*, 920-930.

Bowes, B.G. (1972). Fine-structural observations on necrotic adventitious root apices in *Glechoma hederacea* L. Protoplasma *74*, 41-52.

Bowman, J.L. (2013). Walkabout on the long branches of plant evolution. Current Opinion in Plant Biology *16*, 70-77.

Buda, G.J., Isaacson, T., Matas, A.J., Paolillo, D.J., and Rose, J.K. (2009). Three-dimensional imaging of plant cuticle architecture using confocal scanning laser microscopy. The Plant journal : for cell and molecular biology *60*, 378-385.

Bütehorn, B., Rhody, D., and Franken, P. (2000). Isolation and Characterisation of Pitef1 Encoding the Translation Elongation Factor EF‐1α of the Root Endophyte *Piriformospora indica.* Plant Biology *2*, 687-692.

Chassot, C., Nawrath, C., and Metraux, J.P. (2007). Cuticular defects lead to full immunity to a major plant pathogen. The Plant journal : for cell and molecular biology *49*, 972-980.

Chen, X., Chen, G., Truksa, M., Snyder, C.L., Shah, S., and Weselake, R.J. (2014). Glycerol-3-phosphate acyltransferase 4 is essential for the normal development of reproductive organs and the embryo in *Brassica napus*. Journal of experimental botany *65*, 4201-4215.

Chen, X., Snyder, C.L., Truksa, M., Shah, S., and Weselake, R.J. (2011a). sn-Glycerol-3-phosphate acyltransferases in plants. Plant signaling & behavior *6*, 1695-1699.

Chen, X., Truksa, M., Snyder, C.L., El-Mezawy, A., Shah, S., and Weselake, R.J. (2011b). Three homologous genes encoding sn-glycerol-3-phosphate acyltransferase 4 exhibit different expression patterns and functional divergence in *Brassica napus*. Plant physiology *155*, 851-865.

Clough, S.J., and Bent, A.F. (1998). Floral dip: a simplified method for Agrobacterium-mediated transformation of *Arabidopsis thaliana*. The Plant journal : for cell and molecular biology *16*, 735-743.

Compagnon, V., Diehl, P., Benveniste, I., Meyer, D., Schaller, H., Schreiber, L., Franke, R., and Pinot, F. (2009). CYP86B1 is required for very long chain omega-hydroxyacid and alpha, omega -dicarboxylic acid synthesis in root and seed suberin polyester. Plant physiology *150*, 1831-1843.

Creff, A., Brocard, L., Joubès, J., Taconnat, L., Doll, N.M., Marsollier, A.-C., Pascal, S., Galletti, R., Boeuf, S., Moussu, S*., et al.* (2019). A stress-response-related inter-compartmental signalling pathway regulates embryonic cuticle integrity in *Arabidopsis*. PLoS genetics *15*, e1007847.

Cui, F., Brosché, M., Lehtonen, Mikko T., Amiryousefi, A., Xu, E., Punkkinen, M., Valkonen, Jari P.T., Fujii, H., and Overmyer, K. (2016). Dissecting Abscisic Acid Signaling Pathways Involved in Cuticle Formation. Molecular Plant *9*, 926-938.

Daneshkhah, R., Cabello, S., Rozanska, E., Sobczak, M., Grundler, F.M., Wieczorek, K., and Hofmann, J. (2013). Piriformospora indica antagonizes cyst nematode infection and development in *Arabidopsis* roots. Journal of experimental botany *64*, 3763-3774.

De Giorgi, J., Piskurewicz, U., Loubery, S., Utz-Pugin, A., Bailly, C., Mene-Saffrane, L., and Lopez-Molina, L. (2015). An Endosperm-Associated Cuticle Is Required for *Arabidopsis* Seed Viability, Dormancy and Early Control of Germination. PLoS genetics *11*, e1005708.

de Silva, N. (2018). The roles of suberin biopolymer and associated waxes in protecting plants against abiotic stresses. PhD thesis.

Delude, C., Moussu, S., Joubes, J., Ingram, G., and Domergue, F. (2016). Plant Surface Lipids and Epidermis Development. Sub-cellular biochemistry *86*, 287-313.

Di Ruocco, G., Bertolotti, G., Pacifici, E., Polverari, L., Tsiantis, M., Sabatini, S., Costantino, P., and Dello Ioio, R. (2018). Differential spatial distribution of miR165/6 determines variability in plant root anatomy. Development *145*, dev153858.

Dickman, M.B., Patil, S.S., and Kolattukudy, P.E. (1982). Purification, characterization and rôle in infection of an extracellular cutinolytic enzyme from *Colletotrichum gloeosporioides* Penz. on *Carica papaya* L. Physiological Plant Pathology *20*, 333-347.

Doaigey, A.R., Al-Whaibi, M.H., Siddiqui, M.H., Al Sahli, A.A., and El-Zaidy, M.E. (2013). Effect of GA3 and 2,4-D foliar application on the anatomy of date palm (*Phoenix dactylifera* L.) seedling leaf. Saudi journal of biological sciences *20*, 141-147.

Domergue, F., Vishwanath, S.J., Joubes, J., Ono, J., Lee, J.A., Bourdon, M., Alhattab, R., Lowe, C., Pascal, S., Lessire, R.*, et al.* (2010). Three *Arabidopsis* fatty acyl-coenzyme A reductases, FAR1, FAR4, and FAR5, generate primary fatty alcohols associated with suberin deposition. Plant physiology *153*, 1539-1554.

Domínguez, E., Heredia-Guerrero, J.A., and Heredia, A. (2015). Plant cutin genesis: unanswered questions. Trends in Plant Science *20*, 551-558.

Duan, H., and Schuler, M.A. (2005). Differential Expression and Evolution of the *Arabidopsis* CYP86A Subfamily. Plant physiology *137*, 1067-1081.

Durand, C., Vicré-Gibouin, M., Follet-Gueye, M.L., Duponchel, L., Moreau, M., Lerouge, P., and Driouich, A. (2009). The Organization Pattern of Root Border-Like Cells of Arabidopsis Is Dependent on Cell Wall Homogalacturonan. Plant physiology *150*, 1411-1421.

Edstam, M.M., and Edqvist, J. (2014). Involvement of GPI-anchored lipid transfer proteins in the development of seed coats and pollen in *Arabidopsis thaliana*. Physiol Plant *152*, 32-42.

Ehlting, J., Sauveplane, V., Olry, A., Ginglinger, J.-F., Provart, N.J., and Werck-Reichhart, D. (2008). An extensive (co-)expression analysis tool for the cytochrome P450 superfamily in *Arabidopsis thaliana*. BMC plant biology *8*, 47.

Fabre, G., Garroum, I., Mazurek, S., Daraspe, J., Mucciolo, A., Sankar, M., Humbel, B.M., and Nawrath, C. (2016). The ABCG transporter PEC1/ABCG32 is required for the formation of the developing leaf cuticle in *Arabidopsis*. The New phytologist *209*, 192-201.

Fawke, S., Torode, T.A., Gogleva, A., Fich, E.A., Sørensen, I., Yunusov, T., Rose, J.K., and Schornack, S. (2018). Glycerol phosphate acyltransferase 6 controls filamentous pathogen interactions and cell wall properties of the tomato and *Nicotiana benthamiana* leaf epidermis. bioRxiv, 452102.

Fendrych, M., Van Hautegem, T., Van Durme, M., Olvera-Carrillo, Y., Huysmans, M., Karimi, M., Lippens, S., Guerin, C.J., Krebs, M., Schumacher, K.*, et al.* (2014). Programmed cell death controlled by ANAC033/SOMBRERO determines root cap organ size in *Arabidopsis*. Current biology : CB *24*, 931-940.

Feng, G., Liu, G., and Xiao, J. (2015). The *Arabidopsis* EIN2 restricts organ growth by retarding cell expansion. Plant signaling & behavior *10*, e1017169-e1017169.

Fich, E.A., Segerson, N.A., and Rose, J.K. (2016). The Plant Polyester Cutin: Biosynthesis, Structure, and Biological Roles. Annual review of plant biology *67*, 207-233.

Francis, S.A., Dewey, F.M., and Gurr, S.J. (1996). The role of cutinase in germling development and infection by *Erysiphe gramini* sf.sp.*hordei*. Physiological and Molecular Plant Pathology *49*, 201-211.

Franke, R., Briesen, I., Wojciechowski, T., Faust, A., Yephremov, A., Nawrath, C., and Schreiber, L. (2005). Apoplastic polyesters in Arabidopsis surface tissues--a typical suberin and a particular cutin. Phytochemistry *66*, 2643-2658.

Franke, R., Höfer, R., Briesen, I., Emsermann, M., Efremova, N., Yephremov, A., and Schreiber, L. (2009). The *DAISY* gene from *Arabidopsis* encodes a fatty acid elongase condensing enzyme involved in the biosynthesis of aliphatic suberin in roots and the chalaza-micropyle region of seeds. The Plant Journal *57*, 80-95.

Gidda, S.K., Shockey, J.M., Rothstein, S.J., Dyer, J.M., and Mullen, R.T. (2009). *Arabidopsis thaliana* GPAT8 and GPAT9 are localized to the ER and possess distinct ER retrieval signals: functional divergence of the dilysine ER retrieval motif in plant cells. Plant Physiol Biochem *47*, 867-879.

Gilbert, R.D., Johnson, A.M., and Dean, R.A. (1996). Chemical signals responsible for appressorium formation in the rice blast fungus *Magnaporthe grisea*. Physiological and Molecular Plant Pathology *48*, 335-346.

Goda, H., Sawa, S., Asami, T., Fujioka, S., Shimada, Y., and Yoshida, S. (2004). Comprehensive Comparison of Auxin-Regulated and Brassinosteroid-Regulated Genes in Arabidopsis. Plant physiology *134*, 1555-1573.

Gou, J.Y., Yu, X.H., and Liu, C.J. (2009). A hydroxycinnamoyltransferase responsible for synthesizing suberin aromatics in Arabidopsis. Proceedings of the National Academy of Sciences of the United States of America *106*, 18855-18860.

Grenville, D.J., and Peterson, R.L. (1981). Structure of Aerial and Subterranean Roots of Selaginella kraussiana a. br. Botanical Gazette *142*, 73-81.

Groh, B., Hübner, C., and Lendzian, K.J. (2002). Water and oxygen permeance of phellems isolated from trees: the role of waxes and lenticels. Planta *215*, 794-801.

Haas, D.L., and Carothers, Z.B. (1975). Some Ultrastructural Observations on Endodermal Cell Development in Zea Mays Roots. American Journal of Botany *62*, 336-348.

Haegi, A., Catalano, V., Luongo, L., Vitale, S., Scotton, M., Ficcadenti, N., and Belisario, A. (2013). A newly developed real-time PCR assay for detection and quantification of Fusarium oxysporum and its use in compatible and incompatible interactions with grafted melon genotypes. Phytopathology *103*, 802-810.

Hilfiker, O., Groux, R., Bruessow, F., Kiefer, K., Zeier, J., and Reymond, P. (2014). Insect eggs induce a systemic acquired resistance in Arabidopsis. The Plant journal : for cell and molecular biology *80*, 1085-1094.

Hiruma, K., Gerlach, N., Sacristan, S., Nakano, R.T., Hacquard, S., Kracher, B., Neumann, U., Ramirez, D., Bucher, M., O'Connell, R.J.*, et al.* (2016). Root Endophyte *Colletotrichum tofieldiae* Confers Plant Fitness Benefits that Are Phosphate Status Dependent. Cell *165*, 464-474.

Höfer, R., Briesen, I., Schreiber, L., Beck, M., Franke, R., and Pinot, F. (2008). The Arabidopsis cytochrome P450 CYP86A1 encodes a fatty acid ω-hydroxylase involved in suberin monomer biosynthesis. Journal of experimental botany *59*, 2347-2360.

Holloway, P.J. (1982). The chemical constitution of plant cutins. In the plant cuticle, 45-86.

Hong, L., Brown, J., Segerson, N.A., Rose, J.K., and Roeder, A.H. (2017). CUTIN SYNTHASE2 maintains progressively developing cuticular ridges in *Arabidopsis* sepals. Mol Plant.

Hruz, T., Laule, O., Szabo, G., Wessendorp, F., Bleuler, S., Oertle, L., Widmayer, P., Gruissem, W., and Zimmermann, P. (2008). Genevestigator v3: a reference expression database for the meta-analysis of transcriptomes. Advances in bioinformatics *2008*, 420747.

Huysmans, M., Andrade Buono, R., Skorzinski, N., Cubria Radio, M., De Winter, F., Parizot, B., Mertens, J., Karimi, M., Fendrych, M., and Nowack, M.K. (2018). ANAC087 and ANAC046 control distinct aspects of programmed cell death in the *Arabidopsis* columella and lateral root cap. The Plant cell.

Ingram, G., and Nawrath, C. (2017). The roles of the cuticle in plant development: organ adhesions and beyond. Journal of experimental botany *68*, 5307-5321.

Isaacson, T., Kosma, D.K., Matas, A.J., Buda, G.J., He, Y., Yu, B., Pravitasari, A., Batteas, J.D., Stark, R.E., Jenks, M.A*., et al.* (2009). Cutin deficiency in the tomato fruit cuticle consistently affects resistance to microbial infection and biomechanical properties, but not transpirational water loss. The Plant journal : for cell and molecular biology *60*, 363-377.

Jacobs, S., Zechmann, B., Molitor, A., Trujillo, M., Petutschnig, E., Lipka, V., Kogel, K.H., and Schafer, P. (2011). Broad-spectrum suppression of innate immunity is required for colonization of *Arabidopsis* roots by the fungus *Piriformospora indica*. Plant physiology *156*, 726-740.

Jakobson, L., Lindgren, L.O., Verdier, G., Laanemets, K., Brosche, M., Beisson, F., and Kollist, H. (2016). BODYGUARD is required for the biosynthesis of cutin in *Arabidopsis*. The New phytologist *211*, 614-626.

Jayawardhane, K.N., Singer, S.D., Weselake, R.J., and Chen, G. (2018). Plant sn-Glycerol-3-Phosphate Acyltransferases: Biocatalysts Involved in the Biosynthesis of Intracellular and Extracellular Lipids. Lipids.

Jeffree, C. (2006). The Fine Structure of the Plant Cuticle. In Annual Plant Reviews Volume 23: Biology of the Plant Cuticle.

Jiang, Y., Wang, W., Xie, Q., Liu, N., Liu, L., Wang, D., Zhang, X., Yang, C., Chen, X., Tang, D*., et al.* (2017). Plants transfer lipids to sustain colonization by mutualistic mycorrhizal and parasitic fungi. Science *356*, 1172-1175.

Johnson, J.M., Sherameti, I. , Ludwig, A., Nongbri, P. L., Sun, C., Lou, B., Varma, A., Oelmüller, R. (2011). Protocols for *Arabidopsis thaliana* and *Piriformospora indica* co-cultivation - A model system to study plant beneficial traits. Journal of Endocytobiosis and Cell Research, 101-113.

Kader, J.C. (1996). Lipid-trasnfer proteins in plants. Annual review of plant physiology and plant molecular biology *47*, 627-654.

Kamiya, M., Higashio, S.-Y., Isomoto, A., Kim, J.-M., Seki, M., Miyashima, S., and Nakajima, K. (2016). Control of root cap maturation and cell detachment by BEARSKIN transcription factors in *Arabidopsis*. Development *143*, 4063-4072.

Kandel, S., Morant, M., Benveniste, I., Blee, E., Werck-Reichhart, D., and Pinot, F. (2005). Cloning, functional expression, and characterization of CYP709C1, the first sub-terminal

hydroxylase of long chain fatty acid in plants. Induction by chemicals and methyl jasmonate. The Journal of biological chemistry *280*, 35881-35889.

Kandel, S., Sauveplane, V., Compagnon, V., Franke, R., Millet, Y., Schreiber, L., Werck-Reichhart, D., and Pinot, F. (2007). Characterization of a methyl jasmonate and wounding-responsive cytochrome P450 of *Arabidopsis thaliana* catalyzing dicarboxylic fatty acid formation *in vitro*. Febs j *274*, 5116-5127.

Kannangara, R., Branigan, C., Liu, Y., Penfield, T., Rao, V., Mouille, G., Höfte, H., Pauly, M., Riechmann, J.L., and Broun, P. (2007). The Transcription Factor WIN1/SHN1 Regulates Cutin Biosynthesis in *Arabidopsis thaliana*. The Plant cell *19*, 1278-1294.

Kanno, S., Arrighi, J.F., Chiarenza, S., Bayle, V., Berthome, R., Peret, B., Javot, H., Delannoy, E., Marin, E., Nakanishi, T.M*., et al.* (2016). A novel role for the root cap in phosphate uptake and homeostasis. Elife *5*, e14577.

Kenrick, P., and Crane, P.R. (1997). The origin and early evolution of plants on land. Nature *389*, 33.

Khatabi, B., Molitor, A., Lindermayr, C., Pfiffi, S., Durner, J., von Wettstein, D., Kogel, K.-H., and Schäfer, P. (2012). Ethylene Supports Colonization of Plant Roots by the Mutualistic Fungus *Piriformospora indica*. PLoS ONE *7*, e35502.

Kim, H., Lee, S.B., Kim, H.J., Min, M.K., Hwang, I., and Suh, M.C. (2012). Characterization of glycosylphosphatidylinositol-anchored lipid transfer protein 2 (LTPG2) and overlapping function between LTPG/LTPG1 and LTPG2 in cuticular wax export or accumulation in *Arabidopsis thaliana*. Plant Cell Physiol *53*, 1391-1403.

Kim, J., Jung, J.H., Lee, S.B., Go, Y.S., Kim, H.J., Cahoon, R., Markham, J.E., Cahoon, E.B., and Suh, M.C. (2013). Arabidopsis 3-Ketoacyl-Coenzyme A Synthase 9 Is Involved in the Synthesis of Tetracosanoic Acids as Precursors of Cuticular Waxes, Suberins, Sphingolipids, and Phospholipids. Plant physiology *162*, 567-580.

Kolattukudy, P.E. (2001). Polyesters in higher plants. Advances in biochemical engineering/biotechnology *71*, 1-49.

Kolattukudy, P.E., Rogers, L.M., Li, D., Hwang, C.S., and Flaishman, M.A. (1995). Surface signaling in pathogenesis. Proceedings of the National Academy of Sciences *92*, 4080-4087.

Kosma, D.K., Murmu, J., Razeq, F.M., Santos, P., Bourgault, R., Molina, I., and Rowland, O. (2014). AtMYB41 activates ectopic suberin synthesis and assembly in multiple plant species and cell types. The Plant journal : for cell and molecular biology *80*, 216-229.

Kreszies, T., Schreiber, L., and Ranathunge, K. (2018). Suberized transport barriers in *Arabidopsis*, barley and rice roots: From the model plant to crop species. Journal of plant physiology 227, 75-83.

Kumpf, R.P., and Nowack, M.K. (2015). The root cap: a short story of life and death. Journal of experimental botany.

Kurata, T., Kawabata-Awai, C., Sakuradani, E., Shimizu, S., Okada, K., and Wada, T. (2003). The YORE-YORE gene regulates multiple aspects of epidermal cell differentiation in *Arabidopsis*. The Plant Journal *36*, 55-66.

Kurdyukov, S., Faust, A., Nawrath, C., Bar, S., Voisin, D., Efremova, N., Franke, R., Schreiber, L., Saedler, H., Metraux, J.P*., et al.* (2006a). The epidermis-specific extracellular BODYGUARD controls cuticle development and morphogenesis in *Arabidopsis*. The Plant cell *18*, 321-339.

Kurdyukov, S., Faust, A., Trenkamp, S., Bar, S., Franke, R., Efremova, N., Tietjen, K., Schreiber, L., Saedler, H., and Yephremov, A. (2006b). Genetic and biochemical evidence for involvement of HOTHEAD in the biosynthesis of long-chain alpha-,omega-dicarboxylic fatty acids and formation of extracellular matrix. Planta *224*, 315-329.

Kuroha, T., Tokunaga, H., Kojima, M., Ueda, N., Ishida, T., Nagawa, S., Fukuda, H., Sugimoto, K., and Sakakibara, H. (2009). Functional analyses of LONELY GUY cytokinin-activating enzymes reveal the importance of the direct activation pathway in *Arabidopsis*. The Plant cell *21*, 3152-3169.

L'Haridon, F., Besson-Bard, A., Binda, M., Serrano, M., Abou-Mansour, E., Balet, F., Schoonbeek, H.J., Hess, S., Mir, R., Leon, J*., et al.* (2011). A permeable cuticle is associated with the release of reactive oxygen species and induction of innate immunity. PLoS Pathog *7*, e1002148.

Laplaze, L., Benkova, E., Casimiro, I., Maes, L., Vanneste, S., Swarup, R., Weijers, D., Calvo, V., Parizot, B., Herrera-Rodriguez, M.B*., et al.* (2007). Cytokinins Act Directly on Lateral Root Founder Cells to Inhibit Root Initiation. The Plant cell *19*, 3889-3900.

Lashbrooke, J., Cohen, H., Levy-Samocha, D., Tzfadia, O., Panizel, I., Zeisler, V., Massalha, H., Stern, A., Trainotti, L., Schreiber, L*., et al.* (2016). MYB107 and MYB9 Homologs Regulate Suberin Deposition in Angiosperms. The Plant cell *28*, 2097.

Laskowski, M., Biller, S., Stanley, K., Kajstura, T., and Prusty, R. (2006). Expression profiling of auxin-treated *Arabidopsis* roots: toward a molecular analysis of lateral root emergence. Plant Cell Physiol *47*, 788-792.

Lee, S.B., Go, Y.S., Bae, H.-J., Park, J.H., Cho, S.H., Cho, H.J., Lee, D.S., Park, O.K., Hwang, I., and Suh, M.C. (2009a). Disruption of Glycosylphosphatidylinositol-Anchored Lipid Transfer Protein Gene Altered Cuticular Lipid Composition, Increased Plastoglobules, and Enhanced Susceptibility to Infection by the Fungal Pathogen *Alternaria brassicicola*. Plant physiology *150*, 42-54.

Lee, S.B., Jung, S.J., Go, Y.S., Kim, H.U., Kim, J.K., Cho, H.J., Park, O.K., and Suh, M.C. (2009b). Two Arabidopsis 3-ketoacyl CoA synthase genes, *KCS20* and *KCS2/DAISY*, are functionally redundant in cuticular wax and root suberin biosynthesis, but differentially controlled by osmotic stress. The Plant journal : for cell and molecular biology *60*, 462-475.

Lee, Y., Yoon, T.H., Lee, J., Jeon, S.Y., Lee, J.H., Lee, M.K., Chen, H., Yun, J., Oh, S.Y., Wen, X*., et al.* (2018). A Lignin Molecular Brace Controls Precision Processing of Cell Walls Critical for Surface Integrity in *Arabidopsis*. Cell *173*, 1468-1480.e1469.

Lendzian, K.J. (2006). Survival strategies of plants during secondary growth: barrier properties of phellems and lenticels towards water, oxygen, and carbon dioxide. Journal of experimental botany *57*, 2535-2546.

Li, B., Kamiya, T., Kalmbach, L., Yamagami, M., Yamaguchi, K., Shigenobu, S., Sawa, S., Danku, J.M., Salt, D.E., Geldner, N*., et al.* (2017). Role of LOTR1 in Nutrient Transport through Organization of Spatial Distribution of Root Endodermal Barriers. Current biology : CB *27*, 758-765.

Li, X.-C., Zhu, J., Yang, J., Zhang, G.-R., Xing, W.-F., Zhang, S., and Yang, Z.-N. (2012). Glycerol-3-Phosphate Acyltransferase 6 (GPAT6) Is Important for Tapetum Development in *Arabidopsis* and Plays Multiple Roles in Plant Fertility. Molecular Plant *5*, 131-142.

Li, Y., Beisson, F., Koo, A.J., Molina, I., Pollard, M., and Ohlrogge, J. (2007a). Identification of acyltransferases required for cutin biosynthesis and production of cutin with suberin-like monomers. Proceedings of the National Academy of Sciences of the United States of America *104*, 18339-18344.

Li, Y., Beisson, F., Ohlrogge, J., and Pollard, M. (2007b). Monoacylglycerols are components of root waxes and can be produced in the aerial cuticle by ectopic expression of a suberin-associated acyltransferase. Plant physiology *144*, 1267-1277.

Li-Beisson, Y., Pollard, M., Sauveplane, V., Pinot, F., Ohlrogge, J., and Beisson, F. (2009). Nanoridges that characterize the surface morphology of flowers require the synthesis of cutin polyester. Proceedings of the National Academy of Sciences of the United States of America *106*, 22008-22013.

Li-Beisson, Y., Shorrosh, B., Beisson, F., Andersson, M.X., Arondel, V., Bates, P.D., Baud, S., Bird, D., Debono, A., Durrett, T.P.*, et al.* (2010). Acyl-lipid metabolism. *Arabidopsis* Book *8*, e0133.

Li-Beisson, Y., Verdier, G., Xu, L., and Beisson, F. (2016). Cutin and Suberin Polyesters. In eLS (John Wiley & Sons, Ltd).

Lolle, S.J., Hsu, W., and Pruitt, R.E. (1998). Genetic analysis of organ fusion in *Arabidopsis thaliana*. Genetics *149*, 607-619.

Loubéry, S., De Giorgi, J., Utz-Pugin, A., Demonsais, L., and Lopez-Molina, L. (2018). A Maternally Deposited Endosperm Cuticle Contributes to the Physiological Defects of transparent testa Seeds. Plant physiology *177*, 1218-1233.

Lü, S., Song, T., Kosma, D.K., Parsons, E.P., Rowland, O., and Jenks, M.A. (2009). *Arabidopsis CER8* encodes LONG-CHAIN ACYL-COA SYNTHETASE 1 (LACS1) that has overlapping functions with LACS2 in plant wax and cutin synthesis. The Plant Journal *59*, 553-564.

Luginbuehl, L.H., Menard, G.N., Kurup, S., Van Erp, H., Radhakrishnan, G.V., Breakspear, A., Oldroyd, G.E.D., and Eastmond, P.J. (2017). Fatty acids in arbuscular mycorrhizal fungi are synthesized by the host plant. Science *356*, 1175-1178.

Lulai, E.C., and Corsini, D.L. (1998). Differential deposition of suberin phenolic and aliphatic domains and their roles in resistance to infection during potato tuber (*Solanum tuberosum* L.) wound-healing. Physiological and Molecular Plant Pathology *53*, 209-222.

Lux, A., Morita, S., Abe, J., and Ito, K. (2005). An Improved Method for Clearing and Staining Free-hand Sections and Whole-mount Samples. Annals of Botany *96*, 989-996.

MacGregor, D.R., Deak, K.I., Ingram, P.A., and Malamy, J.E. (2008). Root System Architecture in *Arabidopsis* Grown in Culture Is Regulated by Sucrose Uptake in the Aerial Tissues. The Plant cell *20*, 2643-2660.

Malamy, J.E., and Benfey, P.N. (1997). Organization and cell differentiation in lateral roots of *Arabidopsis thaliana*. Development *124*, 33-44.

Mao, G., Seebeck, T., Schrenker, D., and Yu, O. (2013). CYP709B3, a cytochrome P450 monooxygenase gene involved in salt tolerance in *Arabidopsis thaliana*. BMC plant biology *13*, 169.

Marhava, P., Bassukas, A.E.L., Zourelidou, M., Kolb, M., Moret, B., Fastner, A., Schulze, W.X., Cattaneo, P., Hammes, U.Z., Schwechheimer, C*., et al.* (2018). A molecular rheostat adjusts auxin flux to promote root protophloem differentiation. Nature *558*, 297-300.

Marsollier, A.C., and Ingram, G. (2018). Getting physical: invasive growth events during plant development. Curr Opin Plant Biol *46*, 8-17.

Marum, L., Miguel, A., Ricardo, P.C., and Miguel, C. (2011). Identification of GPAT acyltransferases in cork oak. BMC Proceedings *5*, P69-P69.

Mazurek, S., Garroum, I., Daraspe, J., De Bellis, D., Olsson, V., Mucciolo, A., Butenko, M.A., Humbel, B.M., and Nawrath, C. (2017). Connecting cutin composition to cuticle ultrastructure and physical properties of *Arabidopsis* petals. Plant physiology.

Men, X., Shi, J., Liang, W., Zhang, Q., Lian, G., Quan, S., Zhu, L., Luo, Z., Chen, M., and Zhang, D. (2017). Glycerol-3-Phosphate Acyltransferase 3 (OsGPAT3) is required for anther development and male fertility in rice. Journal of experimental botany *68*, 513-526.

Molina, I., and Kosma, D. (2015). Role of HXXXD-motif/BAHD acyltransferases in the biosynthesis of extracellular lipids. Plant cell reports *34*, 587-601.

Molina, I., Li-Beisson, Y., Beisson, F., Ohlrogge, J.B., and Pollard, M. (2009). Identification of an *Arabidopsis* feruloyl-coenzyme A transferase required for suberin synthesis. Plant physiology *151*, 1317-1328.

Morant, M., and Reichhart, D. (2004). Recherche de cytochromes P450 impliqués dans la tolérance aux herbicides chez le blé (*Triticum aestivum*). Master thesis

Moreira, S., Bishopp, A., Carvalho, H., and Campilho, A. (2013). AHP6 inhibits cytokinin signaling to regulate the orientation of pericycle cell division during lateral root initiation. PLoS One *8*, e56370.

Mostafavi, S., Ray, D., Warde-Farley, D., Grouios, C., and Morris, Q. (2008). GeneMANIA: a real-time multiple association network integration algorithm for predicting gene function. Genome biology *9 Suppl 1*, S4.

Motte, H., and Beeckman, T. (2018). The evolution of root branching: increasing the level of plasticity. Journal of experimental botany, ery409-ery409.

Moussu, S., Doll, N.M., Chamot, S., Brocard, L., Creff, A., Fourquin, C., Widiez, T., Nimchuk, Z.L., and Ingram, G. (2017). ZHOUPI and KERBEROS Mediate Embryo/Endosperm Separation by Promoting the Formation of an Extracuticular Sheath at the Embryo Surface. The Plant cell *29*, 1642-1656.

Murata, N., and Tasaka, Y. (1997). Glycerol-3-phosphate acyltransferase in plants. Biochim Biophys Acta *1348*, 10-16.

Naseer, S., Lee, Y., Lapierre, C., Franke, R., Nawrath, C., and Geldner, N. (2012). Casparian strip diffusion barrier in *Arabidopsis* is made of a lignin polymer without suberin. Proceedings of the National Academy of Sciences of the United States of America *109*, 10101-10106.

Nawrath, C. (2002). The biopolymers cutin and suberin. The *Arabidopsis* book *1*, e0021-e0021.

Nawrath, C., Schreiber, L., Franke, R.B., Geldner, N., Reina-Pinto, J.J., and Kunst, L. (2013). Apoplastic diffusion barriers in *Arabidopsis. Arabidopsis* Book *11*, e0167.

Nelson, B.K., Cai, X., and Nebenfuhr, A. (2007). A multicolored set of in vivo organelle markers for co-localization studies in *Arabidopsis* and other plants. The Plant journal : for cell and molecular biology *51*, 1126-1136.

Olvera-Carrillo, Y., Van Bel, M., Van Hautegem, T., Fendrych, M., Huysmans, M., Simaskova, M., van Durme, M., Buscaill, P., Rivas, S., Coll, N.S*., et al.* (2015). A Conserved Core of Programmed Cell Death Indicator Genes Discriminates Developmentally and Environmentally Induced Programmed Cell Death in Plants. Plant physiology *169*, 2684-2699.

Oshima, Y., Shikata, M., Koyama, T., Ohtsubo, N., Mitsuda, N., and Ohme-Takagi, M. (2013). MIXTA-Like Transcription Factors and WAX INDUCER1/SHINE1 Coordinately Regulate Cuticle Development in *Arabidopsis* and *Torenia fournieri*. The Plant cell *25*, 1609-1624.

Panikashvili, D., Savaldi-Goldstein, S., Mandel, T., Yifhar, T., Franke, R.B., Hofer, R., Schreiber, L., Chory, J., and Aharoni, A. (2007). The *Arabidopsis* DESPERADO/AtWBC11 transporter is required for cutin and wax secretion. Plant physiology *145*, 1345-1360.

Panikashvili, D., Shi, J.X., Bocobza, S., Franke, R.B., Schreiber, L., and Aharoni, A. (2010). The *Arabidopsis* DSO/ABCG11 Transporter Affects Cutin Metabolism in Reproductive Organs and Suberin in Roots. Molecular Plant *3*, 563-575.

Panikashvili, D., Shi, J.X., Schreiber, L., and Aharoni, A. (2009). The *Arabidopsis* DCR encoding a soluble BAHD acyltransferase is required for cutin polyester formation and seed hydration properties. Plant physiology *151*, 1773-1789.

Panikashvili, D., Shi, J.X., Schreiber, L., and Aharoni, A. (2011). The *Arabidopsis* ABCG13 transporter is required for flower cuticle secretion and patterning of the petal epidermis. The New phytologist *190*, 113-124.

Petit, J., Bres, C., Mauxion, J.-P., Wong Jun Tai, F., Martin, L.B.B., Fich, E.A., Joubès, J., Rose, J.K.C., Domergue, F., and Rothan, C. (2016). The glycerol-3-phosphate acyltransferase GPAT6 from tomato plays a central role in fruit cutin biosynthesis. Plant physiology.

Pfister, A., Barberon, M., Alassimone, J., Kalmbach, L., Lee, Y., Vermeer, J.E., Yamazaki, M., Li, G., Maurel, C., Takano, J*., et al.* (2014). A receptor-like kinase mutant with absent endodermal diffusion barrier displays selective nutrient homeostasis defects. Elife *3*, e03115.

Pickett, F.B., Wilson, A.K., and Estelle, M. (1990). The aux1 Mutation of *Arabidopsis* Confers Both Auxin and Ethylene Resistance. Plant physiology *94*, 1462-1466.

Pineau, E., Xu, L., Renault, H., Trolet, A., Navrot, N., Ullmann, P., Légeret, B., Verdier, G., Beisson, F., and Pinot, F. (2017). *Arabidopsis thaliana* EPOXIDE HYDROLASE1 (AtEH1) is a cytosolic epoxide hydrolase involved in the synthesis of poly‐hydroxylated cutin monomers. New Phytologist *215*, 173-186.

Pollard, M., Beisson, F., Li, Y., and Ohlrogge, J.B. (2008). Building lipid barriers: biosynthesis of cutin and suberin. Trends Plant Sci *13*, 236-246.

Qiang, X., Zechmann, B., Reitz, M.U., Kogel, K.H., and Schafer, P. (2012). The mutualistic fungus *Piriformospora indica* colonizes *Arabidopsis* roots by inducing an endoplasmic reticulum stress-triggered caspase-dependent cell death. The Plant cell *24*, 794-809.

Raffaele, S., Leger, A., and Roby, D. (2009). Very long chain fatty acid and lipid signaling in the response of plants to pathogens. Plant signaling & behavior *4*, 94-99.

Ranathunge, K., Thomas, R.H., Fang, X., Peterson, C.A., Gijzen, M., and Bernards, M.A. (2008). Soybean Root Suberin and Partial Resistance to Root Rot Caused by *Phytophthora sojae*. Phytopathology *98*, 1179-1189.

Rani, S.H., Krishna, T.H.A., Saha, S., Negi, A.S., and Rajasekharan, R. (2010). *Defective in Cuticular Ridges (DCR)* of *Arabidopsis thaliana*, a Gene Associated with Surface Cutin Formation, Encodes a Soluble Diacylglycerol Acyltransferase. Journal of Biological Chemistry *285*, 38337-38347.

Rautengarten, C., Ebert, B., Ouellet, M., Nafisi, M., Baidoo, E.E., Benke, P., Stranne, M., Mukhopadhyay, A., Keasling, J.D., Sakuragi, Y.*, et al.* (2012). *Arabidopsis Deficient in Cutin Ferulate* encodes a transferase required for feruloylation of omega-hydroxy fatty acids in cutin polyester. Plant physiology *158*, 654-665.

Reitz, M.U., Bissue, J.K., Zocher, K., Attard, A., Huckelhoven, R., Becker, K., Imani, J., Eichmann, R., and Schafer, P. (2012). The subcellular localization of Tubby-like proteins and participation in stress signaling and root colonization by the mutualist *Piriformospora indica*. Plant physiology *160*, 349-364.

Renault, H., Alber, A., Horst, N.A., Basilio Lopes, A., Fich, E.A., Kriegshauser, L., Wiedemann, G., Ullmann, P., Herrgott, L., Erhardt, M.*, et al.* (2017). A phenol-enriched cuticle is ancestral to lignin evolution in land plants. Nature Communications *8*, 14713.

Richard M. Bateman, Peter R. Crane, William A. DiMichele, Paul R. Kenrick, Nick P. Rowe, Thomas Speck, and Stein, W.E. (1998). Early Evolution of Land Plants: Phylogeny, Physiology, and Ecology of the Primary Terrestrial Radiation. Annual Review of Ecology and Systematics *29*, 263-292.

Roppolo, D., De Rybel, B., Denervaud Tendon, V., Pfister, A., Alassimone, J., Vermeer, J.E., Yamazaki, M., Stierhof, Y.D., Beeckman, T., and Geldner, N. (2011). A novel protein family mediates Casparian strip formation in the endodermis. Nature *473*, 380-383.

Salminen, T.A., Eklund, D.M., Joly, V., Blomqvist, K., Matton, D.P., and Edqvist, J. (2018). Deciphering the Evolution and Development of the Cuticle by Studying Lipid Transfer Proteins in Mosses and Liverworts. Plants (Basel, Switzerland) *7*.

Samuels, L., Kunst, L., and Jetter, R. (2008). Sealing plant surfaces: cuticular wax formation by epidermal cells. Annual review of plant biology *59*, 683-707.

Sauveplane, V., Kandel, S., Kastner, P.E., Ehlting, J., Compagnon, V., Werck-Reichhart, D., and Pinot, F. (2009). *Arabidopsis thaliana* CYP77A4 is the first cytochrome P450 able to catalyze the epoxidation of free fatty acids in plants. Febs j *276*, 719-735.

Schafer, P., Khatabi, B., and Kogel, K.H. (2007). Root cell death and systemic effects of *Piriformospora indica*: a study on mutualism. FEMS Microbiol Lett *275*, 1-7.

Schindelin, J., Arganda-Carreras, I., Frise, E., Kaynig, V., Longair, M., Pietzsch, T., Preibisch, S., Rueden, C., Saalfeld, S., Schmid, B*., et al.* (2012). Fiji: an open-source platform for biological-image analysis. Nat Methods *9*, 676-682.

Schmittgen, T.D., and Livak, K.J. (2008). Analyzing real-time PCR data by the comparative CT method. Nat Protocols *3*, 1101-1108.

Schnurr, J., Shockey, J., and Browse, J. (2004). The acyl-CoA synthetase encoded by *LACS2* is essential for normal cuticle development in *Arabidopsis*. The Plant cell *16*, 629-642.

Schreiber, L. (2010). Transport barriers made of cutin, suberin and associated waxes. Trends Plant Sci *15*, 546-553.

Scott, L.I. (1928). The Root as an Absorbing Organ. II. The Delimitation of the Absorbing Zone. The New phytologist *27*, 141-174.

Serrano, M., Coluccia, F., Torres, M., L'Haridon, F., and Métraux, J.-P. (2014). The cuticle and plant defense to pathogens. Frontiers in Plant Science *5*, 274.

Shi, J.X., Malitsky, S., De Oliveira, S., Branigan, C., Franke, R.B., Schreiber, L., and Aharoni, A. (2011). SHINE transcription factors act redundantly to pattern the archetypal surface of *Arabidopsis* flower organs. PLoS genetics *7*, e1001388.

Shockey, J., Regmi, A., Cotton, K., Adhikari, N., Browse, J., and Bates, P.D. (2015). Identification of *Arabidopsis GPAT9* (At5g60620) as an Essential Gene Involved in Triacylglycerol Biosynthesis. Plant physiology.

Sieber, P., Schorderet, M., Ryser, U., Buchala, A., Kolattukudy, P., Metraux, J.P., and Nawrath, C. (2000). Transgenic Arabidopsis plants expressing a fungal cutinase show alterations in the structure and properties of the cuticle and postgenital organ fusions. The Plant cell *12*, 721-738.

Singer, S.D., Chen, G., Mietkiewska, E., Tomasi, P., Jayawardhane, K., Dyer, J.M., and Weselake, R.J. (2016). *Arabidopsis* GPAT9 contributes to synthesis of intracellular glycerolipids but not surface lipids. Journal of experimental botany *67*, 4627-4638.

Stępiński, D., Kwiatkowska, M., Popłońska, K., Polit, J.T., Wojtczak, A., Domínguez, E., and Heredia, A. (2016). Cutinsomes and cuticle enzymes GPAT6 and DGAT2 seem to travel together from a lipotubuloid metabolon (LM) to extracellular matrix of *O. umbellatum* ovary epidermis. Micron *85*, 51-57.

Stoeckle, D., Thellmann, M., and Vermeer, J.E.M. (2018). Breakout—lateral root emergence in *Arabidopsis thaliana*. Current Opinion in Plant Biology *41*, 67-72.

Sui, N., Tian, S., Wang, W., Wang, M., and Fan, H. (2017). Overexpression of Glycerol-3-Phosphate Acyltransferase from *Suaeda salsa* Improves Salt Tolerance in *Arabidopsis*. Front Plant Sci *8*, 1337.

Szczuka, E.S.A. (2003). Cuticle Fluorescence During Embryogenesis of *Arabidopsis thaliana* (L.) Heynh. Acta Biologica Cracaviensa Serie Botanica *45*, 63-67.

Takahashi, K., Shimada, T., Kondo, M., Tamai, A., Mori, M., Nishimura, M., and Hara-Nishimura, I. (2010). Ectopic expression of an esterase, which is a candidate for the unidentified plant cutinase, causes cuticular defects in *Arabidopsis thaliana*. Plant Cell Physiol *51*, 123-131.

Tang, D., Simonich, M.T., and Innes, R.W. (2007). Mutations in LACS2, a Long-Chain Acyl-Coenzyme A Synthetase, Enhance Susceptibility to Avirulent *Pseudomonas syringae* But Confer Resistance to *Botrytis cinerea* in *Arabidopsis*. Plant physiology *144*, 1093-1103.

Tena, G. (2019). Disposable cuticle for young roots. Nature Plants *5*, 246-246.

Thomas, R., Fang, X., Ranathunge, K., Anderson, T.R., Peterson, C.A., and Bernards, M.A. (2007). Soybean Root Suberin: Anatomical Distribution, Chemical Composition, and Relationship to Partial Resistance to *Phytophthora sojae*. Plant physiology *144*, 299-311.

Tsuwamoto, R., Fukuoka, H., and Takahata, Y. (2008). GASSHO1 and GASSHO2 encoding a putative leucine-rich repeat transmembrane-type receptor kinase are essential for the normal development of the epidermal surface in Arabidopsis embryos. The Plant journal : for cell and molecular biology *54*, 30-42.

Ülker, B., Peiter, E., Dixon, D.P., Moffat, C., Capper, R., Bouché, N., Edwards, R., Sanders, D., Knight, H., and Knight, M.R. (2008). Getting the most out of publicly available T-DNA insertion lines. The Plant Journal *56*, 665-677.

Ursache, R., Andersen, T.G., Marhavy, P., and Geldner, N. (2018). A protocol for combining fluorescent proteins with histological stains for diverse cell wall components. The Plant journal : for cell and molecular biology *93*, 399-412.

Vandenbussche, F., Petrášek, J., Žádníková, P., Hoyerová, K., Pešek, B., Raz, V., Swarup, R., Bennett, M., Zažímalová, E., Benková, E*., et al.* (2010). The auxin influx carriers AUX1 and LAX3 are involved in auxin-ethylene interactions during apical hook development in *Arabidopsis thaliana* seedlings. Development *137*, 597-606.

Varma, A., Savita, V., Sudha, Sahay, N., Butehorn, B., and Franken, P. (1999). *Piriformospora indica*, a cultivable plant-growth-promoting root endophyte. Applied and environmental microbiology *65*, 2741-2744.

Vilches-Barro, A., and Maizel, A. (2015). Talking through walls: mechanisms of lateral root emergence in *Arabidopsis thaliana*. Curr Opin Plant Biol *23*, 31-38.

Vishwanath, S.J., Delude, C., Domergue, F., and Rowland, O. (2015). Suberin: biosynthesis, regulation, and polymer assembly of a protective extracellular barrier. Plant cell reports *34*, 573-586.

Voisin, D., Nawrath, C., Kurdyukov, S., Franke, R.B., Reina-Pinto, J.J., Efremova, N., Will, I., Schreiber, L., and Yephremov, A. (2009). Dissection of the complex phenotype in cuticular mutants of *Arabidopsis* reveals a role of SERRATE as a mediator. PLoS genetics *5*, e1000703.

Voss, U., Wilson, M.H., Kenobi, K., Gould, P.D., Robertson, F.C., Peer, W.A., Lucas, M., Swarup, K., Casimiro, I., Holman, T.J*., et al.* (2015). The circadian clock rephases during lateral root organ initiation in *Arabidopsis thaliana*. Nat Commun *6*, 7641.

Wang, C., Chin, C.-K., and Gianfagna, T. (2000). Relationship between cutin monomers and tomato resistance to powdery mildew infection. Physiological and Molecular Plant Pathology *57*, 55-61.

Wang, E., Schornack, S., Marsh, J.F., Gobbato, E., Schwessinger, B., Eastmond, P., Schultze, M., Kamoun, S., and Oldroyd, G.E. (2012). A common signaling process that promotes mycorrhizal and oomycete colonization of plants. Current biology : CB *22*, 2242-2246.

Wang, L., Chu, H., Li, Z., Wang, J., Li, J., Qiao, Y., Fu, Y., Mou, T., Chen, C., and Xu, J. (2014). Origin and Development of the Root Cap in Rice. Plant physiology *166*, 603-613.

Wang, Z.-Y., Xiong, L., Li, W., Zhu, J.-K., and Zhu, J. (2011). The Plant Cuticle Is Required for Osmotic Stress Regulation of Abscisic Acid Biosynthesis and Osmotic Stress Tolerance in *Arabidopsis*. The Plant cell *23*, 1971-1984.

Waschburger, E., Kulcheski, F.R., Veto, N.M., Margis, R., Margis-Pinheiro, M., and Turchetto-Zolet, A.C. (2018). Genome-wide analysis of the *Glycerol-3-Phosphate Acyltransferase* (*GPAT*) gene family reveals the evolution and diversification of plant GPATs. Genetics and Molecular Biology, 0-0.

Wellesen, K., Durst, F., Pinot, F., Benveniste, I., Nettesheim, K., Wisman, E., Steiner-Lange, S., Saedler, H., and Yephremov, A. (2001). Functional analysis of the LACERATA gene of Arabidopsis provides evidence for different roles of fatty acid omega -hydroxylation in development. Proceedings of the National Academy of Sciences of the United States of America *98*, 9694-9699.

Weng, H., Molina, I., Shockey, J., and Browse, J. (2010). Organ fusion and defective cuticle function in a *lacs1 lacs2* double mutant of *Arabidopsis*. Planta *231*, 1089-1100.

Wilcox, H. (1954). Primary Organization of Active and Dormant Roots of Noble Fir, Abies procera. American Journal of Botany *41*, 812-821.

Willemsen, V., Bauch, M., Bennett, T., Campilho, A., Wolkenfelt, H., Xu, J., Haseloff, J., and Scheres, B. (2016). The NAC Domain Transcription Factors FEZ and SOMBRERO Control the Orientation of Cell Division Plane in *Arabidopsis* Root Stem Cells. Developmental Cell *15*, 913-922.

Winter, D., Vinegar, B., Nahal, H., Ammar, R., Wilson, G.V., and Provart, N.J. (2007). An "Electronic Fluorescent Pictograph" Browser for Exploring and Analyzing Large-Scale Biological Data Sets. PLoS ONE *2*, e718.

Wu, L., Zhou, Z.Y., Zhang, C.G., Chai, J., Zhou, Q., Wang, L., Hirnerova, E., Mrvkova, M., Novak, O., and Guo, G.Q. (2015). Functional roles of three cutin biosynthetic acyltransferases in cytokinin responses and skotomorphogenesis. PLoS One *10*, e0121943.

Wunderling, A., Ripper, D., Barra-Jimenez, A., Mahn, S., Sajak, K., Targem, M.B., and Ragni, L. (2018). A molecular framework to study periderm formation in *Arabidopsis*. The New phytologist.

Xiao, F., Mark Goodwin, S., Xiao, Y., Sun, Z., Baker, D., Tang, X., Jenks, M.A., and Zhou, J.M. (2004). *Arabidopsis* CYP86A2 represses *Pseudomonas syringae* type III genes and is required for cuticle development. The EMBO Journal *23*, 2903-2913.

Xing, Q., Creff, A., Waters, A., Tanaka, H., Goodrich, J., and Ingram, G.C. (2013). ZHOUPI controls embryonic cuticle formation via a signalling pathway involving the subtilisin protease ABNORMAL LEAF-SHAPE1 and the receptor kinases GASSHO1 and GASSHO2. Development *140*, 770-779.

Xuan, W., Band, L.R., Kumpf, R.P., Van Damme, D., Parizot, B., De Rop, G., Opdenacker, D., Möller, B.K., Skorzinski, N., Njo, M.F*., et al.* (2016). Cyclic programmed cell death stimulates hormone signaling and root development in *Arabidopsis*. Science *351*, 384-387.

Yadav, V., Molina, I., Ranathunge, K., Castillo, I.Q., Rothstein, S.J., and Reed, J.W. (2014). ABCG Transporters Are Required for Suberin and Pollen Wall Extracellular Barriers in *Arabidopsis*. The Plant cell *26*, 3569-3588.

Yang, S., Johnston, N., Talideh, E., Mitchell, S., Jeffree, C., Goodrich, J., and Ingram, G. (2008). The endosperm-specific ZHOUPI gene of *Arabidopsis thaliana* regulates endosperm breakdown and embryonic epidermal development. Development *135*, 3501-3509.

Yang, W., Pollard, M., Li-Beisson, Y., Beisson, F., Feig, M., and Ohlrogge, J. (2010). A distinct type of glycerol-3-phosphate acyltransferase with sn-2 preference and phosphatase activity producing 2-monoacylglycerol. Proceedings of the National Academy of Sciences of the United States of America *107*, 12040-12045.

Yang, W., Pollard, M., Li-Beisson, Y., and Ohlrogge, J. (2016). Quantitative analysis of glycerol in dicarboxylic acid-rich cutins provides insights into *Arabidopsis* cutin structure. Phytochemistry *130*, 159-169.

Yang, W., Simpson, J.P., Li-Beisson, Y., Beisson, F., Pollard, M., and Ohlrogge, J.B. (2012). A land-plant-specific glycerol-3-phosphate acyltransferase family in *Arabidopsis*: substrate specificity, sn-2 preference, and evolution. Plant physiology *160*, 638-652.

Yang, X., Zhao, H., Kosma, D.K., Tomasi, P., Dyer, J.M., Li, R., Liu, X., Wang, Z., Parsons, E.P., Jenks, M.A.*, et al.* (2017). The Acyl Desaturase CER17 Is Involved in Producing Wax Unsaturated Primary Alcohols and Cutin Monomers. Plant physiology *173*, 1109-1124.

Yeats, T.H., Huang, W., Chatterjee, S., Viart, H.M.F., Clausen, M.H., Stark, R.E., and Rose, J.K.C. (2014). Tomato Cutin Deficient 1 (CD1) and putative orthologs comprise an ancient family of cutin synthase-like (CUS) proteins that are conserved among land plants. The Plant journal : for cell and molecular biology *77*, 667-675.

Yeats, T.H., Martin, L.B.B., Viart, H.M.F., Isaacson, T., He, Y., Zhao, L., Matas, A.J., Buda, G.J., Domozych, D.S., Clausen, M.H.*, et al.* (2012). The identification of cutin synthase: formation of the plant polyester cutin. Nature Chemical Biology *8*, 609.

Yeats, T.H., and Rose, J.K.C. (2013). The Formation and Function of Plant Cuticles. Plant physiology *163*, 5-20.

Zeier, J., and Schreiber, L. (1998). Comparative investigation of primary and tertiary endodermal cell walls isolated from the roots of five monocotyledoneous species: chemical composition in relation to fine structure. Planta *206*, 349-361.

Zhao, L., Haslam, T.M., Kunst, L., Sonntag, A., and Molina, I. (2019). Functional Overlap of Long-Chain Acyl-CoA Synthetases in *Arabidopsis*.

Zheng, Z., Xia, Q., Dauk, M., Shen, W., Selvaraj, G., and Zou, J. (2003). *Arabidopsis AtGPAT1*, a member of the membrane-bound glycerol-3-phosphate acyltransferase gene family, is essential for tapetum differentiation and male fertility. The Plant cell *15*, 1872-1887.

Zhu, J.-K. (2016). Abiotic stress signaling and responses in plants. Cell *167*, 313-324.

Zubko, E., Kunova, A., and Meyer, P. (2011). Sense and Antisense Transcripts of Convergent Gene Pairs in *Arabidopsis thaliana* Can Share a Common Polyadenylation Region. PLoS ONE *6*, e16769.

Zuccaro, A., Lahrmann, U., Guldener, U., Langen, G., Pfiffi, S., Biedenkopf, D., Wong, P., Samans, B., Grimm, C., Basiewicz, M.*, et al.* (2011). Endophytic life strategies decoded by

genome and transcriptome analyses of the mutualistic root symbiont *Piriformospora indica*. PLoS Pathog *7*, e1002290.

Supplemental Information

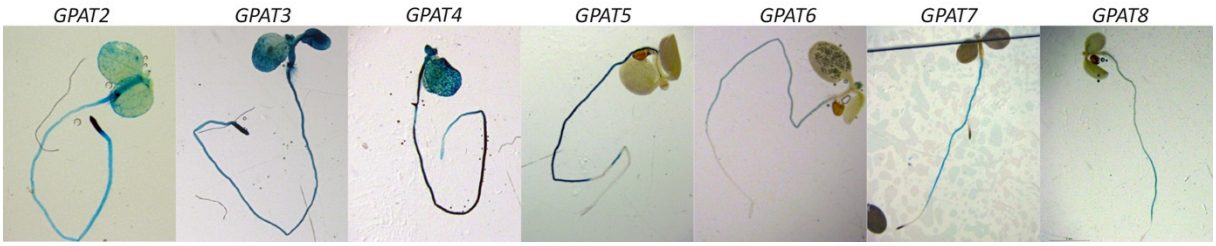

Figure S1: GUS staining of transgenic plants expressing pGPAT::NLS-GFP-GUS at primary root of 5-day-old seedling.

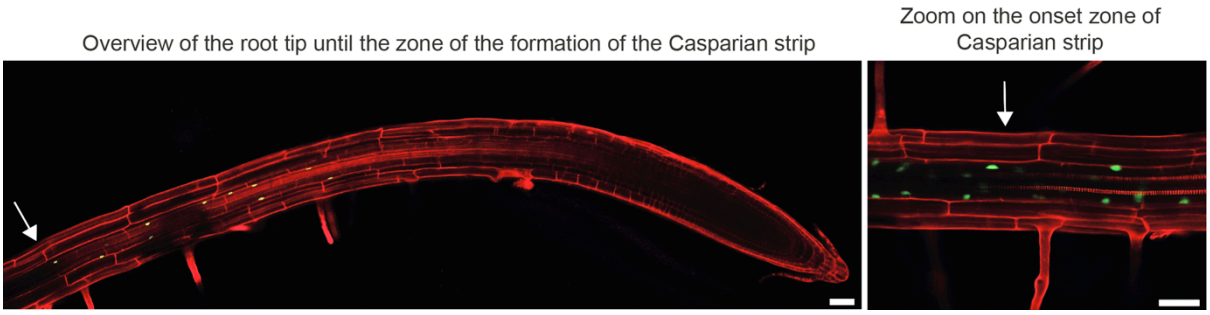

Figure S2: GFP fluorescence of transgenic plants expressing pGPAT4::NLS-GFP-GUS in a 5-day-old root. PI is staining the cell wall. White arrow, onset of the Casparian strip. Scale bars represent 50 µm.

Gene number	Gene name
AT1G52340	*ABA2*
AT1G17840	*ABCG11*
AT3G24650	*ABI3*
AT2G36270	*ABI5*
AT1G80100	*AHP6*
AT5G41040	*ASFT*
AT5G55910	*AUX1*
AT1G64670	*bdg*
AT1G33280	*BRN1*
AT4G10350	*BRN2*
AT4G30140	*CDEF1*
AT5G33370	*CUS2*
AT2G46950	*CYP709B2*
AT5G58860	*CYP86A1*
AT5G23190	*CYP86B1*
AT2G38120	*D6PK*
AT3G48720	*DCF*
AT5G23940	*DCR*
AT3G05600	*EH1*
AT5G03280	*EIN2*
AT1G66340	*ETR1*
AT4G36220	*F5H*

Gene number	Gene name
At3G44540	*FAR4*
AT1G02390	*GPAT2*
AT4G01950	*GPAT3*
AT1G01610	*GPAT4*
AT3G11430	*GPAT5*
AT2G38110	*GPAT6*
AT5G06090	*GPAT7*
AT4G00400	*GPAT8*
AT4G20140	*GSO1*
AT5G44700	*GSO2*
AT1G72970	*HTH*
AT2G37210	*LOG3*
AT3G53450	*LOG4*
AT5G20045	*LOVE1*
AT1G27950	*LTPG1*
AT3G43720	*LTPG2*
AT1G79580	*SMB*
AT4G13260	*YUC2*
AT5G43890	*YUC5*
AT5G25620	*YUC6*
AT4G28720	*YUC8*
AT4G28720	*YUC8*

Table S1: Gene names and numbers

Primer name	Primer sequence	Reference
GPAT2-1_LP	CAGAGTCTAGATTCCAGCGACA	Yang et al. 2012
GPAT2-1_RP	GGGTTTGCCAACTTTTCTTG	
GPAT2-2_LP	TCAATGCATCTCGATTCGTC	Present work
GPAT2-2_RP	AGAGGTCAAAACCATGTCCG	
GPAT2-3_LP	CGGATCTCAGGCAGTATGATC	Present work
GPAT2-3_RP	ATCACCATCGTCTTCAAGCC	
GPAT3-1_LP	ACGCCACACATTGATCTTCA	Yang et al. 2012
GPAT3-1_RP	TCGCAATCAAGCAAGTTGTC	
GPAT3-2_LP	GTCTTGTTCATGTGGGGTCC	SALK primer design
GPAT3-2_RP	TTTATGATGCATGTGCCGAC	
GPAT4_LP	TCTCTTCCCATCGTCATCATC	SALK primer design
GPAT4_RP	ACTGTTGTGGCTGATTTGGTC	
GPAT5_LP	TTGGTTACTATATGCTCCTATTTTGG	Naseer et al. 2012
GPAT5_RP	TTCGGACAAATGGTGAATTTC	
GPAT6_LP	GTTGTAACGGGCGATACGTT	Li et al. 2012
GPAT6-1_RP	CGTGACGTCGTTTTGAGAGA	
GPAT6-2_RP	CACTTGAAAGGTTCCAACAAATC	Present work
GPAT8_LP	TAATGAATTCGAACATGTGGCC	Present work
GPAT8_RP	GAACAGTACCTTGCAGAGAGACATGA	
DCR_LP	ATCCACGTGGCATTTTATGAG	Panikashvili et al. 2019
DCR_RP	ACAATTCCAAACCAAACACAC	
CYP709B2_LP	ACTCGTTAGAGCTTGCAGCTG	Mao et al. 2013
CYP709B2_RP	CTCCTGAGCACGATCAATCTC	
LBAi	TGGTTCACGTAGTGGGCCATCG	SALK primer design

Table S2: Genotyping primers

Primer name	Size (bp)	Primer sequence
pGPAT2-KpnI_F	2070	CATAGGTACCGTTCTCTGTTTTGGTCTTCTTG
pGPAT2-XmaI_R		CATACCCGGGTTTGACCTCTCGTTTTCTAATAAC
pGPAT3-KpnI_F	2223	CATAGGTACCCCTGTTAGCTGGAGATGTTAGG
pGPAT3-XmaI_R		CATACCCGGGGTTTGGATTTTGCAGAAAGC
pGPAT4-KpnI_F	1710	CATAGGTACCAACTTCATTGTTGCATCTTGG
pGPAT4-XmaI_R		CATACCCGGGCTTTCTTGCGGCGAATACT
pGPAT6-KpnI_F	1969	CATAGGTACCGTCGTATTACAATGATGATCAACC
pGPAT6-XmaI_R		CATACCCGGGAGATTTGGAAGGTGAGAATGG
pGPAT7-KpnI_F	1992	CATAGGTACCTGGGAAGATGTAGTCAAGCAC
pGPAT7-XmaI_R		CATACCCGGGCACAACTTAACTTGTTTCTTTTTTTG
pGPAT8-KpnI_F	2118	CATAGGTACCTCAAGTTTTGGGATCTTCATG
pGPAT8-XmaI_R		CATACCCGGGAACTATGAAATATCCACTAAGAGCG
nls-GPF_F	2613	GGGGACAAGTTTGTACAAAAAAGCAGGCTATGCAGCCTTCTCTTAAACG
GUS_R		GGGGACCACTTTGTACAAGAAAGCTGGGTTCATTGTTTGCCTCCCTG
GPAT2-ATT_F	2243	GGGGACAAGTTTGTACAAAAAAGCAGGCTATGTCCGGTAATAAGATC
GPAT2-ATT_R		GGAGTTGTCAAGAAAAAATAAACCCAGCTTTCTTGTACAAAGTGGTCCCC
GPAT3-ATT_F	2114	GAAATCTTGGCGGACATAGCCTGCTTTTTTGTACAAACTTGTCCCC
GPAT3-ATT_R		GGGGACCACTTTGTACAAGAAAGCTGGGTTTAATTTTTCTTAACTACTCCATT ATTACCGG
CYP709B2-ATT_F	2076	AAATTCTAACCGAACAAAATAACATAGCCTGCTTTTTTGTACAAACTTGTCCCC
CYP709B2-ATT_R		GGGGACCACTTTGTACAAGAAAGCTGGGTTCAACCGTCGATAGG
pDCR-KpnI_F	2936	CTACATGGTACCGTTGTCTTGCGATATGCTTG
pDCR-XmaI_R		ATCTAACCCGGGGGTGAAAGAGATTTTAACTGGC
pCYP709B2-KpnI_F	2098	CTACATGGTACCAACCCTGCTTTCTCCATC
pCYP709B2-XmaI_R		ATCTAACCCGGGAGGAGTAATGGAATTTATTTTACATG

Table S3: Cloning primers

Name	Sequence	Reference or Calibration	
GPAT2_R_qPCR	GGCTAAGACGGCGGCGAAT	Li et al. 2012	slope: -2.9383, Y-intercept:36.218, R^2: 0.998, efficiency: 2.189
GPAT2_F_qPCR	GGCAAACCCTACCACAAGA		
GPAT3_F_qPCR	GGTCGTGTTATTGGCATCA	Li et al. 2012	slope: -3.687, Y-intercept:41,688, R^2: 0.998, efficiency: 1.86
GPAT3_R_qPCR	GCTTCGTGGTAGGGTTTGC		
GPAT4_F_qPCR	GTGTCACTTATAGTGTCTCTCGCCTC	This work	slope: -3.432, Y-intercept:40.638, R^2: 0.999, efficiency: 1.956
GPAT4_R_qPCR	GCTCTGCAAATAGAGCACTGAACC		
GPAT5_F_qPCR	TCGTTATGTGAGGAGCATATTCAT	Kosma et al. 2014	slope: -3.366, Y-intercept:37.756, R^2: 0.9999, efficiency: 1.982
GPAT5_R_qPCR	TTGTTGGTCACCGTGGTTGT		
GPAT6_F_qPCR	GTTCATGAACCCGAGGCC	This work	slope: -3.387, Y-intercept:37.756, R^2: 0.999, efficiency: 1.822
GPAT6_R_qPCR	CATCCTCCGATCAATAATCACG		
GPAT7_F_qPCR	GGTCTAGGACGACATATTATCTCGG	This work	slope: -3.387, Y-intercept:41.543, R^2: 0.981, efficiency: 1.973
GPAT7_R_qPCR	GCCGCTGGTTATGACCG		
GPAT8_R_qPCR	GACTATGCGGTTCTTTAAGCGTTC	This work	slope: -3.323, Y-intercept:37.336, R^2: 0.971, efficiency: 1.999
GPAT8_F_qPCR	GTTTGGTAACGAATCACCTGATCTCG		
SAND_F_qPCR	AACTCTATGCAGCATTTGATCCACT	Hilfiker et al. 2014	slope: -3.333, Y-intercept:42,438 R^2: 0.998, efficiency: 1.996
SAND_R_qPCR	TGATTGCATATCTTTATCGCCATC		
AtUBQ5_F_qPCR	CCAAGCCGAAGAAGATCAAG	Daneshkhah *et al.* 2013	slope: -3.333, Y-intercept:42,438 R^2: 0.998, efficiency: 1.996
AtUBQ5_R_qPCR	ACTCCTTCCTCAAACGCTGA		
PiITS_F_qPCR	CAACACATGTGCACGTCGAT	Khatabi et al. 2012	slope: 23.208, Y-intercept: 30.55, R2: 0.995, efficiency: 2.099
PiITS_R_qPCR	CCAATGTGCATTCAGAACGA		

Table S4: qPCR primers